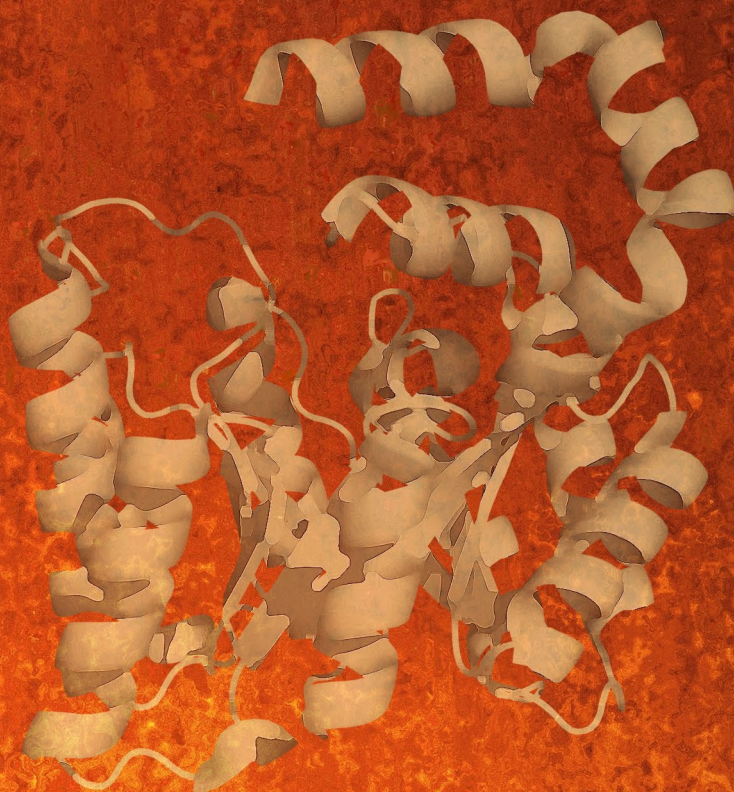


# Trimming proline dehydrogenase

## Protein and cofactor minimization



Mieke M.E. Huijbers





# **Trimming proline dehydrogenase**

**Protein and cofactor minimization**

**Mieke M.E. Huijbers**

## **Thesis committee**

### **Promotor**

Prof. Dr W.J.H. van Berkel

Personal chair at the Laboratory of Biochemistry

Wageningen University & Research

### **Other members**

Prof. Dr J. van der Oost, Wageningen University & Research

Prof. Dr M.W. Fraaije, University of Groningen

Prof. Dr K.H. van Pée, Technical University Dresden, Germany

Prof. Dr J. Pleiss, University of Stuttgart, Germany

This research was conducted under the auspices of the Graduate School VLAG (Advanced studies in Food Technology, Agrobiotechnology, Nutrition and Health Sciences).



# **Trimming proline dehydrogenase**

## **Protein and cofactor minimization**

**Mieke M.E. Huijbers**

### **Thesis**

submitted in fulfilment of the requirements for the degree of doctor  
at Wageningen University  
by the authority of the Rector Magnificus  
Prof. Dr A.P.J. Mol,  
in the presence of the  
Thesis Committee appointed by the Academic Board  
to be defended in public  
on Friday 10 March 2017  
at 1.30 p.m. in the Aula

Mieke M.E. Huijbers

Trimming proline dehydrogenase: protein and cofactor minimization  
182 pages.

PhD thesis, Wageningen University, Wageningen, NL (2017)

With references, with summaries in English and Dutch

ISBN 978-94-6343-051-7

DOI 10.18174/401209

# Contents

<b>List of abbreviations</b>	7
<b>Chapter 1</b>	11
Introduction	
<b>Chapter 2</b>	41
High yields of active <i>Thermus thermophilus</i> proline dehydrogenase are obtained using maltose-binding protein as a solubility tag	
<b>Chapter 3</b>	63
A more polar N-terminal helix releases MBP-tagged <i>Thermus thermophilus</i> proline dehydrogenase from tetramer-polymer self-association	
<b>Chapter 4</b>	81
Functional impact of the N-terminal arm of proline dehydrogenase from <i>Thermus thermophilus</i>	
<b>Chapter 5</b>	103
Dimerization of proline dehydrogenase from <i>Thermus thermophilus</i> is crucial for its thermostability	
<b>Chapter 6</b>	121
Proline dehydrogenase from <i>Thermus thermophilus</i> does not discriminate between FAD and FMN as cofactor	
<b>Chapter 7</b>	145
General discussion	
<b>Summary</b>	167
English summary	
Nederlandse samenvatting	
<b>About the author</b>	175
Acknowledgements	
Curriculum vitae	
Publications	
Overview of completed training activities	





## List of abbreviations

### General

ACP	acyl-carrier protein
ADP	adenosine-5'-diphosphate
AMP	adenosine 5'-monophosphate
ATP	adenosine-5'-triphosphate
BCA	bicinchoninic acid
BOG	n-octyl $\beta$ -D-glucopyranoside
CD	circular dichroism
CTD	C-terminal domain
CP	carrier protein
DBD	DNA-binding domain
DCPIP	dichlorophenolindophenol
DMF	dimethylformamide
DMSO	dimethylsulfoxide
EC	Enzyme Commission
ESI-MS	electron spray ionization mass spectrometry
EtOH	ethanol
FAD	flavin adenine dinucleotide
FMN	flavin mononucleotide
GSA	glutamic semialdehyde
GuHCl	guanidinium hydrochloride
LB	Luria-Bertani
LC-MS/MS	liquid chromatography-tandem mass spectrometry
MBP	maltose-binding protein
NAD	nicotinamide adenine dinucleotide
NADP	nicotinamide adenine dinucleotide phosphate
NMR	nuclear magnetic resonance
NRPS	nonribosomal peptide synthase
PMSF	phenylmethylsulfonyl fluoride
P2C	pyrrole-2-carboxylate
P5C	$\Delta^1$ -pyrroline-5-carboxylate
PCP	peptidyl carrier protein
PCR	polymerase chain reaction
PDB	protein data bank
PKS	polyketide synthase
ROS	reactive oxygen species
SDS	sodium dodecyl sulfate
SDS-PAGE	sodium dodecyl sulfate polyacrylamide gel electrophoresis
TB	terrific broth
TCA	tricarboxylic acid
TFA	trifluoroacetic acid
THFA	L-tetrahydro-2-furoic acid

## Amino acids

Ala	A	alanine
Arg	R	arginine
Asn	N	asparagine
Asp	D	aspartic acid
Cys	C	cysteine
Gln	Q	glutamine
Glu	E	glutamic acid
Gly	G	glycine
His	H	histidine
Ile	I	isoleucine
Leu	L	leucine
Lys	K	lysine
Met	M	methionine
Phe	F	phenylalanine
Pro	P	proline
Ser	S	serine
Thr	T	threonine
Trp	W	tryptophan
Tyr	T	tyrosine
Val	V	valine

## Enzymes

$\alpha$ -KG	$\alpha$ -ketoglutarate
$\gamma$ -GK	$\gamma$ -glutamyl kinase
$\gamma$ -GPR	$\gamma$ -glutamyl phosphate reductase
ACAD	acyl-CoA dehydrogenase
ALDH	aldehyde dehydrogenase
DAAO	D-amino acid oxidase
MTHFR	methylenetetrahydrofolate reductase
OAT	ornithine aminotransferase
P5CDH	$\Delta^1$ -pyrroline-5-carboxylate dehydrogenase
P5CR	P5C reductase
P5CS	P5C synthase
ProDH	proline dehydrogenase
POX	proline oxidase
PutA	proline utilization A
TIM	triosephosphate isomerase

## Organisms

<i>Bj</i>	<i>Bradyrhizobium japonicum</i>
<i>Dr</i>	<i>Deinococcus radiodurans</i>
<i>Ec</i>	<i>Escherichia coli</i>
<i>Gs</i>	<i>Geobacter sulfurreducens</i>
<i>Mt</i>	<i>Mycobacterium tuberculosis</i>
<i>St</i>	<i>Salmonella typhimurium</i>
<i>Ti</i>	<i>Talaromyces islandicus</i>
<i>Tt</i>	<i>Thermus thermophilus</i>



**MBP-*Tt*ProDH variants**

WT	MBP- <i>Tt</i> ProDH wildtype
EE	MBP- <i>Tt</i> ProDH with Phe10 and Leu12 replaced by Glu
$\Delta A$	MBP- <i>Tt</i> ProDH lacking helix $\alpha A$
$\Delta AB$	MBP- <i>Tt</i> ProDH lacking helices $\alpha A$ and $\alpha B$
$\Delta ABC$	MBP- <i>Tt</i> ProDH lacking helices $\alpha A$ , $\alpha B$ and $\alpha C$
$\Delta AB$ V32D	MBP- <i>Tt</i> ProDH $\Delta AB$ with Val32 replaced by Asp
$\Delta AB$ Y35F	MBP- <i>Tt</i> ProDH $\Delta AB$ with Tyr35 replaced by Phe
$\Delta AB$ V36D	MBP- <i>Tt</i> ProDH $\Delta AB$ with Val36 replaced by Asp
EE KK	MBP- <i>Tt</i> ProDH EE with Asp205 and Glu207 replaced by Lys
$\Delta A$ KK	MBP- <i>Tt</i> ProDH $\Delta A$ with Asp205 and Glu207 replaced by Lys
$\Delta AB$ KK	MBP- <i>Tt</i> ProDH $\Delta AB$ with Asp205 and Glu207 replaced by Lys
$\Delta ABC$ KK	MBP- <i>Tt</i> ProDH $\Delta ABC$ with Asp205 and Glu207 replaced by Lys





# Chapter 1

**Introduction**





Cells are the basic functional units of living organisms and the smallest units that can replicate independently. They are composed of molecules, of which proteins occupy a large part (Fig. 1). The exact macromolecular composition of cells varies per cell type. As an example, in wns function as enzymes that catalyze biochemical reactions. Enzymes are highly efficient, accelerate basically all reactions in the cell and are often highly specific in the substrates they accept. To expand their catalytic power, a substantial part of all enzymes is cofactor-dependent. Such cofactors can range from inorganic metal ions to complex organic molecules. Flavins are among the most important organic cofactors.

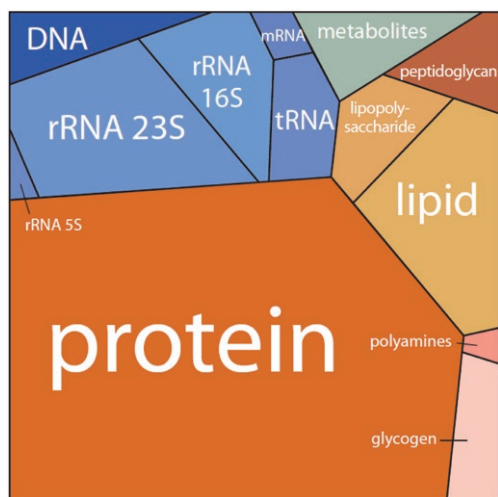


**Figure 1.**

A Voronoi tree diagram showing the composition of an *E. coli* cell growing with a doubling time of 40 min. Each polygon area represents the relative fraction of the corresponding constituent in the cell dry mass. The colors are chosen such that components with related functional role have similar tints. Figure from [2].

## Flavoenzymes

Flavin-containing enzymes are ubiquitous in nature and catalyze a wide variety of reactions. Thereby, they play a critical role in many biological processes, such as energy production, biodegradation, DNA repair, apoptosis, biosynthesis, and more [3,4]. There is a wide variety in the number of genes (0.1 – 3.5%) encoding flavoenzymes among different genomes. Apparently, some organisms are very dependent on flavin-dependent oxidoreductases for degradation or biosynthesis, while other organisms use different protein arsenals for this [5]. Since flavoproteins are so abundant, the implications of mutations in these enzymes are large. In the human genome, two thirds of the flavoproteins are linked to disorders [6].

Flavoenzymes contain a flavin mononucleotide (FMN) or flavin adenine dinucleotide (FAD) cofactor that serves as a redox-active prosthetic group and confers the enzyme a bright yellow appearance (flavus is Latin for yellow). Both FMN and FAD are derived from the precursor riboflavin (vitamin B2). For the *in vivo* synthesis of these cofactors, the ribityl side chain of riboflavin is phosphorylated by riboflavin kinase and additionally adenylated by FMN adenylyltransferase, yielding FMN and FAD respectively. Eukaryotes and some

archaea depend on two separate enzymes for FMN and FAD synthesis [7,8], but in most prokaryotes these two enzymes are fused into a bifunctional protein, FAD synthetase [9-11] (Fig. 2). The redox-active isoalloxazine ring of the flavin is used as a coenzyme in enzymatic reactions and can undergo one- or two-electron reductions. Although more than 90% of the flavin-dependent enzymes are oxidoreductases, these enzymes do not only catalyze redox reactions. About 10% of the flavoenzymes catalyze nonredox reactions and are classified as transferases, lyases, isomerases and ligases.

The majority of flavin-containing enzymes (90%) bind the cofactor non-covalently. Furthermore, FAD is three times more often utilized than FMN. Riboflavin is not used as a redox-active prosthetic group [5,12]. FAD- and FMN-containing enzymes are dominated by different enzyme folds. The Rossmann fold is very common among FAD-containing proteins, while FMN-containing proteins mostly adopt a TIM-barrel or flavodoxin-like fold [5,13].

### The TIM-barrel fold

The  $(\beta\alpha)_8$  TIM-barrel fold is the most common enzyme fold. This fold has first been observed in 1975 in triosephosphate isomerase (TIM) [14], after which it is named. Most TIM-barrels function as enzymes. It is a remarkably versatile scaffold: this fold is found in many different enzyme families and completely unrelated reactions can be catalyzed by enzymes with this fold [15-17]. Enzymes with a TIM-barrel fold are present in 5 out of 6 classes of enzymes as defined by the Enzyme Commission (EC) [17-19]. Most of the reactions that are catalyzed by TIM-barrel enzymes play a role in molecular or energy metabolism and many of these enzymes contain a cofactor that assists in catalysis [19].

Typically, the TIM-barrel domain consists of 250 amino acids [16]. The structure exists of an eightfold repeat of alternating  $\beta$ -strands and  $\alpha$ -helices, sequentially numbered  $\beta$ 1- $\beta$ 8 and  $\alpha$ 1- $\alpha$ 8 from the N-terminus. The loops connecting the strands and helices are referred to as  $\beta\alpha$  and  $\alpha\beta$  loops.  $\beta\alpha$  loop 1 follows after strand  $\beta$ 1 and  $\alpha\beta$  loop 1 follows after helix  $\alpha$ 1. The  $\beta$ -strands form the core of the barrel and are surrounded by the  $\alpha$ -helices (Fig. 3). The TIM-barrel structure is unique: it is the only barrel with a completely parallel  $\beta$ -sheet [17]. The active site of all TIM-barrel enzymes is located at the C-terminal ends of the  $\beta$ -strands (Fig. 3). In addition, the  $\beta\alpha$  loops are important for shaping the active site [16]. As an example, in TIM, three out of the eight  $\beta\alpha$  loops provide catalytic residues [20]. In contrast, the  $\alpha\beta$  loops appear to be important for stability of the TIM-barrel fold [21].

Some enzymes adopt a distorted TIM-barrel fold. One of these enzymes with an interesting distortion is the flavoenzyme proline dehydrogenase, which catalyzes the flavin-dependent oxidation of L-proline to  $\Delta^1$ -pyrroline-5-carboxylate.



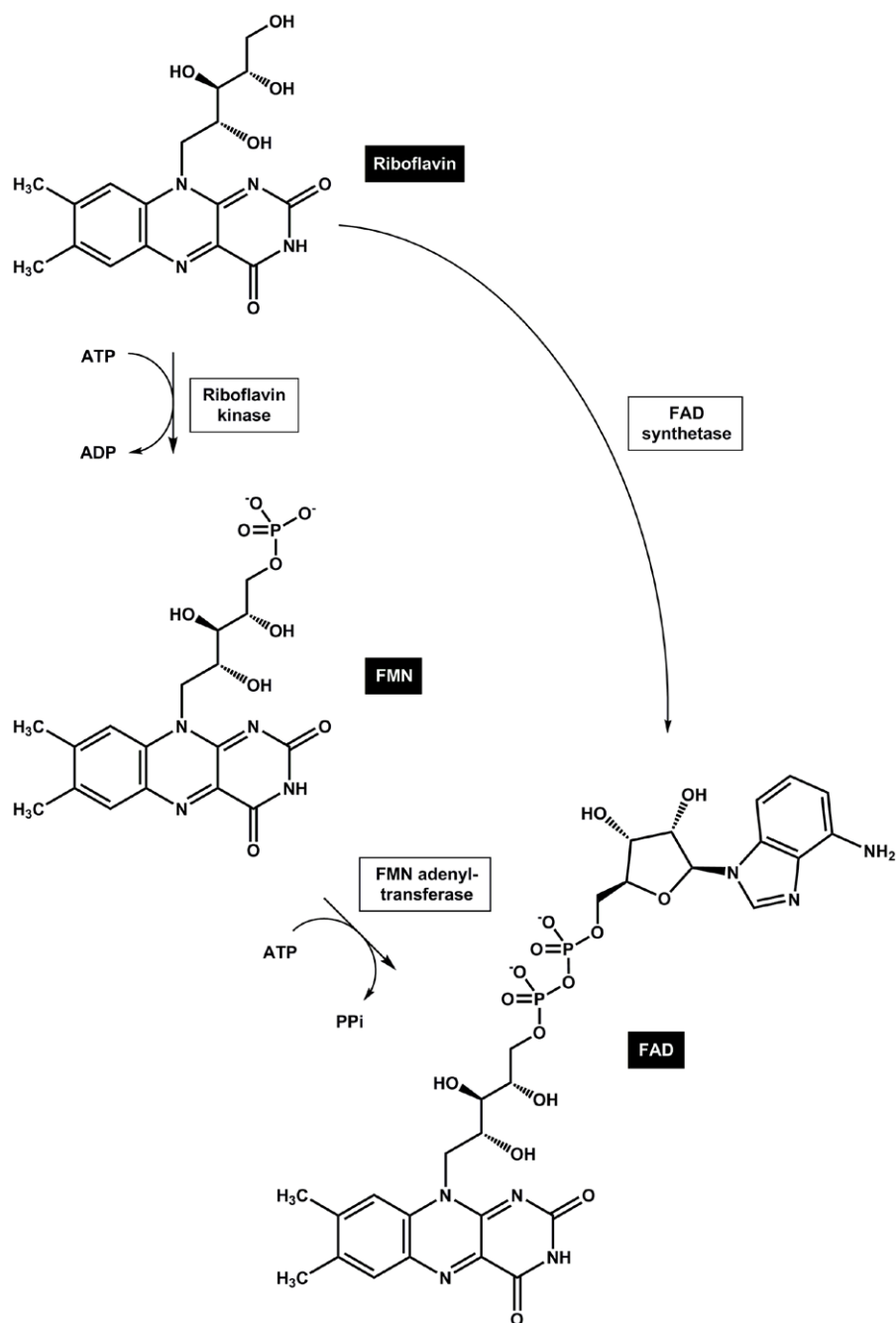


**Figure 2.**

*In vivo* synthesis of FAD and FMN from riboflavin. Eukaryotes and some archaea depend on a riboflavin kinase and a FMN adenylyltransferase for FMN and FAD synthesis, respectively, but in most prokaryotes these two enzymes are fused into a bifunctional protein, FAD synthetase.

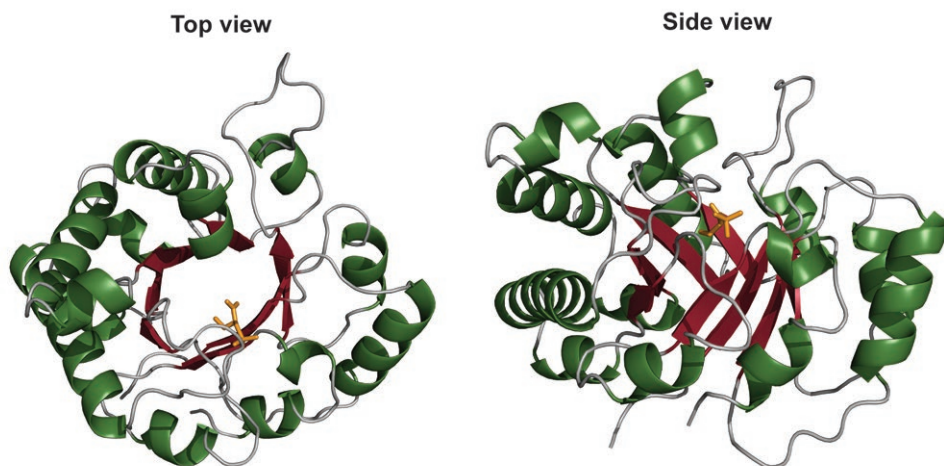


**Figure 3.**

Structural features of the TIM-barrel fold. Trypanosomal triosephosphate isomerase (PDB: 4TIM) with 2-phosphoglycollate as reaction intermediate analogue in the active site (depicted in yellow) is used as an example [22]. The eightfold repeat of alternating  $\beta$ -strands and  $\alpha$ -helices forms the barrel. The active site is located at the C-terminal ends of the  $\beta$ -strands and the  $\beta\alpha$  loops are important for shaping the active site.

## Proline

Proline (L-proline) is one of the proteinogenic amino acids. It is one of the most abundant amino acids in the cell. Together with the posttranslationally modified analogue hydroxyproline, proline is the major component of collagen, which is the major fibrous protein present in animals and accounts for approximately 30% of total human body protein [23].

Proline has an exceptional structure: it is the only amino acid with a secondary amine, meaning that the  $\alpha$ -amino group is directly attached to the side chain. This structural feature provides proline with a conformational rigidity not seen in the other amino acids. Therefore, this imino acid is often present in turns in a protein structure and disfavors  $\alpha$ -helices and  $\beta$ -sheets. It is a non-essential amino acid, since it can be synthesized from L-glutamate. In addition, it can serve as building block for the synthesis of a wide range of peptides and antibiotics [24-28].

Next to serving as one of the amino acids, proline has a central role in metabolism [29]. Proline and its metabolic enzymes are involved in a wide range of cellular processes, including cell signaling, bioenergetics and cellular redox control and the imino acid is widely recognized as a regulator in stress situations [30-33]. Proline protects against oxidative stress by scavenging reactive oxygen species (ROS) during biotic and abiotic stresses, thus acting as an antioxidant and preventing apoptosis [34-36]. In plants, proline accumulation occurs in response to various biotic and abiotic stresses, which has been extensively described [37-41].

Intracellular proline levels can increase >100-fold during adverse environmental conditions [39]. In addition, there is evidence proline does not only accumulate as an osmolyte during stress conditions but also plays a role in plant development and signaling [38,42].

Some organisms can rely on proline as their main energy source under certain circumstances by occupying proline-rich environmental niches, for example *Helicobacter pylori* [43,44] and trypanosomatids [45-47]. In addition, some insects use proline as their main fuel during flight. This is especially well studied for the tsetse fly [48,49], but is also observed for the mosquito *Aedes aegypti* [50] and for bees and wasps [51,52].

## Proline metabolism

Proline metabolism involves the interconversion between L-proline and L-glutamate (Fig. 4). In proline catabolism, the oxidation of proline to glutamate involves two enzymatic reactions that are connected by a non-enzymatic hydrolysis step [29,53] (Fig. 4). First, the FAD-dependent enzyme proline dehydrogenase (ProDH; EC 1.5.5.2) oxidizes L-proline to  $\Delta^1$ -pyrroline-5-carboxylate (P5C). This oxidation involves the transfer of two electrons from the proline substrate to the FAD cofactor, which is subsequently re-oxidized by transferring its electrons to the electron transport chain via the reduction of membrane-bound ubiquinone [54-56]. Produced P5C is then non-enzymatically hydrolyzed to glutamic semialdehyde (GSA). P5C and GSA exist in a highly pH-dependent equilibrium, with P5C favored at pH higher than 6.5 [57,58]. Finally, P5C is oxidized to L-glutamate by  $\Delta^1$ -pyrroline-5-carboxylate dehydrogenase (P5CDH; EC 1.2.1.88), and the two released electrons are transferred to nicotinamide adenine dinucleotide (NAD) [53]. ProDH and P5CDH exist as monofunctional enzymes or can be fused into a bifunctional enzyme called proline utilization A (PutA). The current view is that the occurrence of PutAs is restricted to bacteria, while monofunctional ProDH and P5CDH can occur in both bacteria and eukaryotes [59,60].

Proline biosynthesis from glutamate involves three enzymatic reactions [53] (Fig. 4). The conversion of L-glutamate to GSA is catalyzed by  $\gamma$ -glutamyl kinase ( $\gamma$ -GK; EC 2.7.2.11) and  $\gamma$ -glutamyl phosphate reductase ( $\gamma$ -GPR; EC 1.2.1.41). GK uses adenosine-5'-triphosphate (ATP) to produce  $\gamma$ -glutamyl phosphate, which is subsequently reduced to GSA by the nicotinamide adenine dinucleotide phosphate (NADPH)-dependent GPR [53]. In animals and plants,  $\gamma$ -GK and  $\gamma$ -GPR are fused into the bifunctional enzyme P5C synthetase (P5CS), while they are separate monofunctional enzymes in lower eukaryotes, such as yeast, and bacteria [61,62]. GSA can also be produced from ornithine by the mitochondrial enzyme ornithine aminotransferase (OAT; EC 2.6.1.13). After GSA is formed, it cyclizes non-enzymatically to P5C, which can be reduced to proline by the NADPH-dependent P5C reductase (P5CR; EC 1.5.1.2) [53]. The above mentioned enzymes involved in proline metabolism are all unidirectional, except for OAT. This suggests that proline metabolism is purpose-driven and tightly regulated.

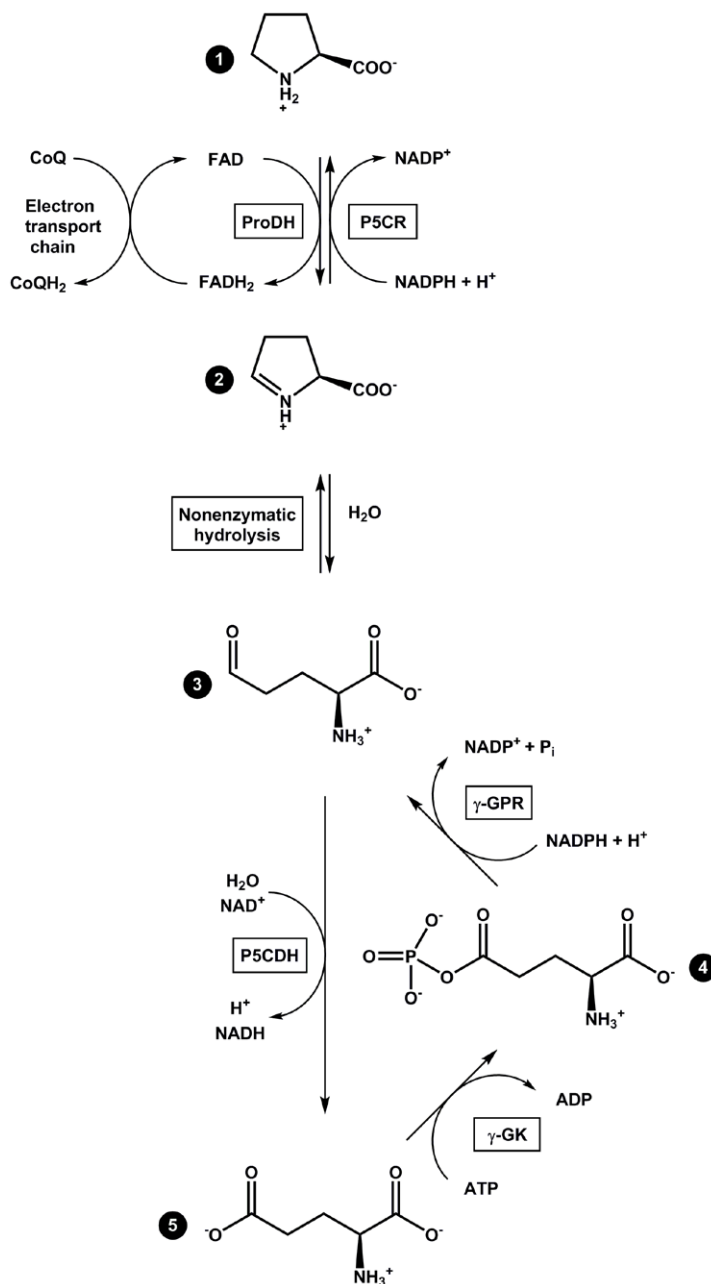
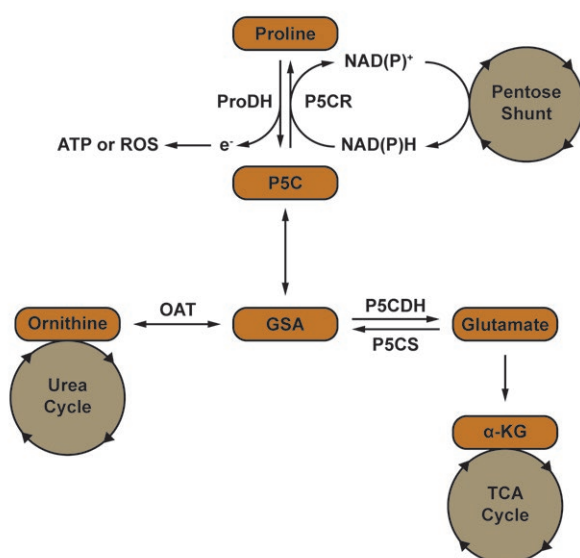


Figure 4.

Enzymes involved in proline metabolism. Reaction intermediates: (1) L-proline, (2)  $\Delta^1$ -pyrroline-5-carboxylate (3) glutamic semialdehyde, (4)  $\gamma$ -glutamyl phosphate, (5) L-glutamate.

Proline and the enzymes involved in its metabolism are linked with several core metabolic pathways in the cell (Fig. 5). Electrons released by the reduction of the FAD cofactor during proline oxidation by ProDH are donated into the electron transport chain, leading to the generation of ROS or ATP [53]. Conversion of P5C to L-proline by P5CR goes via oxidation of NADPH to NADP<sup>+</sup>; this redox couple is a metabolic interlock with the pentose phosphate pathway (pentose shunt) and linked to glucose metabolism [29,63,64]. GSA can be either converted to ornithine, which can enter the urea cycle, or to glutamate, which, is a precursor of  $\alpha$ -ketoglutarate ( $\alpha$ -KG) and can enter the tricarboxylic acid (TCA) cycle.

There is a great interest in understanding the biochemical functions of the proline metabolic enzymes because of their important role in biological pathways and medical issues. In this thesis, we focus on ProDH.



**Figure 5.**

Proline metabolic links. Proline metabolism is closely related with TCA cycle, urea cycle, and pentose phosphate pathway (pentose shunt). Figure based on [65].

## Medical aspects of ProDH

Proline and proline metabolism play an important role in humans and malfunctioning of the proline metabolic enzymes can lead to several medical issues. In addition to being one of the proteinogenic amino acids and playing a role in metabolism, proline is also suggested to function as an inhibitory neurotransmitter in a subset of glutamatergic synapses [66].

In humans, deletion of chromosomal region 22q11 is the most commonly found interstitial deletion and is associated with several syndromes, among which DiGeorge and velo-cardio-facial syndrome. Patients suffering from these syndromes have a high susceptibility for schizophrenia [67-69]. The gene encoding for human ProDH (also known as proline oxidase

(POX)) is located on chromosomal region 22q11 and is a hot-spot for mutations [70]. Therefore, different errors in human inborn proline metabolism have been described [66,71]. Missense mutations in ProDH have been identified in patients suffering from hyperprolinemia and the neuropsychiatric disorder schizophrenia [66,72-77]. Hyperprolinemia occurs when proline is not properly broken down in the cell, leading to elevated levels of the amino acids in the blood. This disorder has been described for the first time in 1961 [78]. There are two types of hyperprolinemia: type I is caused by a deficiency of ProDH [79], and type II is caused by a deficiency of P5CDH [80]. Both are inherited as autosomal recessive traits [66]. Patients do not always show a clinical phenotype, but can show cognitive, neurological, and psychiatric symptoms, such as an increased incidence of seizures and an increased risk of mild mental retardation [73,81].

ProDH plays a role in tumorigenesis and tumor development, since it is influenced by various tumor-associated factors [65]. It is one of the genes markedly induced by tumor suppressor p53 [82,83], which is an important factor in defending against tumor progression since it can control the cell cycle and apoptosis of tumor cells. The role of ProDH in cancer is complicated but is slowly elucidated. ProDH functions as a tumor suppressor by initiating apoptosis through ROS signaling [83-87]. Furthermore, it can inhibit tumor cell growth and proliferation and block the cell cycle, also through ROS signaling [85,88,89]. However, ProDH appears to have a paradoxical role in tumor biology. Under nutrient and hypoxic stress, ProDH is upregulated and serves as tumor survival factor through ATP production [31,64] and through protective ROS-induced autophagy [90-92]. A detailed overview of the factors involved in the dual role of ProDH in cancer is given by Liu and Phang [65].

Recently, ProDH has also been shown to play a role in HIV-1-associated neurological disorders, which can affect patients in the late stages of AIDS. ProDH is a protective stress response metabolic regulator in HIV-1 gp120-associated neurotoxicity by enhancing autophagy through ROS-mediated oxidative stress [93].

### Classification of ProDHs and PutAs

As mentioned before, ProDH and P5CDH can exist as monofunctional enzymes or can be fused into a bifunctional enzyme, protein utilization A (PutA). The occurrence of PutAs seems restricted to bacteria, while monofunctional ProDH and P5CDH can occur in both bacteria and eukaryotes [59,60]. ProDHs exhibit a distorted ( $\beta\alpha$ )<sub>8</sub> TIM-barrel fold, while P5CDHs exhibit an aldehyde dehydrogenase (ALDH) fold [59] (Fig. 6). ProDHs from archaea have a structural fold that is distinct from bacterial and eukaryotic ProDHs [94]; therefore, they will not be discussed here.

Monofunctional ProDH is a membrane-associated enzyme. In animals, it is associated with the inner mitochondrial membrane, while P5CDH is cytosolic [95-97]; this also goes for plants [56,98]. Bacterial monofunctional ProDHs are also presumed to be membrane-associated

[60]. Monofunctional ProDHs with a distorted TIM-barrel fold are typically 200–540 amino acids in length. The polypeptide chain for bacterial monofunctional ProDHs is shorter than for eukaryotic monofunctional ProDHs (Fig. 7). While the catalytic domain is of equal size, eukaryotic ProDHs have an elongated N-terminus [99]; a clear example of this is human ProDH [100]. The function of the N-terminal part of ProDH is unclear [59,100].

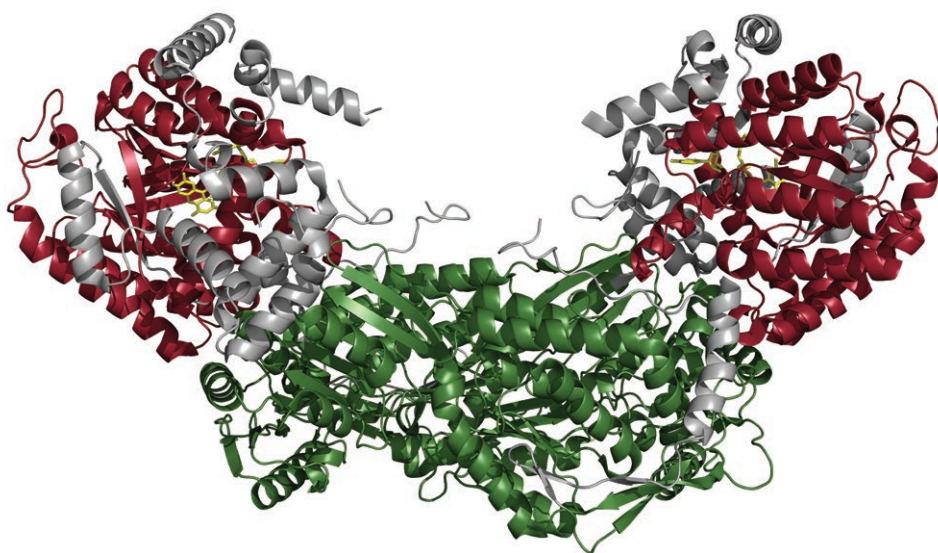


**Figure 6.**

Structure of PutA dimer from *Geobacter sulfurreducens* (PDB: 4NM9) [101]. The ProDH domains are depicted in red and the P5CDH domains are depicted in green. The FAD cofactors in the ProDH domains are depicted in yellow.

PutAs are peripherally membrane associated enzymes that can be subdivided in three different groups: short bifunctional (or minimalist) PutAs, long bifunctional PutAs and trifunctional PutAs [99]. Minimalist PutAs contain only a functional ProDH and P5CDH domain and are about 980-1100 amino acid residues in length. In comparison, long bifunctional PutAs have an additional C-terminal domain (CTD) of unknown function, which consists of about 175 residues. Thereby, these PutAs have a length of about 1100-1200 amino acid residues. Trifunctional PutAs contain, besides a ProDH, P5CDH and C-terminal domain, an N-terminally located 50-residues DNA-binding domain. Clearly, these PutAs are the longest: they encompass about 1300-1400 amino acid residues [99]. For trifunctional PutAs, the proline utilization (*put*) regulon encodes, next to the genes encoding PutA, the proline transporter PutP. Also, there is a regulatory region between the *putA* and *putP* genes [102]. When proline levels are low, PutA can act as a transcriptional repressor by binding to this regulatory region via its DNA-binding domain and thereby suppressing transcription of the *putA* and *putP* genes [102]. In response to high proline concentration in



the external environment, PutAs can undergo functional switching by dissociating from the *put* regulatory site and associating with the inner bacterial membrane. PutA and PutP can then be transcribed and the cells can take up proline via PutP, after which the membrane-associated PutA can oxidize proline, an important step in metabolism of the cell [103,104]. The redox state of the flavin determines whether PutA acts as a transcriptional repressor or as a metabolic enzyme [103,105-108]. In this way trifunctional PutAs link transcription and metabolism in response to proline levels inside and outside the cell.

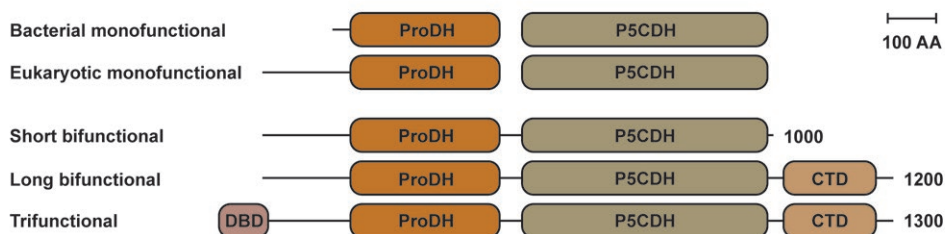


**Figure 7.**

Cartoon representation of the composition of monofunctional ProDHs and PutA proteins. Figure based on [99].

### Channeling of the P5C/GSA intermediate between ProDH and P5CDH

Substrate channeling means that a product of one enzyme is transported to the active site of another enzyme without release of the intermediate into the bulk solvent [109]. In PutA enzymes, the C-terminal fusion of ProDH to P5CDH (Fig. 6 and 7) allows channeling of the P5C/GSA intermediate between the enzymes. Evidence for substrate channeling is provided by studies on *Bradyrhizobium japonicum* PutA (BjPutA) [110,111], *Geobacter sulfurreducens* PutA (GsPutA) [101], *Escherichia coli* PutA (EcPutA) [112], and *Salmonella typhimurium* PutA (StPutA) [113].

Channeling of the P5C/GSA intermediate might be critical to facilitate the hydrolysis of P5C to GSA due to the highly pH-dependent equilibrium between those intermediates [57,58]. Hydrolysis of P5C to GSA is unfavorable at physiological pH: below pH 6.5, protonation of the pyrrolinium ring leads to hydrolysis of P5C to GSA, but above pH 6.5 the equilibrium is favored towards P5C. Channeling would allow an increase in the  $pK_a$  of the pyrrolinium ring at pH above 6.5, shifting the equilibrium towards hydrolysis of P5C to GSA and thereby improving the conversion efficiency of proline to glutamate [114]. In addition, channeling can protect against formation of unwanted products, since P5C and GSA are reactive and unstable intermediates that can inhibit other enzymes or react with metabolites [114]. It has been shown that GSA inhibits several enzymes from *E. coli*: glucosamine-6-phosphate synthase, cytidine 5'-triphosphate synthase, and the aminotransferase domain of carbamoyl phosphate synthetase [57,115,116]. In addition, P5C can form adducts with several ketones and aldehydes, such as pyruvic acid, oxaloacetic acid and acetoacetic acid [117].

Furthermore, P5C can deactivate pyridoxal phosphate. Formation of an inactive adduct results in vitamin B6 deficiency in patients with hyperprolinemia type II [117]. So seemingly, it would be beneficial to control intracellular levels of P5C/GSA by channeling.

According to the Rosetta Stone hypothesis, monofunctional ProDH and P5CDH should also be involved in substrate channeling. This hypothesis states that when two enzymes are separate in some organisms while they are fused in others, this almost always indicates an interaction between these two enzymes in their non-fused form [118]. In fact, evidence for substrate channeling between the monofunctional enzymes ProDH and P5CDH from *Thermus thermophilus* has been found recently [119].

### Structural characteristics of ProDHs and PutAs

Two crystal structures of full-length PutAs have been solved, which are the structures of BjPutA [111] and Gs PutA [101] (Fig. 6). Furthermore, the crystal structure of the ProDH domain of EcPutA [120] (Fig. 8A) is available. The ProDH domain of EcPutA has also been crystallized in complex with various proline analogues [121]. For monofunctional ProDHs, crystal structures of *Thermus thermophilus* ProDH (TtProDH) [60] (Fig. 8A) and *Deinococcus radiodurans* ProDH (DrProDH) [110] have been obtained. All structures contain an FAD cofactor. Next to methylenetetrahydrofolate reductase [122], ProDH is the only known  $(\beta\alpha)_8$  barrel protein binding a FAD cofactor [120]. Furthermore, these structures all show a distorted  $(\beta\alpha)_8$  TIM-barrel fold.

The classic TIM-barrel fold exists of an eightfold repeat of alternating  $\beta$ -strands and  $\alpha$ -helices; the eight  $\beta$ -strands form the core of the barrel that is surrounded by the eight  $\alpha$ -helices. The distorted  $(\beta\alpha)_8$  TIM-barrel fold of ProDH is characterized by the position of helix  $\alpha 8$ , which is on top of the barrel instead of alongside strand  $\beta 8$ . This distortion is caused by the presence of an additional helix ( $\alpha 0$ ), which precedes  $\beta 1$  in the polypeptide chain and is absent in the classic TIM-barrel. This extra helix occupies the place normally reserved for helix  $\alpha 8$ , forcing it to move perpendicular to the barrel [60,120,121]. This unique variation is crucial for the activity of ProDH, since the location of helix  $\alpha 8$  creates the proline-binding pocket. Since this distorted fold is observed for both monofunctional ProDHs and the ProDH domain in PutAs, it is considered to be a conserved defining structural signature in the ProDH superfamily [59,60].

One remarkable difference between PutAs and ProDHs concerns the binding mode of the FAD cofactor. PutAs and monofunctional ProDHs bind the isoalloxazine ring of the FAD cofactor in the same fashion, however, the location of the adenosine moiety differs (Fig. 8B). This might be partially caused by small structural difference between PutAs and ProDHs. PutAs contain an additional helix,  $\alpha 5a$ , which is replaced by a loop in monofunctional ProDHs. This helix contains a tryptophan that stacks against the adenine group of the FAD. Monofunctional ProDHs that lack helix  $\alpha 5a$  do not have an equivalent of this tryptophan for

interaction with the FAD. In addition, PutAs have extra helical components that follow helix  $\alpha 8$ . The additional C-terminal helices in PutAs prevent the conformation of the adenine ring of the FAD cofactor observed in monofunctional ProDHs [60,121].

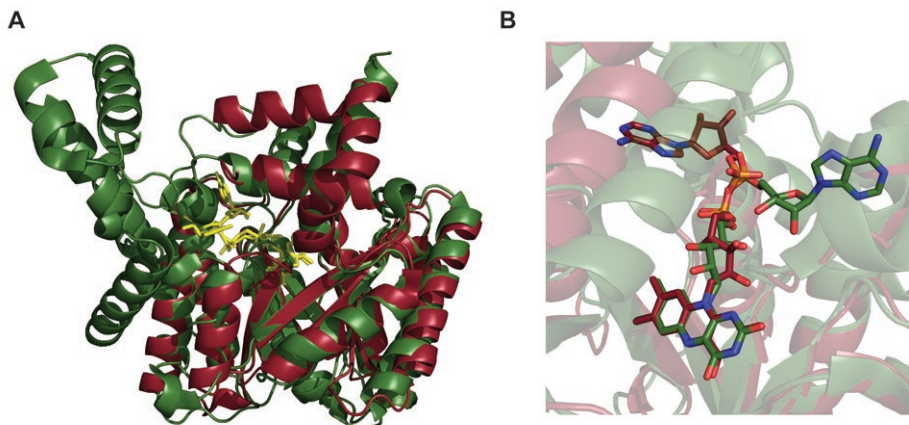


**Figure 8.**

(A) Structure of *Tt*ProDH (red, PDB:2G37) and the ProDH domain of *Ec*PutA (green, PDB: 4O8A) superimposed. The FAD cofactor is depicted in yellow. (B) Different conformations of the FAD cofactor of *Tt*ProDH (red) and *Ec*PutA (green). Both enzymes bind the isoalloxazine group of the FAD cofactor in the same fashion, however, the location of the adenosine group differs.

### The active site of ProDHs

Based on multiple sequence alignments, several fingerprint motifs of bacterial PutA/ProDHs have been identified [60] (Fig. 9). Each motif contains at least one amino acid residue that is conserved throughout the entire family; these conserved residues are clustered around the active site and important for FAD- and/or substrate binding [60]. The active site of ProDH is located at the C-terminal ends of the  $\beta$ -strands, like in the classic TIM-barrel. The proline-binding pocket is between the *si* face of the isoalloxazine ring of the flavin and helix  $\alpha 8$ .

The binding mode of the proline analogue L-tetrahydro-2-furoic acid (THFA) in the ProDH domain of *Ec*PutA has been described in detail [59,121]. Lys329, Arg555 and Arg556 form ion pairs with the carboxylic moiety of THFA, while several other residues form hydrophobic contacts with the pyrrolidine ring (Fig. 10). The ionic interactions and most of the hydrophobic interactions are also described for binding of THFA in *Dr*ProDH [123]. The ring of THFA is oriented nearly parallel to the middle ring of the dimethyl-isoalloxazine moiety of the flavin (Fig. 10B). C5 of THFA is 3.3 Å from flavin N5. This proximity suggests direct hydride transfer from the substrate to the flavin [120,121,124,125]. Such a mechanism has also been proposed for D-amino acid oxidase (DAAO), which has a similar ligand-FAD geometry as observed for ProDH and catalyzes a reaction that is analogous to that of ProDH [126,127]. It is suggested for ProDH that after binding of the proline substrate to the active site, Lys329

and Tyr437 (*E. coli* PutA numbering, Fig. 10B) deprotonate the amino ring nitrogen of the zwitterionic proline to give a neutral amino acid, followed by donation of a hydride ion from C5 to the FAD [121,125].

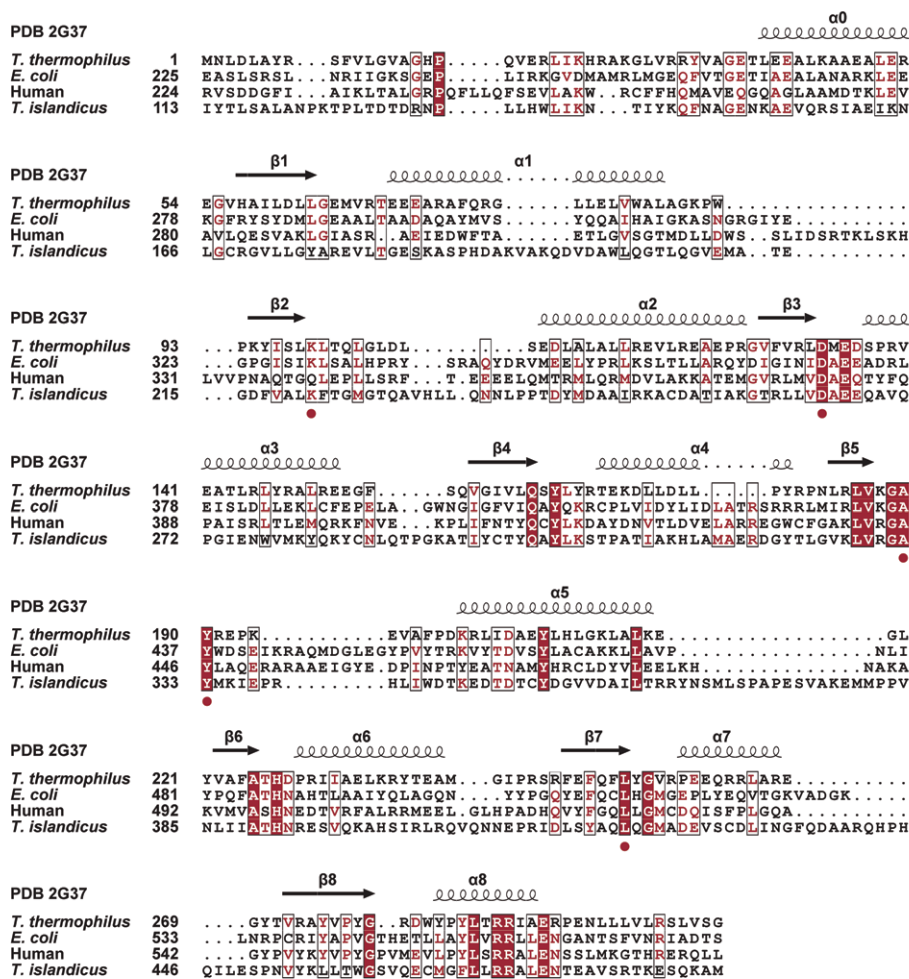
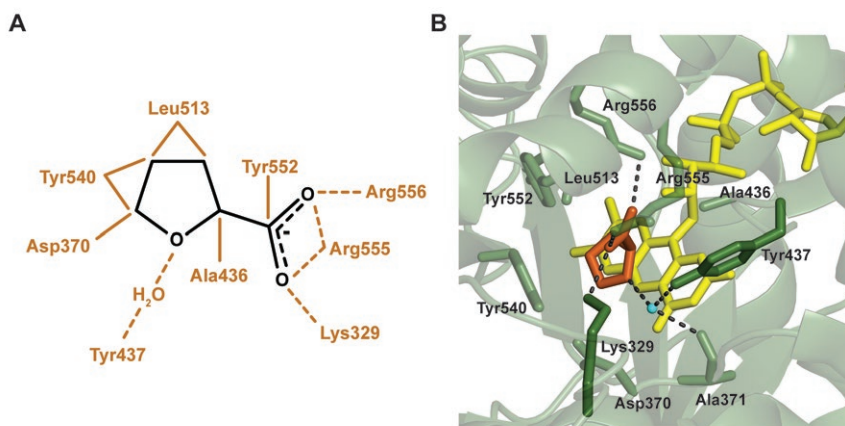


Figure 9.

Structure-based multiple sequence alignment of ProDHs from different organisms. The ProDH amino acid sequences of *T. thermophilus* (UniProt: Q72IB8, PDB: 2G37), *E. coli* (UniProt: P09546, PDB: 4O8A), Human (UniProt: Q43272) and *T. islandicus* (UniProt: A0A0U1M791) were aligned using the PROMALS3D server [128], which also uses structural information in constructing the alignment. The figure showing the alignment was made using ESPrnt 3.0 software [129]. Strictly conserved residues are shown in white on a red background and similar residues are shown in red on a white background. Black boxes indicate similarity in a group of residues. Below the sequence, conserved active site residues are indicated with a red circle.



**Figure 10.**

Binding of THFA in the active site the ProDH domain of *EcPutA*. (A) Schematic representation of the interactions between the ProDH domain of *E. coli* PutA and the proline analogue THFA. Brown solid lines indicate van der Waals interactions; brown dotted lines indicate hydrogen bonds and ion pairs. Figure based on [59]. (B) Active site of the ProDH domain of *EcPutA* (PDB: 1TIW). The active site residues are shown in green with Lys329 and Tyr437 in dark green, the FAD cofactor is shown in yellow and the proline analogue THFA is shown in orange. Hydrogen bonds are indicated by grey dotted lines. A water molecule is indicated in cyan.

### Substrate specificity of ProDHs

As expected for a central metabolic enzyme, ProDH has a restricted substrate scope. Next to L-proline, only 3,4-dehydro-L-proline becomes oxidized by ProDH [60,130]. Other proline analogues such as *trans*-4-hydroxy-L-proline, *cis*-4-hydroxy-L-proline, L-azetidine-2-carboxylic acid, and L-pipecolic acid are neither inhibitors nor substrates of ProDH [60]. However, replacing Tyr540 (Fig. 10) with Ala or Ser in *EcPutA* alters the kinetics: the catalytic efficiency for proline decreases, while the reactivity with hydroxyproline increases. Likely, Tyr540, which is a very conserved residue in the PutA/ProDH family, clashes with the 4-hydroxy moiety of hydroxyproline [131].

The Michaelis-Menten constant ( $K_M$ ) for proline has shown to be in the millimolar range for various bacterial [60,123,125] and eukaryotic [54,100] monofunctional ProDHs as well as PutAs [101,132,133]. The high specificity of ProDHs for proline accompanied by high  $K_M$  values seems to reflect the cellular situation. Due to its central role in metabolism (Fig. 5), ProDHs should have a high substrate specificity to not disturb the metabolic balance in the cell. Furthermore, a low affinity of ProDH for proline might be related to the high availability of proline in the cell and the fact that proline is, next to a metabolic compound, involved in various cellular processes (see above). In addition, it is one of the amino acids that is needed for protein synthesis.

Besides ProDH, monomeric sarcosine oxidase, a flavoprotein with a D-amino acid oxidase fold, is also active with proline. As for ProDH, this enzyme also has  $K_M$  values for proline in the millimolar range [134,135]. In contrast, L-amino acid oxidase is active with a broad range of amino acids, but not with L-proline [136].

### Competitive and mechanism-based inhibition of ProDHs

THFA, L-mandelate, L-lactate and acetate are known competitive inhibitors of ProDH [60,121,137]. THFA is often used as a substrate analogue in crystallographic studies of this enzyme. 4-methylene-L-proline is known to be a mechanism-based inhibitor [138]. In addition, ProDH can be irreversibly inactivated by the suicide inhibitor *N*-propargylglycine (Fig. 11). This inhibition has been studied in detail for *Tt*ProDH and the ProDH domain of *Ec*PutA [139,140]. Inactivation involves the initial oxidation of *N*-propargylglycine to *N*-propargyliminoglycine and the subsequent formation of a bicovalent linkage between flavin N(5) and the  $\epsilon$ -amino group of a lysine in the  $\beta 2$ - $\alpha 2$  loop [139,140] (Fig. 11). This lysine (Lys99 in *Tt*ProDH and Lys239 in *Ec*PutA) is involved in binding the carboxylic moiety of proline [60] (Fig. 11). Upon reaction with *N*-propargylglycine, the FAD cofactor of ProDH is reduced and the enzyme is locked in the reduced state [139,140].

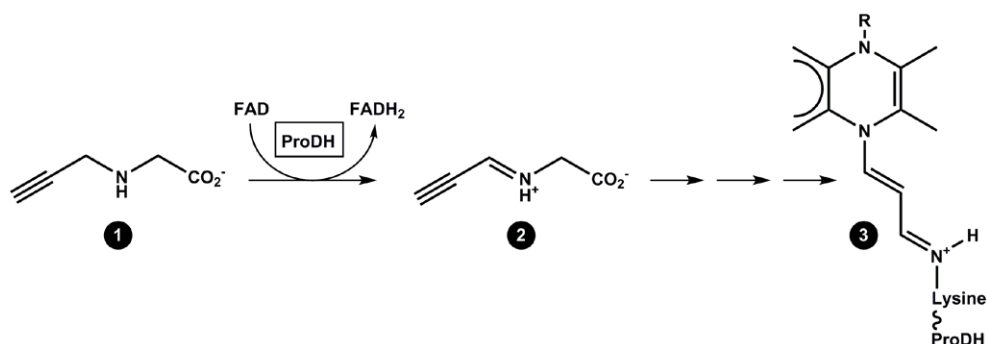


**Figure 11.**

Irreversible mechanism-based inhibition of ProDH by *N*-propargylglycine. Upon reaction of *N*-propargylglycine (1), *N*-propargyliminoglycine (2) is formed and the FAD-cofactor of ProDH is reduced. Subsequently, a covalent Lys-FAD adduct (3) is formed.

### Conformational changes upon substrate binding to ProDHs

The structure of the ligand-free ProDH is suggested to be open, while the presence of the substrate or an inhibitor in the active site leads to a more closed structure. This is nicely shown for *Dr*ProDH, for which crystal structures of the free reduced enzyme as well as the inhibitor-bound oxidized enzyme have been solved [123]. These structures show indeed that the structure of the reduced, ligand-free enzyme is open with the flavin highly solvent exposed. The crystal structure of the enzyme in the presence of THFA shows a more closed



conformation, in which the THFA is completely buried between the *si* face of the FAD and helix  $\alpha 8$  [123]. This closed structure is also seen for the inhibitor-bound ProDH domain of *EcPutA* [120,141], while *TtProDH* without inhibitor shows an active site that is more open [60]. This implies that the active site closes upon substrate binding and opens to allow product release.

Closing/opening of the active site is associated with two major conformational changes in the region of the proline-binding pocket. First, helix  $\alpha 8$  can move away from the proline-binding pocket in the absence of a ligand, as shown for *TtProDH* [121]. When FAD is reduced, helix  $\alpha 8$  can shift even more outward, as shown for *DrProDH* [123]. This suggests that inward movement of helix  $\alpha 8$  towards the proline-binding pocket is important for substrate binding. Helix  $\alpha 8$  contributes three amino acid residues (Tyr-x-x-Arg-Arg) that bind the carboxylic group of the substrate analogue THFA [120,121]. The fact that acetate is a competitive inhibitor of ProDH suggests the carboxylic group to be the minimal functional group that is recognized by the active site [121].

Another conformational change that plays a role in substrate binding is movement of the  $\beta 1$ - $\alpha 1$  loop. A conserved Glu-Arg ion pair between the  $\beta 1$ - $\alpha 1$  loop and helix  $\alpha 8$  assists in stabilizing the active site of the enzyme-substrate complex [120,121]. When there is no ligand present in the active site, the  $\beta 1$ - $\alpha 1$  loop withdraws from the active site, leading the Glu to flip out and point into the solvent [60]. Also, reduction of the FAD leads to a rupture of this ion pair by an outwards movement of this loop [123]. Therefore, the  $\beta 1$ - $\alpha 1$  loop seems to stabilize the active site of the enzyme-substrate complex and its movement is suggested to create a gate for substrate access and product release that is universal in ProDH catalysis [101,111,123].

### ***Thermus thermophilus* ProDH**

*Thermus thermophilus* is a thermophilic gram-negative bacterium originally isolated from a hot spring in Mine, Shizuoka Prefecture, Japan in 1968 [142]. Its optimal growth temperature is between 65 and 72 °C. The genome sequence of *T. thermophilus* was reported in 2004 [143]. This thermophilic organism serves as a biological model and its thermostable enzymes have widespread biotechnological applications [144].

*Thermus thermophilus* proline dehydrogenase (*TtProDH*) is also thermostable [60]. The structure of this enzyme has been elucidated (PDB: 2G37) [60,145]. It adopts the conserved and characteristic distorted ( $\beta\alpha$ )<sub>8</sub> TIM-barrel fold typical for ProDHs [60] (Fig. 12). The additional helix  $\alpha 0$ , typical for ProDHs, is clearly present. The FAD-cofactor in the three-dimensional model of the crystal structure of *TtProDH* is highly solvent-exposed. Since no inhibitor is present in the structure of *TtProDH*, helix  $\alpha 8$  has moved outwards about 4 Å [60]. Furthermore, the enzyme is dimeric in the three-dimensional model of the crystal structure, with helix  $\alpha 5$  being the suggested dimerization interface in this model. Next to the distorted



TIM-barrel, the enzyme contains an N-terminal arm that consists of three helices:  $\alpha A$ ,  $\alpha B$  and  $\alpha C$ . The C-terminal helix  $\alpha 8$  fits into the cleft that is formed by the three N-terminal helices. Together, these four helices form a hydrophobic patch that is thought to be involved in channeling P5C/GSA between *Tt*ProDH and its partner enzyme *Tt*P5CDH [60,119].

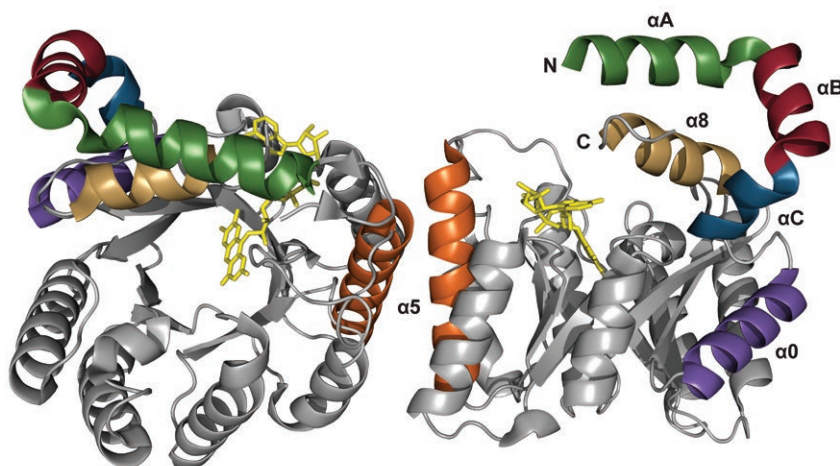


**Figure 12.**

Three-dimensional model of the crystal structure of *Tt*ProDH (PDB: 2G37). The N-terminal helices  $\alpha A$  (green),  $\alpha B$  (red),  $\alpha C$  (blue) and  $\alpha 0$  (purple) are indicated, as well as the helix  $\alpha 5$  (orange) in the dimerization interface and C-terminal helix  $\alpha 8$  (brown). The FAD cofactor is depicted in yellow.

## Scope and outline of this thesis

This project was started as part of the European Research Area Industrial Biotechnology (ERA-IB) project “Multi Enzyme Systems Involved in Astin Biosynthesis and their use in heterologous astin production (MESIAB)”. The goal of this project was to identify gene clusters involved in astin production. Astins are cyclic halogenated pentapeptides isolated from the roots of the plant *Aster tataricus*. They contain the unusual amino acids  $\beta$ -phenylalanine ( $\beta$ Phe), 2-aminobutyric acid (2Abu) and 3,4-dichloroproline (Pro( $Cl_2$ )), resulting in cyclic chlorinated pentapeptide cyclo[Ser- $\beta$ Phe-2Abu-Pro( $Cl_2$ )-2Abu] [146,147] (Fig. 13).

Root extracts of *Aster tataricus* show antibacterial activity and astin derivatives possess a high anti-tumor potential. Since only very low amounts of astins can be isolated from plants and they are difficult to synthesize chemically without negative impacts on the environment, the goal of this project was to produce astin in a heterologous host and establish its biosynthetic pathway. The presence of astins in dried roots and, for the first time, in the roots of freshly grown *A. tataricus* plants could be shown. However, a newly discovered fungus isolated from the inflorescence axis of *A. tataricus*, turned out to be the actual producer of astins [148]. In addition, the production of the hepatotoxic and carcinogenic peptide cyclochlorotine by

the fungus *Talaromyces islandicus* could be demonstrated. Astins and cyclochlorotine are very similar in their chemical structure: the only difference is the replacement of one of the 2-aminobutyrate in astins by a serine in cyclochlorotine (Fig. 13). Therefore, it can be assumed that the pathways and enzymes involved in their biosynthesis are very similar. Since the biosynthetic pathway of cyclochlorotine was also not known, it was decided to sequence the genome of *T. islandicus* to facilitate identification of the cyclochlorotine/astin biosynthetic genes [149]. After the genome sequence was elucidated, gene clusters involved in cyclochlorotine biosynthesis were analyzed [150]. This included elaborate studies on nonribosomal peptide synthetase (NRPS) gene clusters involved in production of the cyclic pentapeptide. In addition, the genome was searched for proline dehydrogenases and halogenases putatively involved in the synthesis of 3,4-dichloroproline. We identified and cloned three putative ProDH genes from *T. islandicus* and did some minor characterization [150]. However, the involvement of ProDH in the synthesis of the dichlorinated proline building block of cyclochlorotine remained doubtful. In addition, expression and purification of these fungal ProDHs was challenging. Therefore, we simultaneously started to express and purify the enzyme from *Thermus thermophilus*. Although a crystal structure of ligand-free TtProDH has been elucidated [60] (Fig. 12), relatively little is known about the biochemical properties of this enzyme.

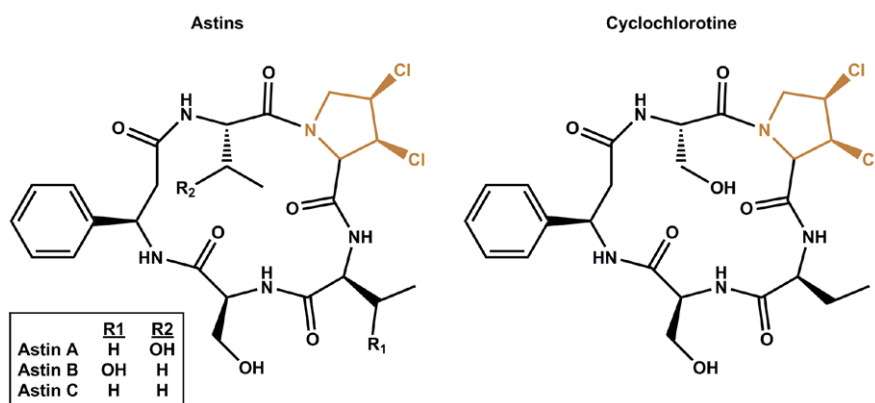


Figure 13.

Chemical structures of astins and cyclochlorotine. Both metabolites are composed of the nonproteinogenic amino acids L-2-aminobutyrate (2Abu), L- $\beta$ -phenylalanine ( $\beta$ Phe), the unique L-cis-3,4-dichloroproline [ $\text{Pro}(\text{Cl}_2)$ ] and L-serine (Ser), which results in the cyclic chlorinated pentapeptides cyclo[Ser- $\beta$ Phe-Ser- $\text{Pro}(\text{Cl}_2)$ -2Abu] and cyclo[Ser- $\beta$ Phe-Ser- $\text{Pro}(\text{Cl}_2)$ -2Abu], respectively. The dichlorinated proline is shown in brown.

This thesis deals with the engineering of TtProDH in order to gain more insight into the structure-function relationship of this thermo-resistant flavoenzyme. For *in vitro* studies, substantial amounts of highly pure enzyme are required. **Chapter 2** describes the production and purification of TtProDH. Using maltose-binding protein (MBP) as solubility tag, high

yields of holoenzyme were obtained. The MBP-tag can be efficiently removed from the fusion protein with trypsin. The thus obtained native enzyme is stable at high temperatures and tolerant against organic solvents, but forms undesirable soluble aggregates. The hydrophobic N-terminal helix  $\alpha A$  of *Tt*ProDH is responsible for this self-association, as we describe in **Chapter 3**. After replacing the hydrophobic surface residues Phe10 and Leu12 by glutamates, MBP-*Tt*ProDH almost exclusively forms tetramers. This variant, EE, is an excellent catalyst, but selective removal of the MBP-tag is difficult. Therefore, in subsequent studies we used MBP-tagged enzymes.

To gain more insight into the functionality of the N-terminal arm of *Tt*ProDH, we created N-terminally truncated variants that are described in **Chapter 4**. These variants, lacking respectively one ( $\Delta A$ ), two ( $\Delta AB$ ), or three ( $\Delta ABC$ ) N-terminal helices show that helix  $\alpha A$  and  $\alpha B$  are not important for *in vitro* activity, while  $\alpha C$  has a crucial role in the activity of the enzyme. Additional enzyme variants show in more detail that disrupting interactions between helix  $\alpha C$  and  $\alpha 8$  impairs ProDH activity. This suggests that helix  $\alpha C$  controls the location and flexibility of helix  $\alpha 8$ , the latter being crucial for substrate recognition. In addition, helix  $\alpha C$  is involved in tetramerization of *Tt*ProDH.

To investigate the quaternary structure in more detail, the dimerization interface of the enzyme was studied in **Chapter 5**. Disrupting ionic interactions at the dimeric interface yields monomeric protein. This monomeric form is fully active but has a lowered thermostability.

Next to knowledge about the function of several  $\alpha$ -helices, we also gained insight into cofactor binding of *Tt*ProDH. In **Chapter 6**, the production of *Tt*ProDH apoprotein is described. Binding studies revealed that *Tt*ProDH binds FMN and FAD with equal rates and affinities. We also established that ProDH overproduced in *E. coli* contains significant amounts of FMN. Therefore, classification of *Tt*ProDH as an FAD-binding enzyme should be reconsidered.

Finally, the novel findings of this thesis and future perspectives are in **Chapter 7**.

## References

- [1] Goodsell, D. S., Inside a living cell. *Trends Biochem. Sci.* (1991), 16, 203-206.
- [2] Milo, R. and Philips, R., Cell biology by the numbers, Garland Science, 2015.
- [3] Joosten, V. and van Berkel, W. J. H., Flavoenzymes. *Curr. Opin. Chem. Biol.* (2007), 11, 195-202.
- [4] Walsh, C. T. and Wencewicz, T. A., Flavoenzymes: versatile catalysts in biosynthetic pathways. *Nat. Prod. Rep.* (2012), 30, 175-200.
- [5] Macheroux, P., Kappes, B., Ealick, S. E., Flavogenomics - a genomic and structural view of flavin-dependent proteins. *Febs Journal* (2011), 278, 2625-2634.
- [6] Lienhart, W. D., Gudipati, V., Macheroux, P., The human flavoproteome. *Arch. Biochem. Biophys.* (2013), 535, 150-162.
- [7] Santos, M. A., Jiménez, A., Revuelta, J. L., Molecular characterization of *FMN1*, the structural gene for the monofunctional flavokinase of *Saccharomyces cerevisiae*. *J. Biol. Chem.* (2000), 275, 28618-28624.
- [8] Wu, M., Repetto, B., Glerum, D. M., Tzagoloff, A., Cloning and characterization of FAD1, the structural gene for flavin adenine dinucleotide synthetase of *Saccharomyces cerevisiae*. *Mol. Cell. Biol.* (1995), 15, 264-271.
- [9] Mack, M., van Loon, A. P. G. M., Hohmann, H. P., Regulation of riboflavin biosynthesis in *Bacillus subtilis* is affected by the activity of the flavokinase/flavin adenine dinucleotide synthetase encoded by *ribC*. *J. Bacteriol.* (1998), 180, 950-955.
- [10] Manstein, D. J. and Pai, E. F., Purification and characterization of FAD synthetase from *Brevibacterium ammoniagenes*. *J. Biol. Chem.* (1986), 261, 16169-16173.
- [11] Serrano, A., Ferreira, P., Martínez-Júlvez, M., Medina, M., The prokaryotic FAD synthetase family: a potential drug target. *Curr. Pharm. Des.* (2013), 19, 2637-2648.
- [12] de Gonzalo, G., Smit, C., Jin, J., Minnaard, A. J., Fraaije, M. W., Turning a riboflavin-binding protein into a self-sufficient monooxygenase by cofactor redesign. *Chem. Commun.* (2011), 47, 11050-11052.
- [13] Huijbers, M. M. E., Montersino, S., Westphal, A. H., Tischler, D., van Berkel, W. J. H., Flavin dependent monooxygenases. *Arch. Biochem. Biophys.* (2014), 544, 2-17.
- [14] Banner, D. W., Bloomer, A. C., Petsko, G. A. *et al.*, Structure of chicken muscle triose phosphate isomerase determined crystallographically at 2.5 Å resolution: using amino acid sequence data. *Nature* (1975), 255, 609-614.
- [15] Hegyi, H. and Gerstein, M., The relationship between protein structure and function: a comprehensive survey with application to the yeast genome. *J. Mol. Biol.* (1999), 288, 147-164.
- [16] Wierenga, R. K., The TIM-barrel fold: a versatile framework for efficient enzymes. *FEBS Lett.* (2001), 492, 193-198.
- [17] Nagano, N., Hutchinson, E. G., Thornton, J. M., Barrel structures in proteins: automatic identification and classification including a sequence analysis of TIM barrels. *Protein Sci.* (1999), 8, 2072-2084.
- [18] Webb, E. C., Enzyme nomenclature 1992: recommendations of the Nomenclature Committee of the International Union of Biochemistry and Molecular Biology on the nomenclature and classification of enzymes, Academic Press, New York, 1992.
- [19] Nagano, N., Orengo, C. A., Thornton, J. M., One fold with many functions: the evolutionary relationships between TIM barrel families based on their sequences, structures and functions. *J. Mol. Biol.* (2002), 321, 741-765.
- [20] Wierenga, R. K., Kapetaniou, E. G., Venkatesan, R., Triosephosphate isomerase: a highly evolved biocatalyst. *Cell. Mol. Life Sci.* (2010), 67, 3961-3982.
- [21] Urfer, R. and Kirschner, K., The importance of surface loops for stabilizing an eightfold beta alpha barrel protein. *Protein Sci.* (1992), 1, 31-45.
- [22] Noble, M. E. M., Verlinde, C. L. M. J., Groendijk, H. *et al.*, Crystallographic and molecular modeling studies on trypanosomal triosephosphate isomerase: a critical assessment of the predicted and observed structures of the complex with 2-phosphoglycerate. *J. Med. Chem.* (1991), 34, 2709-2718.
- [23] Deber, C. M., Brodsky, B., Rath, A., Proline residues in proteins, eLS, John Wiley & Sons, Ltd, 2001.

- [24] Chang, W. C., Guo, Y., Wang, C. *et al.*, Mechanism of the C5 stereoinversion reaction in the biosynthesis of carbapenem antibiotics. *Science* (2014), 343, 1140-1144.
- [25] Li, C., Roege, K. E., Kelly, W. L., Analysis of the indanomycin biosynthetic gene cluster from *Streptomyces antibioticus* NRRL 8167. *ChemBioChem* (2009), 10, 1064-1072.
- [26] Méjean, A., Mann, S., Maldiney, T. *et al.*, Evidence that biosynthesis of the neurotoxic alkaloids anatoxin-a and homoanatoxin-a in the cyanobacterium *oscillatoria* PCC 6506 occurs on a modular polyketide synthase initiated by L-proline. *J. Am. Chem. Soc.* (2009), 131, 7512-7513.
- [27] Thomas, M. G., Burkart, M. D., Walsh, C. T., Conversion of L-proline to pyrrolyl-2-carboxyl-S-PCP during undecylprodigiosin and pyoluteorin biosynthesis. *Chem. Biol.* (2002), 9, 171-184.
- [28] Xu, H. M., Yi, H., Zhou, W. B. *et al.*, Tataricins A and B, two novel cyclotetrapeptides from *Aster tataricus*, and their absolute configuration assignment. *Tetrahedron Lett.* (2013), 54, 1380-1383.
- [29] Phang, J. M., The regulatory functions of proline and pyrroline-5-carboxylic acid. *Curr. Top. Cell. Regul.* (1985), 25, 91-132.
- [30] Phang, J. M., Pandhare, J., Liu, Y. M., The metabolism of proline as microenvironmental stress substrate. *J. Nutr.* (2008), 138, 2008S-2015S.
- [31] Phang, J. M., Donald, S. P., Pandhare, J., Liu, Y., The metabolism of proline, a stress substrate, modulates carcinogenic pathways. *Amino Acids* (2008), 35, 681-690.
- [32] Liang, X. W., Zhang, L., Natarajan, S. K., Becker, D. F., Proline mechanisms of stress survival. *Antioxid. Redox Sign.* (2013), 19, 998-1011.
- [33] Phang, J. M., Liu, W., Zabinryk, O., Proline metabolism and microenvironmental stress, *Annu. Rev. Nutr.* Vol. 30, 2010, 441-463.
- [34] Krishnan, N., Dickman, M. B., Becker, D. F., Proline modulates the intracellular redox environment and protects mammalian cells against oxidative stress. *Free Radic. Biol. Med.* (2008), 44, 671-681.
- [35] Chen, C. B. and Dickman, M. B., Proline suppresses apoptosis in the fungal pathogen *Colletotrichum trifolii*. *Proc. Natl. Acad. Sci. USA* (2005), 102, 3459-3464.
- [36] Chen, C. B., Wanduragala, S., Becker, D. F., Dickman, M. B., Tomato QM-like protein protects *Saccharomyces cerevisiae* cells against oxidative stress by regulating intracellular proline levels. *Appl. Environ. Microbiol.* (2006), 72, 4001-4006.
- [37] Kishor, P. B. K., Sangam, S., Amrutha, R. N. *et al.*, Regulation of proline biosynthesis, degradation, uptake and transport in higher plants: its implications in plant growth and abiotic stress tolerance. *Curr. Sci.* (2005), 88, 424-438.
- [38] Szabados, L. and Savouré, A., Proline: a multifunctional amino acid. *Trends Plant Sci.* (2009), 15, 89-97.
- [39] Verbruggen, N. and Hermans, C., Proline accumulation in plants: a review. *Amino Acids* (2008), 35, 753-759.
- [40] Hare, P. D. and Cress, W. A., Metabolic implications of stress-induced proline accumulation in plants. *Plant Growth Regul.* (1997), 21, 79-102.
- [41] Qamar, A., Mysore, K. S., Senthil-Kumar, M., Role of proline and pyrroline-5-carboxylate metabolism in plant defense against invading pathogens. *Front. Plant Sci.* (2015), 6, 503.
- [42] Mattioli, R., Costantino, P., Trovato, M., Proline accumulation in plants: not only stress. *Plant Signal. Behav.* (2009), 4, 1016-1018.
- [43] Nagata, K., Nagata, Y., Sato, T. *et al.*, L-Serine, D- and L-proline and alanine as respiratory substrates of *Helicobacter pylori*: correlation between *in vitro* and *in vivo* amino acid levels. *Microbiol. Rev.* (2003), 149, 2023-2030.
- [44] Nakajima, K., Inatsu, S., Mizote, T. *et al.*, Possible involvement of *put A* gene in *Helicobacter pylori* colonization in the stomach and motility. *Biomed. Res.* (2008), 29, 9-18.
- [45] Bringaud, F., Rivi re, L., Coustou, V., Energy metabolism of trypanosomatids: adaptation to available carbon sources. *Mol. Biochem. Parasitol.* (2006), 149, 1-9.
- [46] Lamour, N., Rivi re, L., Coustou, V. *et al.*, Proline metabolism in procyclic *Trypanosoma brucei* is down-regulated in the presence of glucose. *J. Biol. Chem.* (2005), 280, 11902-11910.
- [47] Paes, L. S., Mantilla, B. S., Zimbres, F. M. *et al.*, Proline dehydrogenase regulates redox state and respiratory


- metabolism in *Trypanosoma cruzi*. *PLoS ONE* (2013), 8, e69419. doi:69410.61371/journal.pone.0069419.
- [48] Bursell, E., Aspects of the metabolism of amino acids in the tsetse fly, *Glossina* (Diptera). *J. Insect Physiol.* (1963), 9, 439-452.
- [49] Bursell, E., Substrates of oxidative metabolism in dipteran flight muscle. *Comp. Biochem. Physiol. B* (1975), 52, 235-238.
- [50] Scaraffia, P. Y. and Wells, M. A., Proline can be utilized as an energy substrate during flight of *Aedes aegypti* females. *J. Insect Physiol.* (2003), 49, 591-601.
- [51] Teulier, L., Weber, J., Crevier, J., Darveau, C., Proline as a fuel for insect flight: enhancing carbohydrate oxidation in hymenopterans. *Proc. R. Soc. B* (2016), 283.
- [52] Micheu, S., Crailsheim, K., Leonhard, B., Importance of proline and other amino acids during honeybee flight *Amino Acids* (2000), 18, 157-175.
- [53] Adams, E. and Frank, L., Metabolism of proline and the hydroxyprolines. *Annu. Rev. Biochem.* (1980), 49, 1005-1061.
- [54] Wanduragala, S., Sanyal, N., Liang, X. W., Becker, D. F., Purification and characterization of Put1p from *Saccharomyces cerevisiae*. *Arch. Biochem. Biophys.* (2010), 498, 136-142.
- [55] Moxley, M. A., Tanner, J. J., Becker, D. F., Steady-state kinetic mechanism of the proline:ubiquinone oxidoreductase activity of proline utilization A (PutA) from *Escherichia coli*. *Arch. Biochem. Biophys.* (2011), 516, 113-120.
- [56] Schertl, P. and Braun, H., Respiratory electron transfer pathways in plant mitochondria. *Front. Plant Sci.* (2014), 5.
- [57] Bearne, S. L. and Wolfenden, R., Glutamate  $\gamma$ -semialdehyde as a natural transition state analog inhibitor of *Escherichia coli* glucosamine-6-phosphate synthase. *Biochemistry* (1995), 34, 11515-11520.
- [58] Lewis, M. L., Rowe, C. J., Sewald, N. *et al.*, The effect of pH on the solution structure of  $\delta^1$ -pyrroline-2-carboxylic acid as revealed by NMR and electrospray mass spectroscopy. *Bioorg. Med. Chem. Lett.* (1993), 3, 1193-1196.
- [59] Tanner, J. J., Structural biology of proline catabolism. *Amino Acids* (2008), 35, 719-730.
- [60] White, T. A., Krishnan, N., Becker, D. F., Tanner, J. J., Structure and kinetics of monofunctional proline dehydrogenase from *Thermus thermophilus*. *J. Biol. Chem.* (2007), 282, 14316-14327.
- [61] Hu, C. A., Delauney, A. J., Verma, D. P. S., A bifunctional enzyme ( $\Delta^1$ -pyrroline-5-carboxylate synthetase) catalyzes the first two steps in proline biosynthesis in plants. *Proc. Natl. Acad. Sci. USA* (1992), 89, 9354-9358.
- [62] Savouré, A., Jaoua, S., Hua, X. *et al.*, Isolation, characterization, and chromosomal location of a gene encoding the  $\Delta^1$ -pyrroline-5-carboxylate synthetase in *Arabidopsis thaliana*. *FEBS Lett.* (1995), 372, 13-19.
- [63] Hagedorn, C. H. and Phang, J. M., Catalytic transfer of hydride ions from NADPH to oxygen by the interconversions of proline and  $\Delta^1$ -pyrroline-5-carboxylate. *Arch. Biochem. Biophys.* (1986), 248, 166-174.
- [64] Pandhare, J., Cooper, S. K., Donald, S. P., Phang, J. M., Regulation and function of proline oxidase under nutrient stress. *J. Cell. Biochem.* (2009), 107, 759-768.
- [65] Liu, W. and Phang, J. M., Proline dehydrogenase (oxidase) in cancer. *Biofactors* (2012), 38, 398-406.
- [66] Phang, J. M., Hu, C. A., Valle, D., Disorders of proline and hydroxyproline metabolism, *Metabolic and Molecular Bases of Inherited Disease*, McGraw-Hill, 2001, 1821-1838.
- [67] Scambler, P. J., The 22q11 deletion syndromes. *Hum. Mol. Genet.* (2000), 9, 2421-2426.
- [68] Kobrynski, L. J. and Sullivan, K. E., Velocardiofacial syndrome, DiGeorge syndrome: the chromosome 22q11.2 deletion syndromes. *Lancet* (2007), 370, 1443-1452.
- [69] Murphy, K. C., Schizophrenia and velo-cardio-facial syndrome. *Lancet* (2002), 359, 426-430.
- [70] Hu, C. A., Williams, D. B., Zhaorigetu, S. *et al.*, Functional genomics and SNP analysis of human genes encoding proline metabolic enzymes. *Amino Acids* (2008), 35, 655-664.
- [71] Mitsubuchi, H., Nakamura, K., Matsumoto, S., Endo, F., Inborn errors of proline metabolism. *J. Nutr.* (2008), 138, 2016S-2020S.
- [72] Jacquet, H., Raux, G., Thibaut, F. *et al.*, PRODH mutations and hyperprolinemia in a subset of schizophrenic patients. *Hum. Mol. Genet.* (2002), 11, 2243-2249.



- [73] Willis, A., Bender, H. U., Steel, G., Valle, D., PRODH variants and risk for schizophrenia. *Amino Acids* (2008), 35, 673-679.
- [74] Bender, H. U., Almashanu, S., Steel, G. *et al.*, Functional consequences of PRODH missense mutations. *Am. J. Hum. Genet.* (2005), 76, 409-420.
- [75] Jacquet, H., Demily, C., Houy, E. *et al.*, Hyperprolinemia is a risk factor for schizoaffective disorder. *Mol. Psychiatry* (2004), 10, 479-485.
- [76] Liu, H., Abecasis, G. R., Heath, S. C. *et al.*, Genetic variation in the 22q11 locus and susceptibility to schizophrenia. *Proc. Natl. Acad. Sci. USA* (2002), 99, 16859-16864.
- [77] Liu, H., Heath, S. C., Sobin, C. *et al.*, Genetic variation at the 22q11 *PRODH2/DGCR6* locus presents an unusual pattern and increases susceptibility to schizophrenia. *Proc. Natl. Acad. Sci. USA* (2002), 99, 3717-3722.
- [78] Sriver, C. R., Schafer, I. A., Efron, M. L., New renal tubular amino-acid transport system and a new hereditary disorder of amino-acid metabolism. *Nature* (1961), 192, 672-673.
- [79] Efron, M. L., Familial hyperprolinemia. *N. Engl. J. Med.* (1965), 272, 1243-1254.
- [80] Valle, D., Goodman, S. I., Applegarth, D. A., Shih, V. E., Phang, J. M., Type II hyperprolinemia. D<sup>1</sup>-pyrroline-5-carboxylic acid dehydrogenase deficiency in cultured skin fibroblasts and circulating lymphocytes. *J. Clin. Invest.* (1976), 58, 598-603.
- [81] Raux, G., Bumsel, E., Hecketsweiler, B. *et al.*, Involvement of hyperprolinemia in cognitive and psychiatric features of the 22q11 deletion syndrome. *Hum. Mol. Genet.* (2007), 16, 83-91.
- [82] Polyak, K., Xia, Y., Zweier, J. L., Kinzler, K. W., Vogelstein, B., A model for p53-induced apoptosis. *Nature* (1997), 389, 300-305.
- [83] Donald, S. P., Sun, X. Y., Hu, C. A. A. *et al.*, Proline oxidase, encoded by p53-induced gene-6, catalyzes the generation of proline-dependent reactive oxygen species. *Cancer Res.* (2001), 61, 1810-1815.
- [84] Maxwell, S. A. and Rivera, A., Proline oxidase induces apoptosis in tumor cells, and its expression is frequently absent or reduced in renal carcinomas. *J. Biol. Chem.* (2003), 278, 9784-9789.
- [85] Liu, Y., Borchert, G. L., Surazynski, A., Hu, C. A., Phang, J. M., Proline oxidase activates both intrinsic and extrinsic pathways for apoptosis: the role of ROS/superoxides, NFAT and MEK//ERK signaling. *Oncogene* (2006), 25, 5640-5647.
- [86] Rivera, A. and Maxwell, S. A., The p53-induced gene-6 (proline oxidase) mediates apoptosis through a calcineurin-dependent pathway. *J. Biol. Chem.* (2005), 280, 29346-29354.
- [87] Pandhare, J., Cooper, S. K., Phang, J. M., Proline oxidase, a proapoptotic gene, is induced by troglitazone: evidence for both peroxisome proliferator-activated receptor  $\gamma$ -dependent and -independent mechanisms. *J. Biol. Chem.* (2006), 281, 2044-2052.
- [88] Liu, Y., Borchert, G. L., Donald, S. P. *et al.*, Proline oxidase functions as a mitochondrial tumor suppressor in human cancers. *Cancer Res.* (2009), 69, 6414-6422.
- [89] Liu, Y., Borchert, G. L., Surazynski, A., Phang, J. M., Proline oxidase, a p53-induced gene, targets COX-2/PGE2 signaling to induce apoptosis and inhibit tumor growth in colorectal cancers. *Oncogene* (2008), 27, 6729-6737.
- [90] Liu, W., Glunde, K., Bhujwalla, Z. M. *et al.*, Proline oxidase promotes tumor cell survival in hypoxic tumor microenvironments. *Cancer Res.* (2012), 72, 3677-3686.
- [91] Zabinryk, O., Liu, W., Khalil, S., Sharma, A., Phang, J. M., Oxidized low-density lipoproteins upregulate proline oxidase to initiate ROS-dependent autophagy. *Carcinogenesis* (2010), 31, 446-454.
- [92] Liu, W. and Phang, J. M., Proline dehydrogenase (oxidase), a mitochondrial tumor suppressor, and autophagy under the hypoxia microenvironment. *Autophagy* (2012), 8, 1407-1409.
- [93] Pandhare, J., Dash, S., Jones, B., Villalta, F., Dash, C., A novel role of proline oxidase in HIV-1 envelope glycoprotein induced neuronal autophagy. *J. Biol. Chem.* (2015), 290, 25439-25451.
- [94] Kawakami, R., Satomura, T., Sakuraba, H., Ohshima, T., L-proline dehydrogenases in hyperthermophilic archaea: distribution, function, structure, and application. *Appl. Microbiol. Biotechnol.* (2011), 93, 83-93.
- [95] Wang, S. S. and Brandriss, M. C., Proline utilization in *Saccharomyces cerevisiae*: sequence, regulation, and mitochondrial localization of the PUT1 gene product. *Mol. Cell. Biol.* (1987), 7, 4431-4440.

- [96] Brunner, G. and Neupert, W., Localisation of proline oxidase and  $\Delta^1$ -pyrroline-5-carboxylic acid dehydrogenase in rat liver. *FEBS Lett.* (1969), 3, 283-286.
- [97] Balboni, E. and Hecht, R. I., Studies on the inner mitochondrial membrane localization of proline dehydrogenase. *Biochim. Biophys. Acta* (1977), 462, 171-176.
- [98] Elthon, T. E. and Stewart, C. R., Submitochondrial location and electron transport characteristics of enzymes involved in proline oxidation. *Plant Physiol.* (1981), 67, 780-784.
- [99] Tanner, J. J. and Becker, D. F., PutA and proline metabolism, Handbook of flavoproteins. Volume 1 - oxidases, dehydrogenases and related systems, De Gruyter, 2012.
- [100] Tallarita, E., Pollegioni, L., Servi, S., Molla, G., Expression in *Escherichia coli* of the catalytic domain of human proline oxidase. *Protein Expr. Purif.* (2012), 82, 345-351.
- [101] Singh, H., Arentson, B. W., Becker, D. F., Tanner, J. J., Structures of the PutA peripheral membrane flavoenzyme reveal a dynamic substrate-channeling tunnel and the quinone-binding site. *Proc. Natl. Acad. Sci. USA* (2014), 111, 3389-3394.
- [102] Zhou, Y., Larson, J. D., Bottoms, C. A. *et al.*, Structural basis of the transcriptional regulation of the proline utilization regulon by multifunctional PutA. *J. Mol. Biol.* (2008), 381, 174-188.
- [103] Wood, J. M., Membrane association of proline dehydrogenase in *Escherichia coli* is redox dependent. *Proc. Natl. Acad. Sci. USA* (1987), 84, 373-377.
- [104] Ostrovsky de Spicer, P. and Maloy, S., PutA protein, a membrane-associated flavin dehydrogenase, acts as a redox-dependent transcriptional regulator. *Proc. Natl. Acad. Sci. USA* (1993), 90, 4295-4298.
- [105] Zhang, W. M., Zhang, M., Zhu, W. D. *et al.*, Redox-induced changes in flavin structure and roles of flavin N(5) and the ribityl 2'-OH group in regulating PutA-membrane binding. *Biochemistry* (2007), 46, 483-491.
- [106] Brown, E. D. and Wood, J. M., Conformational change and membrane association of the PutA protein are coincident with reduction of its FAD cofactor by proline. *J. Biol. Chem.* (1993), 268, 8972-8979.
- [107] Zhang, W. M., Zhou, Y., Becker, D. F., Regulation of PutA-membrane associations by FAD reduction. *Biochemistry* (2004), 43, 13165-13174.
- [108] Surber, M. W. and Maloy, S., Regulation of flavin dehydrogenase compartmentalization: requirements for PutA-membrane association in *Salmonella typhimurium*. *Biochim. Biophys. Acta* (1999), 1421, 5-18.
- [109] Ovádi, J., Physiological significance of metabolic channelling. *J. Theor. Biol.* (1991), 152, 1-22.
- [110] Arentson, B. W., Luo, M., Pemberton, T. A., Tanner, J. J., Becker, D. F., Kinetic and structural characterization of tunnel-perturbing mutants in *Bradyrhizobium japonicum* proline utilization A. *Biochemistry* (2014), 53, 5150-5161.
- [111] Srivastava, D., Schuermann, J. P., White, T. A. *et al.*, Crystal structure of the bifunctional proline utilization A flavoenzyme from *Bradyrhizobium japonicum*. *Proc. Natl. Acad. Sci. USA* (2010), 107, 2878-2883.
- [112] Moxley, M. A., Sanyal, N., Krishnan, N., Tanner, J. J., Becker, D. F., Evidence for hysteretic substrate channeling in the proline dehydrogenase and  $\Delta^1$ -pyrroline-5-carboxylate dehydrogenase coupled reaction of proline utilization A (PutA). *J. Biol. Chem.* (2014), 289, 3639-3651.
- [113] Surber, M. W. and Maloy, S., The PutA protein of *Salmonella typhimurium* catalyzes the two steps of proline degradation via a leaky channel. *Arch. Biochem. Biophys.* (1998), 354, 281-287.
- [114] Arentson, B. W., Sanyal, N., Becker, D. F., Substrate channeling in proline metabolism. *Front. Biosci. (Landmark Ed.)* (2012), 17, 375-388.
- [115] Bearne, S. L., Hekmat, O., Macdonnell, J. E., Inhibition of *Escherichia coli* CTP synthase by glutamate gamma-semialdehyde and the role of the allosteric effector GTP in glutamine hydrolysis. *Biochem. J.* (2001), 356, 223-232.
- [116] Thoden, J. B., Huang, X., Raushel, F. M., Holden, H. M., The small subunit of carbamoyl phosphate synthetase: snapshots along the reaction pathway. *Biochemistry* (1999), 38, 16158-16166.
- [117] Farrant, R. D., Walker, V., Mills, G. A., Mellor, J. M., Langley, G. J., Pyridoxal phosphate de-activation by pyrroline-5-carboxylic acid. Increased risk of vitamin B-6 deficiency and seizures in hyperprolinemia type II. *J. Biol. Chem.* (2001), 276, 15107-15116.
- [118] Marcotte, E. M., Pellegrini, M., Ng, H. L. *et al.*, Detecting protein function and protein-protein interactions from genome sequences. *Science* (1999), 285, 751-753.

- [119] Sanyal, N., Arentson, B. W., Luo, M., Tanner, J. J., Becker, D. F., First evidence for substrate channeling between proline catabolic enzymes: a validation of domain fusion analysis for predicting protein-protein interactions. *J. Biol. Chem.* (2015), 290, 2225-2234.
- [120] Lee, Y. H., Nadaraja, S., Gu, D., Becker, D. F., Tanner, J. J., Structure of the proline dehydrogenase domain of the multifunctional PutA flavoprotein. *Nat. Struct. Biol.* (2003), 10, 109-114.
- [121] Zhang, M., White, T. A., Schuermann, J. P. *et al.*, Structures of the *Escherichia coli* PutA proline dehydrogenase domain in complex with competitive inhibitors. *Biochemistry* (2004), 43, 12539-12548.
- [122] Guenther, B. D., Sheppard, C. A., Tran, P. *et al.*, The structure and properties of methylenetetrahydrofolate reductase from *Escherichia coli* suggest how folate ameliorates human hyperhomocysteinemia. *Nat. Struct. Biol.* (1999), 6, 359-365.
- [123] Luo, M., Arentson, B. W., Srivastava, D., Becker, D. F., Tanner, J. J., Crystal structures and kinetics of monofunctional proline dehydrogenase provide insight into substrate recognition and conformational changes associated with flavin reduction and product release. *Biochemistry* (2012), 51, 10099-10108.
- [124] Fraaije, M. W. and Mattevi, A., Flavoenzymes: diverse catalysts with recurrent features. *Trends Biochem. Sci.* (2000), 25, 126-132.
- [125] Serrano, H. and Blanchard, J. S., Kinetic and isotopic characterization of L-proline dehydrogenase from *Mycobacterium tuberculosis*. *Biochemistry* (2013), 52, 5009-5015.
- [126] Kurtz, K. A., Rishavy, M. A., Cleland, W. W., Fitzpatrick, P. F., Nitrogen isotope effects as probes of the mechanism of D-amino acid oxidase. *J. Am. Chem. Soc.* (2000), 122, 12896-12897.
- [127] Umhau, S., Pollegioni, L., Molla, G. *et al.*, The x-ray structure of D-amino acid oxidase at very high resolution identifies the chemical mechanism of flavin-dependent substrate dehydrogenation. *Proc. Natl. Acad. Sci. USA* (2000), 97, 12463-12468.
- [128] Pei, J., Kim, B. H., Grishin, N. V., PROMALS3D: a tool for multiple protein sequence and structure alignments. *Nucl. Acids Res.* (2008), 36, 2295-2300.
- [129] Robert, X. and Gouet, P., Deciphering key features in protein structures with the new ENDscript server. *Nucl. Acids Res.* (2014), 42, W320-W324.
- [130] Wood, J. M., Genetics of L-proline utilization in *Escherichia coli*. *J. Bacteriol.* (1981), 146, 895-901.
- [131] Ostrander, E. L., Larson, J. D., Schuermann, J. P., Tanner, J. J., A conserved active site tyrosine residue of proline dehydrogenase helps enforce the preference for proline over hydroxyproline as the substrate. *Biochemistry* (2009), 48, 951-959.
- [132] Vinod, M. P., Bellur, P., Becker, D. F., Electrochemical and functional characterization of the proline dehydrogenase domain of the PutA flavoprotein from *Escherichia coli*. *Biochemistry* (2002), 41, 6525-6532.
- [133] Krishnan, N. and Becker, D. F., Oxygen reactivity of PutA from *Helicobacter* species and proline-linked oxidative stress. *J. Bacteriol.* (2006), 188, 1227-1235.
- [134] Zhao, G. and Jorns, M., Ionization of zwitterionic amine substrates bound to monomeric sarcosine oxidase. *Biochemistry* (2005), 44, 16866-16874.
- [135] Zhao, G. and Jorns, M., Monomeric sarcosine oxidase: evidence for an ionizable group in the E-S complex. *Biochemistry* (2002), 41, 9747-9750.
- [136] Geueke, B. and Hummel, W., A new bacterial L-amino acid oxidase with a broad substrate specificity: purification and characterization. *Enzyme Microb. Technol.* (2002), 31, 77-87.
- [137] Zhu, W. D., Gincher, Y., Docherty, P., Spilling, C. D., Becker, D. F., Effects of proline analog binding on the spectroscopic and redox properties of PutA. *Arch. Biochem. Biophys.* (2002), 408, 131-136.
- [138] Tritsch, D., Mawlawi, H., Biellmann, J. F., Mechanism-based inhibition of proline dehydrogenase by proline analogs. *Biochim. Biophys. Acta* (1993), 1202, 77-81.
- [139] Srivastava, D., Zhu, W., Johnson Jr., W. H. *et al.*, The structure of the proline utilization A proline dehydrogenase domain inactivated by N-propargylglycine provides insight into conformational changes induced by substrate binding and flavin reduction. *Biochemistry* (2010), 49, 560-569.
- [140] White, T. A., Johnson Jr., W. H., Whitman, C. P., Tanner, J. J., Structural basis for the inactivation of *Thermus thermophilus* proline dehydrogenase by N-propargylglycine. *Biochemistry* (2008), 47, 5573-5580.

- 
- [141] Srivastava, D., Zhu, W., Johnson, W. H., Jr. *et al.*, The structure of the proline utilization A proline dehydrogenase domain inactivated by N-propargylglycine provides insight into conformational changes induced by substrate binding and flavin reduction. *Biochemistry* (2010), 49, 560-569.
- [142] Oshima, T. and Imahori, K., Description of *Thermus thermophilus* (Yoshida and Oshima) comb. nov., a nonsporulating thermophilic bacterium from a Japanese thermal spa. *Int. J. Syst. Evol. Microbiol.* (1974), 24, 102-112.
- [143] Henne, A., Bruggemann, H., Raasch, C. *et al.*, The genome sequence of the extreme thermophile *Thermus thermophilus*. *Nat. Biotech.* (2004), 22, 547-553.
- [144] Cava, F., Hidalgo, A., Berenguer, J., *Thermus thermophilus* as biological model. *Extremophiles* (2009), 13, 213-231.
- [145] White, T. A. and Tanner, J. J., Cloning, purification and crystallization of *Thermus thermophilus* proline dehydrogenase. *Acta Crystallogr. F Struct. Biol. Cryst. Commun.* (2005), 61, 737-739.
- [146] Kosemura, S., Ogawa, T., Totsuka, K., Isolation and structure of asterin, a new halogenated cyclic pentapeptide from *Aster tataricus*. *Tetrahedron Lett.* (1993), 34, 1291-1294.
- [147] Morita, H., Nagashima, S., Takeya, K., Itokawa, H., Astins A and B, antitumor cyclic pentapeptides from *Aster tataricus*. *Chem. Pharm. Bull. (Tokyo)* (1993), 41, 992-993.
- [148] Jahn, L., Schafhauser, T., Pan, S. *et al.*, A new ostropalean fungus (*Villosirosea asteris* gen. nov., sp. nov.) from the inflorescence axis of *Aster tataricus*. *Submitted*.
- [149] Schafhauser, T., Wibberg, D., Rückert, C. *et al.*, Draft genome sequence of *Talaromyces islandicus* ("*Penicillium islandicum*") WF-38-12, a neglected mold with significant biotechnological potential. *J. Biotechnol.* (2015), 211, 101-102.
- [150] Schafhauser, T., Kirchner, N., Kulik, A. *et al.*, The cyclochlorotine mycotoxin is produced by the nonribosomal peptide synthetase CctN in *Talaromyces islandicus* ("*Penicillium islandicum*"). *Environ. Microbiol.* (2016).







# Chapter 2

**High yields of active *Thermus thermophilus* proline dehydrogenase are obtained using maltose-binding protein as a solubility tag**

*Biotechnology Journal (2015), 10, 395-403*

**Mieke M.E. Huijbers  
Willem J.H. van Berkel**

Laboratory of Biochemistry, Wageningen University & Research, Stippeneng 4, 6708 WE Wageningen, the Netherlands





## Abstract

Proline dehydrogenase (ProDH) catalyzes the FAD-dependent oxidation of proline to  $\Delta^1$ -pyrroline-5-carboxylate, the first step of proline catabolism in many organisms. Next to being involved in a number of physiological processes, ProDH is of interest for practical applications because the proline imino acid can serve as building block for a wide range of peptides and antibiotics. ProDH is a membrane-associated protein and recombinant soluble forms of the enzyme have only been obtained in limited amounts. We here report on the heterologous production of ProDH from *Thermus thermophilus* (*TtProDH*) in *Escherichia coli*. Using maltose-binding protein (MBP) as solubility tag, high yields of active holoenzyme are obtained. Native *TtProDH* can be produced from cleaving the purified fusion protein with trypsin. Size-exclusion chromatography shows that fused and clipped *TtProDH* form oligomers. Thermal stability and co-solvent tolerance indicate the conformational robustness of *TtProDH*. These properties together with the high yield make *TtProDH* attractive for industrial applications.

## Keywords

flavoenzyme, maltose-binding protein, proline dehydrogenase, protein stability, solubility tag

## Introduction

Proline dehydrogenase (ProDH; EC 1.5.5.2) catalyzes the flavin adenine dinucleotide (FAD)-dependent oxidation of proline to  $\Delta^1$ -pyrroline-5-carboxylate (P5C), the first step of proline catabolism in many organisms. P5C can be non-enzymatically hydrolyzed to glutamic semialdehyde (GSA), which is further oxidized by P5C dehydrogenase (P5CDH; EC 1.2.1.88) to L-glutamate. ProDH and P5CDH are separate monofunctional enzymes in eukaryotes and some bacteria, whereas they are fused in other bacteria [1]. This fusion results in a bifunctional enzyme called Proline Utilization A (PutA), which allows channeling of the GSA intermediate between the active sites [2-4].

Except from contributing to the cellular energy supply, ProDH plays important roles in oxidative stress, apoptosis, cancer and schizophrenia [5-8]. In plants, proline accumulates in response to environmental stress such as drought, high salinity and UV irradiation [6,9,10]. ProDHs and related enzymes are also of interest for biocatalytic applications because the proline imino acid can serve as building block for the synthesis of a wide range of peptides and antibiotics [11-15].

To date, two crystal structures of full-length PutA have been solved, which are the structures of *Bradyrhizobium japonicum* PutA [16] and *Geobacter sulfurreducens* PutA [3]. Furthermore, the crystal structure of the ProDH domain of *Escherichia coli* PutA [17] is available. For monofunctional ProDHs, crystal structures of *Thermus thermophilus* ProDH [1] and *Deinococcus radiodurans* ProDH [18] have been obtained. These structures indicate a distorted ( $\beta\alpha$ )<sub>8</sub> TIM-barrel fold [19].

ProDH is a membrane-associated enzyme [1]. When human ProDH is produced in *E. coli*, very low activity is observed [20,21]. Some biochemical data on ProDH from *Saccharomyces cerevisiae* [22] and *Trypanosoma cruzi* [23] have been reported, but no details were given about the production levels of the recombinant enzymes. All recombinant expressions of ProDH reported so far include a His-tagged protein and purification by metal affinity chromatography [18,21-27]. However, obtaining soluble protein in preparative amounts has remained problematic [21,26]. Furthermore, it has been reported repeatedly that heterologous expression of ProDH in *E. coli* yields protein aggregates [24,27].

For application of ProDH under non-natural conditions, the development of experimental strategies that allow for the production of large amounts of soluble ProDH is highly desirable. We here report on the heterologous production of ProDH from *T. thermophilus* (TtProDH) in *E. coli*. Using maltose-binding protein (MBP) as solubility tag, impressive yields of active holoenzyme are obtained. The hydrodynamic and conformational stability properties of fused and clipped TtProDH are presented as well.

## Materials & Methods

### Cloning of *TtProDH*

The synthetic *T. thermophilus* ProDH gene (Eurogentec; codon optimized for *E. coli*) encoding for amino acid residues 1-307 (NCBI RefSeq code YP\_005183) and two additional C-terminal amino acids (Leu-Glu) was PCR amplified using the primers 5' AAT TAG AAT TCA TGA ACC TGG ACC TGG CTT ACC G 3' (forward) and 5' GCC CAA GCT TTC ATT CCA GAC CGC TAA CCA G 3' (reverse), introducing *EcoRI* and *HindIII* restriction sites (underlined). The amplified fragment was introduced into a pBAD-MBP vector [28] using the *EcoRI* and *HindIII* restriction sites, resulting in an N-terminal fusion of *TtProDH* to MBP. The resulting MBP-*TtProDH* construct consisting of 700 amino acid residues (Fig. S1) was verified by automated sequencing of both strands (Macrogen) and the plasmid was transformed to *E. coli* TOP10 host cells for recombinant expression.

### Purification of MBP-*TtProDH*

An Äkta explorer FPLC system (GE Healthcare) was used for all purification steps. For enzyme production, 10 mL pre-cultures inoculated with *E. coli* TOP10 cells harboring a pBAD-MBP-*TtProDH* plasmid were grown overnight at 37 °C in terrific broth (TB) medium containing 100 µg/mL ampicillin. The pre-cultures were used to inoculate six 2 L erlenmeyer flasks, each containing 500 mL TB medium and 100 µg/mL ampicillin. The cells were grown at 37 °C until OD<sub>600</sub> = 0.8. Protein expression was induced with 0.02% (w/v) L-arabinose at 20 °C with a shaking rate of 200 rpm for 20 h. Cells (15 g, wet weight) were harvested by centrifugation (7000 g at 4 °C for 10 min) and resuspended in 50 mM sodium phosphate, pH 7.4. After adding 1 mg DNaseI, 1 mM MgCl<sub>2</sub> and a Complete Protease Inhibitor Cocktail Tablet (Roche Diagnostics), cells were lysed by passing them three times through a pre-cooled French Press (SLM Aminco Instruments) at 10000 psi. Cell lysate was centrifuged at 26000 g at 4 °C for 1 h. The soluble fraction was loaded on an amylose resin (16 x 75 mm) column (New England Biolabs), pre-equilibrated in 50 mM sodium phosphate, pH 7.4. After washing, bound protein was eluted with 10 mM maltose, dissolved in the same buffer. MBP-*TtProDH* (630 mg) with a concentration of 8.2 mg/mL, was flash-frozen in liquid nitrogen and stored at -80 °C.

### Limited proteolysis of MBP-*TtProDH* and purification of native *TtProDH*

Before proteolysis, MBP-*TtProDH* (82 mg) was fractionated on a Superdex 75 26/600 column (GE-Healthcare), pre-equilibrated in 50 mM sodium phosphate, 150 mM NaCl, pH 7.4. Peak fractions were concentrated to 16.8 mg/mL by using a 10 kDa cut off Vivaspinn 20 spinfilter (GE Healthcare), flash-frozen in liquid nitrogen and stored at -80 °C. 25 mg of purified

MBP-*TtProDH* was incubated with 12 µg trypsin from bovine pancreas (product no. 109 819, Boehringer Mannheim) in 50 mM sodium phosphate, 150 mM NaCl, pH 7.4 in the presence of 20 mM *n*-octyl β-D-glucopyranoside (BOG). After 20 min incubation at 37 °C, phenylmethylsulfonyl fluoride (PMSF) (Merck) was added to a final concentration of 2 mM to inactivate the protease. The PMSF-treated samples were left at room temperature for 1 h. Subsequently, cleaved fusion protein was loaded on a Source Q-15 anion-exchange (16 x 90 mm) column (GE-Healthcare), pre-equilibrated in 20 mM Bis-Tris, pH, 7.4. After washing with one volume of starting buffer and three volumes of 20 mM Bis-Tris, 100 mM NaCl, pH 7.4 to remove free MBP, the enzyme was eluted with a linear gradient of 0.1 – 1 M NaCl in the same buffer. Purified protein was concentrated to 2.3 mg/mL by using a 10 kDa cut off Vivaspinn 6 spinfilter (GE Healthcare) and dialyzed against 50 mM sodium phosphate, pH 7.4 at 4 °C for 16 h. *TtProDH* was then flash-frozen in liquid nitrogen and stored at -80 °C.

### **Protein analysis**

Enzyme purity was checked with sodium dodecyl sulfate polyacrylamide gel electrophoresis (SDS-PAGE) using 10% polyacrylamide slab gels. Proteins were stained using Coomassie Brilliant Blue R-250. The molecular weight marker used on all gels was Precision Plus Protein Standard (Biorad).

### **Peptide mapping**

Purified MBP-*TtProDH*, *TtProDH* and MBP were loaded on SDS-PAGE using 10% polyacrylamide slab gels. Gels were stained using a Colloidal Blue staining kit (Invitrogen). Destaining was performed in water. Bands corresponding to the fusion protein, *TtProDH* and MBP were cut out of the gel, supplemented with 50 µL of 5 ng/µL sequencing-grade bovine trypsin (Roche) in 50 mM ammonium bicarbonate, pH 8.0 and incubated at 45 °C for 2 h. 10% trifluoroacetic acid (TFA) was added up to a pH between 2 and 4, the samples were sonicated for 1 s in an ultrasonic water bath and a clean-up was performed using a Lichroprep C18 µcolumn. For this, the peptide mixtures were dissolved in 100 µL 0.1% formic acid, loaded on the column, washed with 0.1% formic acid and eluted with 50 µL 0.05% formic acid, containing 50% acetonitrile. After reduction of the acetonitrile content in a concentrator at 45 °C, the peptide mixtures were analyzed by liquid chromatography-tandem mass spectrometry (LC-MS/MS) as described previously [29]. MaxQuant [30] was used for peptide identification, essentially as described in [31].

### **ESI-MS**

For determining the exact molecular masses of MBP-*TtProDH*, *TtProDH* and MBP, nanoflow electrospray ionization mass spectrometry (ESI-MS) analysis under denaturing conditions

was performed. Enzyme samples were prepared in 50 mM ammonium acetate pH 6.5 and diluted to a final concentration of 5  $\mu$ M (MBP-*Tt*ProDH and MBP) or 10  $\mu$ M (*Tt*ProDH) in 5% formic acid. Analysis was performed on a LC-T nanoflow ESI orthogonal TOF mass spectrometer (Micromass, Manchester, UK), equipped with a Z-spray nano-electrospray ionization source. All measurements were performed by operating in the positive ion mode and by using gold-coated needles, made with boro-silicate glass capillaries (Kwik-Fill; World precision Instruments, Sarasota) on a P-97 puller (Sutter Instruments, Novato). Gold coating of the needles was performed by an Edwards Scancoat sic Pirani 501 sputter coater (Edwards laboratories, Milpitas). Mass spectra were recorded with a capillary voltage of 1.2 kV and cone voltage of 30 V. All spectra were mass calibrated by using an aqueous solution of cesium iodine (25 mg/mL).

### Gel filtration analysis

The hydrodynamic properties of *Tt*ProDH were analyzed using size exclusion chromatography. For this, MBP-*Tt*ProDH and *Tt*ProDH were pre-incubated for 16 h at room temperature in the absence or presence of 20 mM BOG, 10% glycerol, 0.5 M guanidinium hydrochloride (GuHCl), or 1 M GuHCl. Furthermore, *Tt*ProDH was incubated at 80 °C for 15 min. Protein samples were loaded on a Superdex 200 10/300 GL column (GE Healthcare), running in 50 mM sodium phosphate, 150 mM NaCl, pH 7.4. Apparent molecular masses were determined from running calibration proteins in parallel, essentially as described elsewhere [32].

### Spectral analysis

Absorption spectra of MBP-*Tt*ProDH and *Tt*ProDH were recorded at 25 °C on a Hewlett Packard 8453 diode array spectrophotometer in 50 mM sodium phosphate, pH 7.4. Spectra were collected and analyzed using the UV-Visible ChemStation software package (Hewlett Packard). The molar absorption coefficient of enzyme-bound FAD was determined by recording the absorption spectrum of 2.7 mg/mL MBP-*Tt*ProDH in the absence and presence of 0.5% (w/v) SDS, assuming a molar absorption coefficient for free FAD of 11.3 mM<sup>-1</sup> cm<sup>-1</sup> at 450 nm. Purified enzyme concentrations were routinely determined by measuring the absorbance at 450 nm using the estimated molar absorption coefficient for protein-bound FAD (12.4 mM<sup>-1</sup> cm<sup>-1</sup>).

### Enzyme activity

*Tt*ProDH activity was routinely determined at 25 °C using the proline: dichlorophenolindophenol (DCPIP) oxidoreductase assay. The activity assay was performed in a volume of 600  $\mu$ L containing 20 mM Hepes, pH 8.0, 100 mM L-proline and 70  $\mu$ M DCPIP.

The reaction was initiated by the addition of catalytic amounts of enzyme and the decrease in absorbance at 600 nm ( $\Delta\epsilon = 16100 \text{ M}^{-1} \text{ cm}^{-1}$ ) was followed with a Hewlett-Packard 8453 diode array spectrophotometer. One unit of enzyme (U) is defined as the amount of ProDH that transfers electrons from 1  $\mu\text{mol}$  of proline to DCPIP per min at 25 °C.

### Circular dichroism spectroscopy

Far-UV circular dichroism (CD) spectra of TtProDH and MBP-TtProDH were acquired on a Jasco J-715 spectropolarimeter equipped with a Peltier thermostat (Jasco). Data were collected from 195 to 260 nm with a data pitch of 0.5 nm, scanning speed of 50 nm/min, response time of 1 s and 2 nm bandwidth. Spectra were recorded at 25 °C using 1 mm quartz cuvettes and 30 scans were averaged and baseline corrected. Samples contained 0.52  $\mu\text{M}$  MBP-TtProDH or 1.6  $\mu\text{M}$  TtProDH in 50 mM sodium phosphate, pH 7.4, both before and after incubation at 80 °C for 15 min. After heat treatment, samples were centrifuged before recording spectra.

### Fluorescence spectroscopy

Protein tryptophan (Trp) fluorescence was measured using a Cary Eclipse fluorescence spectrophotometer (Varian). Temperature-induced unfolding of 0.21  $\mu\text{M}$  MBP-TtProDH, 0.62  $\mu\text{M}$  TtProDH and 0.26  $\mu\text{M}$  MBP in 20 mM Hepes, pH 8.0 was evaluated by increasing the temperature from 20 – 80 °C at a rate of 0.5 °C/min. Data points were collected every 0.2 °C. Reversibility of TtProDH unfolding was monitored by decreasing the temperature from 80 – 20 °C with the same settings. Trp excitation was at 295 nm and fluorescence emission was monitored at 350 nm. Emission and excitation slits were set to 5 nm. Midpoints of transition were determined by fitting a sigmoid curve.

### Enzyme stability

The thermal stability of MBP-TtProDH was determined at various temperatures. 10.4  $\mu\text{M}$  MBP-TtProDH and 6.2  $\mu\text{M}$  TtProDH were incubated in 20 mM Hepes, pH 8.0 for 90 min at 60, 70, 80, 85, 90, and 95 °C, respectively. The time-dependent loss of activity was followed by the standard activity assay procedure. 10  $\mu\text{L}$  aliquots were removed from the incubation mixtures at various time points up to 90 min and directly assayed for residual enzyme activity at 25 °C.

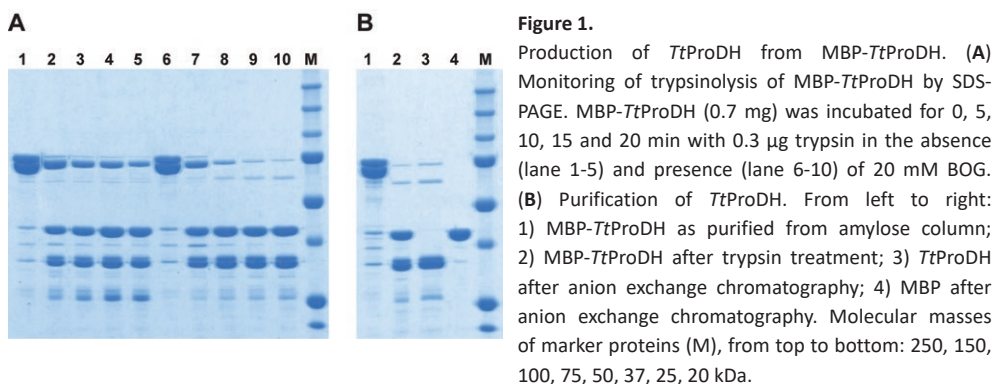
Enzyme stability in organic solvents was assessed by incubating 9.8  $\mu\text{M}$  TtProDH in 20 mM Hepes, pH 8.0 supplemented with 20%, 40%, 60% or 80% ethanol (EtOH), dimethyl sulfoxide (DMSO) or dimethylformamide (DMF). 10  $\mu\text{L}$  aliquots were removed after 1 h of incubation and directly assayed for residual enzyme activity at 25 °C. As a control, TtProDH was incubated in 20 mM Hepes, pH 8.0 for 1 h.



## Results

### Overexpression of MBP-*Tt*ProDH in *E. coli*

*Tt*ProDH can be overexpressed in *E. coli* in large amounts as a soluble protein by using an N-terminal MBP tag. Expressed MBP-*Tt*ProDH comprises about 50% of total protein content of the cell, and 80% of the yellow fusion protein is present in the soluble fraction after lysing the cells. Using an amylose affinity column, more than 250 mg of MBP-*Tt*ProDH is obtained per liter of *E. coli* culture. SDS-PAGE shows two bands, which both correspond to the fusion protein (Fig. 1A). Peptide mapping indicates that both bands comprise the complete fusion construct (Fig. S2). ESI-MS reveals masses of  $78677.3 \pm 3.7$  and  $81756.9 \pm 2.0$  Da (Fig. S3A), of which the first mass is the mass of the fusion protein (theoretical mass 78674.9 Da, including the initial methionine), while the second mass corresponds to an elongated form of the fusion protein (*vide infra*).



### Hydrodynamic properties of MBP-*Tt*ProDH

Analytical gel filtration revealed that MBP-*Tt*ProDH consists of multiple oligomeric protein species (Fig. 2A). It was reported before that BOG is effective in solubilizing *Tt*ProDH aggregates [1,24,27]. In agreement, we found that the fusion protein becomes more homogeneous after treatment with 20 mM BOG (Fig. 2B). An even better defined MBP-*Tt*ProDH species was obtained when the protein was treated for 16 h with 1 M GuHCl (Fig. 2C). An incubation time of 1 h or lowering the concentration of GuHCl to 0.5 M was not sufficient to fully solubilize the larger protein aggregates (not shown). From running calibration proteins in parallel, the minimum apparent molecular mass of GuHCl-solubilized MBP-*Tt*ProDH (Fig. 2C) was estimated to be  $380 \pm 10$  kDa.

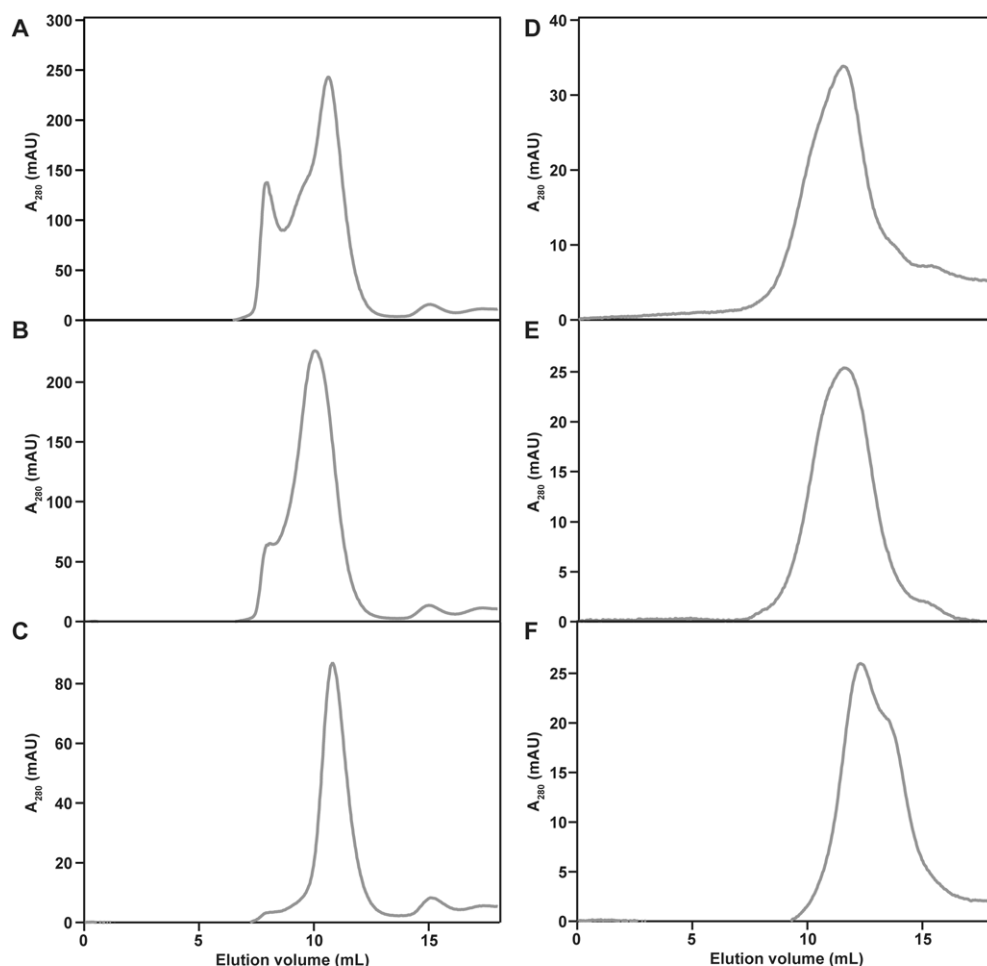


**Figure 2.**

Hydrodynamic properties of MBP-*TtProDH* and *TtProDH* as monitored by Superdex 200 size-exclusion chromatography. (A) MBP-*TtProDH* (100  $\mu$ L, 94  $\mu$ M) as eluted from the amylose column; (B) MBP-*TtProDH* (100  $\mu$ L, 27  $\mu$ M) after 16 h incubation with 20 mM BOG; (C) MBP-*TtProDH* (100  $\mu$ L, 27  $\mu$ M) after 16 h incubation with 1 M GuHCl; (D) *TtProDH* (100  $\mu$ L, 51  $\mu$ M) as eluted from the amylose column; (E) *TtProDH* (100  $\mu$ L, 51  $\mu$ M) after 16 h incubation with 20 mM BOG; (F) *TtProDH* (100  $\mu$ L, 51  $\mu$ M) after 16 h incubation with 1 M GuHCl. Absorption was monitored at 280 nm.

### Proteolytic cleavage of MBP-*TtProDH*

Proteolysis of MBP-*TtProDH* with Factor Xa protease was not effective, despite the presence of a Factor Xa protease cleavage site in the linker region. Since the linker also contains a cleavage site for trypsin [28] (Fig. S1), this protease was used to obtain native *TtProDH*. Trypsinolysis in the presence of 20 mM BOG is more effective, since in the presence of

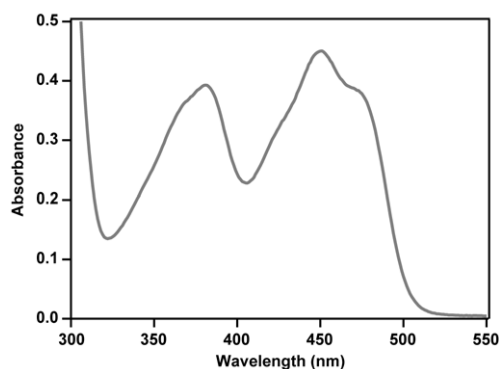
this detergent MBP-*Tt*ProDH is cleaved faster without significant further degradation (Fig. 1A). For preparative purposes, purified MBP-*Tt*ProDH was cleaved with trypsin in the presence of 20 mM BOG. The cleavage products were easily separated on a Source 15-Q column (see Materials & Methods), as confirmed by SDS-PAGE (Fig. 1B). *Tt*ProDH shows, like MBP-*Tt*ProDH, two bands on SDS-PAGE. Peptide mapping indicates both bands comprise the complete protein sequence (Fig. S2). ESI-MS reveals masses of  $36210.7 \pm 1.1$  and  $37178.5 \pm 1.3$  Da (Fig. S3B), of which the first mass is the mass of *Tt*ProDH (theoretical mass 36211.0 Da), while the second mass corresponds to an elongated form of *Tt*ProDH (*vide infra*). MBP displays a single band on gel and peptide mapping shows coverage of the complete protein sequence (Fig. S2). ESI-MS gives a mass of  $42483.8 \pm 1.1$  for MBP (Fig. S3C), which is in agreement with the predicted theoretical mass (42481.9 Da, including the initial methionine).

### Hydrodynamic properties of *Tt*ProDH

His-tagged *Tt*ProDH as expressed in *E. coli* forms large protein aggregates, which can be solubilized with BOG to give monomers [27], or a mixture of monomeric and dimeric species [1]. We found that *Tt*ProDH, originating from BOG-treated MBP-*Tt*ProDH, mainly forms oligomers with an apparent molecular mass of  $260 \pm 10$  kDa (Fig. 2D). An extra treatment with 20 mM BOG did not significantly change the hydrodynamic properties of *Tt*ProDH (Fig. 2E). However, treatment of *Tt*ProDH with 1 M GuHCl yields a mixture of oligomeric species with apparent molecular masses ranging from 100 to 180 kDa (Fig. 2F). Heating of *Tt*ProDH at 80 °C for 15 min results in a more uniform oligomeric species with an apparent molecular mass of  $240 \pm 10$  kDa (data not shown). Keeping the heated protein at room temperature for 16 h gives the same result.

### Spectral properties

The visible flavin absorption spectrum of purified MBP-*Tt*ProDH shows maxima at 381 nm and 451 nm and shoulders at 376, 426 and 476 nm, respectively (Fig. 3). The absorption ratio  $A_{381}/A_{451}$  of 0.87 is significantly lower than that of His-tagged *Tt*ProDH [1]. The shape (vibrational fine structure) of the flavin absorption spectrum does hardly change after cleavage of the MBP fusion partner (not shown). The molar absorption coefficient of *Tt*ProDH-bound FAD is  $12.4 \text{ mM}^{-1} \text{ cm}^{-1}$  at 451 nm, as deduced from SDS unfolding experiments. *Tt*ProDH is rather resistant to SDS-mediated unfolding. After 1 h of incubation in 0.2% SDS, MBP-*Tt*ProDH still shows the absorption spectrum of the folded flavoprotein. Complete unfolding of the holoprotein at room temperature requires incubation in 0.5% SDS. MBP-*Tt*ProDH has an absorption ratio of  $A_{279}/A_{451}$  of 17.5, while this ratio is 6.4 for *Tt*ProDH. These absorption ratios are in good agreement with the number of aromatic residues of MBP and *Tt*ProDH, and indicate that both MBP-*Tt*ProDH and *Tt*ProDH are fully saturated with FAD.

**Figure 3.**

Flavin absorption spectrum of purified MBP-*TtProDH* (35.6  $\mu$ M) in 50 mM sodium phosphate, pH 7.4.

## Catalytic properties

Purified MBP-*TtProDH* has a specific activity of  $4 \pm 1$  U/mg at 25 °C. Addition of excess FAD hardly improves the enzyme activity, confirming that the enzyme is fully saturated with FAD. The specific activity of MBP-*TtProDH* is in the same range as reported for His-tagged ProDH [1]. Proteolytic cleavage of MBP-*TtProDH* does not significantly change the activity of *TtProDH*. The same holds when MBP-*TtProDH* or *TtProDH* are treated for 16 h with 20 mM BOG or 1 M GuHCl.

## Protein stability

The structural stability of the enzyme was determined by CD spectroscopy. At 25 °C, MBP-*TtProDH* (Fig. 4A) and *TtProDH* (Fig. 4B) are clearly well-structured. After incubating at 80 °C for 15 min, the fusion protein forms visible aggregates due to unfolding of MBP. This is reflected in a severe loss of CD signal. *TtProDH* on the other hand retains its structural features after incubation at 80 °C, although a small amount of protein is lost because of aggregation.

Thermal unfolding of MBP-*TtProDH* (11 Trp residues), *TtProDH* (3 Trp residues) and MBP (8 Trp) was also monitored by Trp fluorescence spectroscopy (Fig. 4C). Upon incubation of MBP-*TtProDH* at increasing temperature, the Trp fluorescence emission drops with a midpoint of transition around 53 °C. For free MBP, the midpoint of transition is around 56 °C. When increasing the temperature from 20 - 80 °C, the fluorescence emission of *TtProDH* gradually decreases without a clear transition. This, and the fact that the quantum yield of Trp fluorescence decreases with increasing temperature [33], suggests that *TtProDH* does not unfold under the conditions applied. Decreasing the temperature of the heated *TtProDH* sample shows that the Trp fluorescence behavior is not fully reversible. The transition in Trp fluorescence observed during heating of MBP-*TtProDH* is due to unfolding of MBP, since *TtProDH* does not unfold at these temperatures.

The thermostability of fused and clipped *Tt*ProDH was also assessed by incubating MBP-*Tt*ProDH and *Tt*ProDH at elevated temperatures and monitoring the residual activity as a function of the incubation time. With MBP-*Tt*ProDH, more than 50% of the activity is retained after 90 min incubation at 60, 70 and 80 °C (Fig. 4D). When incubating MBP-*Tt*ProDH at 90 °C, the activity gets readily lost. *Tt*ProDH is more stable than MBP-*Tt*ProDH. Fig. 4E shows that with the native enzyme, rapid loss of activity only occurs at temperatures above 90 °C, in good agreement with results obtained for His-tagged ProDH [1]. Note that for *Tt*ProDH, the activity initially increases when the enzyme is incubated at elevated temperatures.

The storage stability of *Tt*ProDH in organic solvents was assessed by incubating the enzyme in different concentrations of EtOH, DMSO and DMF. As can be seen from Fig. 4F, *Tt*ProDH is rather stable in these co-solvents. After 1 h incubation, more than 50% of residual activity is observed in 40% EtOH, 60% DMF, and 60% DMSO, respectively. In 80% of all three organic solvents, the activity of *Tt*ProDH is more readily lost, although still more than 15% of activity is retained in 80% DMF after 1 h incubation

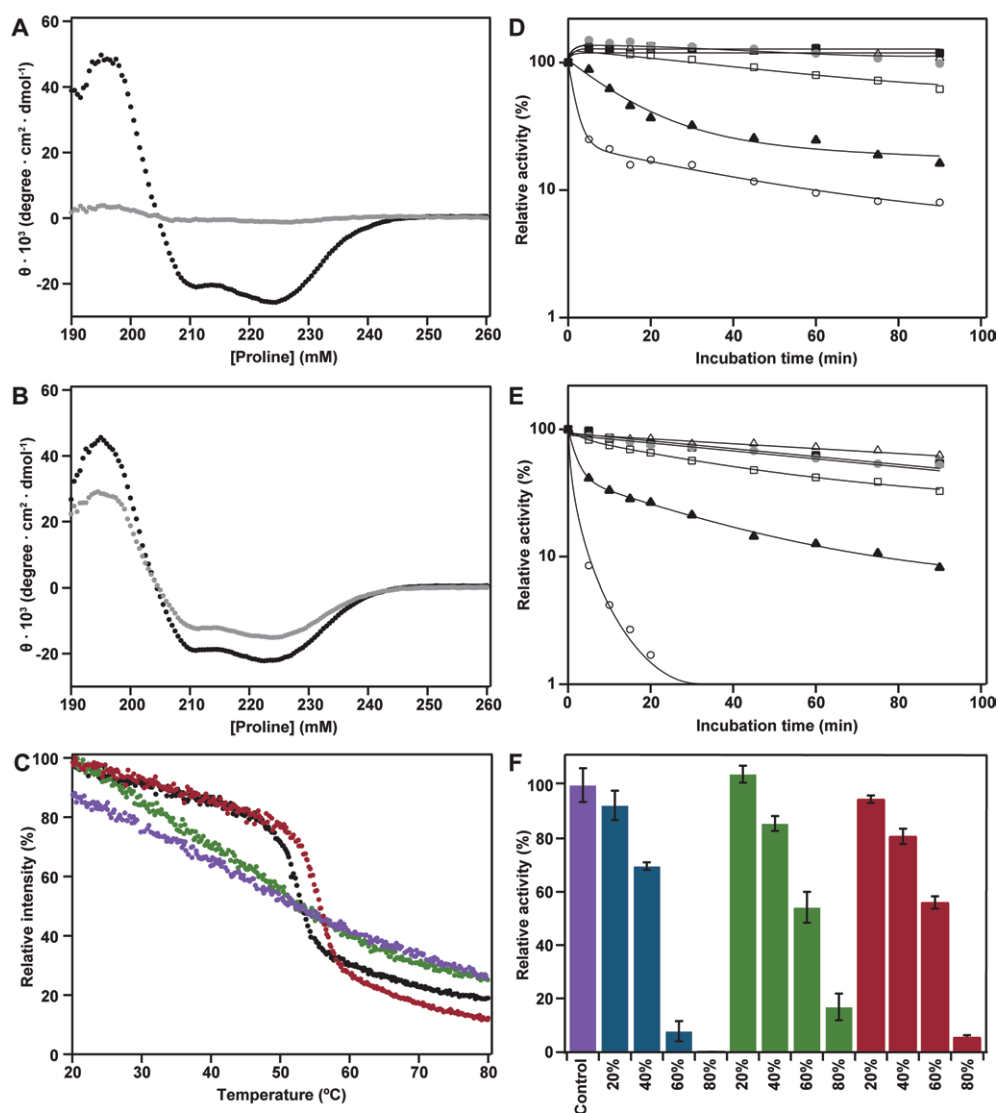


Figure 4.

Stability of MBP-TtProDH and TtProDH. (A) CD spectra of MBP-TtProDH (0.52  $\mu\text{M}$ ) before (black) and after (gray) incubation of the sample at 80  $^{\circ}\text{C}$ . (B) CD spectra of TtProDH (1.6  $\mu\text{M}$ ) before (black) and after (gray) incubation of the sample at 80  $^{\circ}\text{C}$ . (C) Thermal unfolding of MBP-TtProDH (0.21  $\mu\text{M}$ ), MBP (0.26  $\mu\text{M}$ ) and TtProDH (0.62  $\mu\text{M}$ ) as monitored by tryptophan fluorescence spectroscopy. Black: MBP-TtProDH; green: TtProDH (unfolding); purple: TtProDH (refolding); red: MBP; (D) Thermoinactivation of MBP-TtProDH (10.4  $\mu\text{M}$ ) as a function of temperature. (E) Thermoinactivation of TtProDH (6.2  $\mu\text{M}$ ) as a function of temperature. For (D) and (E): black squares: 60  $^{\circ}\text{C}$ ; open triangles: 70  $^{\circ}\text{C}$ ; gray circles: 80  $^{\circ}\text{C}$ ; open squares 85  $^{\circ}\text{C}$ ; black triangles 90  $^{\circ}\text{C}$ ; open circles 95  $^{\circ}\text{C}$ . (F) Residual activity of TtProDH (6.2  $\mu\text{M}$ ) in different organic solvents. Each measurement was performed in triplicate. Purple: control; blue: EtOH; green: DMF; red: DMSO.

## Discussion

MBP is widely recognized as a carrier protein for the production of soluble recombinant proteins in *E. coli* [34,35]. In this report, we show that MBP can efficiently assist in the production of large amounts of soluble *Tt*ProDH in *E. coli*. The MBP tag inhibits the self-association of *Tt*ProDH, preventing to a large extent the formation of insoluble protein aggregates. Size-exclusion chromatography revealed that MBP-*Tt*ProDH has a complex quaternary structure and that incubation with BOG or GuHCl results in oligomeric species that are composed of at least four polypeptide chains. MBP-bound *Tt*ProDH is fully saturated with FAD, raising the question if flavin incorporation precedes oligomerization.

Cleavage of MBP-*Tt*ProDH with Factor Xa was not successful, possibly because of steric hindrance. The inability of Factor Xa to efficiently cleave fusion proteins has been reported before [36-38]. Trypsin is more effective in cleaving MBP-*Tt*ProDH. Especially in the presence of BOG, rather pure forms of free MBP and *Tt*ProDH are obtained. The fact that *Tt*ProDH itself is not degraded by trypsin indicates a stable and well-folded protein.

Analytical gel filtration established that *Tt*ProDH resembles MBP-*Tt*ProDH in stabilizing a quaternary structure composed of at least four polypeptide chains. Determination of the precise geometry of MBP-*Tt*ProDH and *Tt*ProDH requires further studies, directed at determining the subunit arrangement and intermolecular interactions of the biomolecules. This is particularly interesting because N-terminally His-tagged *Tt*ProDH as treated with BOG was found to be a mixture of dimers and monomers [1]. Moreover, several other ProDHs have been described as dimers [21,23,39] while in some cases, the oligomerization state of ProDH was not reported [22,24,26].

SDS-PAGE indicated that the *E. coli* cells produce two forms of MBP-*Tt*ProDH. Peptide mapping revealed that both forms comprise the complete sequence of the fusion protein. The lower band on gel corresponds to full-length MBP-*Tt*ProDH, while the upper band corresponds to a read-through protein extended by 25 amino acids. This read-through is produced because of the selected stop codon, TGA, which can be recognized by the tRNA coding for Trp, TGG [40,41]. The amino acid sequence of the read-through protein (Fig. S4) corresponds to a theoretical mass of 81751.3 Da, which is in fair agreement with the measured mass of  $81756.9 \pm 2.0$  Da. *Tt*ProDH is also present in two forms as shown on SDS-PAGE. The lower band again corresponds to full-length enzyme while the upper band corresponds to a read-through protein, this time extended by only 7 amino acids (Fig. S4). This shorter extension is due to cleavage of the additional C-terminal part by trypsin. The measured mass of  $37178.5 \pm 1.3$  Da corresponds to the theoretical mass of 37178.1 kDa.

Thermoinactivation studies showed that *Tt*ProDH has a melting temperature around 87 °C. MBP-*Tt*ProDH is less stable, most probably because ProDH-bound MBP unfolds around 53 °C. Free MBP isolated in this study unfolds at 56 °C. This value is somewhat lower than



the corresponding value of 62 °C reported for wild-type MBP [42], possibly because of the presence of the asparagine-rich linker sequence (Fig. S1). Trp fluorescence and CD analysis revealed that TtProDH does not unfold upon heating from 20 °C to 80 °C. However, the thermal process is not fully reversible. Gel filtration suggests that during heating some irreversible change in oligomerization behavior occurs. This change apparently results in a more active enzyme, as indicated by the increased activity of the enzyme when incubating at elevated temperatures.

Next to being useful for structure-function relationship studies, the overexpression of MBP-TtProDH is of interest from an industrial point of view. Large amounts of active holoenzyme can be obtained through a simple cultivation procedure and one-step purification of the fusion protein. MBP-TtProDH is a rather stable enzyme, which can be used in synthetic and biosensor applications. In cases where it would be desirable to apply the more thermostable native enzyme, which is also compatible with several organic solvents, tryptic cleavage of MBP-TtProDH can be readily achieved.

## **Acknowledgements**

We thank Evans Asamoah Gyimah and Adrie Westphal for technical assistance. We thank Sjeff Boeren for help with LC-MS/MS and Arjan Barendregt (Biomolecular Mass Spectrometry and Proteomics Group, Bijvoet Centre for Biomolecular Research, Utrecht University) for help with ESI-MS. MH received financial support from the Netherlands Organization for Scientific Research (NWO) through the ERA-NET Industrial Biotechnology program (ERA-IB-2) of the European Community.

## References

- [1] White, T. A., Krishnan, N., Becker, D. F., Tanner, J. J., Structure and kinetics of monofunctional proline dehydrogenase from *Thermus thermophilus*. *J. Biol. Chem.* (2007), 282, 14316-14327.
- [2] Arentson, B. W., Sanyal, N., Becker, D. F., Substrate channeling in proline metabolism. *Front. Biosci.* (2012), 17, 375-388.
- [3] Singh, H., Arentson, B. W., Becker, D. F., Tanner, J. J., Structures of the PutA peripheral membrane flavoenzyme reveal a dynamic substrate-channeling tunnel and the quinone-binding site. *Proc. Natl. Acad. Sci. USA* (2014), 111, 3389-3394.
- [4] Surber, M. W. and Maloy, S., The PutA protein of *Salmonella typhimurium* catalyzes the two steps of proline degradation via a leaky channel. *Archives of Biochemistry and Biophysics* (1998), 354, 281-287.
- [5] Jacquet, H., Raux, G., Thibaut, F. *et al.*, PRODH mutations and hyperprolinemia in a subset of schizophrenic patients. *Hum. Mol. Genet.* (2002), 11, 2243-2249.
- [6] Liang, X. W., Zhang, L., Natarajan, S. K., Becker, D. F., Proline mechanisms of stress survival. *Antioxid. Redox Sign.* (2013), 19, 998-1011.
- [7] Liu, W. and Phang, J. M., Proline dehydrogenase (oxidase) in cancer. *Biofactors* (2012), 38, 398-406.
- [8] Phang, J. M., Liu, W., Zabirnyk, O., Proline metabolism and microenvironmental stress, *Annu. Rev. Nutr.* Vol. 30, 2010, 441-463.
- [9] Hare, P. D. and Cress, W. A., Metabolic implications of stress-induced proline accumulation in plants. *Plant Growth Regul.* (1997), 21, 79-102.
- [10] Szabados, L. and Savaouré, A., Proline: a multifunctional amino acid. *Trends Plant Sci.* (2009), 15, 89-97.
- [11] Chang, W. C., Guo, Y., Wang, C. *et al.*, Mechanism of the C5 stereoinversion reaction in the biosynthesis of carbapenem antibiotics. *Science* (2014), 343, 1140-1144.
- [12] Li, C., Roege, K. E., Kelly, W. L., Analysis of the indanomycin biosynthetic gene cluster from *Streptomyces antibioticus* NRRL 8167. *ChemBioChem* (2009), 10, 1064-1072.
- [13] Méjean, A., Mann, S., Maldiney, T. *et al.*, Evidence that biosynthesis of the neurotoxic alkaloids anatoxin-a and homoanatoxin-a in the cyanobacterium *oscillatoria* PCC 6506 occurs on a modular polyketide synthase initiated by L-proline. *J. Am. Chem. Soc.* (2009), 131, 7512-7513.
- [14] Thomas, M. G., Burkart, M. D., Walsh, C. T., Conversion of L-proline to pyrrolyl-2-carboxyl-S-PCP during undecylprodigiosin and pyoluteorin biosynthesis. *Chem. Biol.* (2002), 9, 171-184.
- [15] Xu, H. M., Yi, H., Zhou, W. B. *et al.*, Tataricins A and B, two novel cyclotetrapeptides from *Aster tataricus*, and their absolute configuration assignment. *Tetrahedron Lett.* (2013), 54, 1380-1383.
- [16] Srivastava, D., Schuermann, J. P., White, T. A. *et al.*, Crystal structure of the bifunctional proline utilization A flavoenzyme from *Bradyrhizobium japonicum*. *Proc. Natl. Acad. Sci. USA* (2010), 107, 2878-2883.
- [17] Lee, Y. H., Nadaraia, S., Gu, D., Becker, D. F., Tanner, J. J., Structure of the proline dehydrogenase domain of the multifunctional PutA flavoprotein. *Nat. Struct. Biol.* (2003), 10, 109-114.
- [18] Luo, M., Arentson, B. W., Srivastava, D., Becker, D. F., Tanner, J. J., Crystal structures and kinetics of monofunctional proline dehydrogenase provide insight into substrate recognition and conformational changes associated with flavin reduction and product release. *Biochemistry* (2012), 51, 10099-10108.
- [19] Tanner, J. J., Structural biology of proline catabolism. *Amino Acids* (2008), 35, 719-730.
- [20] Krishnan, N., Dickman, M. B., Becker, D. F., Proline modulates the intracellular redox environment and protects mammalian cells against oxidative stress. *Free Radic. Biol. Med.* (2008), 44, 671-681.
- [21] Tallarita, E., Pollegioni, L., Servi, S., Molla, G., Expression in *Escherichia coli* of the catalytic domain of human proline oxidase. *Protein Expr. Purif.* (2012), 82, 345-351.
- [22] Wanduragala, S., Sanyal, N., Liang, X. W., Becker, D. F., Purification and characterization of Put1p from *Saccharomyces cerevisiae*. *Archives of Biochemistry and Biophysics* (2010), 498, 136-142.
- [23] Paes, L. S., Suárez Mantilla, B., Zimbres, F. M. *et al.*, Proline dehydrogenase regulates redox state and respiratory metabolism in *Trypanosoma cruzi*. *PLoS ONE* (2013), 8, e69419. doi:69410.61371/journal.pone.0069419.
- [24] Lagautriere, T., Bashiri, G., Paterson, N. G. *et al.*, Characterization of the proline-utilization pathway in

- Mycobacterium tuberculosis* through structural and functional studies. *Acta Crystallogr. D Biol. Crystallogr.* (2014), 70, 968-980.
- [25] Nadaraia, S., Lee, Y. H., Becker, D. F., Tanner, J. J., Crystallization and preliminary crystallographic analysis of the proline dehydrogenase domain of the multifunctional PutA flavoprotein from *Escherichia coli*. *Acta Crystallogr. D Biol. Crystallogr.* (2001), 57, 1925-1927.
- [26] Serrano, H. and Blanchard, J. S., Kinetic and isotopic characterization of L-proline dehydrogenase from *Mycobacterium tuberculosis*. *Biochemistry* (2013), 52, 5009-5015.
- [27] White, T. A. and Tanner, J. J., Cloning, purification and crystallization of *Thermus thermophilus* proline dehydrogenase. *Acta Crystallogr. F Struct. Biol. Cryst. Commun.* (2005), 61, 737-739.
- [28] Heuts, D. P. H. M., van Hellemond, E. W., Janssen, D. B., Fraaije, M. W., Discovery, characterization, and kinetic analysis of an alditol oxidase from *Streptomyces coelicolor*. *J. Biol. Chem.* (2007), 282, 20283-20291.
- [29] Lu, J., Boeren, S., de Vries, S. C. *et al.*, Filter-aided sample preparation with dimethyl labeling to identify and quantify milk fat globule membrane proteins. *J. Proteomics* (2011), 75, 34-43.
- [30] Cox, J. and Mann, M., MaxQuant enables high peptide identification rates, individualized p.p.b.-range mass accuracies and proteome-wide protein quantification. *Nat. Biotechnol.* (2008), 26, 1367-1372.
- [31] Smaczniak, C., Li, N., Boeren, S. *et al.*, Proteomics-based identification of low-abundance signaling and regulatory protein complexes in native plant tissues. *Nat. Protoc.* (2012), 7, 2144-2158.
- [32] Montersino, S. and van Berkel, W. J. H., Functional annotation and characterization of 3-hydroxybenzoate 6-hydroxylase from *Rhodococcus jostii* RHAI. *Biochim. Biophys. Acta P&P* (2012), 1824, 433-442.
- [33] Schmid, F. X., Spectral methods of characterizing protein conformation and conformational changes, Protein structure: a practical approach, IRL Press, 1989, 251-285.
- [34] di Guana, C., Lib, P., Riggsa, P. D., Inouyeb, H., Vectors that facilitate the expression and purification of foreign peptides in *Escherichia coli* by fusion to maltose-binding protein. *Gene* (1988), 67, 21-30.
- [35] Lebendiker, M. and Danieli, T., Production of prone-to-aggregate proteins. *FEBS Lett.* (2014), 588, 236-246.
- [36] Ko, Y. H., Thomas, P. J., Delannoy, M. R., Pedersen, P. L., The cystic fibrosis transmembrane conductance regulator. Overexpression, purification, and characterization of wild type and  $\Delta F508$  mutant forms of the first nucleotide binding fold in fusion with the maltose-binding protein. *J. Biol. Chem.* (1993), 268, 24330-24338.
- [37] Sachdev, D. and Chirgwin, J. M., Fusions to maltose-binding protein: control of folding and solubility in protein purification, *Method. Enzymol.*, 2000, 312-321.
- [38] Sharma, S. and Rose, D. R., Cloning, Overexpression, Purification, and Characterization of the Carboxyl-terminal Nucleotide Binding Domain of P-glycoprotein. *Journal of Biological Chemistry* (1995), 270, 14085-14093.
- [39] Vinod, M. P., Bellur, P., Becker, D. F., Electrochemical and functional characterization of the proline dehydrogenase domain of the PutA flavoprotein from *Escherichia coli*. *Biochemistry* (2002), 41, 6525-6532.
- [40] Hirsh, D. and Gold, L., Translation of UGA triplet *in vitro* by tryptophan transfer RNA's. *J. Mol. Biol.* (1971), 58, 459-468.
- [41] Eggertsson, G. and Söll, D., Transfer ribonucleic acid-mediated suppression of termination codons in *Escherichia coli*. *Microbiol. Rev.* (1988), 52, 354-374.
- [42] Ganesh, C., Shah, A. N., Swaminathan, C. P., Surolia, A., Varadarajan, R., Thermodynamic characterization of the reversible, two-state unfolding of maltose-binding protein, a large two-domain protein. *Biochemistry* (1997), 36, 5020-5028.

## Supporting information

atgaaatcgaagaaggtaaacttgtaactctggattaacggcgataaaggctataacggt  
 M K I E E G K L V I W I N G D K G Y N G  
 ctgcgtgaagtcggttaagaattccgagaagataccggaattaaagtcaccgttgagcat  
 L A E V G K K F E K D T G I K V T V E H  
 ccggataaactggaagaaattccacaggttgccgcaactggcgatggccctgacatt  
 P D K L E E K F P Q V A A T G D G P D I  
 atcttctgggcacacgaccgttgggtggctacgtcaatctggcctgtggctgaaatc  
 I F W A H D R F G G Y A Q S G L L A E I  
 accccggacaaagcgttccaggacaagctgtatccgtttacctgggatggcgtacgttac  
 T P D K A F Q D K L Y P F T W D A V R Y 100  
 aacggcaagctgattgcttaccgcatcgctgttgaaagcgttatcgctgattatacaaaa  
 N G K L I A Y P I A V E A L S L I Y N K  
 gatctgctgccgaacccgcaaaaacctgggaagagatcccgcgctggataaagaactg  
 D L L P N P P K T W E E I P A L D K E L  
 aaagcgaaagtgaaagcgctgatgttcaacctgcaagaaccgtacttcaacctggccg  
 K A K G K S A L M F N L Q E P Y F T W P  
 ctgattgctgctgggggttatcgcttcaagtatgaaaacggcaagtcagacataaa  
 L I A A D G G Y A F K Y E N G K Y D I K  
 gacgtggcgctggataacgctggcgcaaaagcggctgacacctcctggttgacctgatt  
 D V G V D N A G A K A G L T F L V D L I 200  
 aaaaacaaacacatgaatgcagacacgattactccatcgcaagctgccttataataaa  
 K N K H M N A D T D Y S I A E A F N K  
 ggcgaaacagcgatgaccatcaacggccgctggcgatggtccaacatcgacacagcaaa  
 G E T A M T I N G P W A W S N I D T S K  
 gtgaattatggtgaacggtactgcgaccttcaagggtcaacctcaaacgcttcggt  
 V N Y G V T V L P T F K G Q P S K F F V  
 ggcgtgctgagcgcaggtattaaacggcgccagtcgaacaaaagagctggcaaaagagttc  
 G V L S A G I N A A S P N K E L A K E F  
 ctcgaaaactatctgctgactgatgaaggtctggaagcgggttaataaagacaaacgcgtg  
 L E N Y L L T D E G L E A V N K D K P L 300  
 ggtgcccgtagcgtgaagttcttacggaagagttggcgaaagatccacgtattggccgc  
 G A V A L K S Y E E E L A K D P R I A A  
 actatggaaaacgcccgaaggtgaaatcatgcgaacatcccgagatgcgcctttc  
 T M E N A Q K G E I M P N I P Q M S A F  
 tggatgcgcgtgactgcggtgatcaacgcgcgacggtgcgcagactgtcgtatgaa  
 W Y A V R T A V I N A A S G R Q T V D E  
 gcctgaaagacgcgcagactaattcgagctcgaacaaacaaacataacataaacaac  
 A L K D A Q T N S S S N N N N N N N N  
 aaactcgggatcgagggaaggttccagaattcatgaacctggacctggttaccgtagc  
 N L G I E G R I S E F M N L D L A Y R S 400  
 ttgttctgggtgttgctgaggtcatccgaggttgaaactgtgataaacatcggtgcaaaa  
 F V L G V A G H P Q V E R L I K H R A K  
 ggtctggttgcgttattgttgcgggtgaaacctggaagaagcactgaaagcagcgaa  
 G L V R R Y V A G E T L E E A L K A A E  
 gcactggaacgtgaaggttccatgcaatcctggatctgctgggtgaaatggttctgtacc  
 A L E R E G V H A I L D L L G E M V R T  
 gaagaagagcgcgcgcatcttcagcgtggtctgctggaactggttggcgactggcaggt  
 E E E A R A F Q R G L L E L V W A L A G  
 aaacgtggccgcaaatatcatcagcctgaaactgacacagctgggactggtatcgagcga  
 K P W P K Y I S L K L T Q L G L D L S E 500  
 gatctggcactggcctgctgctggaagtctgcgcgaagcagaaccgctggtgtttt  
 D L A L A L L R E V L R E A E P R G V F  
 gttcgtctgatatggaagatagtcgcgctgttgaaagcaacctgcgtctgtatcgtgca  
 V R L D M E D S P R V E A T L R L Y R A  
 ctgcgtgaggaaggttttagccaggttggtattgttctgcagagctatctgtatcgacc  
 L R E E G F S Q V G I V L Q S Y L Y R T  
 gaaaaagacctgctgctgctgctgctgcaaatctgctgctggtttaaaggtgca  
 E K D L L D L L P Y R P N L R L V K G A  
 tatcgtgaacggaagaagttgcatttccggataaacgcctgattgatgcgaatatctg  
 Y R E P K E V A F P D K R L I D A E Y L 600  
 catctgggtaaactggcgctgaaagaaggtctgtacgttgcatttgcacccatgacccg  
 H L G K L A L K E G L Y V A F A T H D P  
 cgtattattgcagaactgaaacgttataccgaagcaatgggtattccgcgtgacgcgtttt  
 R I I A E L K R Y T E A M G I P R S R F  
 gaatttcagtttctgtatggtgttcgtcctgaagaacagcgtcgtctgacgcggaaggt  
 E F Q F L Y G V R P E E Q R R L A R E G  
 tatacgttctgctatgttccgtatggtcgtgattggtatcgtatcgtatcgaccctgct  
 Y T V R A Y V P Y G R D W Y P Y L T R  
 attgcgaacgtcggaataatctgctgctggttctgctgtagcctggttagcgttgga  
 I A E R P E N L L V L R S L V S G L E 700  
 tga  
 -

Figure S1.

DNA and amino sequence of the MBP-*Tt*ProDH fusion protein. MBP: residues 1-367; *Tt*ProDH: residues 392-700; The linker amino acid sequence (residues 368-391) is underlined with the factor Xa cleavage site (residues 384-387) indicated in bold. Trypsin cleaves the construct after the arginine present in the linker (Arg387).

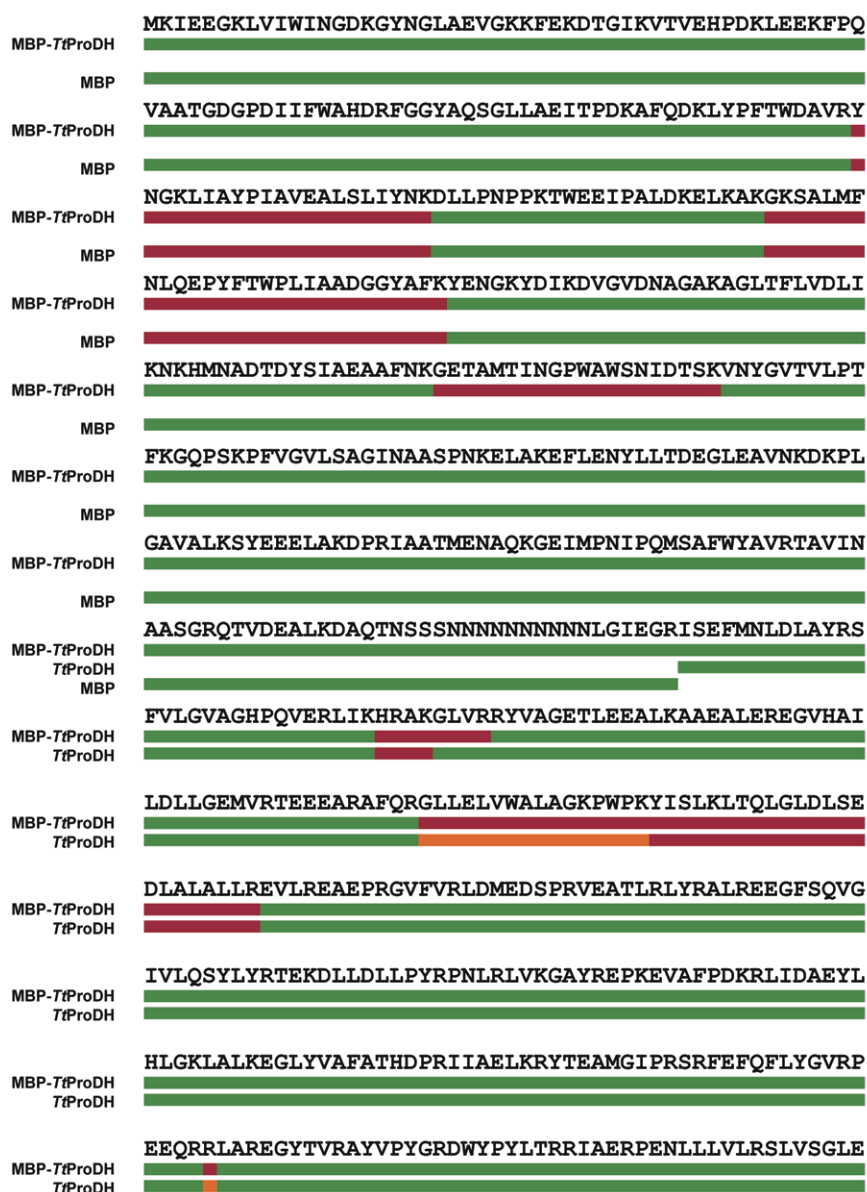


Figure S2.

Peptide mapping of MBP-TtProDH, TtProDH and MBP. Peak intensities of the peptides were normalized to 1 for each sample separately. In green, peptides with relative peak intensities >0.0005 are depicted, they are assumed as being present. In red, peptides with relative peak intensities <0.0005 are depicted, they are assumed as being present in very low amounts or being absent. For MBP-TtProDH and TtProDH, both bands corresponding to the enzyme on gel were analyzed separately although they are shown as one sample in this figure. Peptides present in one while absent in the other are depicted in orange.

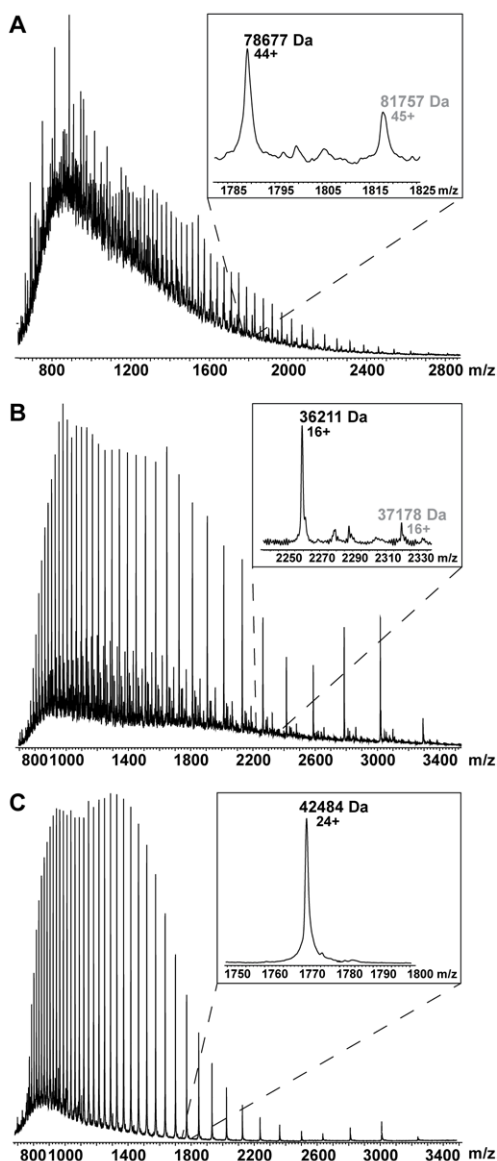


Figure S3.

(A) ESI-MS spectrum of MBP-TtProDH. Masses of  $78677.3 \pm 3.7$  and  $81756.9 \pm 2.0$  Da are revealed, of which the first mass is the mass of the fusion protein (theoretical mass 78674.9 Da, including the initial methionine), while the second mass corresponds to a read-through protein extended by 25 amino acids (theoretical mass 81751.3 Da). (B) ESI-MS spectrum of TtProDH. Masses of  $36210.7 \pm 1.1$  and  $37178.5 \pm 1.3$  Da are revealed, of which the first mass is the mass of TtProDH (theoretical mass 36211.0 Da), while the second mass corresponds to a read-through protein (which is additionally cut by trypsin) by 7 amino acids (theoretical mass 37178.1 kDa). (C) ESI-MS spectrum of MBP. A mass of  $42483.8 \pm 1.1$  is revealed which is in agreement with the predicted theoretical mass (42481.9 Da, including the initial methionine).

atgaaaatcgaagaaggtaaactggtaattctggattaacggcgataaaggctataacggt  
 M K I E E G K L V I W I N G D K G Y N G  
 ctgcgtgaagtcggttaagaatttcgagaagataccggaattaaagtcaccgttgagcat  
 L A E V G K K F E K D T G I K V T V E H  
 ccgataaaactggaagagaattccccacaggttcggcgaactggcgatggccctgacatt  
 P D K L E E K F P Q V A A T G D G P D I  
 atcttctgggcacacgacccgttttggtggctacgtcaatctggcctgttggtgaaatc  
 I F W A H D R F G G Y A Q S G L L A E I  
 accccggacaaaagcgttccaggacaagctgtatccgtttacctgggatccgtacgttac  
 T P D K A F Q D K L Y P F T W D A V R Y  
 aacggcgaagctgattgcttaccgatcgctgttgaagcgttatcgctgatttatacaaaa  
 N G K L I A Y P I A V E A L S L I Y N K  
 gatctgctgcgaacccgcgaacaaacctgggaagatcccgcgctggataaagaactg  
 D L L P N P P K T W E E I P A L D K E L  
 aaagcgaagagcgcgctgatgttcaacctgcaagaacgctacttcacctggcgcg  
 K A A K G K S A L M F N L Q E P Y F T W P  
 ctgattgctgtagcggggttatgcttcaagtatgaaaacggcaagtacgacattaaa  
 L I A A D G G Y A F K Y E N G K Y D I K  
 gacgtggcgctggataacgctggcgcaagcgggtctgaccttctggttgacctgatt  
 D V G V D N A G A K A G L T F L V D I G  
 aaaaacaaacacatgaatgcagacacccgattactccatcgagaagctgccttaataaaa  
 K N K H M N A D T D Y S I A E A F N K  
 ggcgaaacagcgatgaccatcaacggcccgctggcgatggtccaacatcgacacacgcaaa  
 G E T A M T I N G P W A W S N I D T S K  
 gtgaattatggtgaacggtactgccgacctcaagggtcaaccatccaaacccgttcgtt  
 V N Y G V T V L P T F K G Q P S K P F V  
 ggcgtgctgagcgaggtattaaacgcgcagtcggaacaaagagctggcaaaagagttc  
 G V L S A G I N A A S P N K E L A K E F  
 ctcgaaaactatctgctgactgatgaaggtctggaagcgtttaataaagacaaacccgtg  
 L E N Y L L T D E G L E A V N K D K P L  
 ggtgcctgtagcgtgaagtcctacgaggaagagttggcgaagatccacgtatttggccgc  
 G A V A L K S Y E E E L A K D P R I A A  
 actatggaaaacgccagaaggtgaatcatgcccgaacatcccgcagatgtccgcttct  
 T M E N A Q K G E I M P N I P Q M S A F  
 tggatccgctgctgactgcggtgatcaacgcgcacggctcgctcagactgtcgatgaa  
 W Y A V R T A V I N A A S G R Q T V D E  
 gccctgaagacgcgcagactaatctcgagctcgaaacaaacaaacaaacaaacaaac  
 A L K D A Q T N S S S S N N N N N N N N  
 aacctcgggatcgagggaaggttccagaattatgaacctggacctggcttaccgtagc  
 N L G I E G R I S E F M N L D L A Y R S  
 tttgttctgggtgttgacggtcatccgcaggttgaacgtctgattaaacatcgtgcaaaa  
 F V L G V A G H P Q V E R L I K H R A K  
 ggtctggttcgtgcttattgttgcggtgaaacccctggaagaagcactgaaagcagcgaa  
 G L V R R Y V A G E T L E E A L K A A E  
 gcactggaacgtgaaggtgttcacgcaatccgtgattctgctgggtgaaatggttcgtacc  
 A L E R E G V H A I L D L L G E M V R T  
 gaagaagagcgacgcgcatcttcagcgtggtctgctggaactggtttgggcactggcaggt  
 E E E A R A F Q R G L L E L V W A L A G  
 aaacgtggccggaatatatcagcctgaaactgacacagctgggaactggatctgagcgaa  
 K P W P K Y I S L K L T Q L G L D L S E  
 gatctggcactggccctgctgctggaagtcttcgcgcgaagcagaacccggtggtgtttt  
 D L A L A L L R E V L R E A E P R G V F  
 gttcgtctggataggaatagtcgcgctgttgaagcaacccctgcgtctgtatcgtgca  
 V R L D M E D S P R V E A T L R L Y R A  
 ctgcgtgaggaaggttttagccaggttggtattgttctgcagagctatctgtatcgcacc  
 L R E E G F S Q V G I V L Q S Y L Y R T  
 gaaaagacactgctggtatcgtcgcgtatcgtccgaatctgctgtctggttaaggtgca  
 E K D L L D L L P Y R P N L R L V K G A  
 tatcgtgaaccgaaagaagttgcatctccgataaacgcctgattgatgccgaatatctg  
 Y R E P K E V A F P D K R L I D A E Y L  
 catctgggtaaaactggcgctgaaagaaggtctgtacgttgcatcttgcaacccatgatccg  
 H L G K L A L K E G L Y V A F A T H D P  
 cgtattattgcagaactgaaacgttataccgaagcaatgggtattccgcgtagcgtttt  
 R I I A E L K R Y T E A M G I P R S R F  
 gaatttcagtttctgtatggtgttctgctggaagacagcgtctgtggcagcggaaggt  
 E F Q F L Y G V R P E E Q R R L A R E G  
 tatacgttctgctgctatggttcgtatggtgattggtatcgtatcgtgaccctgct  
 Y T V R A Y V P Y G R D W Y P Y L T R R  
 attcgcaacgtccggaatatcgtgctggttctgctgtagcctggttagcgttggaa  
 I A E R P E N L L L L V L R S L V S G L E  
 tgggaagctgggcccgaacaaaactcatctcagaagaggatctgaatagcgcgctgcac  
 W K L G P E Q K L I S E E D L N S A V D  
 catcatcatcatcatcattga  
 H H H H H H -

Figure S4.

DNA and amino sequence of the MBP-*TtProDH* fusion protein after read-through of the stopcodon. The stopcodon TGA is changed into TGG during a read-through, incorporating a tryptophan, shown in white on a black background. The lysine after which trypsin cleaves, producing a shortened read-through protein of *TtProDH*, is shown in white on a gray background.







# Chapter 3

## **A more polar N-terminal helix releases MBP-tagged *Thermus thermophilus* proline dehydrogenase from tetramer-polymer self-association**

*Journal of Molecular Catalysis B: Enzymatic* (2016), 134, 340-346

**Mieke M.E. Huijbers  
Willem J.H. van Berkel**

Laboratory of Biochemistry, Wageningen University & Research, Stippeneng 4, 6708 WE Wageningen, the Netherlands





## Abstract

Proline dehydrogenase (ProDH) is a ubiquitous flavoenzyme involved in the biosynthesis of L-glutamate. ProDH is of interest for biocatalysis because the protein might be applied in multi-enzyme reactions for the synthesis of structurally complex molecules. We recently demonstrated that the thermotolerant ProDH from *Thermus thermophilus* (TtProDH) is overproduced in *Escherichia coli* when using maltose-binding protein (MBP) as a solubility tag. However, MBP-TtProDH and MBP-clipped TtProDH are prone to aggregation through non-native self-association. Here we provide evidence that the hydrophobic N-terminal helix of TtProDH is responsible for the self-association process. The more polar MBP-tagged F10E/L12E variant exclusively forms tetramers and exhibits excellent catalytic features over a wide range of temperatures. Understanding the hydrodynamic and catalytic properties of thermostable enzymes is important for the development of industrial biocatalysts as well as for pharmaceutical applications.

## Keywords

flavoprotein, molecular self-association, proline dehydrogenase, protein oligomerization, *Thermus thermophilus*

## Introduction

Protein oligomerization is a commonly observed cellular process. Dimers (about 40%) and tetramers (about 20%) are the most common protein species in the cell, of which the majority is homo-oligomeric [1,2]. *In vivo*, protein oligomerization might be advantageous for many reasons, such as catalysis, cooperativity, improved stability and a reduction of surface area [1,3-6].

The oligomeric state of an *in vitro* produced enzyme does not necessarily represent the *in vivo* situation. Many intrinsic and extrinsic factors can influence the *in vitro* oligomeric state of proteins [7] and there are different types of 'non-native' oligomerization pathways [7,8]. One such pathway concerns aggregation through self-association, which means that proteins can associate into aggregates directly from the native state. This process can lead to soluble aggregates and is not always reversible.

Interacting protein surfaces are more hydrophobic than free protein surfaces. Furthermore, the subunit interface in oligomers is on average more hydrophobic than the average protein-protein interface [9-12]. Hydrophobic regions in proteins can also indicate regions sensitive to aggregation [13-15]. Knowing the location and properties of regions that are sensitive to aggregation can help in rationalizing what kind of effects sequence changes can have on the aggregation behavior of the protein [15]. Introducing so-called sequence breakers, for example an amino acid that disrupts a hydrophobic region in a sequence, can decrease the aggregation propensity of a protein [14,16,17]. By using negative design, formation of undesirable non-native structures can be avoided [18-20].

We are investigating the molecular properties of *Thermus thermophilus* proline dehydrogenase (TtProDH; EC 1.5.5.2) for potential application in multi-enzyme reactions. TtProDH is an extremely stable flavin adenine dinucleotide (FAD)-dependent enzyme involved in proline catabolism (Fig. 1).

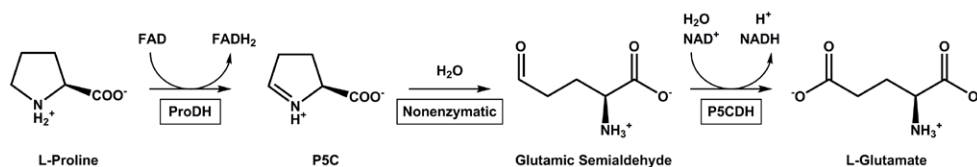


**Figure 1.**

Conversion of L-proline to L-glutamate by ProDH and P5CDH.

It has a conserved distorted ( $\beta\alpha$ )<sub>8</sub> TIM-barrel fold and an N-terminal arm that consists of three helices:  $\alpha$ A,  $\alpha$ B and  $\alpha$ C [21] (Fig. 2A). The C-terminal helix  $\alpha$ 8 fits into the cleft that is formed by helices  $\alpha$ A,  $\alpha$ B and  $\alpha$ C. Together, these four helices form a hydrophobic patch

that is thought to be involved in channeling  $\Delta^1$ -pyrroline-5-carboxylate (P5C)/glutamic semialdehyde (GSA) between *Tt*ProDH and its partner enzyme  $\Delta^1$ -pyrroline-5-carboxylate dehydrogenase (*Tt*P5CDH) [21,22]. Applying the selectivity of *Tt*ProDH in tandem reactions with other enzymes might be a powerful tool to efficiently produce structurally complex molecules from L-proline.

Several ProDHs from various sources have been described as dimers [23-25]. However, the oligomeric state of *Tt*ProDH remains ambiguous. N-terminally His-tagged *Tt*ProDH treated with *n*-octyl  $\beta$ -D-glucopyranoside (BOG) was described as a mixture of dimers and monomers [21]. We produced *Tt*ProDH with maltose-binding protein (MBP) as a solubility tag and found that, both in the absence and presence of BOG, MBP-*Tt*ProDH and MBP-clipped *Tt*ProDH consist of oligomers and soluble aggregates [26]. The non-native self-association observed might be related to the hydrophobic nature of the N-terminal helix of *Tt*ProDH. To address this issue, we increased the polarity of helix  $\alpha$ A by introducing sequence-breakers via site-directed mutagenesis. Phe10 and Leu12, located at the protein surface (Fig. 2B), were replaced by glutamates, generating the F10E/L12E variant of MBP-*Tt*ProDH. The biochemical properties of MBP-*Tt*ProDH wildtype and MBP-*Tt*ProDH F10E/L12E (further referred herein as WT and EE, respectively) are compared in this chapter.

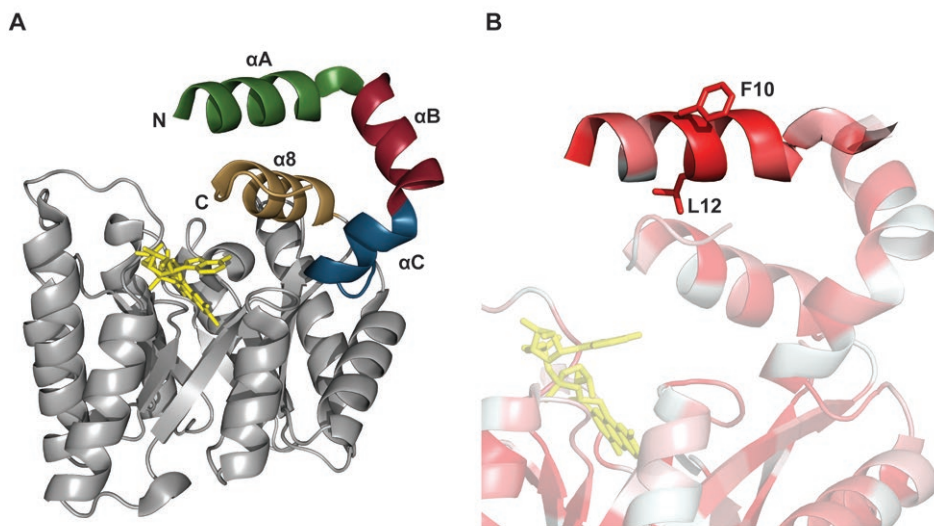


**Figure 2.**

Structural features of *Tt*ProDH. **(A)** Three-dimensional model of the crystal structure of *Tt*ProDH (PDB entry 2G37). The N-terminal helices  $\alpha$ A (green),  $\alpha$ B (red) and  $\alpha$ C (blue) are indicated, as well as the C-terminal helix  $\alpha$ 8 (brown). The FAD cofactor is depicted in yellow. **(B)** Hydrophobicity of the N-terminal helix (5-LAYRSFVLGVAGHP-18) of *Tt*ProDH. The intensity of the red color is correlated to the hydrophobicity of the residue. Phe10 and Leu12 are shown in sticks. The N-terminal helix  $\alpha$ A is shown bright, N-terminal helices  $\alpha$ B,  $\alpha$ C and the catalytic domain with the FAD cofactor are shown transparent.

## Materials and methods

### Cloning and site-directed mutagenesis of TtProDH variants

In our previous research, we obtained two forms of MBP-TtProDH [26]. With peptide mapping and mass spectrometry, we showed that one form corresponded to full-length MBP-TtProDH while the other form corresponded to an elongated form of the enzyme. This elongated form was due to a read-through of the stop codon. Here, the stop codon was changed from TGA to TAA, resulting in the production of a single form of WT. This was done in a one-step PCR and ligation reaction, using the pBAD-MBP vector containing the synthetic ProDH gene from *Thermus thermophilus* [26] as template plasmid. A single primer (5' G GTT AGC GGT CTA GAA TAA AAG CTT GGG CCC GAA C 3' (nucleotide change underlined)) was used to introduce the mutation. The PCR product was treated with *DpnI* and directly transformed to *E. coli* dh5 $\alpha$  cells. Positive constructs were identified through automated sequencing of both strands (Macrogen). Subsequently, the correct plasmid was transformed to *E. coli* TOP10 host cells for recombinant expression.

The gene encoding the F10E/L12E variant of WT was constructed by using the same one-step PCR and ligation reaction as was used for the stop codon change. pBAD WT with the corrected stop codon (TAA) was used as template DNA, and the primer used was 5' GCT TAC CGT AGC GAA GTT GAA GGT GTT GCA GGT C 3' (nucleotide changes underlined).

### Purification of MBP-TtProDH variants

WT and EE were purified according to a protocol described previously [26]. After the amylose column (New England Biolabs, 80 mL in XK 26/10), an additional polishing step was performed. 100  $\mu$ M FAD was added to the enzyme, which was subsequently loaded onto a Q-Sepharose column (GE Healthcare, 60 mL in XK 26/10), pre-equilibrated in 20 mM Bis-Tris pH, 7.4. Next, the column was washed with one volume of starting buffer and three volumes of 20 mM Bis-Tris, 100 mM NaCl, pH 7.4. Subsequently, the enzyme was eluted with a linear gradient of 0.1 – 0.5 M NaCl in the same buffer. Purified protein was concentrated to a protein content of 5-10 mg/mL using a 10 kDa cut off Amicon filter and subsequently dialyzed against 5 L of 50 mM sodium phosphate, pH 7.4 at 4 °C for 16 h. The purified enzymes were flash-frozen in liquid nitrogen and stored at -80 °C.

### Limited proteolysis

Limited proteolysis was performed using diphenyl carbamyl chloride treated trypsin (Sigma). 240  $\mu$ g of the target enzyme was incubated with 0.12  $\mu$ g of protease in a final volume of 60  $\mu$ L. The reactions were performed in 50 mM sodium phosphate, pH 7.4, in the presence

and absence of 20 mM BOG. Proteolysis was performed at 37 °C. Before proteolysis and after 2, 5, 10, 20, 30, 60 min of incubation, a 5 µL sample was taken and immediately added to pre-heated loading buffer to stop the reaction. The samples were subsequently analyzed using sodium dodecyl sulfate polyacrylamide gel electrophoresis (SDS-PAGE). 12% polyacrylamide slab gels were used and the proteins were stained with Coomassie Brilliant Blue R-250. As a molecular weight marker, Precision Plus Protein Standard (Biorad) was used.

### Analytical gel filtration

The hydrodynamic properties of WT and EE were analyzed by size exclusion chromatography, essentially as described before [26]. 200 µL of a 40 µM enzyme solution was loaded on a Superdex 200 10/300 GL (GE Healthcare), equilibrated in 50 mM sodium phosphate, 150 mM NaCl, pH 7.4.

### Electrospray ionization mass spectrometry

The native and subunit masses of WT and EE were determined using nanoflow electrospray ionization mass spectrometry (ESI-MS), according to a method described before [26]. Free MBP served as a reference. Protein samples were prepared in 50 mM ammonium acetate, pH 6.5. For analysis under native conditions, the enzymes were diluted to a final concentration of 5 - 10 µM. For analysis under denatured conditions enzyme samples were diluted in 5% formic acid, to a final concentration of 10 µM.

### Spectral analysis

Flavin absorption spectra were recorded at 25 °C on a Hewlett-Packard 8453 diode array spectrophotometer, essentially as described before [26]. Protein concentration of the samples was 40 µM; enzymes were present in 50 mM sodium phosphate, pH 7.4. Enzyme concentrations were routinely determined by measuring the absorbance at 450 nm, using the estimated molar absorption coefficient for protein-bound FAD of 12.4 mM<sup>-1</sup> cm<sup>-1</sup> [26].

Circular dichroism (CD) spectra were acquired on a Jasco J-715 spectropolarimeter equipped with a Peltier thermostat (Jasco). Far-UV CD spectra of 0.5 µM enzyme in 50 mM sodium phosphate, pH 7.4 were recorded at 25 °C using 1 mm quartz cuvettes. 30 scans were averaged and baseline corrected. Data were collected from 195 to 260 nm with a data pitch of 0.5 nm, scanning speed of 50 nm min<sup>-1</sup>, response time of 1 s and a bandwidth of 2 nm. Visible CD spectra of 40 µM enzyme in 50 mM sodium phosphate, pH 7.4 were recorded at 25 °C using 1 cm quartz cuvettes. 10 scans were averaged and baseline corrected. Data were collected from 300 to 600 nm with a data pitch of 0.2 nm, a scanning speed of 100 nm/min, a response time of 2 s and a bandwidth of 1 nm.



## Enzyme activity

Enzyme activity was determined at 25 °C and 45 °C on a Hewlett Packard 8453 diode array spectrophotometer using the proline:dichlorophenolindophenol (DCPIP) oxidoreductase assay, according to a protocol described previously [26]. For estimation of Michaelis-Menten kinetic parameters, the activity assay contained different amounts of L-proline (0.5, 2.5, 5, 10, 20, 35, 50, 75, 100, 150, 200 mM) and 65 µM DCPIP in 50 mM sodium phosphate, pH 7.4. The reaction was performed in a total volume of 600 µL and initiated by the addition of catalytic amounts of enzyme. Every data point was retrieved in triplicate. Using IGOR Pro 6.10A, rates ( $v$ ) and apparent rates ( $v_{app}$ ) were fitted to the Michaelis-Menten equation (1) and the Haldane equation (2), respectively, where the latter takes substrate inhibition into account:

$$v = \frac{v_{MAX} \cdot [S]}{K_M + [S]} \quad (1)$$

$$v_{app} = \frac{v_{MAX} \cdot [S]}{K_M + [S] + \left( \frac{[S]^2}{K_I} \right)} \quad (2)$$

[S] is the substrate concentration, and  $V_{MAX}$  and  $K_M$  are the limiting rate and Michaelis constant, respectively.  $K_I$  is the inhibition constant.

## Results

### Overproduction and purification of MBP-*Tt*ProDH variants

WT and EE were overproduced in *E. coli* with equally high yields. From 1 L culture, about 200–250 mg of each variant was purified. The purity of the enzymes can be judged from the SDS-PAGE analysis depicted in Fig. 3.

### Limited proteolysis

For removal of the MBP-tag, WT and EE (both 78.7 kDa) were incubated with trypsin, either in the absence or presence of BOG. In agreement with earlier findings [26], splitting of WT with trypsin works well, yielding free MBP (42.5 kDa) and free *Tt*ProDH (36.2 kDa) (Fig. 3A). Trypsinolysis in the presence of BOG is more effective compared to cleavage in the absence of BOG: in the presence of the detergent, WT is cleaved faster and without significant further degradation.

Limited proteolysis of EE with trypsin does not result in homogeneous preparations (Fig. 3B). Immediately after addition of the protease, further degradation bands start to appear. In time, EE is degraded to a final and stable degradation product. This appears to be the same degradation product that can be seen on SDS-PAGE when WT is incubated with trypsin. As for WT, cleavage of EE in the absence of BOG is faster, which can be judged from the intensity of the final degradation band.

Since removal of the MBP-tag is not straightforward, and its presence does not significantly affect the activity and oligomerization behavior of the enzyme [26], further experiments were performed with the MBP-tagged variants of *Tt*ProDH.

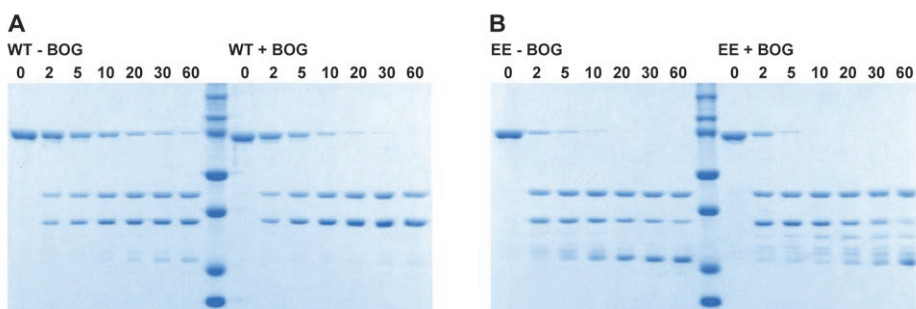


**Figure 3.**

Limited proteolysis of (A) WT and (B) EE. Both enzymes were incubated with trypsin in the absence and presence of 20 mM BOG. From left to right, time samples from 0 to 60 min incubation are shown. Molecular masses of marker proteins (M), from top to bottom: 150, 100, 75, 50, 37, 25, 20 kDa.

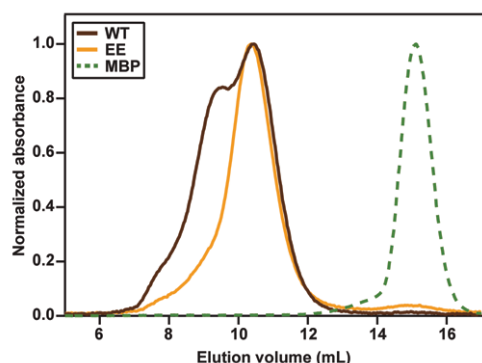


**Figure 4.**

Hydrodynamic properties of WT and EE as monitored by Superdex 200 size-exclusion chromatography. MBP serves as control.

### Oligomerization state of MBP-TtProDH

We reported before that WT purifies as a mixture of oligomers and soluble aggregates [26]. The extent of aggregation of WT is somewhat dependent on the batch of purified enzyme. Analytical gel filtration of the preparation described here suggests the presence of tetramers and soluble aggregates of various sizes (Fig. 4).

EE has two point mutations in helix  $\alpha$ A. This helix contains several hydrophobic residues (Fig. 2B). Therefore, we hypothesized that introducing charged residues in this helix might diminish the non-native aggregation of TtProDH. Analytical gel filtration reveals that EE almost exclusively forms tetramers (Fig. 4).

As a control, free MBP was analyzed using gel filtration. The apparent molecular mass of 47.6 kDa of the protein eluting at 15.1 mL is close to the theoretical value of 42.5 kDa for the MBP monomer (Fig. 4).

Native ESI-MS confirms that WT and EE form tetramers (Fig. 5 and Table 1). WT aggregates present in solution could not be identified using native ESI-MS. Both WT and EE mass spectra reveal, next to tetramers, significant amounts of dimers. As dimers are not observed in analytical gel filtration, this points to dissociation of tetramers in the gas phase. ESI-MS of denatured WT and EE confirms that the ProDH tetramers consist of identical subunits.

ESI-MS experiments of free MBP under native and denatured conditions reveal molecular masses for the MBP monomer in excellent agreement with the predicted mass derived from the MBP sequence (Table 1).

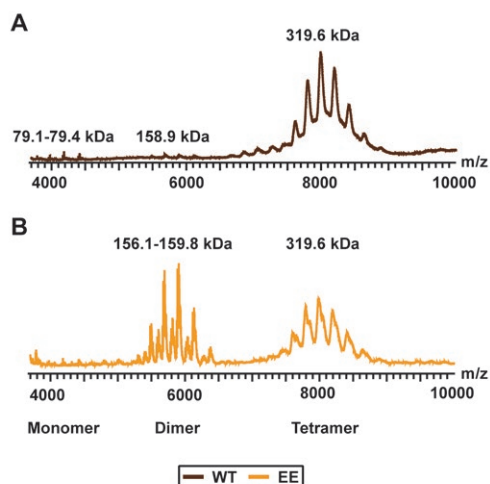


**Figure 5.**  
ESI-MS spectra of (A) WT and (B) EE.

**Table 1.**

Molecular masses of WT, EE and MBP as determined by native and denatured ESI-MS. Both predicted (Pred.) as well as experimental (Exp.) masses are given. All native masses are given in kDa and all denatured masses in Da. For calculation of the predicted native masses, it has been taken into account that each subunit contains a non-covalently bound FAD cofactor (molecular mass 785.56 Da).

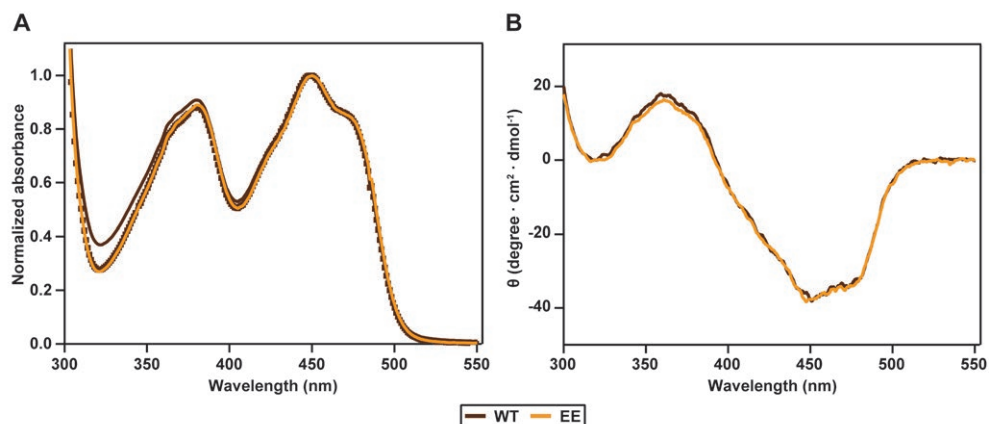
	Native						Denatured	
	Tetramer		Dimer		Monomer		Pred.	Exp.
	Pred.	Exp.	Pred.	Exp.	Pred.	Exp.		
WT	317.8	319.6	158.9	158.9	79.5	79.1-79.4	78674.9	78686.7 ± 1.9
EE	317.8	319.6	158.9	156.1-159.8	-	-	78672.8	78692.1 ± 1.6
MBP	-	-	-	-	42.5	42.5-43.5	42481.9	42492.2 ± 1.7

## Spectral properties

The visible flavin absorption spectra of WT and EE show maxima at 381 nm and 451 nm [26] (Fig. 6A). However, the absorption ratio  $A_{381/451}$  is somewhat higher in WT compared to EE. When the spectrum of WT is corrected for Rayleigh scattering, the spectra of WT and EE completely overlap. This indicates that the microenvironment around the flavin isoalloxazine ring in EE is similar to WT, and that the increased absorption of WT at lower wavelength is related to the formation of soluble aggregates.

In our previous research we showed that *Tt*ProDH is very thermostable and solvent tolerant and that the enzyme only loses secondary structure and activity after long-term incubations above 80 °C [26]. Far-UV CD analysis of WT and EE confirm that the secondary structural properties of both enzyme forms are identical (not shown). The visible CD spectra of WT and EE are also very similar (Fig. 6B). These spectra confirm that the background absorption in

the flavin absorption spectrum of WT is due to the presence of soluble aggregates and that the microenvironment around the flavin isoalloxazine ring in EE has not changed compared to WT.

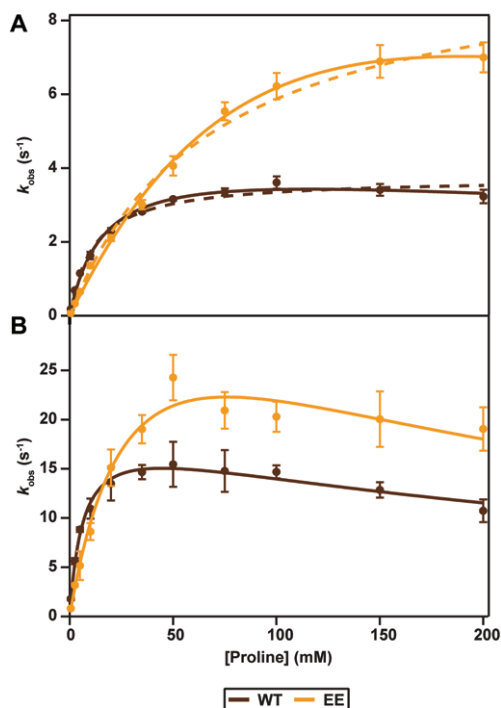


**Figure 6.**

Flavin spectral properties of WT and EE. **(A)** Absorption spectra. The spectrum of WT has been corrected for Rayleigh scattering, resulting in the dotted line. **(B)** Circular dichroism spectra.

### Enzyme activity of MBP-TtProDH

Steady-state kinetic parameters of WT and EE were determined using the proline:DCPIP oxidoreductase assay (Fig. 7 and Table 2). The activity was determined at 25 °C and at 45 °C. 25 °C is the temperature often used for ProDH kinetic measurements in literature. Because TtProDH is a thermophilic enzyme, we increased the temperature to 45 °C, which is more close to its natural physiological condition. We did not increase the temperature further, due to the instability of the MBP-tag [26] and DCPIP at higher temperatures. Both for WT and EE,  $k_{\text{cat}}$  increases when the temperature is raised from 25 °C and 45 °C. Furthermore, both enzymes show a lower  $K_{\text{M}}$  for proline at higher temperature. This leads to a remarkable tenfold increase in catalytic efficiency between 25 and 45 °C. However, from Fig. 7 and Table 2 it can also be inferred that substrate inhibition, observed for both WT and EE, becomes more pronounced at higher temperature. Since substrate inhibition is weak, especially at lower temperatures, the kinetic constants at 25 °C have been determined with the Michaelis-Menten equation as well as with the Haldane equation, the latter taking substrate inhibition into account.

**Figure 7.**

Kinetic data of WT and EE at (A) 25 °C and (B) 45 °C as determined with the proline:DCPIP assay. The dashed lines indicate the fitted curve retrieved from the Michaelis-Menten equation while the solid lines indicate the fitted curve retrieved from the Haldane equation.

**Table 2.**

Kinetic parameters for WT and EE, at 25 °C and 45 °C as determined with the proline:DCPIP assay. The kinetic parameters at 25 °C have been determined both with the Michaelis-Menten and the Haldane equation.

			$k_{cat}$ (s <sup>-1</sup> )	$K_M$ (mM)	$k_{cat} / K_M$ (s <sup>-1</sup> M <sup>-1</sup> )	$K_I$ (mM)
WT	25 °C	Michaelis-Menten	$3.7 \pm 0.1$	$11.5 \pm 1.4$	325	-
	25 °C	Haldane	$4.4 \pm 0.3$	$16.3 \pm 2.2$	269	$825 \pm 308$
	45 °C	Haldane	$19.4 \pm 1.0$	$6.5 \pm 0.9$	2979	$306 \pm 57$
EE	25 °C	Michaelis-Menten	$9.8 \pm 0.5$	$67.6 \pm 8.2$	146	-
	25 °C	Haldane	$20.0 \pm 5.5$	$175.1 \pm 60.3$	114	$206 \pm 110$
	45 °C	Haldane	$42.1 \pm 8.5$	$33.8 \pm 11.6$	1247	$171 \pm 75$

## Discussion

Aggregation through self-association of the native state is regularly observed for proteins produced *in vitro*. We describe the disruption of the self-association of MBP-tagged TtProDH (WT). Using site-directed mutagenesis, we generated the F10E/L12E variant (EE) to increase the polarity of helix  $\alpha$ A.

From analytical gel filtration studies we previously suggested that WT and MBP-clipped TtProDH form mixtures of tetramers and larger aggregates, and that the aggregates can be partially removed by the addition of BOG [26]. In contrast, BOG-treated His-tagged TtProDH was reported to be a mixture of monomers and dimers [21]. Here, we found support from analytical gel filtration and native MS that WT forms, besides aggregates, homotetramers and that replacement of Phe10 and Leu12 with Glu residues completely eliminates the formation of the aggregates. From this we conclude that helix  $\alpha$ A of TtProDH is responsible for the formation of aggregates through self-association. Our present findings also imply that there is a - so far not identified - interaction that leads to the formation of TtProDH tetramers. These tetramers might arise from dimers, of which the latter are formed through interaction between the  $\alpha$ 5 helices of two TtProDH subunits, as deduced from the crystal structure [21].

Tetrameric species are often observed with thermostable enzymes and there are many examples of thermostable enzymes that occur in a higher oligomeric state compared to their mesophilic counterparts [27-32]. Increasing the number of interactions and decreasing the surface to volume ratio contributes to enhanced protein stability [33-37]. For several enzymes with a TIM-barrel fold, it has been shown that the mesophilic enzyme appears as dimer, while the thermophilic enzyme appears as tetramer, assembled as a dimer of dimers [38,39]. Indeed, several ProDHs from mesophilic sources have been described as dimers [23-25].

Unfortunately, we did not obtain a homogeneous preparation of trypsin-treated EE (Fig. 3B). Therefore, at this stage we cannot rule out completely that the tetrameric nature of the MBP-fused enzyme is due to the presence of the bulky protein tag which is close to the hydrophobic patch formed by helices  $\alpha$ A,  $\alpha$ B and  $\alpha$ C (together with the C-terminal helix  $\alpha$ 8). However, the hydrodynamic properties of MBP-clipped TtProDH [26] support that also native TtProDH forms tetramers.

WT and EE show weak substrate binding (Table 2). As a result, high concentrations of proline are needed in the activity assay, giving rise to substrate inhibition (Fig. 7). The steady-state kinetic properties at 25 °C of EE are remarkably different from those of WT. EE has a higher  $k_{cat}$  than WT, but an increased Michaelis constant for the imino acid substrate. This might be related to the self-association of WT, which makes the enzyme more rigid. The change in kinetic parameters might also be caused by the negative charges introduced in helix  $\alpha$ A, which might influence the degree of substrate inhibition.



Since the kinetics of *Tt*ProDH at 25 °C is difficult to interpret, we raised the temperature to 45 °C, which is closer to the natural physiological condition of the *Thermus thermophilus* enzyme. Our results show that the catalytic efficiency of both MBP-*Tt*ProDH variants strongly increases between 25 and 45 °C. This is in line with the idea that conformational flexibility is crucial for optimal enzyme catalysis and that thermostable enzymes are rather stiff at room temperature [37]. At higher temperature, substrate inhibition becomes more pronounced. This seems not related to enzyme aggregation, as it is also observed with EE.

Our results suggest that the hydrophobic N-terminus of *Tt*ProDH is not crucial for the enzyme activity. As stated before, helices  $\alpha$ A,  $\alpha$ B,  $\alpha$ C and  $\alpha$ 8 are assumed to be involved in channeling P5C/GSA between *Tt*ProDH and *Tt*P5CDH [21,22]. Furthermore, *Tt*ProDH is suggested to be membrane-associated [21]. We suggest helix  $\alpha$ A plays an important role in these *in vivo* interactions.

In conclusion, we show that MBP-tagged *Tt*ProDH is a homotetramer and that the tendency of the enzyme to self-associate can be successfully repressed by replacing Phe10 and Leu12 in the N-terminal helix with glutamates. The newly produced homogeneous form of the thermostable enzyme shows proper flavin binding characteristics and excellent catalytic features. Specific removal of the MBP-tag remains challenging and will be a subject of future studies.

### Acknowledgements

We thank Adrie Westphal for technical assistance. We thank Arjan Barendregt (Biomolecular Mass Spectrometry and Proteomics Group, Bijvoet Centre for Biomolecular Research, Utrecht University) for help with ESI-MS. This work was supported by the Netherlands Organization for Scientific Research (NWO) and The Graduate School VLAG (Wageningen, The Netherlands) through the ERA-NET Industrial Biotechnology program (project EIB.10.004) of the European Community.

## References

- [1] Goodsell, D. S. and Olson, A. J., Structural symmetry and protein function. *Annu. Rev. Biophys. Biomol. Struct.* (2000), 29, 105-153.
- [2] Matthews, J. M. and Sunde, M., Dimers, oligomers, everywhere, Protein dimerization and oligomerization in biology, Landes Bioscience and Springer Science+Business Media, 2012, 1-18.
- [3] Ali, M. H. and Imperiali, B., Protein oligomerization: how and why. *Bioorg. Med. Chem.* (2005), 13, 5013-5020.
- [4] Griffin, M. D. W. and Gerrard, J. A., The relationship between oligomeric state and protein function, Protein dimerization and oligomerization in biology, Landes Bioscience and Springer Science+Business Media, 2012, 74-90.
- [5] Hashimoto, K. and Panchenko, A. R., Mechanisms of protein oligomerization, the critical role of insertions and deletions in maintaining different oligomeric states. *Proc. Natl. Acad. Sci. USA* (2010), 107, 20352-20357.
- [6] Marianayagam, N. J., Sunde, M., Matthews, J. M., The power of two: protein dimerization in biology. *Trends Biochem. Sci.* (2004), 29, 618-625.
- [7] Wang, W., Nema, S., Teagarden, D., Protein aggregation - pathways and influencing factors. *Int. J. Pharm.* (2010), 390, 89-99.
- [8] Philo, J. S. and Arakawa, T., Mechanisms of protein aggregation. *Curr. Pharm. Biotechnol.* (2009), 10, 348-351.
- [9] Conte, L. L., Chothia, C., Janin, J., The atomic structure of protein-protein recognition sites. *J. Mol. Biol.* (1999), 285, 2177-2198.
- [10] Janin, J., Miller, S., Chothia, C., Surface, subunit interfaces and interior of oligomeric proteins. *J. Mol. Biol.* (1988), 204, 155-164.
- [11] Jones, S. and Thornton, J. M., Principles of protein-protein interactions. *Proc. Natl. Acad. Sci. USA* (1996), 93, 13-20.
- [12] Miller, S., The structure of interfaces between subunits of dimeric and tetrameric proteins. *Protein Eng.* (1989), 3, 77-83.
- [13] Schwartz, R., Istrail, S., King, J., Frequencies of amino acid strings in globular protein sequences indicate suppression of blocks of consecutive hydrophobic residues. *Protein Sci.* (2001), 10, 1023-1031.
- [14] Chiti, F., Taddei, N., Baroni, F. *et al.*, Kinetic partitioning of protein folding and aggregation. *Nat. Struct. Mol. Biol.* (2002), 9, 137-143.
- [15] Pawar, A. P., DuBay, K. F., Zurdo, J. *et al.*, Prediction of "aggregation-prone" and "aggregation-susceptible" regions in proteins associated with neurodegenerative diseases. *J. Mol. Biol.* (2005), 350, 379-392.
- [16] Richardson, J. S. and Richardson, D. C., Natural  $\beta$ -sheet proteins use negative design to avoid edge-to-edge aggregation. *Proc. Natl. Acad. Sci. USA* (2002), 99, 2754-2759.
- [17] Wang, W. and Hecht, M. H., Rationally designed mutations convert *de novo* amyloid-like fibrils into monomeric  $\beta$ -sheet proteins. *Proc. Natl. Acad. Sci. USA* (2002), 99, 2760-2765.
- [18] Berezovsky, I. N., Zeldovich, K. B., Shakhnovich, E. I., Positive and negative design in stability and thermal adaptation of natural proteins. *PLoS Comp. Biol.* (2007), 3, 498-507.
- [19] Hecht, M. H., Richardson, J. S., Richardson, D. C., Ogden, R. C., *De novo* design, expression, and characterization of Felix: A four-helix bundle protein of native-like sequence. *Science* (1990), 249, 884-891.
- [20] Hellinga, H. W., Rational protein design: combining theory and experiment. *Proc. Nat. Acad. Sci. USA* (1997), 94, 10015-10017.
- [21] White, T. A., Krishnan, N., Becker, D. F., Tanner, J. J., Structure and kinetics of monofunctional proline dehydrogenase from *Thermus thermophilus*. *J. Biol. Chem.* (2007), 282, 14316-14327.
- [22] Sanyal, N., Arentson, B. W., Luo, M., Tanner, J. J., Becker, D. F., First evidence for substrate channeling between proline catabolic enzymes: a validation of domain fusion analysis for predicting protein-protein interactions. *J. Biol. Chem.* (2015), 290, 2225-2234.
- [23] Paes, L. S., Mantilla, B. S., Zimbres, F. M. *et al.*, Proline dehydrogenase regulates redox state and respiratory

- metabolism in *Trypanosoma cruzi*. *PLoS ONE* (2013), 8.
- [24] Tallarita, E., Pollegioni, L., Servi, S., Molla, G., Expression in *Escherichia coli* of the catalytic domain of human proline oxidase. *Protein Expr. Purif.* (2012), 82, 345-351.
- [25] Vinod, M. P., Bellur, P., Becker, D. F., Electrochemical and functional characterization of the proline dehydrogenase domain of the PutA flavoprotein from *Escherichia coli*. *Biochemistry* (2002), 41, 6525-6532.
- [26] Huijbers, M. M. E. and van Berkel, W. J. H., High yields of active *Thermus thermophilus* proline dehydrogenase are obtained using maltose-binding protein as a solubility tag. *Biotechnol. J.* (2015), 10, 395-403.
- [27] Dalhus, B., Saarinen, M., Sauer, U. H. *et al.*, Structural basis for thermophilic protein stability: structures of thermophilic and mesophilic malate dehydrogenases. *J. Mol. Biol.* (2002), 318, 707-721.
- [28] Dams, T., Auerbach, G., Bader, G. *et al.*, The crystal structure of dihydrofolate reductase from *Thermotoga maritima*: molecular features of thermostability. *J. Mol. Biol.* (2000), 297, 659-672.
- [29] Kohlhoff, M., Dahm, A., Hensel, R., Tetrameric triosephosphate isomerase from hyperthermophilic Archaea. *FEBS Lett.* (1996), 383, 245-250.
- [30] Tanaka, Y., Tsumoto, K., Yasutake, Y. *et al.*, How oligomerization contributes to the thermostability of an Archaeon protein - Protein L-isoadipyl-O-methyltransferase from *Sulfolobus tokodaii*. *J. Biol. Chem.* (2004), 279, 32957-32967.
- [31] Thoma, R., Hennig, M., Sterner, R., Kirschner, K., Structure and function of mutationally generated monomers of dimeric phosphoribosylanthranilate isomerase from *Thermotoga maritima*. *Structure* (2000), 8, 265-276.
- [32] Villeret, V., Clantin, B., Tricot, C. *et al.*, The crystal structure of *Pyrococcus furiosus* ornithine carbamoyltransferase reveals a key role for oligomerization in enzyme stability at extremely high temperatures. *Proc. Natl. Acad. Sci. USA* (1998), 95, 2801-2806.
- [33] Kumar, S., Tsai, C., Nussinov, R., Factors enhancing protein thermostability. *Protein Eng.* (2000), 13, 179-191.
- [34] Razvi, A. and Scholtz, J. M., Lessons in stability from thermophilic proteins. *Protein Sci.* (2006), 15, 1569-1578.
- [35] Jaenicke, R. and Böhm, G., The stability of proteins in extreme environments. *Curr. Opin. Struct. Biol.* (1998), 8, 738-748.
- [36] Backmann, J. and Schäfer, G., Thermodynamic analysis of hyperthermostable oligomeric proteins, *Methods Enzymol.*, Vol 334, The Academic Press, 2001, 328-342.
- [37] Vieille, C. and Zeikus, G. J., Hyperthermophilic enzymes: sources, uses, and molecular mechanisms for thermostability. *Microbiol. Mol. Biol. Rev.* (2001), 65, 1-43.
- [38] Maes, D., Zeelen, J. P., Thanki, N. *et al.*, The crystal structure of triosephosphate isomerase (TIM) from *Thermotoga maritima*: a comparative thermostability structural analysis of ten different TIM structures. *Proteins Struct. Funct. Genet.* (1999), 37, 441-453.
- [39] Walden, H., Bell, G. S., Russell, R. J. M. *et al.*, Tiny TIM: a small, tetrameric, hyperthermostable triosephosphate isomerase. *J. Mol. Biol.* (2001), 306, 745-757.







# Chapter 4

## Functional impact of the N-terminal arm of proline dehydrogenase from *Thermus thermophilus*

*Manuscript submitted*

Mieke M.E. Huijbers<sup>1</sup>

Ilona van Alen<sup>1</sup>

Jenny W. Wu<sup>1</sup>

Arjan Barendregt<sup>2,3</sup>

Albert J.R. Heck<sup>2,3</sup>

Willem J.H. van Berkel<sup>1</sup>

<sup>1</sup> Laboratory of Biochemistry, Wageningen University & Research, Stippeneng 4, 6708 WE Wageningen, the Netherlands

<sup>2</sup> Biomolecular Mass Spectrometry and Proteomics, Bijvoet Center for Biomolecular Research and Utrecht Institute of Pharmaceutical Sciences, Utrecht University, Padualaan 8, 3584 Utrecht, The Netherlands

<sup>3</sup> Netherlands Proteomics Center, Padualaan 8, 3584 Utrecht, The Netherlands





## Abstract

Proline dehydrogenase (ProDH) is a ubiquitous flavoenzyme that catalyzes the oxidation of proline to  $\Delta^1$ -pyrroline-5-carboxylate, the initial step in proline catabolism. *Thermus thermophilus* ProDH (TtProDH) is composed of a distorted TIM-barrel and three N-terminal helices,  $\alpha$ A,  $\alpha$ B and  $\alpha$ C, of which the function is not well understood. Here we report the characterization of the helical arm-truncated variants  $\Delta$ A,  $\Delta$ AB and  $\Delta$ ABC. All three truncated variants, expressed as N-terminal fusions with maltose-binding protein, show similar flavin spectral properties, indicative of a conserved microenvironment of their active sites.  $\Delta$ A and  $\Delta$ AB are highly active tetramers that rapidly react with the suicide inhibitor *N*-propargylglycine. Removal of the complete N-terminal arm ( $\Delta$ ABC) results in poorly active dimers that are not capable of forming a flavin adduct with *N*-propargylglycine. The catalytic and hydrodynamic properties of single variants V32D and V36D show that disrupting a hydrophobic patch between helix  $\alpha$ C and  $\alpha$ 8 also leads to dimer formation, loss of activity and decreased reactivity with *N*-propargylglycine. Together, this substantiates that helix  $\alpha$ C is crucial for TtProDH catalysis and tetramerization through positioning of helix  $\alpha$ 8.

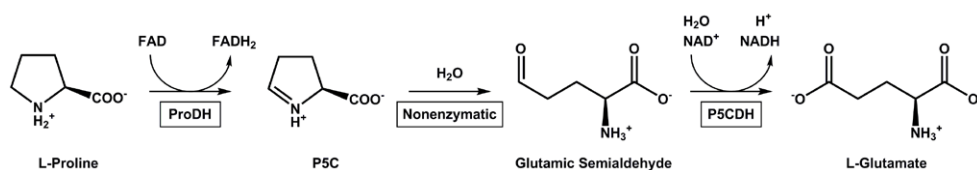
## Keywords

flavoprotein, proline dehydrogenase, protein oligomerization, suicide inhibition, TIM-barrel



## Introduction

Proline dehydrogenase (ProDH; EC 1.5.5.2) is a ubiquitous enzyme involved in proline catabolism. ProDH catalyzes the flavin adenine dinucleotide (FAD)-dependent oxidation of L-proline to  $\Delta^1$ -pyrroline-5-carboxylate (P5C). After P5C hydrolysis, the resulting glutamic semialdehyde (GSA) is oxidized to glutamate by  $\Delta^1$ -pyrroline-5-carboxylate dehydrogenase (P5CDH; EC 1.2.1.88) (Scheme 1). ProDH and P5CDH exist as separate monofunctional enzymes in eukaryotes and some bacteria, but are fused into a bifunctional enzyme in other bacteria [1]. In this two-component enzyme, called proline utilization A (PutA), the C-terminus of ProDH is fused to P5CDH, allowing channeling of the P5C/GSA intermediate between the enzymes [2-6].



**Scheme 1.**

Conversion of L-proline to L-glutamate by ProDH and P5CDH.

ProDH has a distorted  $(\beta\alpha)_8$  TIM-barrel fold (Fig. 1A), which is conserved throughout the PutA/ProDH family [7,8]. Opposed to the classic TIM-barrel fold, the ProDH barrel begins with a helix ( $\alpha_0$ ) rather than a strand (Fig. 1). This extra helix occupies the location that is normally reserved for  $\alpha_8$ . As a consequence,  $\alpha_8$  is not located alongside  $\beta_8$ , but on top of the barrel [1,9,10]. The distorted location of  $\alpha_8$  is crucial for catalysis, since it contributes three strictly conserved residues (Tyr-x-x-Arg-Arg) that interact with the substrate [9,10].

The N-terminal sequence of ProDH is poorly conserved. Monofunctional eukaryotic ProDHs, including the human enzyme [11], have an elongated N-terminus compared to monofunctional bacterial ProDHs [7,8]. ProDH from *Thermus thermophilus* (TtProDH) contains an N-terminal arm consisting of three helices:  $\alpha_A$ ,  $\alpha_B$  and  $\alpha_C$  (Fig. 1). Helix  $\alpha_8$  fits into the cleft which is formed by helices  $\alpha_A$ ,  $\alpha_B$  and  $\alpha_C$  and together they form a hydrophobic patch. This patch is assumed to be involved in channeling P5C/GSA between TtProDH and TtP5CDH [1,12].

Previously, we showed that TtProDH is overproduced in *E. coli* when its N-terminus is fused to maltose-binding protein (MBP). Although fully active, MBP-TtProDH is prone to non-native self-association [13]. Replacing Phe10 and Leu12 in helix  $\alpha_A$  with Glu residues successfully eliminated this aggregation behavior, yielding homogeneous MBP-TtProDH tetramers [14].

To investigate the functional impact of the N-terminal arm of *Tt*ProDH in further detail, we constructed three MBP-fused variants, lacking respectively one ( $\Delta A$ ), two ( $\Delta AB$ ), or three ( $\Delta ABC$ ) N-terminal helices. The hydrodynamic and catalytic properties of these arm-truncated variants were explored and compared to those of MBP-*Tt*ProDH F10E/L12E (EE). In addition, we addressed the properties of site-directed variants V32D, Y35F and V36D, all situated in helix  $\alpha C$ , to probe the interaction between helix  $\alpha C$  and helix  $\alpha 8$ .

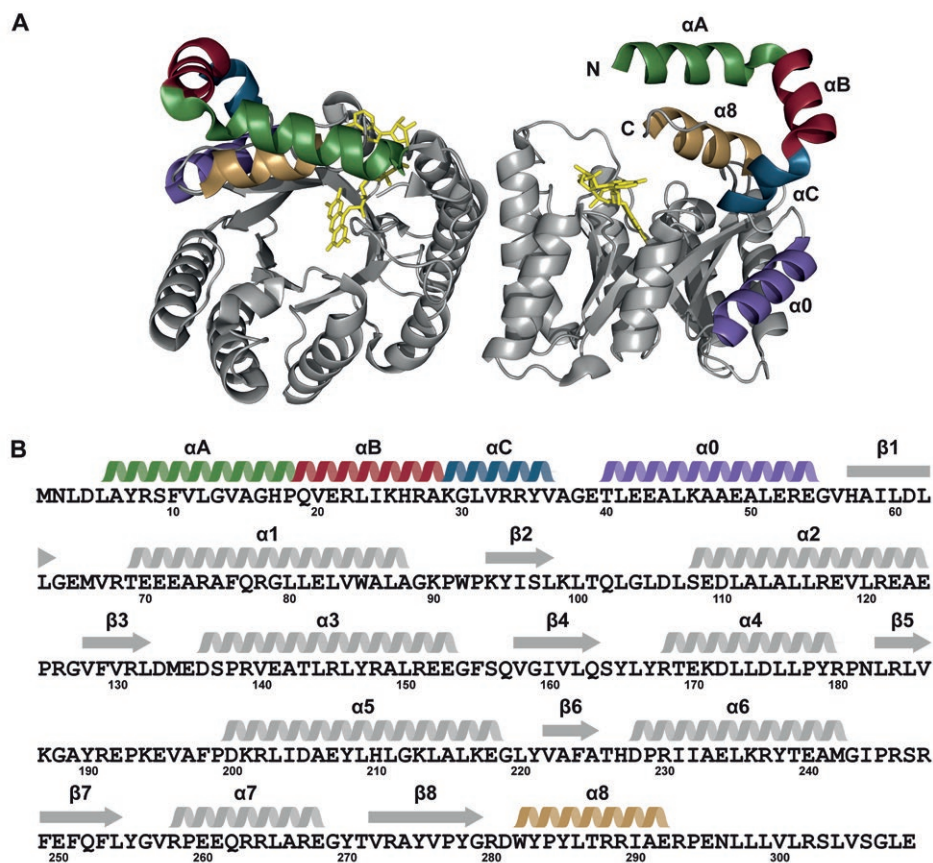


**Figure 1.**

Structural features of *Tt*ProDH. (A) Three-dimensional model of the crystal structure of the *Tt*ProDH dimer (PDB entry 2G37). The N-terminal helices  $\alpha A$  (green),  $\alpha B$  (red) and  $\alpha C$  (blue) are indicated, as well as helix  $\alpha 0$  (purple) and the C-terminal helix  $\alpha 8$  (brown). (B) Amino acid sequence of *Tt*ProDH. Secondary structural elements on top of the sequence have the same colors as in Fig. 1A.

## Materials and Methods

### Construction of MBP-*TtProDH* variants

Three N-terminally shortened MBP-fused variants were constructed; each variant was shortened with one additional N-terminal helix. To amplify the DNA, pBAD-MBP-*TtProDH* [14] was used as template DNA. The primers listed in Table 1 were used for amplification. Using *EcoRI* and *HindIII* restriction sites, the amplified fragments were introduced into a pBAD-MBP vector, which resulted in N-terminal fusions of the *TtProDH* variants to MBP. The resulting constructs MBP-*TtProDH*  $\Delta A$ , MBP-*TtProDH*  $\Delta AB$  and MBP-*TtProDH*  $\Delta ABC$  were verified by automated sequencing of both strands (Macrogen) and the plasmids were transformed to *E. coli* TOP10 host cells for recombinant expression.

The obtained plasmid for MBP-*TtProDH*  $\Delta AB$  was used as a template to construct point mutations in helix  $\alpha C$ . V32D, Y35F and V36D were constructed using the procedure described earlier [14], with the exception that in this case both a forward and a reverse primer were used (Table 1).

**Table 1.**

Oligonucleotides used for the construction of the various MBP-*TtProDH* variants. For the helix  $\alpha C$  variants, codon changes are underlined.

Variant	Oligonucleotide sequence (5' to 3')
$\Delta A$ , forward	AATTAGAATTCAGGTTGAACGTCTGATTAAACATCGTGCAAAAGG
$\Delta AB$ , forward	AATTAGAATTCAAAGGTCTGGTTCGTCGTTATGTTGCCGGTG
$\Delta ABC$ , forward	AATTAGAATTCGAAACCCTGGAAGAAGCACTGAAAGCAG
$\Delta A$ , $\Delta AB$ , $\Delta ABC$ , reverse	GCCCAAGCTTTTATTCTAGACCGCTAACCAGGC
$\Delta AB$ , V32D, forward*	CGAGGGAAGGATTCAGAATTCAAAGGTCTG <u>GAT</u> CGTCGTTATGTTGCCGGTGAAACCCTGG
$\Delta AB$ , Y35F, forward*	CGAGGGAAGGATTCAGAATTCAAAGGTCTGGTTCGTCG <u>TTT</u> GTTGCCGGTGAAACCCTGG
$\Delta AB$ , V36D, forward*	CGAGGGAAGGATTCAGAATTCAAAGGTCTGGTTCGTCGTTAT <u>GAT</u> GCCGGTGAAACCCTGG

\* As a reverse primer, the complement reverse sequence of the forward primer was used.

### Expression and purification of MBP-*TtProDH* variants

The MBP-*TtProDH* variants were purified following a previously described procedure [14]. In short, the variants were produced in *E. coli* TOP10 cells and purified using amylose affinity and anion-exchange chromatography.

## Protein analysis

Enzyme purity was checked with sodium dodecyl sulfate polyacrylamide gel electrophoresis (SDS-PAGE). 10% polyacrylamide slab gels were used and the proteins were stained with Coomassie Brilliant Blue R-250. 0.5  $\mu\text{g}$  of purified N-terminal variants was loaded per lane. As a molecular weight marker, Precision Plus Protein Standard (Biorad) was used.

## Analytical gel filtration

The hydrodynamic properties of the MBP-TtProDH variants were analyzed by size exclusion chromatography as described previously [14]. In addition, 20  $\mu\text{M}$  EE and 20  $\mu\text{M}$   $\Delta\text{ABC}$  in 50 mM sodium phosphate, pH 7.4 were mixed, incubated at room temperature overnight and subsequently analyzed by size exclusion chromatography.

## ESI-MS

The native and denatured masses of the MBP-TtProDH variants were determined using nanoflow electrospray ionization mass spectrometry (ESI-MS) according to a previously established procedure [13,14], whereby the settings were optimized for the current application. Source backing pressure was increased to 7.8 mbar and the cone voltage was varied between 100-150 V.

## Spectral analysis

Far-UV circular dichroism (CD) spectra of the MBP-TtProDH variants were recorded as described before [13]. 1  $\mu\text{M}$  samples were prepared in 50 mM sodium phosphate, pH 7.4. Optical flavin absorption spectra of the MBP-TtProDH variants were recorded as has been described previously [14].

## Enzyme activity

Enzyme activity of the MBP-TtProDH variants was determined at 25 °C on a Hewlett Packard 8453 diode array spectrophotometer using the proline:dichlorophenolindophenol (DCPIP) oxidoreductase assay [13]. For the standard assay, catalytic amounts of enzyme were added to a 600  $\mu\text{L}$  reaction mixture containing 65  $\mu\text{M}$  DCPIP and 100 mM L-proline in 50 mM sodium phosphate, pH 7.4. Steady-state kinetic parameters were determined at 25 °C, essentially as described previously [14].

Proline oxidase activity of the MBP-TtProDH variants was determined at 25 °C in air-saturated 50 mM sodium phosphate, pH 7.4, containing 3.5 - 7.5  $\mu\text{M}$  enzyme, using a Hansatech Oxytherm system (Hansatech Instruments). Reactions were started by the addition of 100 mM L-proline.

### Inactivation with *N*-propargylglycine

The synthesis of *N*-propargylglycine was based on a procedure described before [15]. A clear solution of iodoacetic acid (1.05 g, 5.6 mmol) and *N*-propargylamine (2.6 g, 47 mmol) was refluxed in 50 mL aqueous ethanol for 24 h. The dark mixture was cooled to room temperature and the solvent was removed *in vacuo*. The crude product was precipitated from 1:1 ethanol:ethyl acetate. Recrystallization from aqueous ethanol and ethyl acetate and final drying under high vacuum yielded the *N*-propargylglycine as a white solid (28 mg, 4%).  $^1\text{H}$  NMR (DMSO- $d_6$ ):  $\delta$  = 3.42 (d, 2H,  $J$ =2.4 Hz), 3.24 (s, 2H), 3.16 (t, 1H,  $J$ =2.4 Hz).

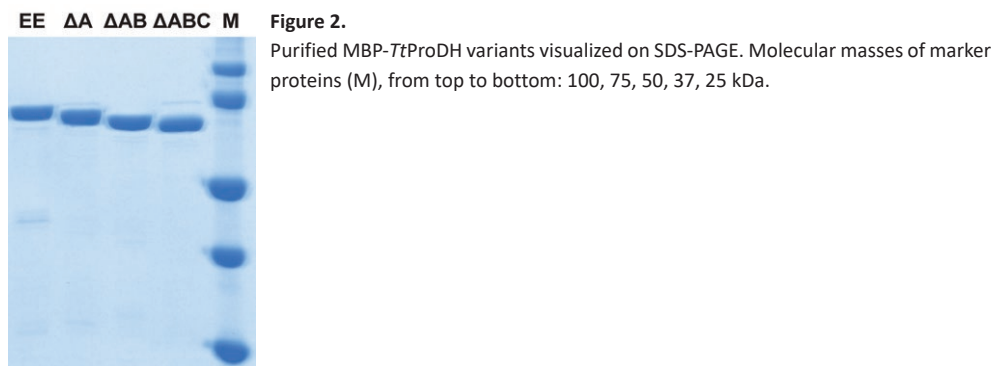
Spectral changes associated with the reaction of TtProDH with *N*-propargylglycine were monitored at 25 °C on a Hewlett Packard 8453 diode array spectrophotometer. A fresh stock solution of 75 mM *N*-propargylglycine was prepared in 50 mM sodium phosphate, pH 7.4. 40  $\mu\text{M}$  of the MBP-TtProDH variants in 50 mM sodium phosphate, pH 7.4 was incubated with a final concentration of 2.5 mM *N*-propargylglycine. Immediately after the addition of *N*-propargylglycine, the first spectrum was recorded. Subsequent spectra were recorded at 1 min intervals for 90 min. Before and after the incubation of the enzyme variants with *N*-propargylglycine, 10  $\mu\text{L}$  aliquots were removed from the cuvette and the enzyme activity was determined with the standard assay. Activity measurements were performed in triplicate.

## Results

### Protein expression and purification

MBP-*Tt*ProDH EE,  $\Delta A$ ,  $\Delta AB$  and  $\Delta ABC$  were overproduced in *E. coli* TOP10 cells. From 1 L of culture about 200-250 mg of each variant was purified, yields that we have described before for the heterologous production of MBP-*Tt*ProDH [13,14]. From SDS-PAGE analysis of the purified enzymes it can be appreciated that sequential removal of three helices results in a gradual decrease of subunit molecular mass (Fig. 2).

Previously we demonstrated that removal of the MBP fusion tag with trypsin does not significantly affect the spectral and catalytic properties of the enzyme [13]. As found with EE [14], trypsinolysis of the arm-truncated variants did not result in homogeneous preparations. Therefore, we used the MBP-fused variants for further studies.



### Spectral properties

The far-UV CD spectra of EE and the N-terminal variants are very similar (Fig. 3A) and comparable to that of WT [13]. The visible flavin absorption spectra of EE and the arm-truncated variants (Fig. 3B) are also nearly identical to that of WT [13,14], except that the lowest energy absorption band of  $\Delta ABC$  has shifted about 2 nm to higher wavelengths. These data support that there are no major structural changes and that deletion of the N-terminal helices does not significantly alter the microenvironment of the flavin isoalloxazine ring.

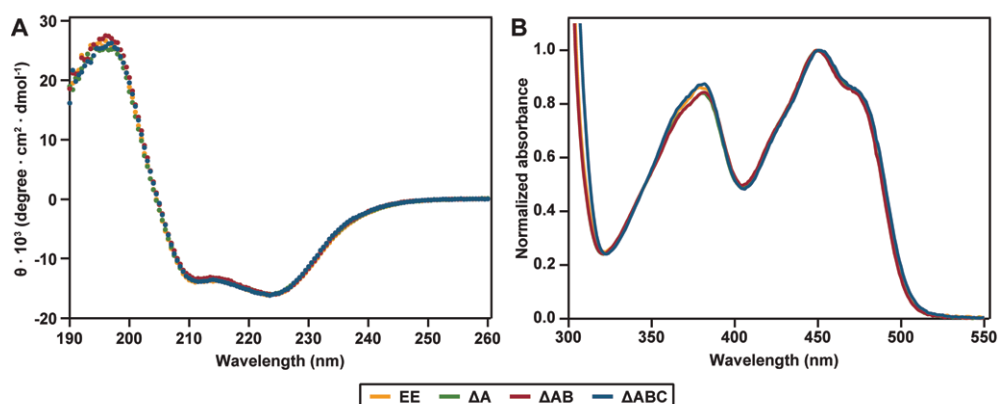


Figure 3.

Spectral properties of EE,  $\Delta A$ ,  $\Delta AB$  and  $\Delta ABC$ . (A) Far-UV CD spectra. (B) Visible flavin absorption spectra.

### Hydrodynamic properties

Due to its more polar N-terminal helix, EE purifies as a tetramer and does not aggregate as MBP-*TtProDH* wildtype (WT) does in solution [13,14]. The truncated variants  $\Delta A$  and  $\Delta AB$  also form tetramers as indicated by size exclusion chromatography (Fig. 4A).  $\Delta ABC$  elutes mainly as a dimer (Fig. 4A), suggesting that  $\alpha C$  plays a role in the tetramerization process.

Mixing of EE and  $\Delta ABC$  followed by analytical gel filtration reveals two separate peaks, a peak for the tetrameric species of EE and a peak for the dimeric species of  $\Delta ABC$  (Fig. 4B). This indicates that mixing of the two enzyme forms does not lead to protein aggregation. Moreover, SDS-PAGE of the gel filtration fractions shows that no subunit exchange occurs (inset Fig. 4B).

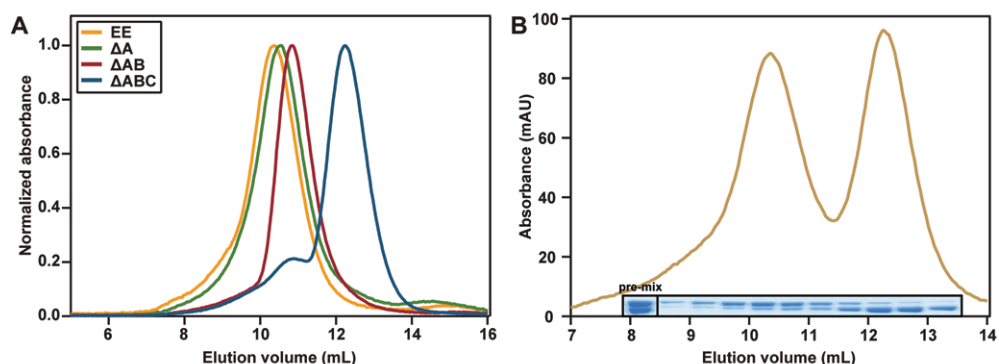


Figure 4.

Hydrodynamic properties of EE,  $\Delta A$ ,  $\Delta AB$  and  $\Delta ABC$  as monitored by Superdex 200 size-exclusion chromatography. (A) Elution pattern of the MBP-*TtProDH* variants. (B) Hydrodynamic properties of EE and  $\Delta ABC$ , mixed in equal amounts and equilibrated at room temperature overnight. SDS-PAGE of the gel filtration fractions is also shown.



Additional information about the oligomeric state of the different variants was obtained by native mass spectrometry. The estimated masses (Table 2) confirm that  $\Delta A$  and  $\Delta AB$  exist predominantly as tetramers, and  $\Delta ABC$  as dimer. With  $\Delta ABC$ , low amounts of tetramers are present, in agreement with the analytical gel filtration results (Fig. 4A). For  $\Delta A$  and  $\Delta AB$ , also some dimers are observed with native mass spectrometry, and for  $\Delta ABC$  monomers, although their abundance is rather low. Denaturing the different complexes enabled an accurate mass measurement of the individual subunits (Table 2). These masses show that all variants exist of identical subunits.

The experimental masses of native and denatured  $\Delta ABC$  do not correspond with the predicted masses. The observed species appears to be C-terminally truncated. Based on the estimated mass, cleavage occurs before Arg288, leading to the removal of a part of the C-terminal tail with sequence (288-RRIAERPENLLVLRSLVSGLE-309). This truncated form has a predicted subunit mass of 71884.9 Da, close to the measured mass of 71899.3 Da.

**Table 2.**

Molecular masses of EE,  $\Delta A$ ,  $\Delta AB$  and  $\Delta ABC$  as determined by native and denatured ESI-MS. Both predicted (Pred.) as well as experimental (Exp.) masses are given in kDa with experimental errors less than 0.01%. For calculation of the predicted native masses, it has been taken into account that each subunit contains a non-covalently bound FAD cofactor (molecular mass 786 Da).

	Native						Denatured	
	Tetramer		Dimer		Monomer			
	Pred.	Exp.	Pred.	Exp.	Pred.	Exp.	Pred.	Exp.
<b>MBP-<i>Tt</i>ProDH EE*</b>	317.8	319.6	158.9	158.9	79.5	-	78.7	78.7
<b>MBP-<i>Tt</i>ProDH <math>\Delta A</math></b>	310.1	311.3	155.0	154.9-155.7	77.5	-	76.7	76.8
<b>MBP-<i>Tt</i>ProDH <math>\Delta AB</math></b>	305.1	307.6-307.8	152.6	152.6-153.7	76.3	-	75.5	75.5
<b>MBP-<i>Tt</i>ProDH <math>\Delta ABC</math></b>	300.7	290.0-290.7	150.4	145.0-146.0	75.2	71.9-72.7	74.4	71.9
<b>MBP-<i>Tt</i>ProDH <math>\Delta AB</math> V32D</b>	305.2	296.2-304.4	152.6	146.5-149.0	76.3	73.0-76.0	75.5	73.0 75.5
<b>MBP-<i>Tt</i>ProDH <math>\Delta AB</math> Y35F</b>	305.1	307.4	152.5	152.3-152.9	76.3	-	75.5	73.0
<b>MBP-<i>Tt</i>ProDH <math>\Delta AB</math> V36D</b>	305.2	296.2	152.6	151.1-151.9	76.3	-	75.5	73.0 75.5

\* As determined previously [14].

## Catalytic properties

Fig. 5 presents an overview of the steady-state kinetic properties of the MBP-*Tt*ProDH variants. The kinetic parameters derived from these experiments are summarized in Table 3. The proline  $K_M$  values of EE,  $\Delta A$ ,  $\Delta AB$  and  $\Delta ABC$  are comparable. However,  $\Delta A$  and  $\Delta AB$  have a slightly higher activity than EE and  $\Delta ABC$  is almost inactive. From these data it is clear that

$\alpha$ A and  $\alpha$ B are not required for optimal activity. Further deletion of helix  $\alpha$ C, on the other hand, seems critical for catalysis.

Since TtProDH has a low but significant proline oxidase activity [1], it was of interest to address the oxygen reactivity of the N-terminal arm variants. For all variants described above, micromolar concentrations of enzyme were needed to reliably measure consumption of oxygen, and very low specific activities were observed (Table 3). Nevertheless, these data confirm that removal of the complete N-terminal arm ( $\Delta$ ABC) also impairs the proline oxidase activity of MBP-TtProDH.

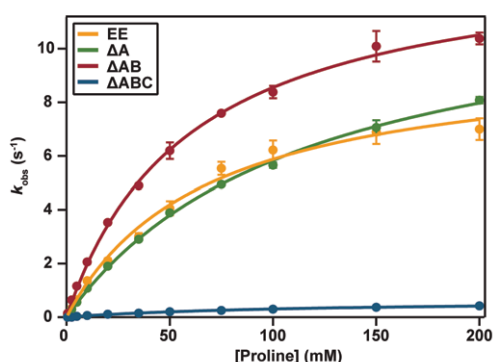


**Figure 5.**

Steady-state kinetics of EE,  $\Delta$ A,  $\Delta$ AB and  $\Delta$ ABC as determined with the proline:DCPIP assay. The fitted curves are retrieved from non-linear regression analysis applying the Michaelis-Menten equation.

**Table 3.**

Kinetic parameters of the MBP-TtProDH variants at 25 °C, pH 7.4 as determined with the proline:DCPIP oxidoreductase assay, using proline as the variable substrate, and specific activities of the MBP-TtProDH variants as determined by the proline:O<sub>2</sub> assay, at a concentration of 100 mM proline.

	Proline:DCPIP assay			Proline:O <sub>2</sub> assay
	$K_M$ (mM)	$k_{cat}$ (s <sup>-1</sup> )	$k_{cat}/K_M$ (s <sup>-1</sup> M <sup>-1</sup> )	Specific activity (mU/mg)
MBP-TtProDH EE*	68 ± 8	9.8 ± 0.5	146	266 ± 12
MBP-TtProDH $\Delta$ A	116 ± 5	12.6 ± 0.3	109	405 ± 15
MBP-TtProDH $\Delta$ AB	60 ± 3	13.6 ± 0.3	229	228 ± 8
MBP-TtProDH $\Delta$ ABC	116 ± 11	0.6 ± 0.02	6	20 ± 1
MBP-TtProDH $\Delta$ AB V32D	309 ± 25	3.2 ± 0.2	10	265 ± 4
MBP-TtProDH $\Delta$ AB Y35F	161 ± 29	14.1 ± 1.5	88	388 ± 5
MBP-TtProDH $\Delta$ AB V36D	189 ± 27	0.3 ± 0.03	1.6	21 ± 1

\* As determined previously [14].

## Reaction with *N*-propargylglycine

*TtProDH* is irreversibly inactivated by the suicide inhibitor *N*-propargylglycine [16]. Inactivation involves the initial oxidation of *N*-propargylglycine to *N*-propargyliminoglycine and the subsequent formation of a bicovalent linkage between flavin N(5) and the  $\epsilon$ -amino group of Lys99 (Fig. 6C). This residue is located in the loop between  $\beta 2$  and  $\alpha 2$  and involved in binding the carboxylic moiety of proline [1]. Upon reaction with *N*-propargylglycine the absorption maximum of *TtProDH* at 450 nm disappears, while the maximum around 380 nm gradually increases. Furthermore, the peak at 380 nm shifts to longer wavelengths. This behavior is indicative of the initial reduction of the flavin and the subsequent formation of the covalent Lys99-FAD adduct [16,17]. After reaction with *N*-propargylglycine, the enzyme is locked in the reduced state.

To probe the catalytic features of the MBP-*TtProDH* variants in further detail, we investigated the reactivity of EE and the arm-truncated variants with *N*-propargylglycine. Fig. 6A shows that all variants except  $\Delta ABC$  form a covalent flavin adduct, and that the reactions result in similar absorption changes as observed before with *TtProDH* [16]. However, a more careful analysis of the kinetics of the reactions reveals significant differences.

For EE,  $\Delta A$  and  $\Delta AB$ , flavin reduction and adduct formation are clearly observed (Fig. 6A). Reduction of EE by *N*-propargylglycine is relatively slow as evidenced from the time-dependent decrease in absorption at 450 nm. Flavin reduction is immediately followed by covalent adduct formation as evidenced from the absorbance increase around 380 and 405 nm. Variants  $\Delta A$  and  $\Delta AB$  reveal an increased rate of reduction compared to EE. This corresponds with the increased  $k_{\text{cat}}$  values for these variants (Table 3). The peak at 380 nm shows a red shift to 385 nm for EE and to 388 nm for  $\Delta A$  and  $\Delta AB$ . Furthermore, both for  $\Delta A$  and  $\Delta AB$ , the increase in absorbance around 388 nm is more pronounced.

$\Delta ABC$  shows neither flavin reduction nor formation of a flavin adduct (Fig. 6A). However, a slow rise in absorption with a maximum at 290 nm is observed in the near-UV region, pointing to the conversion of *N*-propargylglycine to *N*-propargyliminoglycine. Activity measurements with DCPIP suggest that *N*-propargylglycine indeed is a poor substrate for  $\Delta ABC$  (data not shown).

Activity of the different enzyme variants before and after incubation with 2.5 mM of *N*-propargylglycine was measured (Fig. 6B). For EE, residual activity after 90 min of incubation with the inhibitor is about 13%. For  $\Delta A$  and  $\Delta AB$  the activity loss is even more pronounced, in good agreement with the spectral results. The residual activity of  $\Delta ABC$  after 90 min incubation with *N*-propargylglycine is rather low (Fig. 6B).

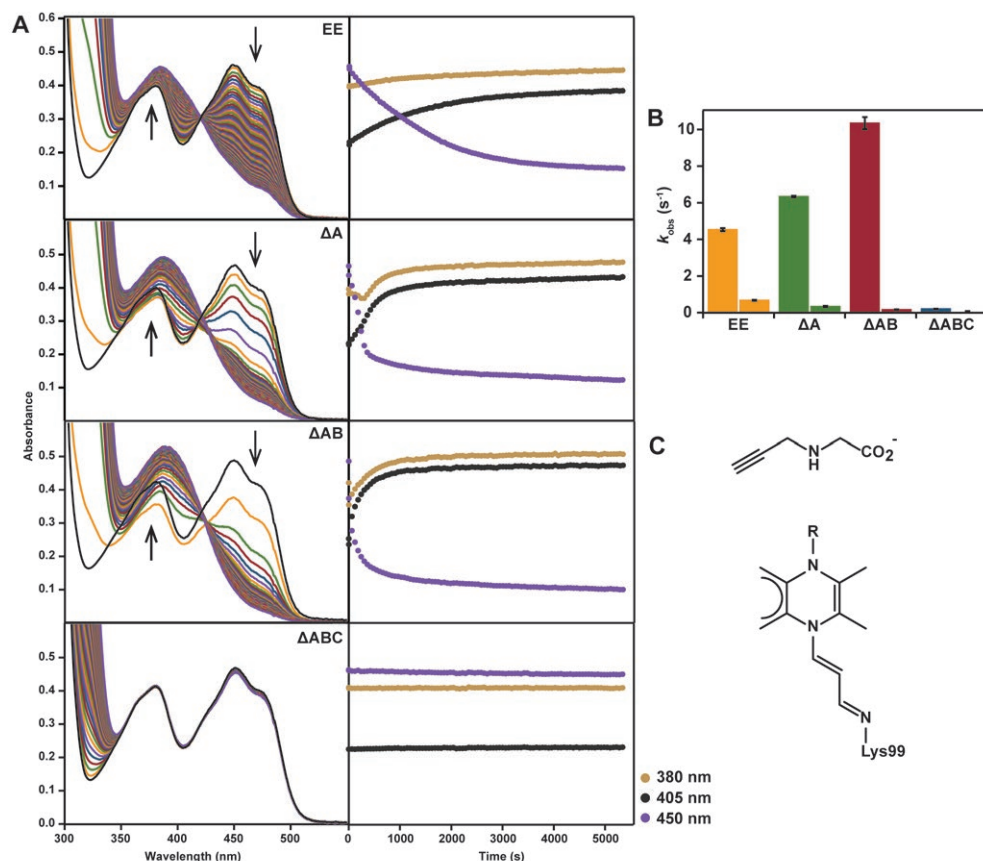


**Figure 6.**

Reactivities of the N-terminal arm TtProDH variants with N-propargylglycine. (A) Left: absorption spectral changes of the variants upon incubation with N-propargylglycine. The black line indicates the spectrum before the addition of N-propargylglycine. Spectra were recorded at 1 min intervals for 90 min. Right: absorbance changes of the variants upon incubation with N-propargylglycine followed at 380, 405 and 450 nm. (B) Activity of the different enzyme variants before and after incubation with N-propargylglycine. (C) Chemical structure of N-propargylglycine and the covalent Lys99-FAD adduct.

### Interactions between helix $\alpha C$ and $\alpha 8$

$\Delta ABC$  is produced as a catalytically impaired dimer. In addition, this MBP-TtProDH variant is truncated at its C-terminal helix  $\alpha 8$ . This suggests that helix  $\alpha C$  is important for the stabilization of helix  $\alpha 8$ . The three-dimensional model of the crystal structure of TtProDH suggests that there is a hydrogen bond between Tyr35 of  $\alpha C$  and Glu295 of  $\alpha 8$  (Fig. 7). Glu295 is part of the sequence that is cleaved off in  $\Delta ABC$ . To investigate whether the Tyr-Glu interaction is important for stabilization of helix  $\alpha 8$ , we changed Tyr35 to Phe. In addition, there is a hydrophobic patch between helix  $\alpha C$  and  $\alpha 8$  (Fig. 7). To examine the importance

of this patch for the stabilization of helix  $\alpha 8$ , Val32 and Val36 individually were changed into Asp. The single amino acid substitutions were introduced in MBP-7tProDH  $\Delta$ AB, since this variant is fully active and forms stable tetramers. In this way we only look at the interaction between helix  $\alpha$ C and  $\alpha 8$  without possible interference of helix  $\alpha$ A and  $\alpha$ B.

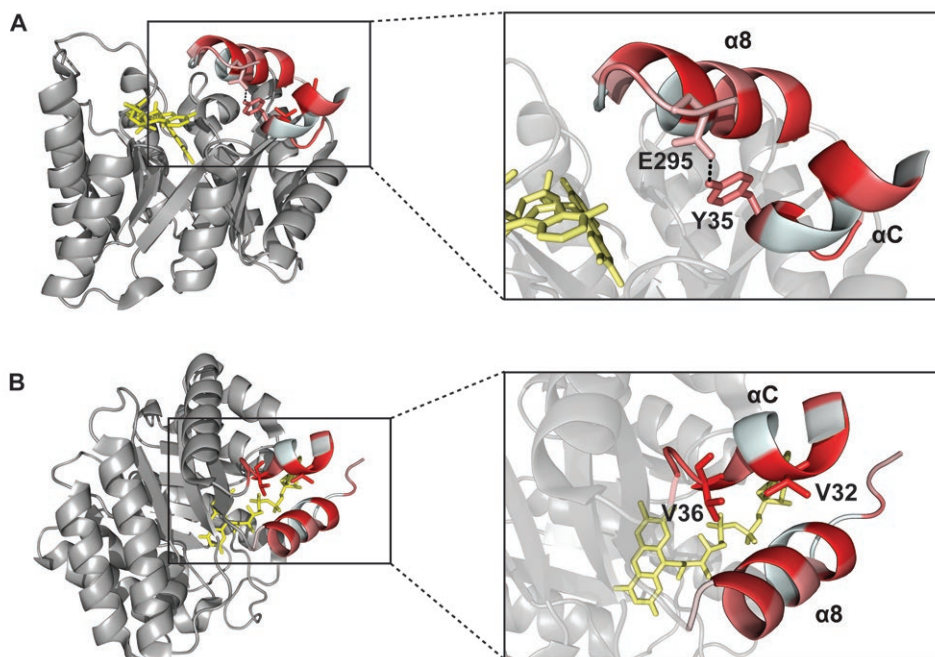


**Figure 7.**

Interactions between helix  $\alpha$ C and helix  $\alpha 8$ . The intensity of the red color is correlated to the hydrophobicity of the residue. Helices  $\alpha$ C and  $\alpha 8$  are colored by hydrophobicity, the remaining part of the catalytic domain is shown in gray and the FAD cofactor is shown in yellow. (A) Ion pair Tyr35 ( $\alpha$ C) and Glu295 ( $\alpha 8$ ). (B) Hydrophobic patch between  $\alpha$ C and  $\alpha 8$  with Val32 ( $\alpha$ C) and Val36 ( $\alpha 8$ ) indicated.

The far-UV CD spectra of V32D, Y35F and V36D (Fig. 8A) are identical to the far-UV CD-spectra of the N-terminal variants (Fig. 3A). The visible flavin absorption properties of the  $\Delta$ AB variants show that the low energy absorption bands of V32D and V36D have shifted about 2 nm to higher wavelength, compared to those of  $\Delta$ AB and Y35F (Fig. 3B and 8B). Thus, the flavin absorption properties of V32D and V36D resemble those of  $\Delta$ ABC (Fig. 3B).

Size exclusion chromatography of Y35F indicates that substitution of Tyr35 with Phe does not affect the tetrameric nature of  $\Delta$ AB (Fig. 8C). Therefore, this interaction does not seem critical for stabilization of helix  $\alpha 8$ . However, V32D and V36D elute much later than Y35F, suggesting that these variants mainly form dimers (Fig. 8C). Native MS of Y35F confirms the presence of tetramers. Furthermore, V32D and V36D are present both as tetramers and

dimers (Table 2). The mass of denatured Y35F shows the presence of identical subunits, while V32D and V36D show two subunit masses, of which one corresponds with the predicted mass (Table 2). The differences between the subunit masses suggest that both V32D and V36D are partially intact and partially cleaved before R288 (predicted mass 73001.2 Da), indicating flexibility and instability of helix  $\alpha 8$ .

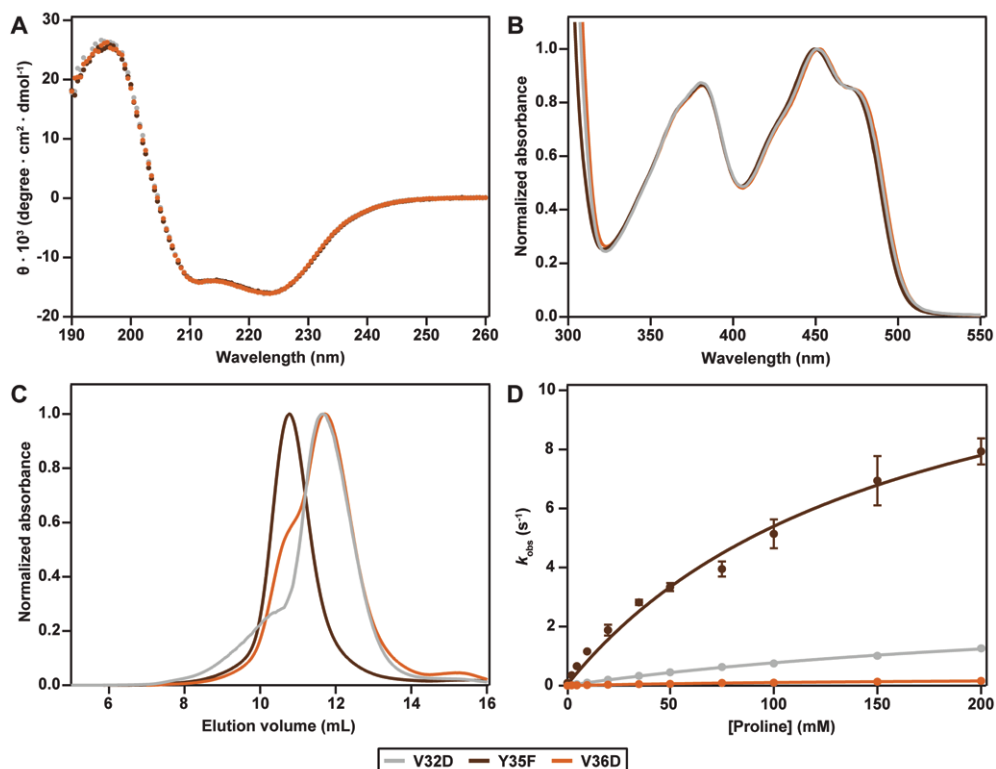


**Figure 8.**

Properties of helix  $\alpha C$  variants. (A) Far-UV CD spectra. (B) Visible flavin absorption spectra. (C) Hydrodynamic properties as monitored by Superdex 200 size-exclusion chromatography. (D) Steady-state kinetic data as determined with the proline:DCPIP assay.

Analysis of the catalytic properties of Y35F confirms that the interaction between Tyr35 and Glu295 is not crucial for the functioning of TtProDH (Fig. 8D). The minor decrease in catalytic efficiency compared to  $\Delta AB$  mainly results from a slight increase in  $K_M$  for the proline substrate (Table 3). V32D and V36D, on the other hand, are poorly active (Fig. 8D). With these variants, a considerable decrease in catalytic efficiency is observed (Table 3). Oxidase activity of especially V36D is very low (Table 3), as found with  $\Delta ABC$ .



The catalytic features of the helix  $\alpha$ C variants were investigated in more detail by probing their reactivity with the suicide inhibitor *N*-propargylglycine (Fig. 9). For Y35F (Fig. 9A), the rates for flavin reduction and adduct formation are similar as found for  $\Delta$ AB (Fig. 6A). For V32D, flavin reduction and adduct formation are also observed (Fig. 9A), but these processes are much slower than for  $\Delta$ AB. The flavin prosthetic group of V36D is not reduced by *N*-propargylglycine and the typical absorption increase around 380 nm, indicative for adduct formation, is also not observed (Fig. 9A). However, as for  $\Delta$ ABC, a slow rise in absorption occurs in the region 300–350 nm, pointing to the conversion of *N*-propargylglycine to *N*-propargyliminoglycine.

All helix  $\alpha$ C variants lose activity when treated with *N*-propargylglycine. After incubation for 90 min, Y35F is almost completely inactivated, but V32D and V36D retain 30% and 63% of their original activity (Fig. 9B).

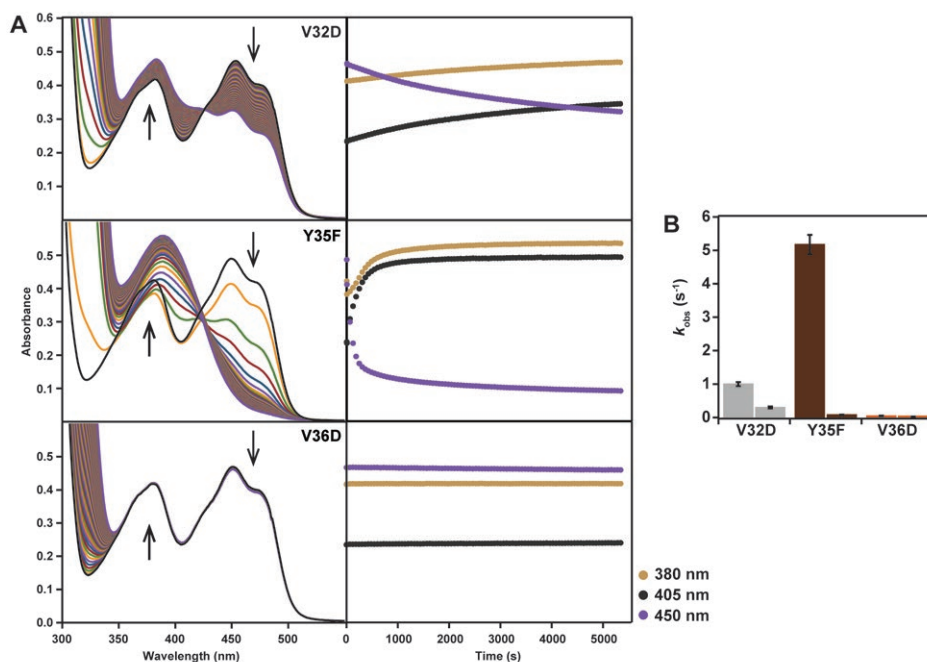


**Figure 9.**

Reactivities of helix  $\alpha$ C TtProDH variants with *N*-propargylglycine. (A) Left: absorption spectral changes of the variants upon incubation with *N*-propargylglycine. The black line indicates the spectrum before the addition of *N*-propargylglycine. Spectra were recorded at 1 min intervals for 90 min. Right: absorbance changes of the variants upon incubation with *N*-propargylglycine followed at 380, 405 and 450 nm. (B) Activity of the different enzyme variants before and after incubation with *N*-propargylglycine.

## Discussion

Proline dehydrogenases contain a conserved  $(\beta\alpha)_8$  TIM-barrel domain and an N-terminal arm that differs in length among monofunctional bacterial and eukaryotic ProDHs. In this study, we investigated the functional impact of the N-terminal arm of *Thermus thermophilus* ProDH. We analyzed variants that lack one ( $\Delta A$ ), two ( $\Delta AB$ ) or three ( $\Delta ABC$ ) N-terminal helices and compared these variants to the EE variant of MBP-fused TtProDH. The latter variant is a highly active soluble form of the enzyme that exclusively forms tetramers [14]. Spectral analysis showed that truncation of the N-terminal arm of TtProDH does neither affect the binding of the FAD cofactor nor the microenvironment of the flavin isoalloxazine ring.

We already showed that non-native aggregation of WT is due to the hydrophobicity of helix  $\alpha A$ . Replacing Phe10 and Leu12 of  $\alpha A$  with glutamates eliminates the formation of larger aggregates [14]. Here we established that the complete removal of helix  $\alpha A$  ( $\Delta A$ ), or removal of helices  $\alpha A$  and  $\alpha B$  ( $\Delta AB$ ), has the same effect: no aggregates are observed and  $\Delta A$  and  $\Delta AB$  exclusively form tetramers. This confirms that  $\alpha A$  is responsible for the *in vitro* aggregation of WT and that both helices  $\alpha A$  and  $\alpha B$  are not essential for the tetramerization process. Furthermore, estimation of kinetic parameters revealed that  $\alpha A$  and  $\alpha B$  are not essential for the enzymatic activity of MBP-TtProDH. Actually,  $\Delta AB$  is the most active MBP-fused TtProDH variant reported thus far. Incubations with the mechanism-based inhibitor *N*-propargylglycine yielded supporting information about the catalytic competence and structural integrity of  $\Delta A$  and  $\Delta AB$ . The flavin cofactor of both arm-truncated variants is rapidly reduced, immediately followed by covalent adduct formation. This leads to irreversible suicide inactivation of the enzymes by *N*-propargylglycine (Fig. 6).

Helix  $\alpha C$  turned out to be more crucial for oligomerization and catalysis. Removal of the complete N-terminal arm ( $\Delta ABC$ ) resulted in catalytically impaired dimers and poor reactivity with *N*-propargylglycine. MS analysis showed that  $\Delta ABC$  has lost 22 residues at the C-terminus, including Arg288 and Arg289 involved in proline binding [1]. Thus, the dissociation of tetramers into dimers and loss in catalytic performance of  $\Delta ABC$  might be caused by the removal of  $\alpha C$  and/or the partial absence of helix  $\alpha 8$ . We do not have indications that the loss in activity is caused by dimer formation, since the dimer-dimer interactions in the tetramer seem to be relatively weak. The oxidase activity remains low for all deletion variants, suggesting that removal of the N-terminal helices does not improve the access of oxygen to the flavin.

For *Deinococcus radiodurans* ProDH (DrProDH, PDB 4H6Q) [18], *Bradyrhizobium japonicum* PutA (BrPutA, PDB 3HAZ) [5] and *Geobacter sulfurreducens* PutA (GsPutA, PDB 4NM9) [4], a conserved Arg-Glu ion pair (Arg288-Glu65 in TtProDH) is suggested to act as an active site gate. Arg288 is present in helix  $\alpha 8$  while Glu65 is present in the  $\beta 1$ - $\alpha 1$  loop. In the presence

of substrate, this loop moves towards the active site and the Arg-Glu ion pair can form. In  $\Delta ABC$ , helix  $\alpha 8$  is cleaved before Arg288, thereby disrupting this ion pair and excluding this possibility for active site stabilization.

Triggered by the properties of  $\Delta ABC$ , we introduced single amino acid substitutions in  $\Delta AB$  that might disrupt the interaction between helix  $\alpha C$  and helix  $\alpha 8$  in a more delicate way. Replacement of Tyr35 with Phe showed that the hydrogen bond interaction between Tyr35 and Glu259 is not crucial for the catalytic performance of the enzyme, and also not for protein tetramerization. Incubation with *N*-propargylglycine confirmed that the flavin reactivity and structural integrity of Y35F are highly comparable to that of  $\Delta AB$ .

The Tyr35 – Glu295 interaction is not conserved in *DrProDH*, although both amino acid residues are present in a region with highly conserved sequence. The latter enzyme is the only other monofunctional ProDH of which a crystal structure is available [18]. In *DrProDH*, Tyr35 is replaced by a phenylalanine (Phe34), while Glu295 is replaced by an arginine (Arg298). The absence of the Tyr-Glu interaction in *DrProDH* is another indication that this ion pair is not of great importance for the structural integrity of *TtProDH*.

The V32D and V36D variants of  $\Delta AB$  provided further insight into the functional role of helix  $\alpha C$ . Both variants mainly form dimers, show partial proteolytic processing at the C-terminus and display low catalytic efficiencies. This lends support to the proposal that the hydrophobic patch between helix  $\alpha C$  and  $\alpha 8$  (Fig. 7) is not only important for tetramer formation, but also for the proper functioning of the active site. Assessment of the reactivity of V32D and V36D with *N*-propargylglycine revealed interesting differences. While slow flavin reduction and covalent adduct formation are observed for V32D, these processes do not take place with V36D. In agreement with this, V36D is less active with proline than V32D, and resembles  $\Delta ABC$  in this respect (Table 3). When we compare the hydrophobicity of helices  $\alpha C$  and  $\alpha 8$  against their counterparts in *DrProDH*, we observe a similar hydrophobic patch between both helices. In addition, analysis of the crystal structures of *Escherichia coli* PutA (PDB 4O8A), *BjPutA* and *GsPutA* suggests that helix  $\alpha 8$  might also be stabilized by hydrophobic contacts, although in PutA enzymes helix  $\alpha 8$  might also be stabilized by additional N- and C-terminal helices.

For V36D (Fig. 9) and  $\Delta ABC$  (Fig. 6), the steady increase in absorption in the near-UV region is indicative for the slow conversion of *N*-propargylglycine to *N*-propargyliminoglycine. As this increase in absorption is not observed in the absence of enzyme, we propose that during reaction with *N*-propargylglycine, both V36D and  $\Delta ABC$  get reduced and that the reduced enzymes are slowly reoxidized by molecular oxygen. As a result, with V36D and  $\Delta ABC$ , hardly any reduction of the FAD cofactor is observed.

In conclusion, our results strengthen the idea that helix  $\alpha C$  is involved in TtProDH tetramerization and stabilization of helix  $\alpha 8$ . The hydrophobic patch between helix  $\alpha C$  and helix  $\alpha 8$  stimulates tetramerization and is important for catalysis because it orients helix  $\alpha 8$  for proper binding of the substrate and interaction with the active site.

We have shown that helix  $\alpha A$  and  $\alpha B$  of TtProDH are not crucial for the *in vitro* activity of the enzyme. However,  $\alpha A$  and  $\alpha B$  of TtProDH might be of importance *in vivo*, by serving as a docking interface for partner enzyme TtP5CDH during channeling [12] and/or for interaction with the membrane. Concerning these issues, it is of interest to study the function of the elongated N-terminus of monofunctional eukaryotic ProDHs, especially of human ProDH [11].

## Acknowledgements

We thank Adrie Westphal (Laboratory of Biochemistry, Wageningen University & Research) for technical assistance. We are indebted to Sebastiaan A. van den Berg (Laboratory of Organic Chemistry, Wageningen University & Research) for the synthesis of *N*-propargylglycine. MH received financial support from the Netherlands Organization for Scientific Research (NWO) and The Graduate School VLAG (Wageningen, The Netherlands) through the ERA-NET Industrial Biotechnology program (ERA-IB-2, project EIB.10.004) of the European Community. The mass spectrometry research was performed within the framework of the Netherlands Organization for Scientific Research (NWO) and supported by the large scale proteomics facility Proteins@Work (project 184.032.201) embedded in The Netherlands Proteomics Centre.

## References

- [1] White, T. A., Krishnan, N., Becker, D. F., Tanner, J. J., Structure and kinetics of monofunctional proline dehydrogenase from *Thermus thermophilus*. *J. Biol. Chem.* (2007), 282, 14316-14327.
- [2] Arentson, B. W., Luo, M., Pemberton, T. A., Tanner, J. J., Becker, D. F., Kinetic and structural characterization of tunnel-perturbing mutants in *Bradyrhizobium japonicum* proline utilization A. *Biochemistry* (2014), 53, 5150-5161.
- [3] Moxley, M. A., Sanyal, N., Krishnan, N., Tanner, J. J., Becker, D. F., Evidence for hysteretic substrate channeling in the proline dehydrogenase and  $\Delta^1$ -pyrroline-5-carboxylate dehydrogenase coupled reaction of proline utilization A (PutA). *J. Biol. Chem.* (2014), 289, 3639-3651.
- [4] Singh, H., Arentson, B. W., Becker, D. F., Tanner, J. J., Structures of the PutA peripheral membrane flavoenzyme reveal a dynamic substrate-channeling tunnel and the quinone-binding site. *Proc. Natl. Acad. Sci. USA* (2014), 111, 3389-3394.
- [5] Srivastava, D., Schuermann, J. P., White, T. A. et al., Crystal structure of the bifunctional proline utilization A flavoenzyme from *Bradyrhizobium japonicum*. *Proc. Natl. Acad. Sci. USA* (2010), 107, 2878-2883.
- [6] Surber, M. W. and Maloy, S., The PutA protein of *Salmonella typhimurium* catalyzes the two steps of proline degradation via a leaky channel. *Arch. Biochem. Biophys.* (1998), 354, 281-287.
- [7] Tanner, J. J. and Becker, D. F., PutA and proline metabolism, Handbook of flavoproteins. Volume 1 - oxidases, dehydrogenases and related systems, De Gruyter, 2012.
- [8] Tanner, J. J., Structural biology of proline catabolism. *Amino Acids* (2008), 35, 719-730.
- [9] Lee, Y. H., Nadaraja, S., Gu, D., Becker, D. F., Tanner, J. J., Structure of the proline dehydrogenase domain of the multifunctional PutA flavoprotein. *Nat. Struct. Biol.* (2003), 10, 109-114.
- [10] Zhang, M., White, T. A., Schuermann, J. P. et al., Structures of the *Escherichia coli* PutA proline dehydrogenase domain in complex with competitive inhibitors. *Biochemistry* (2004), 43, 12539-12548.
- [11] Tallarita, E., Pollegioni, L., Servi, S., Molla, G., Expression in *Escherichia coli* of the catalytic domain of human proline oxidase. *Protein Expr. Purif.* (2012), 82, 345-351.
- [12] Sanyal, N., Arentson, B. W., Luo, M., Tanner, J. J., Becker, D. F., First evidence for substrate channeling between proline catabolic enzymes: a validation of domain fusion analysis for predicting protein-protein interactions. *J. Biol. Chem.* (2015), 290, 2225-2234.
- [13] Huijbers, M. M. E. and van Berkel, W. J. H., High yields of active *Thermus thermophilus* proline dehydrogenase are obtained using maltose-binding protein as a solubility tag. *Biotechnol. J.* (2015), 10, 395-403.
- [14] Huijbers, M. M. E. and van Berkel, W. J. H., A more polar N-terminal helix releases *Thermus thermophilus* proline dehydrogenase from self-association. *J. Mol. Catal. B* (2016), 134, 340-346.
- [15] Rowley, G. L., Greenleaf, A. L., Kenyon, G. L., On the specificity of creatine kinase. New glycosylamines and glycosylamine analogs related to creatine. *J. Am. Chem. Soc.* (1971), 93, 5542-5551.
- [16] White, T. A., Johnson Jr., W. H., Whitman, C. P., Tanner, J. J., Structural basis for the inactivation of *Thermus thermophilus* proline dehydrogenase by N-propargylglycine. *Biochemistry* (2008), 47, 5573-5580.
- [17] Srivastava, D., Zhu, W., Johnson Jr., W. H. et al., The structure of the proline utilization A proline dehydrogenase domain inactivated by N-propargylglycine provides insight into conformational changes induced by substrate binding and flavin reduction. *Biochemistry* (2010), 49, 560-569.
- [18] Luo, M., Arentson, B. W., Srivastava, D., Becker, D. F., Tanner, J. J., Crystal structures and kinetics of monofunctional proline dehydrogenase provide insight into substrate recognition and conformational changes associated with flavin reduction and product release. *Biochemistry* (2012), 51, 10099-10108.









# Chapter 5

## **Dimerization of proline dehydrogenase from *Thermus thermophilus* is crucial for its thermostability**

*Manuscript in preparation*

**Mieke M.E. Huijbers  
Jenny W. Wu  
Willem J.H. van Berkel**

Laboratory of Biochemistry, Wageningen University & Research, Stippeneng 4, 6708 WE Wageningen, the Netherlands





## Abstract

*Thermus thermophilus* proline dehydrogenase (*TtProDH*) catalyzes the first step in proline catabolism. The thermostable flavoenzyme consists of a distorted TIM-barrel and three N-terminal helices,  $\alpha$ A,  $\alpha$ B and  $\alpha$ C. Using maltose-binding protein (MBP)-fused constructs, we recently demonstrated that helix  $\alpha$ C is crucial for *TtProDH* catalysis and tetramerization through positioning of helix  $\alpha$ 8. Here we report on the structural features that determine the thermostability of *TtProDH*. Selective disruption of two ion pairs in the dimerization interface of several MBP-*TtProDH* variants resulted in the formation of monomers. The newly created monomers have improved catalytic properties but their melting temperatures are decreased by more than 20 °C. In summary, intermolecular ion pairs improve the thermostability of *TtProDH* and a trade-off is made between thermostability and catalytic activity.

## Keywords

flavoprotein, protein oligomerization, proline dehydrogenase, thermostability, *Thermus thermophilus*

## Introduction

Quite some microorganisms are able to live under harsh environmental conditions, such as extreme pH, pressure or temperature. Especially extremophilic bacteria and archaea living at very high temperatures have attracted a lot of attention because of the considerable biotechnological potential of their thermostable enzymes [1-5].

In most cases, proteins from (hyper)thermophilic organisms have been found to be structurally similar to their mesophilic counterparts, except for minor differences [6,7]. There is not one single clear defining feature that confers thermostability to enzymes. Many factors have been suggested to contribute to the enhanced stability of thermophilic proteins, such as an increase in subunit contacts, hydrophobic interactions and hydrogen bonding, shorter loops and fewer cavities [6-11]. One feature that seems common to almost all (hyper)thermophilic proteins is an increase in electrostatic interactions [12-15]. Also, increasing the number of interactions and decreasing the surface to volume ratio through oligomerization seems to be a common strategy to enhance protein thermostability [8,10]. There are many examples of thermostable enzymes that occur in a higher oligomeric state compared to their mesophilic counterparts [16-24].

*Thermus thermophilus* is a thermophilic gram-negative bacterium originally isolated from a hot spring in Mine, Shizuoka Prefecture, Japan in 1968 [25]. Its optimal growth temperature is between 65 and 72 °C. The genome sequence of *T. thermophilus* was reported in 2004 [26]. This thermophilic organism serves as a biological model and its thermostable enzymes have widespread biotechnological applications [27].

One of the thermostable enzymes from *T. thermophilus* is proline dehydrogenase (TtProDH). It is a flavin-dependent enzyme that catalyzes the conversion of L-proline to  $\Delta^1$ -pyrroline-5-carboxylate (P5C), the first step in the conversion of proline to glutamate. TtProDH is composed of a distorted TIM-barrel and a helical N-terminal arm which consists of three helices:  $\alpha$ A,  $\alpha$ B and  $\alpha$ C [28]. These helices are part of a hydrophobic patch that is thought to be involved in substrate channeling [28,29].

We have developed an overexpression and purification protocol for TtProDH, in which the enzyme is fused to maltose-binding protein (MBP). Wildtype MBP-TtProDH (WT) purifies as a mixture of soluble aggregates and tetramers [30,31]. Increasing the polarity of helix  $\alpha$ A (variant MBP-TtProDH F10E/L12E (EE)) eliminates the formation of aggregates [31]. In addition, we constructed variants of TtProDH in which we sequentially removed one, two or three N-terminal helices, resulting in variants  $\Delta$ A,  $\Delta$ AB and  $\Delta$ ABC [32]. While  $\Delta$ A and  $\Delta$ AB form active tetramers,  $\Delta$ ABC mainly consists of poorly active dimers.

From the crystal structure of TtProDH (PDB 2G37) it can be deduced that helices  $\alpha$ 5 form the interface of the dimer, and that Asp205 and Glu207 form ion pairs with Arg202 and

Lys213, respectively, of the other subunit [28] (Fig. 1). To investigate the influence of the oligomerization state of *Tt*ProDH on its thermostability, we created variants in which we changed Asp205 and Glu207 of EE,  $\Delta$ A,  $\Delta$ AB and  $\Delta$ ABC into lysines. These MBP-*Tt*ProDH KK variants, as well as their non-KK counterparts were assessed for their hydrodynamic properties as well as their conformational stability.

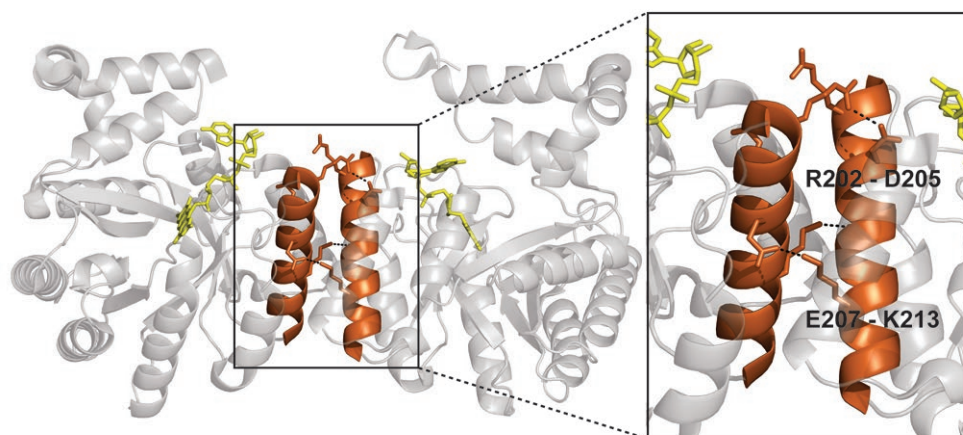


**Figure 1.**

Interactions between helices 5 of both subunits in the three-dimensional model of the crystal structure of *Tt*ProDH (PDB entry 2G37). Helices 5 are shown in orange, the FAD cofactor depicted in yellow, and the remaining part of the *Tt*ProDH structure is shown gray and transparent. The ion pairs R202-D205 and E207-K213 are indicated.

## Materials and Methods

### Cloning, expression and purification of the TtProDH variants

In MBP-TtProDH EE, ΔA, ΔB and ΔABC, Asp205 and Glu207 were changed into lysines (D205K and D207K). This was done in a one-step PCR and ligation reaction, as we have described before [31] with the exception that in this case both a forward and reverse primer were used for introducing the mutations. The plasmids pBAD-MBP-TtProDH EE, ΔA, ΔAB and ΔABC were used as template DNA. Amplification was done using the forward primer 5' CCG GAT AAA CGC CTG ATT AAA GCC AAA TAT CTG CAT CTG GGT AAG CTT GCG CTG AAA GAA GGT C 3' (codon changes underlined). As a reverse primer, the reverse complement sequence of the forward primer was used.

The MBP-TtProDH variants were expressed and purified according to a protocol described previously [31]. In short, the variants were produced in *E.coli* TOP10 cells and purified using amylose affinity and anion-exchange chromatography.

### Subunit composition

The oligomeric state of the MBP-TtProDH KK variants was analyzed by size exclusion chromatography [31]. 200 μL of a 40 μM or 250 μM enzyme solution was loaded on a Superdex 200 10/300 GL (GE Healthcare), equilibrated in 50 mM sodium phosphate, 150 mM NaCl, pH 7.4. Apparent molecular masses were determined from running calibration proteins in parallel, as described elsewhere [33].

The native and subunit masses of the MBP-TtProDH KK variants were determined by nanoflow electrospray ionization mass spectrometry (ESI-MS), essentially as described earlier [32].

### Spectral analysis

Flavin absorption spectra [31] and far-UV circular dichroism (CD) spectra [30] of the MBP-TtProDH variants were recorded according to previously described protocols. For these spectra, enzyme solutions of respectively 40 μM and 1 μM enzyme in 50 mM sodium phosphate, pH 7.4 were prepared.

Temperature-induced unfolding was monitored using CD by following the mean residue molar ellipticity at 224 nm while increasing the temperature from 20 to 95 °C at a rate of 0.5 °C min<sup>-1</sup>. Data points were collected after every 0.5 °C increase. Midpoints of transition were determined by fitting the data to a model described by a sigmoidal or double sigmoidal function. As for the far-UV CD-spectra, protein samples (1 μM) were prepared in 50 mM sodium phosphate, pH 7.4.



### Enzyme activity

Enzyme activity of the MBP-*Tt*ProDH variants was determined on a Hewlett Packard 8453 diode array spectrophotometer using the proline:dichlorophenolindophenol (DCPIP) oxidoreductase assay [30]. Steady-state kinetic parameters were determined at 25 °C, essentially as described previously [31]. Thermoinactivation of the MBP-*Tt*ProDH variants was determined based on an earlier established protocol [30]. 10 µM enzyme solutions in 20 mM Hepes, pH 8.0 were incubated at 65 °C. The time-dependent loss of activity was followed by removing aliquots from the incubation mixtures at various time points up to 30 min. These aliquots were directly assayed for residual enzyme activity at 25 °C by adding them to a 600 µL reaction mixture containing 65 µM DCPIP and 100 mM L-proline in 20 mM Hepes, pH 8.0.

## Results

### Protein expression and purification

All MBP-*Tt*ProDH variants were expressed and purified successfully and with high yields, as we have reported before for different MBP-*Tt*ProDH variants [30-32]. From 1 L culture, about 200-250 mg of each variant was purified. We have demonstrated that the MBP fusion tag does not significantly affect the spectral and catalytic properties of the enzyme [30]. Therefore, we used the MBP-fused variants for further studies.

### Spectral properties

The far-UV CD spectra of the KK-variants of MBP-*Tt*ProDH are very similar (Fig. 2A) and resemble those of the non-KK variants [32]. In addition, the visible flavin absorption spectra of the KK-variants of MBP-*Tt*ProDH (Fig. 2B) are all nearly identical to those of the non-KK variants [32]. Therefore, the D205K and E207K replacements do not alter the secondary structure of the enzyme, nor the local environment of the flavin isoalloxazine ring.

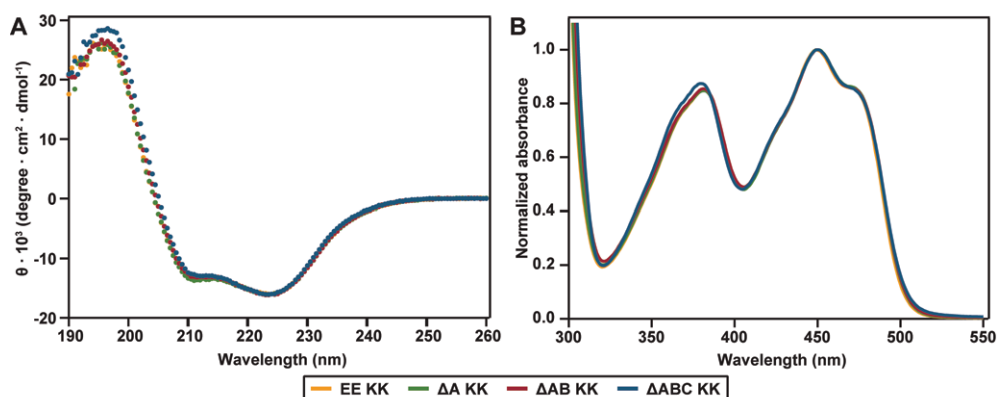


Figure 2.

Spectral properties of the MBP-*Tt*ProDH KK variants. (A) Near-UV CD-spectra. (B) Visible flavin absorption spectra.

### Hydrodynamic properties

The hydrophobic N-terminus of *Tt*ProDH is responsible for its self-association *in vitro* [31]. While MBP-*Tt*ProDH WT forms soluble aggregates and tetramers, the EE variant with a more polar N-terminal helix exclusively forms tetramers [31]. The truncated variants  $\Delta A$  and  $\Delta AB$  form tetramers as well, while  $\Delta ABC$  purifies as a dimer [32]. Introducing Lys205 and Lys207 in the  $\alpha 5$  interface helices of *Tt*ProDH clearly changes the oligomerization state of the protein. Size exclusion chromatography indicates that EE KK forms dimers, while  $\Delta A$  KK,

$\Delta$ AB KK and  $\Delta$ ABC KK mainly form monomers (Fig. 3A). When analyzing the elution patterns at high protein concentrations (250  $\mu$ M instead of 40  $\mu$ M),  $\Delta$ A KK and  $\Delta$ AB KK increase in size (Fig. 3A). The elution pattern of EE KK and  $\Delta$ ABC KK at 40 and 250  $\mu$ M is the same.

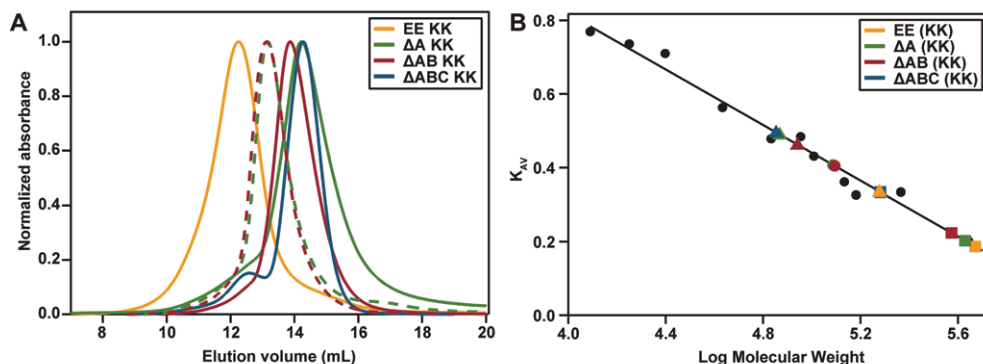


**Figure 3.**

Hydrodynamic properties of the MBP-TtProDH variants as monitored by Superdex 200 size-exclusion chromatography. **(A)** Gel filtration of the KK variants. All samples were loaded with a concentration of 40  $\mu$ M. In dotted lines, the elution pattern of  $\Delta$ A KK and  $\Delta$ AB KK at 250  $\mu$ M is depicted. **(B)**  $K_{AV}$  versus log molecular weight plot. Reference proteins, used to calibrate the column and calculate the MBP-TtProDH apparent masses, are depicted as black circles: cytochrome c (12.3 kDa), myoglobin (17.8 kDa),  $\alpha$ -chymotrypsin (25 kDa), ovalbumin (43 kDa), bovine serum albumin (68 and 136 kDa), 4-hydroxybenzoate 3-hydroxylase (90 kDa), lipamide dehydrogenase (102 kDa), phenol 2-hydroxylase (152 kDa), catalase (232 kDa), ferretin (440 kDa), and vanillyl-alcohol oxidase (510 kDa). MBP-TtProDH variants: squares, non-KK variants 40  $\mu$ M; triangles, KK variants 40  $\mu$ M; circles, KK variants 250  $\mu$ M.

For comparison, the  $K_{AV}$  values of all variants are depicted in Fig. 3B. The difference in oligomerization behavior is immediately clear from this graph. EE,  $\Delta$ A and  $\Delta$ AB have a similar low  $K_{AV}$  value ( $K_{AV} = 0.204 \pm 0.018$ ) corresponding to the size of tetramers.  $\Delta$ ABC and EE KK have a somewhat higher  $K_{AV}$  value ( $K_{AV} = 0.335 \pm 0.001$ ) and form dimers.  $\Delta$ A KK,  $\Delta$ AB KK and  $\Delta$ ABC KK elute as monomers ( $K_{AV} = 0.482 \pm 0.018$ ), while  $\Delta$ A KK and  $\Delta$ AB KK elute in between dimers and monomers ( $K_{AV} = 0.406 \pm 0.001$ ) when applied at high protein concentration. This points to a weak interaction between the monomers of these KK variants.

The oligomerization behavior of the KK variants was also addressed by ESI-MS, as has been done before for the non-KK variants [32]. Table 1 shows dimers as well as monomers for all KK-variants. Dimers are not observed for  $\Delta$ A KK,  $\Delta$ AB KK and  $\Delta$ ABC KK using size exclusion chromatography, but  $\Delta$ A KK,  $\Delta$ AB KK do form dimers at high concentrations (Fig. 3A). Therefore, it is likely that at high concentrations in the mass spectrometer, the enzymes described here partially form dimers.

While the denatured masses of EE KK and  $\Delta$ AB KK indicate that these variants exist of identical subunits, this is not the case for  $\Delta$ A KK and  $\Delta$ ABC KK (Table 1). For  $\Delta$ ABC, we have already shown that the protein is C-terminally truncated after purification from *E. coli* [32].  $\Delta$ ABC

KK has the same truncation (removal of sequence 288-RRIAERPENLLLVLRSLVSGLE-309); however, it does not occur in the entire enzyme population. For  $\Delta A$  KK, the truncation appears to be only a few amino acids.

**Table 1.**

Molecular masses of EE KK,  $\Delta A$  KK,  $\Delta AB$  KK and  $\Delta ABC$  KK as determined by native and denatured ESI-MS. Both predicted (Pred.) as well as experimental (Exp.) masses are given in kDa with experimental errors less than 0.05%. For calculation of the predicted native masses, it has been taken into account that each subunit contains a non-covalently bound FAD cofactor (molecular mass 786 Da).

	Native				Denatured	
	Dimer		Monomer			
	Pred.	Exp.	Pred.	Exp.	Pred.	Exp.
<b>MBP-<i>Tt</i>ProDH EE KK</b>	159.8	159.2 – 159.8	79.5	79.6 – 80.3	78.7	78.7
<b>MBP-<i>Tt</i>ProDH <math>\Delta A</math> KK</b>	155.1	156.6	77.5	77.6 – 78.1	76.7	76.8 75.7
<b>MBP-<i>Tt</i>ProDH <math>\Delta AB</math> KK</b>	153.8	153.8	76.3	76.6	75.5	75.6
<b>MBP-<i>Tt</i>ProDH <math>\Delta ABC</math> KK</b>	145.0	144.3 – 145.3	75.2	72.4 – 73.4	74.4	74.5 71.9

## Catalytic properties

The steady-state kinetic properties of the MBP-*Tt*ProDH variants are shown in Fig. 4 and the corresponding kinetic parameters are summarized in Table 2. EE KK,  $\Delta A$  KK and  $\Delta AB$  KK have a significant improved catalytic efficiency at 25 °C compared to their non-KK counterparts [32] (Table 2).  $\Delta ABC$  KK is poorly active, which is not surprising since we have already shown that helix  $\alpha C$  is crucial for the catalytic function of *Tt*ProDH. [32].

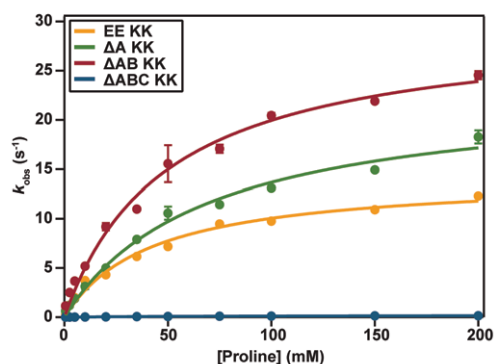


**Figure 4.**

Steady-state kinetics of the MBP-*Tt*ProDH KK variants as determined with the proline:DCPIP assay. The fitted curves are retrieved from non-linear regression analysis applying the Michaelis-Menten equation.

**Table 2.**Kinetic parameters for the MBP-*Tt*ProDH KK variants at 25 °C as determined with the proline:DCPIP assay.

	$K_M$ (mM)	$k_{cat}$ (s <sup>-1</sup> )	$k_{cat}/K_M$ (s <sup>-1</sup> M <sup>-1</sup> )
MBP- <i>Tt</i> ProDH EE*	68 ± 8	9.8 ± 0.5	146
MBP- <i>Tt</i> ProDH ΔA*	116 ± 5	12.6 ± 0.3	109
MBP- <i>Tt</i> ProDH ΔAB*	60 ± 3	13.6 ± 0.3	229
MBP- <i>Tt</i> ProDH ΔABC*	116 ± 11	0.6 ± 0.02	6
MBP- <i>Tt</i> ProDH EE KK	42 ± 6	14.3 ± 0.7	339
MBP- <i>Tt</i> ProDH ΔA KK	69 ± 10	23.1 ± 1.4	335
MBP- <i>Tt</i> ProDH ΔAB KK	49 ± 6	29.8 ± 1.4	603
MBP- <i>Tt</i> ProDH ΔABC KK	84 ± 10	0.2 ± 0.01	3

\* As determined previously [31,32].

## Thermal stability

The thermal stability of the KK MBP-*Tt*ProDH variants was assessed by monitoring the loss of secondary structure using CD spectroscopy. From following the mean residue molar ellipticity at 224 nm while increasing the temperature from 20 to 95 °C, two separate transitions for EE, ΔA, ΔAB and ΔABC are observed (Fig. 5A and Table 3). This indicates non-cooperative unfolding for the MBP and *Tt*ProDH domains [30]. The first transition with a midpoint of unfolding of 50-52 °C reflects the unfolding of the MBP domain, while the thermostable *Tt*ProDH domain unfolds around 88 °C. ΔAB is slightly less stable, with a midpoint of unfolding at 84 °C.

The unfolding temperature for the KK variants has decreased severely, since they start to unfold between 60 and 70 °C (Fig. 5B). The exact midpoints of unfolding of the KK variants are more difficult to determine, since the transitions for unfolding of the MBP- and *Tt*ProDH-domains overlap. However, it can be seen that EE KK and ΔABC KK are slightly more stable than ΔA KK and ΔAB KK (Fig. 5B and Table 3).

**Table 3.**Midpoints of unfolding for the MBP-*Tt*ProDH variants, as monitored by CD spectroscopy. Mean residue molar ellipticity was monitored at 224 nm.

	$T_m$ (°C) MBP	$T_m$ (°C) <i>Tt</i> ProDH		$T_m$ (°C) MBP	$T_m$ (°C) <i>Tt</i> ProDH
MBP- <i>Tt</i> ProDH EE	51.6 ± 0.3	88.2 ± 0.3	MBP- <i>Tt</i> ProDH EE KK	52.0 ± 0.4	70.0 ± 0.4
MBP- <i>Tt</i> ProDH ΔA	50.4 ± 0.3	91.7 ± 1.8	MBP- <i>Tt</i> ProDH ΔA KK	52.0 ± 0.3	63.0 ± 0.2
MBP- <i>Tt</i> ProDH ΔAB	50.4 ± 0.2	84.2 ± 0.1	MBP- <i>Tt</i> ProDH ΔAB KK	52.5 ± 0.3	65.4 ± 0.2
MBP- <i>Tt</i> ProDH ΔABC	52.0 ± 0.3	88.7 ± 0.4	MBP- <i>Tt</i> ProDH ΔABC KK	53.9 ± 0.4	71.8 ± 0.3

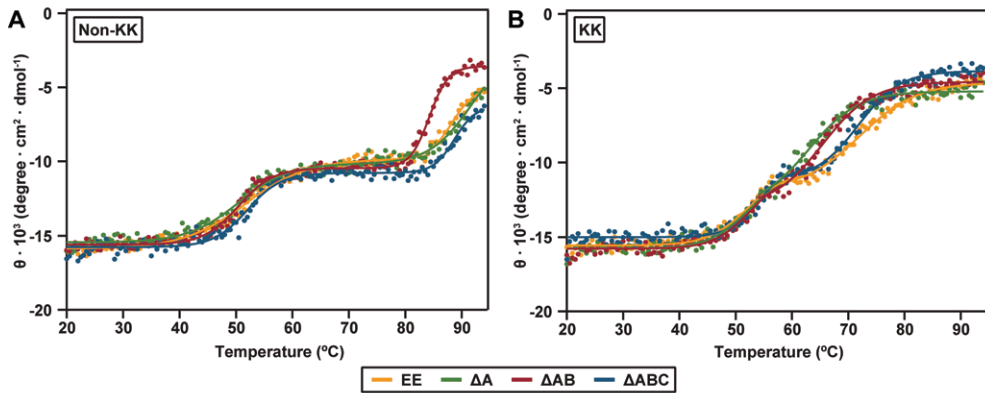


**Figure 5.**

Thermal unfolding of the MBP-*Tt*ProDH variants as monitored by CD spectroscopy. Ellipticity was monitored at 224 nm. (A) MBP-*Tt*ProDH non-KK variants. (B) MBP-*Tt*ProDH KK variants.

The thermostability of the MBP-*Tt*ProDH variants was also evaluated by incubating the different enzymes at 65 °C and monitoring the residual activity as a function of incubation time (Fig. 6). EE and  $\Delta A$  show a slight initial increase in activity when incubated at 65 °C. After 30 min of incubation, EE and  $\Delta A$  still retain 105 and 90% residual activity, respectively.  $\Delta AB$  quickly loses part of its activity upon incubation at 65 °C; however, after this initial activity loss the residual activity stays around 70%. In contrast, the KK-variants of EE,  $\Delta A$  and  $\Delta AB$  all lose fairly quickly upon incubation at 65 °C. EE KK appears to be slightly more thermostable compared to  $\Delta A$  KK and  $\Delta AB$  KK, with about 34% of residual activity after 30 min incubation, compared to 24% for  $\Delta A$  KK and  $\Delta AB$  KK. Since  $\Delta ABC$  and  $\Delta ABC$  KK are almost inactive, thermostability was not assessed for these variants.

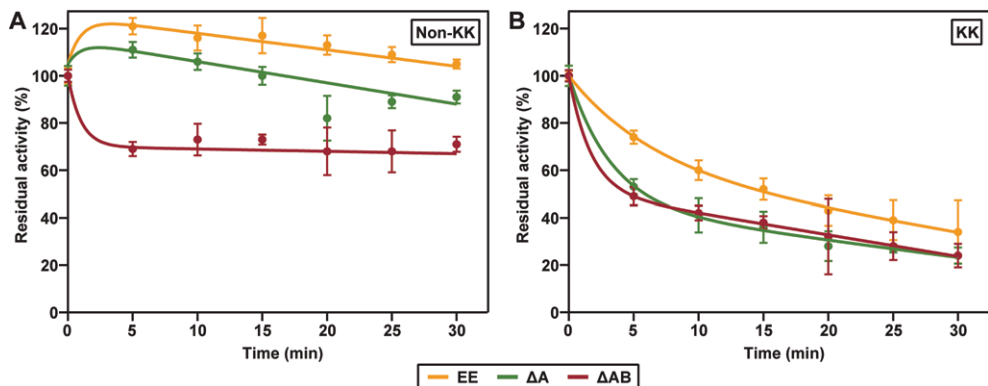


**Figure 6.**

Thermoinactivation at 65 °C of the MBP-*Tt*ProDH variants as a function of time. (A) MBP-*Tt*ProDH non-KK variants. (B) MBP-*Tt*ProDH KK variants.



## Discussion

Many factors have been suggested to contribute to the enhanced stability of thermophilic proteins. We investigated the effect of the oligomerization state of proline dehydrogenase from *Thermus thermophilus* on its thermostability. By altering two negatively charged residues (Asp205 and Glu207) in the dimerization interface of *Tt*ProDH into positively charged lysines (KK), two ion pairs are disrupted. We investigated the effects of this disruption for several MBP-*Tt*ProDH variants (EE,  $\Delta A$ ,  $\Delta AB$  and  $\Delta ABC$ ) and compared their properties to their non-KK counterparts.

The MBP-*Tt*ProDH KK variants are all purified as active holoenzymes. Their flavin spectral properties and secondary structures are nearly identical and hardly differ from their non-KK counterparts [31,32]. However, the hydrodynamic properties have changed, as revealed by gel filtration and native mass spectrometry. While EE,  $\Delta A$  and  $\Delta AB$  form tetramers, EE KK forms dimers and  $\Delta A$  KK and  $\Delta AB$  KK form monomers.  $\Delta ABC$  KK also forms monomers, in contrast to  $\Delta ABC$  which forms dimers. An overview of the oligomeric states of the different variants is given in Fig. 7. We can clearly conclude that helices  $\alpha 5$  form the interface of the dimer through ionic interactions. Helix  $\alpha C$  is involved in tetramerization; however, the exact mode of dimer-dimer interaction remains elusive so far.

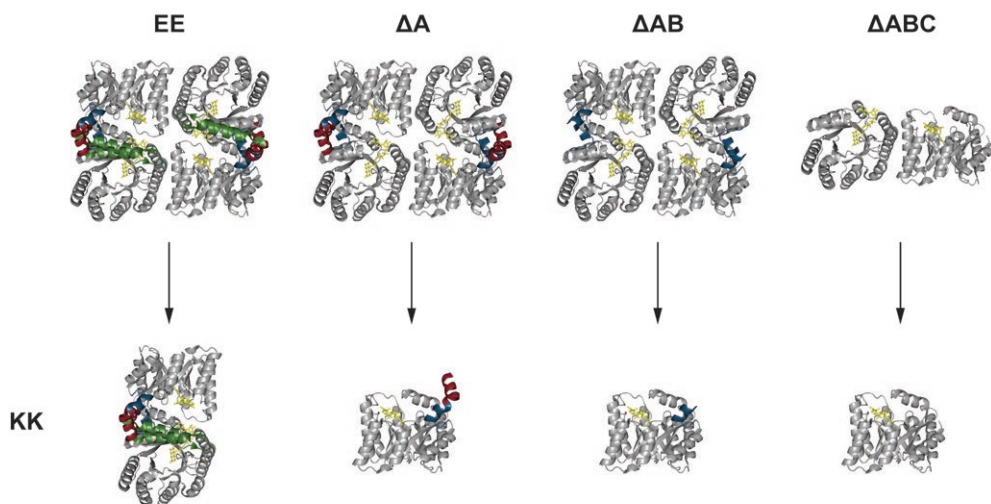


**Figure 7.**

Overview of the different oligomeric species observed for EE,  $\Delta A$ ,  $\Delta AB$  and  $\Delta ABC$ . Helix  $\alpha A$  is depicted in green, helix  $\alpha B$  in red and helix  $\alpha C$  in blue. The FAD cofactor is shown in yellow. For simplicity, MBP is not depicted. Please note that the exact dimer-dimer interactions in the tetramer are unknown.

Steady-state kinetic experiments revealed that all KK variants have an improved catalytic efficiency compared to their non-KK counterparts (Fig. 4 and Table 2). We have shown before that  $\Delta A$  and  $\Delta AB$  have an increased activity compared to EE. The same is true for the KK variants of  $\Delta A$  and  $\Delta AB$  compared to  $\Delta EE$  KK. In fact,  $\Delta AB$  KK is the most active form of TtProDH we have engineered. These results unambiguously show that the TtProDH monomer is active and suggest that the loss of interactions between the dimers and tetramers makes the enzyme less rigid for catalysis.

Thermal unfolding experiments revealed a severe destabilization of the KK variants. The non-KK variants are resistant to temperatures above 80 °C, while the KK variants already start to unfold between 60 and 70 °C (Fig. 5). Thermostability of the variants was also monitored by incubating the enzymes at 65 °C and monitoring the residual activity as a function of incubation time. EE and  $\Delta A$  initially become more active when incubated at 65 °C (Fig. 6A). This might be related to an increase in protein flexibility, as observed before for TtProDH [30].  $\Delta AB$  is a bit less stable than EE and  $\Delta A$  (Fig. 6A). This corresponds to the thermal unfolding, in which  $\Delta AB$  has a lower melting temperature compared to EE and  $\Delta A$  (Fig. 5A). The KK variants all lose activity fairly quick upon incubation at 65 °C, but EE KK appears to be slightly more thermostable compared to  $\Delta A$  KK and  $\Delta AB$  KK (Fig. 6B). This is in agreement with the thermal unfolding curves, which show that EE starts to unfold later than  $\Delta A$  KK and  $\Delta AB$  KK (Fig. 5B). These results indicate that removal of the N-terminal helices only slightly influences the conformational stability of the enzyme, while disruption of the dimerization interface severely affects this stability.

In summary, we show that two amino acid replacements in the dimerization interface of TtProDH alter the oligomerization state of the enzyme from tetramer to monomer. This monomerization improves the catalytic efficiencies of the enzyme, but at the cost of its thermostability. Thus, a tradeoff between activity and thermostability is made, in which the higher-order oligomeric species display the greatest thermostability and lowest catalytic activity. Tradeoffs between catalytic activity and stability are seen often in enzymes [34-36]. Psychrophilic (cold adapted) enzymes show a tradeoff between a low thermal stability, so a high structural flexibility, and a high activity at low temperatures [37-39] while thermostable enzymes show a tradeoff between a high thermal stability and a low activity at moderate temperatures. One of the strategies to increase thermostability is to provide rigidity through oligomerization [8,10]. Tradeoffs between thermal stability and activity made via a higher oligomeric species have been reported [40,41] and our results confirm that oligomerization might be a common strategy for to confer thermostability to an enzyme at the expense of its catalytic activity.

Since tradeoffs between thermal stability and activity seem quite general, the process of engineering enzymes with both high thermostability and high activity is challenging. Nevertheless, an increasing number of examples shows that the activity-stability trade-off can be overcome by genetically or chemically modifying enzymes [42-46]

## Acknowledgements

We thank Adrie Westphal for technical assistance. We thank Arjan Barendregt (Biomolecular Mass Spectrometry and Proteomics Group, Bijvoet Centre for Biomolecular Research, Utrecht University) for help with ESI-MS. This work is supported by the Netherlands Organization for Scientific Research (NWO) and The Graduate School VLAG (Wageningen, The Netherlands) through the ERA-NET Industrial Biotechnology program (ERA-IB-2, project EIB.10.004) of the European Community.

## References

- [1] Turner, P., Mamo, G., Karlsson, E. N., Potential and utilization of thermophiles and thermostable enzymes in biorefining. *Microb. Cell Fact.* (2007), 6, 9-9.
- [2] Tango, M. S. A. and Islam, M. R., Potential of extremophiles for biotechnological and petroleum applications. *Energy Sources* (2002), 24, 543-559.
- [3] Littlechild, J. A., Thermophilic archaeal enzymes and applications in biocatalysis. *Biochem. Soc. Trans.* (2011), 39, 155.
- [4] Willies, S., Isupov, M., Littlechild, J., Thermophilic enzymes and their applications in biocatalysis: a robust aldo-keto reductase. *Environ. Technol.* (2010), 31, 1159-1167.
- [5] Zamost, B. L., Nielsen, H. K., Starnes, R. L., Thermostable enzymes for industrial applications. *J. Ind. Microbiol.* (1991), 8, 71-81.
- [6] Razvi, A. and Scholtz, J. M., Lessons in stability from thermophilic proteins. *Protein Sci.* (2006), 15, 1569-1578.
- [7] Szilágyi, A. and Závodszky, P., Structural differences between mesophilic, moderately thermophilic and extremely thermophilic protein subunits: results of a comprehensive survey. *Structure* (2000), 8, 493-504.
- [8] Backmann, J. and Schäfer, G., Thermodynamic analysis of hyperthermostable oligomeric proteins, *Methods Enzymol.*, Vol 334, The Academic Press, 2001, 328-342.
- [9] Jaenicke, R. and Böhm, G., The stability of proteins in extreme environments. *Curr. Opin. Struct. Biol.* (1998), 8, 738-748.
- [10] Vieille, C. and Zeikus, G. J., Hyperthermophilic enzymes: sources, uses, and molecular mechanisms for thermostability. *Microbiol. Mol. Biol. Rev.* (2001), 65, 1-43.
- [11] Kumar, S., Tsai, C., Nussinov, R., Factors enhancing protein thermostability. *Protein Eng.* (2000), 13, 179-191.
- [12] Isupov, M. N., Fleming, T. M., Dalby, A. R. *et al.*, Crystal structure of the glyceraldehyde-3-phosphate dehydrogenase from the hyperthermophilic archaeon *Sulfolobus solfataricus*. *J. Mol. Biol.* (1999), 291, 651-660.
- [13] Xiao, L. and Honig, B., Electrostatic contributions to the stability of hyperthermophilic proteins. *J. Mol. Biol.* (1999), 289, 1435-1444.
- [14] Perl, D., Mueller, U., Heinemann, U., Schmid, F. X., Two exposed amino acid residues confer thermostability on a cold shock protein. *Nat. Struct. Mol. Biol.* (2000), 7, 380-383.
- [15] Lebink, J. H. G., Knapp, S., van der Oost, J. *et al.*, Engineering activity and stability of *Thermotoga maritima* glutamate dehydrogenase. II: construction of a 16-residue ion-pair network at the subunit interface. *J. Mol. Biol.* (1999), 289, 357-369.
- [16] Dalhus, B., Saarinen, M., Sauer, U. H. *et al.*, Structural basis for thermophilic protein stability: structures of thermophilic and mesophilic malate dehydrogenases. *J. Mol. Biol.* (2002), 318, 707-721.
- [17] Dams, T., Auerbach, G., Bader, G. *et al.*, The crystal structure of dihydrofolate reductase from *Thermotoga maritima*: molecular features of thermostability. *J. Mol. Biol.* (2000), 297, 659-672.
- [18] Kohlhoff, M., Dahm, A., Hensel, R., Tetrameric triosephosphate isomerase from hyperthermophilic Archaea. *FEBS Lett.* (1996), 383, 245-250.
- [19] Tanaka, Y., Tsumoto, K., Yasutake, Y. *et al.*, How oligomerization contributes to the thermostability of an Archaeon protein - Protein L-isoaspartyl-O-methyltransferase from *Sulfolobus tokodaii*. *J. Biol. Chem.* (2004), 279, 32957-32967.
- [20] Thoma, R., Hennig, M., Sterner, R., Kirschner, K., Structure and function of mutationally generated monomers of dimeric phosphoribosylanthranilate isomerase from *Thermotoga maritima*. *Structure* (2000), 8, 265-276.
- [21] Villeret, V., Clantin, B., Tricot, C. *et al.*, The crystal structure of *Pyrococcus furiosus* ornithine carbamoyltransferase reveals a key role for oligomerization in enzyme stability at extremely high temperatures. *Proc. Natl. Acad. Sci. USA* (1998), 95, 2801-2806.
- [22] Lokanath, N. K., Shiromizu, I., Ohshima, N. *et al.*, Structure of aldolase from *Thermus thermophilus* HB8

- showing the contribution of oligomeric state to thermostability. *Acta Crystallogr. D* (2004), 60, 1816-1823.
- [23] Maes, D., Zeelen, J. P., Thanki, N. *et al.*, The crystal structure of triosephosphate isomerase (TIM) from *Thermotoga maritima*: a comparative thermostability structural analysis of ten different TIM structures. *Proteins* (1999), 37, 441-453.
- [24] Walden, H., Bell, G. S., Russell, R. J. M. *et al.*, Tiny TIM: a small, tetrameric, hyperthermostable triosephosphate isomerase. *J. Mol. Biol.* (2001), 306, 745-757.
- [25] Oshima, T. and Imahori, K., Description of *Thermus thermophilus* (Yoshida and Oshima) comb. nov., a nonsporulating thermophilic bacterium from a Japanese thermal spa. *Int. J. Syst. Evol. Microbiol.* (1974), 24, 102-112.
- [26] Henne, A., Bruggemann, H., Raasch, C. *et al.*, The genome sequence of the extreme thermophile *Thermus thermophilus*. *Nat. Biotech.* (2004), 22, 547-553.
- [27] Cava, F., Hidalgo, A., Berenguer, J., *Thermus thermophilus* as biological model. *Extremophiles* (2009), 13, 213-231.
- [28] White, T. A., Krishnan, N., Becker, D. F., Tanner, J. J., Structure and kinetics of monofunctional proline dehydrogenase from *Thermus thermophilus*. *J. Biol. Chem.* (2007), 282, 14316-14327.
- [29] Sanyal, N., Arentson, B. W., Luo, M., Tanner, J. J., Becker, D. F., First evidence for substrate channeling between proline catabolic enzymes: a validation of domain fusion analysis for predicting protein-protein interactions. *J. Biol. Chem.* (2015), 290, 2225-2234.
- [30] Huijbers, M. M. E. and van Berkel, W. J. H., High yields of active *Thermus thermophilus* proline dehydrogenase are obtained using maltose-binding protein as a solubility tag. *Biotechnol. J.* (2015), 10, 395-403.
- [31] Huijbers, M. M. E. and van Berkel, W. J. H., A more polar N-terminal helix releases MBP-tagged *Thermus thermophilus* proline dehydrogenase from tetramer-polymer self-association. *J. Mol. Catal. B* (2016), 134, 340-346.
- [32] Huijbers, M. M. E., van Alen, I., Wu, J. W. *et al.*, Functional impact of the N-terminal arm of proline dehydrogenase from *Thermus thermophilus*. *Manuscript submitted* (2017).
- [33] Monterisino, S. and van Berkel, W. J. H., Functional annotation and characterization of 3-hydroxybenzoate 6-hydroxylase from *Rhodococcus jostii* RHA1. *Biochim. Biophys. Acta P&P* (2012), 1824, 433-442.
- [34] Beadle, B. M. and Shoichet, B. K., Structural bases of stability-function tradeoffs in enzymes. *J. Mol. Biol.* (2002), 321, 285-296.
- [35] Georges, F., Protein stability and enzyme activity at extreme biological temperatures. *J. Phys. Condens. Matter* (2010), 22, 323101.
- [36] Sterner, R. and Liebl, W., Thermophilic adaptation of proteins. *Crit. Rev. Biochem. Mol. Biol.* (2001), 36, 39-106.
- [37] Feller, G. and Gerday, C., Psychrophilic enzymes: hot topics in cold adaptation. *Nat. Rev. Microbiol.* (2003), 1, 200-208.
- [38] Georlette, D., Blaise, V., Collins, T. *et al.*, Some like it cold: biocatalysis at low temperatures. *FEMS Microbiol. Rev.* (2004), 28, 25-42.
- [39] Feller, G., Psychrophilic enzymes: from folding to function and biotechnology. *Scientifica* (2013), 2013, 1-28.
- [40] Fraser, N. J., Liu, J., Mabbitt, P. D. *et al.*, Evolution of protein quaternary structure in response to selective pressure for increased thermostability. *J. Mol. Biol.* (2016), 428, 2359-2371.
- [41] Dick, M., Weiergräber, O. H., Classen, T. *et al.*, Trading off stability against activity in extremophilic aldolases. *Sci. Rep.* (2016), 6, 17908.
- [42] Siddiqui, K. S., Defying the activity-stability trade-off in enzymes: taking advantage of entropy to enhance activity and thermostability. *Crit. Rev. Biotechnol.* (2016), 1-14.
- [43] Xu, B., Dai, M., Chen, Y. *et al.*, Improving the thermostability and activity of a thermophilic subtilase by incorporating structural elements of its psychrophilic counterpart. *Appl. Environ. Microbiol.* (2015), 81, 6302-6313.
- [44] Asghari, S. M., Pazhang, M., Ehtesham, S. *et al.*, Remarkable improvements of a neutral protease activity

- and stability share the same structural origins. *Protein Eng. Des. Sel.* (2010), 23, 599-606.
- [45] Siddiqui, K. S. and Cavicchioli, R., Improved thermal stability and activity in the cold-adapted lipase B from *Candida antarctica* following chemical modification with oxidized polysaccharides. *Extremophiles* (2005), 9, 471-476.
- [46] García-Ruiz, E., Maté, D., Ballesteros, A., Martínez, A. T., Alcalde, M., Evolving thermostability in mutant libraries of ligninolytic oxidoreductases expressed in yeast. *Microb. Cell Fact.* (2010), 9, 17.







# Chapter 6

## **Proline dehydrogenase from *Thermus thermophilus* does not discriminate between FAD and FMN as cofactor**

*Manuscript accepted, Scientific Reports (2017)*

**Mieke M.E. Huijbers<sup>1</sup>**

**Marta Martínez-Júlvez<sup>2</sup>**

**Adrie H. Westphal<sup>1</sup>**

**Estela Delgado-Arciniega<sup>1</sup>**

**Milagros Medina<sup>2</sup>**

**Willem J.H. van Berkel<sup>1</sup>**

<sup>1</sup> Laboratory of Biochemistry, Wageningen University & Research, Stippeneng 4, 6708 WE Wageningen, the Netherlands

<sup>2</sup> Department of Biochemistry and Molecular Cell Biology and Institute for Biocomputation and Physics of Complex Systems, University of Zaragoza, Pedro Cerbuna 12, 50009-Zaragoza, Spain





## Abstract

Flavoenzymes are versatile biocatalysts containing either FAD or FMN as cofactor. FAD often binds to a Rossmann fold, while FMN prefers a TIM-barrel or flavodoxin-like fold. Proline dehydrogenase is denoted as an exception: it possesses a TIM-barrel-like fold while binding FAD. Using a riboflavin auxotrophic *Escherichia coli* strain and maltose-binding protein as solubility tag, we produced the apoprotein of *Thermus thermophilus* ProDH (MBP-*Tt*ProDH). Remarkably, reconstitution with FAD or FMN revealed that MBP-*Tt*ProDH has no preference for either of the two prosthetic groups. Kinetic parameters of both holo forms are similar, as are the dissociation constants for FAD and FMN release. Furthermore, we show that the holo form of MBP-*Tt*ProDH, as produced in *E. coli* TOP10 cells, contains about three times more FMN than FAD. In line with this flavin content, the crystal structure of *Tt*ProDH variant  $\Delta$ ABC, which lacks helices  $\alpha$ A,  $\alpha$ B and  $\alpha$ C, shows no electron density for an AMP moiety of the cofactor. To the best of our knowledge, this is the first example of a flavoenzyme that does not discriminate between FAD and FMN as cofactor. Therefore, classification of *Tt*ProDH as an FAD-binding enzyme should be reconsidered.

## Keywords

apoprotein, cofactor, flavoprotein, proline dehydrogenase, TIM-barrel

## Introduction

Flavoenzymes are ubiquitous in nature and function as versatile biocatalysts. They play an essential role in various biological processes such as biosynthesis, energy production, light emission, biodegradation, chromatin remodeling, DNA repair, apoptosis, protein folding, detoxification, and neural development [1].

Flavoenzymes usually contain flavin mononucleotide (FMN) or flavin adenine dinucleotide (FAD) as redox active prosthetic group (Fig. 1). These cofactors are synthesized from riboflavin (vitamin B2) through the action of riboflavin kinase (E.C. 2.7.1.26) and FMN adenyltransferase (E.C. 2.7.7.2), respectively. Eukaryotes and some archaea depend on two separate enzymes for FMN and FAD synthesis [2,3], but in most prokaryotes these two enzymes are fused into a bifunctional protein, FAD synthetase [4-6]. FAD is utilized three times more often than FMN as enzyme prosthetic group, while riboflavin is not used for this purpose [7,8].

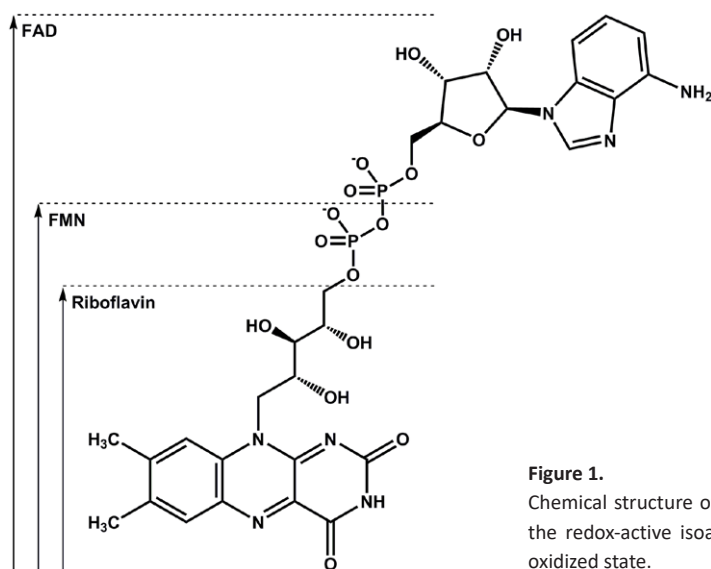


**Figure 1.**

Chemical structure of riboflavin, FMN and FAD, with the redox-active isoalloxazine ring presented in the oxidized state.

FMN- and FAD-dependent enzymes have a preference for certain protein folds. While FMN enzymes show a preference for a TIM-barrel or flavodoxin-like fold, FAD enzymes often use a Rossmann fold for binding the ADP dinucleotide moiety of the cofactor [7]. Some flavoenzymes, like NADPH cytochrome P450 oxidoreductase and nitric oxide synthase, use both flavin cofactors for the transport of electrons through separate domains [9,10].

The majority (90%) of flavoproteins bind their cofactor non-covalently [7]. Flavin dissociation provides the opportunity of studying the properties of the apoenzyme [11,12], and allows for reconstituting the holoprotein with isotopically enriched [13] or artificial [14] flavins.

Furthermore, apoflavoenzymes can be selectively immobilized by anchoring to a flavin-containing carrier [15]. Different methods have been explored to dissociate flavoproteins into apoprotein and flavin prosthetic group [16]. Traditional methods include precipitation procedures and dialysis [17]. However, these approaches may give low yields, since many apoflavoproteins cannot withstand the harsh and/or time-consuming conditions employed. More recent methods for apoprotein preparation focus on reversible immobilization strategies, which allow deflavination and reconstitution of preparative amounts of flavoprotein [18,19]. Particularly for flavoproteins with a more complex quaternary structure, production of fully reconstitutable apoprotein remains challenging.

In some flavoproteins the flavin is covalently bound to the polypeptide chain [20,21]. By replacing the target residue(s) of covalent flavinylation through site-directed mutagenesis, the apoprotein can be obtained [22,23]. For vanillyl-alcohol oxidase it could be established that the FAD becomes covalently linked to the protein in an autocatalytic process, and that the initial non-covalent binding of FAD to the apo dimer stimulates enzyme octamerization [24,25].

An alternative approach for the preparation of apoenzyme is the use of riboflavin-deficient expression systems. The *E. coli* strain BSV11 is riboflavin auxotrophic [26]. It carries a mutation in the *ribB* gene, which encodes for 3,4-dihydroxy-2-butanone-4-phosphate synthase, an essential enzyme in the riboflavin biosynthesis pathway [27]. Using riboflavin auxotrophic strains, both flavoenzymes that bind their flavin covalently or non-covalently can be produced in their apo-form. Examples include sarcosine oxidase [28] and vanillyl-alcohol oxidase [29].

Proline dehydrogenase (ProDH, EC 1.5.5.2) is a ubiquitous flavoenzyme involved in proline catabolism [30,31]. It oxidizes L-proline to  $\Delta^1$ -pyrroline-5-carboxylate (P5C), which is non-enzymatically hydrolyzed to glutamic semialdehyde (GSA). P5C dehydrogenase (P5CDH, EC 1.2.1.88) oxidizes GSA to L-glutamate. ProDH and P5CDH exist as monofunctional enzymes in some bacteria and in eukaryotes; however, in other bacteria they are fused into a bifunctional enzyme called proline utilization A (PutA) [32,33].

In humans, malfunctioning of the proline metabolic enzymes can lead to several medical issues [34,35]. The gene encoding for human ProDH (also known as proline oxidase) is a hot-spot for mutations [36]. Missense mutations in ProDH have been identified in patients suffering from hyperprolinemia and the neuropsychiatric disorder schizophrenia [37-40]. Furthermore, ProDH is one of the genes markedly induced by tumor suppressor p53 [41,42] and plays a role in tumorigenesis and tumor development [43].

ProDH adopts a distorted ( $\beta\alpha$ )<sub>8</sub> TIM-barrel fold [32,33,44]. Next to methylenetetrahydrofolate reductase (MTHFR) [45], ProDH is the only known TIM-barrel enzyme that contains an FAD cofactor. Due to this property, ProDH and MTHFR have been structurally classified as separate clans of FAD oxidoreductases [7].

Previously, we described the properties of *Thermus thermophilus* ProDH (*TtProDH*), produced through fusion with maltose-binding protein (MBP) [46]. Because MBP-*TtProDH* appeared to be prone to aggregation, we constructed a variant with a more polar N-terminus (F10E/L12E). This MBP-*TtProDH* variant, here further referred to as EE, forms homogeneous tetramers [47]. Each *TtProDH* subunit binds a FAD cofactor [32]. However, molecular details of FAD incorporation are currently unknown.

This research describes the properties of the EE apoprotein. Using a riboflavin auxotrophic expression strain, properly folded apoenzyme was obtained. Intriguingly, we discovered that EE accepts both FAD and FMN as prosthetic group. Based on this finding, the flavin composition and mode of cofactor binding of *TtProDH* was further investigated.



## Materials and Methods

### Enzyme production and purification

*E. coli* TOP10 cells containing a pBAD plasmid (pBAD-EE), in which the changes F10E/L12E were introduced in the gene encoding MBP-*Tt*ProDH [47], were used for heterologous expression of holo MBP-*Tt*ProDH EE. The holo EE was purified as described previously [47], except that no extra FAD was added during purification. Riboflavin auxotrophic *E. coli* BSV11 strain was used as expression host for production of apo-EE. This strain is defective in riboflavin synthesis and was obtained by Tn5 transposon mutagenesis [13]. For enzyme production, a 10 mL pre-culture inoculated with cells harbouring the pBAD-EE plasmid was grown o/n at 37 °C in Luria-Bertani (LB) medium containing 100 µg/mL ampicillin and 50 µM riboflavin. The pre-culture was used to inoculate two 2 L Erlenmeyer flasks, each containing 500 mL LB medium, 100 µg mL<sup>-1</sup> ampicillin and 50 µM riboflavin. The cells were grown at 37 °C until OD<sub>600</sub> = 0.8. Cells were spun down (7000 g for 10 min) and washed three times with riboflavin-free LB. After the third washing step, the cells were divided over two 2 L erlenmeyer flasks, both containing 500 mL riboflavin-free LB medium and 100 µg/mL ampicillin. After one hour shaking (200 rpm) at 20 °C, protein expression was induced by adding 0.02% (w/v) L-arabinose, and growth and expression continued for 14 h. Cells (6 g, wet weight) were harvested by centrifugation (7000 g for 10 min at 4 °C) and resuspended in 50 mM sodium phosphate, pH 7.4. After addition of 1 mg DNaseI, 1 mM MgCl<sub>2</sub> and a Complete Protease Inhibitor Cocktail Tablet (Roche Diagnostics), cells were lysed by passing them three times through a pre-cooled French Press pressure cell (SLM Amicon Instruments) at 10000 psi. Cell lysate was centrifuged at 26000 g for 1 h at 4 °C. Apo-EE was purified using an amylose column (New England Biolabs, 20 mL in XK 16/10), and a Source 15Q column (GE Healthcare, 20 mL in XK 16/10), according to a protocol that has been described before for the holoenzyme [46,47]. In addition, after the ion exchange column, the enzyme was concentrated using a 10 kDa cut off Amicon filter and loaded on a preparative Superdex200 XK26/1000 column (GE Healthcare), equilibrated in 50 mM sodium phosphate, 150 mM NaCl, pH 7.4. The eluted protein was concentrated and simultaneously the buffer was changed to 50 mM sodium phosphate, pH 7.4 by using a 30 kDa cutoff Vivaspin 6 spinfilter (GE Healthcare). Protein concentrations were determined using the bicinchoninic acid (BCA) assay (Thermo Scientific) and the purified apoenzyme with a concentration of 7.5 mg/mL was flash-frozen in liquid nitrogen and stored at -80 °C. The native mass of apo-EE was determined using nanoflow electrospray ionization mass spectrometry (ESI-MS), as described before [46,47].

A helical arm-truncated variant lacking N-terminal helices αA, αB and αC was constructed. The plasmid pBAD-MBP-*Tt*ProDH [47] was PCR-amplified using the primers 5'AAT TAG AAT TCA TGG CGA AAA TTG AAA CCC TGG AAG AAG CAC TG 3' (forward) and 5' GCC CAA GCT

TTT ATT CTA GAC CGC TAA CCA GGC 3' (reverse). Using *EcoRI* and *HindIII* restriction sites (underlined in the primers), the amplified fragment was introduced into a pBAD-MBP vector, which resulted in an N-terminal fusion of the *TtProDH*  $\Delta$ ABC variant to MBP. The resulting construct was verified by automated sequencing of both strands (Macrogen). *E. coli* TOP10 cells were transformed with the plasmid for recombinant expression. MBP-*TtProDH*  $\Delta$ ABC was produced and purified as described previously [47]. The denatured mass of apo-EE was determined using nanoflow electrospray ionization mass spectrometry (ESI-MS) [46]. Removal of the MBP-tag and purification of native  $\Delta$ ABC was achieved by slight modification of the trypsin-treatment reported before [46]. In this case, 25 mg purified MBP-*TtProDH*  $\Delta$ ABC in 50 mM sodium phosphate, pH 7.4 was incubated with 36  $\mu$ g trypsin at 37 °C for 1 h. After that, phenylmethylsulfonyl fluoride (PMSF, Merck) was added to a final concentration of 2 mM to inactivate trypsin and the protocol to purify  $\Delta$ ABC was proceeded as described [46]. Trypsinolysis of MBP-*TtProDH*  $\Delta$ ABC and purification of  $\Delta$ ABC was visualized with sodium dodecyl sulphate polyacrylamide gel electrophoresis (SDS-PAGE), using 12% polyacrylamide slab gels. Proteins were stained using Coomassie Brilliant Blue R-250. As a molecular weight marker, Precision Plus Protein Standard (Biorad) was used.

### Spectral analysis

Holo-EE (10  $\mu$ M) and apo-EE (10  $\mu$ M) were incubated with 50  $\mu$ M FAD or FMN, in 50 mM sodium phosphate, pH 7.4 at room temperature for 1 hour. Excess FAD/FMN was removed using a 10 kDa cut off spin filter and flavin absorption spectra of holo-EE, apo-EE and reconstituted enzymes were recorded at 25 °C on a Hewlett-Packard 8453 diode array spectrophotometer, essentially as described before [46].

Far-UV circular dichroism (CD) spectra of holo-EE, apo-EE and apo-EE reconstituted with FAD or FMN were acquired on a Jasco J-715 spectropolarimeter equipped with a Peltier thermostat (Jasco). Samples contained 1  $\mu$ M enzyme in 50 sodium phosphate, pH 7.4 and spectra were recorded as described previously [46]. Temperature-induced unfolding was monitored by increasing the temperature from 20 – 95 °C at a rate of 0.5 °C min<sup>-1</sup>. Data points were collected every 0.5 °C increase. Midpoints of transition were determined by fitting the data to a model described by a double sigmoidal function.

### Enzyme activity

Enzyme activity of apo-EE, apo-EE reconstituted with FAD or FMN, and holo-EE was determined at 25 °C on a Hewlett Packard 8453 diode array spectrophotometer using the proline:dichlorophenolindophenol (DCPIP) oxidoreductase assay [46]. For the standard assay, catalytic amounts of enzyme were added to a 600  $\mu$ L reaction mixture containing 65  $\mu$ M DCPIP and 100 mM L-proline in 50 mM sodium phosphate, pH 7.4. Steady-state kinetic parameters were determined at 25 °C, essentially as described previously [47].

## Fluorescence spectroscopy

Dissociation constants of apo-EE-flavin complexes were determined by using the quenching of flavin fluorescence upon binding of the flavin cofactor to the apoenzyme. 200 nM solutions of FAD, FMN or riboflavin in 50 mM sodium phosphate, pH 7.4, were prepared based on the molar absorption coefficients of  $11300 \text{ M}^{-1} \text{ cm}^{-1}$  at 450 nm for free FAD,  $12200 \text{ M}^{-1} \text{ cm}^{-1}$  at 445 nm for free FMN and  $12500 \text{ M}^{-1} \text{ cm}^{-1}$  at 445 nm for free riboflavin. 1.3 mL of the 200 nM FAD, FMN or riboflavin solutions were titrated with 5  $\mu\text{L}$  aliquots of 5  $\mu\text{M}$  apoenzyme in the same buffer. In total, 250  $\mu\text{L}$  of the enzyme solution was added. After addition of each aliquot of enzyme, fluorescence emission was recorded during 30 sec. Excitation was at 445 nm (bandwidth 5 nm) and emission at 525 nm (bandwidth 10 nm) and the photomultiplier potential was set at 975 V. As control, buffer (50 mM sodium phosphate, pH 7.4) was titrated with apoenzyme under the same conditions.

The dissociation constants ( $K_D$ ) of the apo-EE-FAD/FMN complexes were determined using Igor Pro 6.10, by fitting the fluorescence emission data ( $F_{\text{total}}$ ) to the model described by equation 1:

$$F_{\text{total}} = f_{\text{flavin}} \cdot [\text{flavin}]_{\text{free}} + f_{\text{complex}} \cdot [\text{complex}] + f_{\text{apo}} \cdot [\text{apo}] \quad (1),$$

where

$$[\text{complex}] = \frac{([\text{flavin}]_{\text{total}} + K_D + [\text{apo}]_{\text{total}}) - \sqrt{([\text{flavin}]_{\text{total}} + K_D + [\text{apo}]_{\text{total}})^2 - ([\text{flavin}]_{\text{total}} \cdot [\text{apo}]_{\text{total}})}}{2}$$

and  $[\text{flavin}]_{\text{total}}$  and  $[\text{apo}]_{\text{total}}$  are the concentrations of flavin and apoenzyme at each point in the titrations.  $f_{\text{flavin}}$ ,  $f_{\text{complex}}$  and  $f_{\text{apo}}$  are the fluorescence conversion factors for each species, respectively.

Fluorescence emission spectra of 0.9  $\mu\text{M}$  FAD, 0.9  $\mu\text{M}$  FMN, 0.9  $\mu\text{M}$  apo-EE reconstituted with FAD, and 0.9  $\mu\text{M}$  apo-EE reconstituted with FMN were recorded. All solutions were prepared in 50 mM sodium phosphate, pH 7.4. Excitation was at 445 nm (bandwidth 5 nm) and emission at 470-650 nm (bandwidth 10 nm). The photomultiplier potential was set at 820 V and 10 scans were recorded and averaged.

In addition, fluorescence emission spectra of 0.9  $\mu\text{M}$  purified holo-EE [47] and 0.9  $\mu\text{M}$  denatured EE were recorded. EE was denatured by incubating 0.9  $\mu\text{M}$  enzyme in 50 mM sodium phosphate, pH 7.4, containing 0.5% sodium dodecyl sulfate (SDS) [46]. After incubation at room temperature for several minutes, fluorescence emission spectra of holo- and denatured EE were recorded as described above. Flavin composition of the denatured sample could be calculated using equations (2) and (3):

$$f_{\text{fin}} = F_{\text{FMN}} \cdot f_{\text{FMN}} + F_{\text{FAD}} \cdot f_{\text{FAD}} \quad (2)$$

$$f_{\text{FMN}} = 1 - f_{\text{FAD}} \quad (3)$$

where  $F_{\text{fin}}$  is the final fluorescence emission after incubation of 0.9  $\mu\text{M}$  holo enzyme with 0.5% SDS, and  $F_{\text{FMN}}$  and  $F_{\text{FAD}}$  are the fluorescence emissions of 0.9  $\mu\text{M}$  FMN and 0.9  $\mu\text{M}$  FAD, respectively.  $f_{\text{FMN}}$  and  $f_{\text{FAD}}$  are the fractions of FMN and FAD present in the sample.

## Mass spectrometry

To determine the FAD/FMN ratio in purified holoenzyme, the flavin cofactor was released from the enzyme by extraction with ethanol. A 10  $\mu\text{M}$  holo-EE solution was incubated with 60% ethanol for about 30 min. Subsequently, the solution was centrifuged to remove aggregates. The solution was passed through a 10 kDa cut-off Vivaspin 6 spinfilter (GE Healthcare) and the flow-through was collected. The solution was freeze-dried and the obtained pellet dissolved in 120  $\mu\text{L}$  pure water. Two microliter of this solution were loaded onto a UPLC column (Discovery HS F5-3 2.1 mm I.D. x 150 mm, 3  $\mu\text{m}$  particles, Sigma Aldrich). Separation was performed at 40  $^{\circ}\text{C}$  with a gradient from 100%  $\text{H}_2\text{O}$  (with 0.1% formic acid) to 35% acetonitrile (with 0.1% formic acid) in 15 min at a flow rate of 250  $\mu\text{L}/\text{min}$ . FMN and FAD were identified and quantified using a Shimadzu UPLC-triple quad mass spectrometer (LCMS-8040). The triple quad mass spectrometer was operating with 3 L/min nebulizing gas flow and 15 L/min drying gas flow. The DI temperature was set to 250  $^{\circ}\text{C}$  and the heat block temperature to 400  $^{\circ}\text{C}$ . Electrospray ionization was used. The machine was calibrated with a reference set of FAD and FMN.

## Crystal growth, data collection and structure refinement for *TtProDH* $\Delta\text{ABC}$

*TtProDH*  $\Delta\text{ABC}$  crystals were obtained by the hanging-drop vapor-diffusion method at 292 K. Drops contained 0.5  $\mu\text{L}$  of 2.2  $\text{mg mL}^{-1}$  protein solution buffered with 50 mM Hepes, 500 mM sodium chloride, pH 8.0, and 0.5  $\mu\text{L}$  of reservoir solution containing 20% (v/v) 2-propanol, 0.2 M calcium chloride dihydrate and 0.1 M sodium acetate, pH 4.6, and were equilibrated against 60  $\mu\text{L}$  of reservoir solution. A mixture of 70% of reservoir solution and 30% of glycerol was used as cryoprotectant solution. Data set from one  $\Delta\text{ABC}$  monocrystal was collected in the beamline I02 of Diamond Light Source (Oxfordshire, UK) at a wavelength of 0.97949  $\text{\AA}$  and a temperature of 100 K. The data were processed and scaled using the XDS package [48] and CCP4 software [49]. The crystal structure was solved by molecular replacement using the MOLREP program [50] and the WT structure (PDB 2G37) as search model. Refinements were performed automatically by REFMAC 5 from CCP4 [51] and manually by COOT [52]. PROCHECK [53] was used to assess and validate the final structure. *TtProDH*  $\Delta\text{ABC}$  diffracted up to 2.2  $\text{\AA}$  and belongs to the  $\text{P6}_2$  cubic space group.  $V_m$  value is 2.84  $\text{\AA}^3/\text{Da}$ , with one protein molecule in the asymmetric unit and 56.68% of solvent content. Amino acid residues 280-296 and the AMP moiety of FAD, lacking observed electron density, are not included in the model. The Ramachandran plot shows that 97.08 %, 2.5 % and 0.42 % of the amino acid residues are in most favored, allowed and disallowed regions, respectively.

## Results

### Preparation of apo-EE

Initial attempts of producing reconstitutable apoprotein from purified holo-EE were not successful. When using precipitation, dialysis or affinity chromatography-based deflavinylolation protocols [16], irreversible aggregation of the apoenzyme occurred. Therefore, we focused our attention on producing apo-EE in a cellular environment. Using the riboflavin auxotrophic *E. coli* strain BSV11 as expression host, the apoenzyme was properly produced with purification yields of approximately 10 mg/L culture. The preparation contained mainly apo-EE and a minor amount of holo-EE, as judged from the low flavin absorbance in the visible region and the low activity compared with native enzyme (*vide infra*).

### Reconstitution of apo-EE

Apo-EE shows a low flavin absorption in the visible region, yielding an  $A_{280}/A_{450}$  ratio of 58.9 (Fig. 2). The apoenzyme can be successfully reconstituted with FAD or FMN, yielding absorption spectra similar to that of holo-EE (Fig. 2). The  $A_{280}/A_{450}$  ratios for apoenzyme reconstituted with FAD (11.4) and FMN (12.0) are similar to that of holo-EE, pre-incubated with excess FAD (11.8) or FMN (12.1). Holo-EE, as purified here in the absence of excess FAD, shows an  $A_{280}/A_{450}$  ratio of 13.3. This indicates that holo-EE contains a small amount of apoprotein.

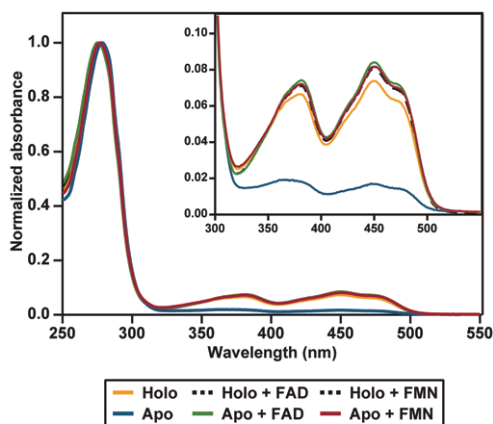


**Figure 2.**

Absorption spectra of holo-EE, apo-EE and apo-EE reconstituted with FAD or FMN.

Far-UV CD spectra of holo-EE, apo-EE and reconstituted apo-EE are all very similar, indicating no large changes in secondary structure (Fig. 3A). Thermal unfolding monitored by CD spectroscopy shows two separate transitions for each sample (Fig. 3B). This indicates non-cooperative unfolding for the MBP and TtProDH domains [46]. The first transition reflects unfolding of MBP, with a midpoint of unfolding around 55 °C. The thermostable TtProDH domain has a midpoint of unfolding around 90 °C. When comparing the thermal stability of apo-EE to that of reconstituted apo-EE or holo-EE, no large differences are observed. Results from native mass spectrometry have shown that holo-EE forms tetramers with a mass of  $319.6 \pm 33$  kDa [47]. Apo-EE is also a tetramer, with a native mass of  $310.7 \pm 31$  kDa. Therefore, the oligomerization state of the enzyme is not affected in the absence of the flavin cofactor.

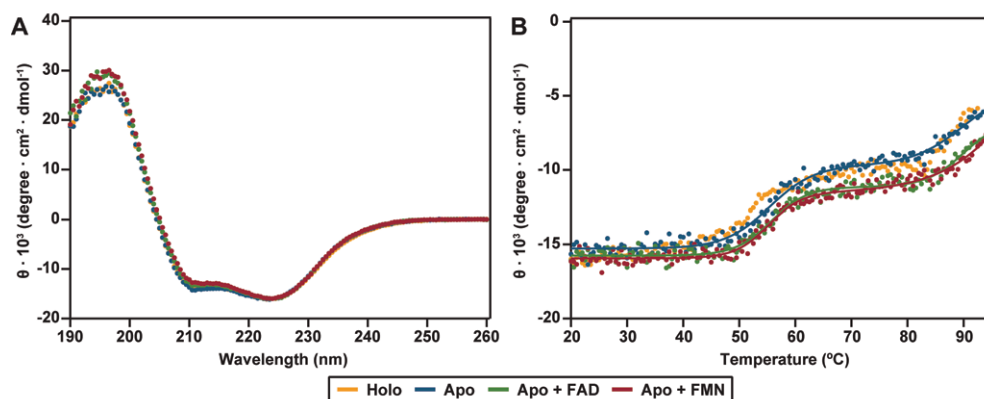


**Figure 3.**

Secondary structure and thermal stability of holo-, apo-, and reconstituted EE. (A) Far-UV CD spectra. (B) Thermal unfolding monitored by CD at 224 nm.

### Catalytic properties of reconstituted apo-EE

Comparison of the specific activities of apo-EE and holo-EE shows that the obtained apoprotein preparation contains about 17% residual activity (Table 1). Apo-EE reconstituted with FAD or FMN shows equal specific activities as holo-EE, indicating that the apoenzyme can be fully reconstituted with either of the flavin cofactors. The kinetic parameters of apo-EE, reconstituted with FAD or FMN, are very similar to those described for holo-EE (Table 1 and Fig. 4), indicating no preference for either of the prosthetic groups in catalysis.

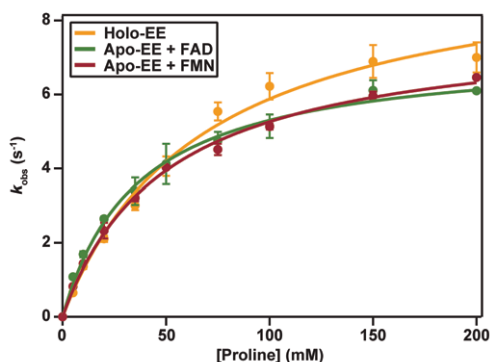


**Table 1.**

Specific activities and kinetic parameters of holo-EE, apo-EE and apo-EE reconstituted with FAD or FMN. Activity measurements were done at 25 °C, pH 7.4 with the proline:DCPIP oxidoreductase assay.

	Specific activity (U mg <sup>-1</sup> )	$k_{\text{cat}}$ (s <sup>-1</sup> )	$K_{\text{M}}$ (mM)	$k_{\text{cat}}/K_{\text{M}}$ (s <sup>-1</sup> M <sup>-1</sup> )
Holo-EE*	4.74 ± 0.27	9.8 ± 0.5	67.6 ± 8.2	146
Apo-EE	0.84 ± 0.01	ND	ND	ND
Apo-EE + FAD	4.83 ± 0.07	7.2 ± 0.2	36.6 ± 3.2	198
Apo-EE + FMN	4.95 ± 0.10	7.9 ± 0.2	50.1 ± 3.4	158

\* As determined previously [47].

**Figure 4.**

Steady-state kinetics of holo-EE and apo-EE reconstituted with FAD and FMN, as determined with the proline:DCPIP assay.

### Cofactor binding of apo-EE

The equilibrium constants for dissociation of FAD and FMN from EE were determined using fluorescence spectroscopy. Upon binding to the apoprotein, fluorescence of the flavin is severely quenched within seconds. From titrating aliquots of apoenzyme to an FAD or FMN containing solution (Fig. 5), tight binding is observed and equal dissociation constants for the apo-FAD ( $K_{\text{D}} = 18.0 \pm 0.5$  nM) and apo-FMN ( $K_{\text{D}} = 19.5 \pm 0.8$  nM) complexes are estimated. Of note is that riboflavin shows a very weak binding to the apoenzyme (data not shown). From Fig. 5 it is evident that the fluorescence quantum yield of the apo-FAD complex is lower than the fluorescence quantum yield of the apo-FMN complex. The increase in flavin fluorescence at the end of the FAD titration (Fig. 5A) can be attributed to the residual amount of flavin present in the apoprotein preparation.

FAD in solution is about 9 times less fluorescent than FMN (Fig. 6A). This is due to stacking of the adenine part onto the isoalloxazine ring of FAD, which quenches its fluorescence [54,55]. In *Tt*ProDH, FAD binds in an extended conformation, as deduced from the crystal structure [32]. Nevertheless, binding to the apoprotein severely quenches the fluorescence of FAD (Fig. 5A, Fig. 6B). This is also true for FMN, but the fluorescence quantum yield of the apoenzyme reconstituted with FMN is significantly higher than the fluorescence quantum yield of the apoenzyme reconstituted with FAD (Fig. 5B, Fig. 6B).

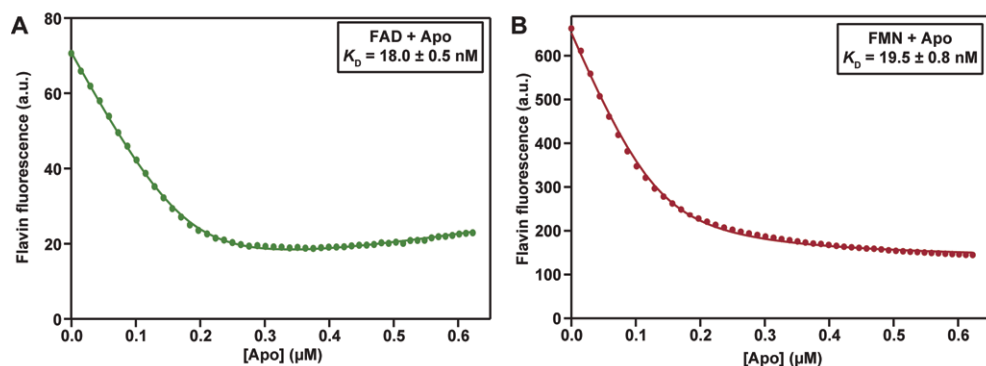


**Figure 5.**

Titration of an FAD or FMN solution with apo-EE to determine the dissociation constants of the apoenzyme-FAD/FMN complex. Flavin fluorescence emission was monitored at 525 nm, excitation was at 445 nm. (A) 200 nM FAD titrated with 5  $\mu$ M of apo EE and (B) 200 nM FMN titrated with 5  $\mu$ M apo EE.

The emission spectrum of holo-EE, isolated from *E. coli*, shows much higher fluorescence intensity than that of the reconstituted apo-FAD complex (Fig. 6B). This suggests that next to FAD, holo-EE might also contain FMN. By denaturing holo-EE with 0.5% SDS (Fig. 6A), the flavin cofactor composition could be measured more accurately. From fluorescence calibration curves of FMN and FAD, it was estimated that  $75 \pm 3\%$  of the released flavin is FMN. To confirm that the enzyme incubated with 0.5% SDS had released all its cofactor, part of the sample was passed through a 10 kDa cut off spin filter to remove the enzyme before measuring fluorescence emission spectra and part of the sample was measured directly. The obtained spectra were identical, indicating all enzyme had released its cofactor and only the fluorescence of flavin free in solution was recorded. As mentioned, no extra flavin was added during purification of holo-EE, therefore, the FAD/FMN ratio was not altered by experimental procedures.

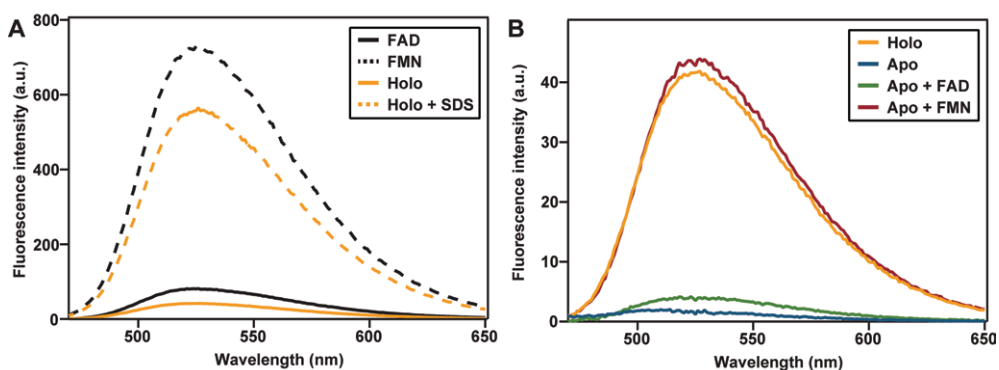


**Figure 6.**

Fluorescence emission spectra of holo- and apo-EE. Excitation was at 445 nm. (A) Spectra of 0.9  $\mu$ M FAD, 0.9  $\mu$ M FMN, 0.9  $\mu$ M holo-EE and 0.9  $\mu$ M holo-EE denatured in 0.5% SDS. (B) Spectra of 0.9  $\mu$ M apo-EE and 0.9  $\mu$ M apo-EE reconstituted with FAD or FMN. For comparison, the spectrum of holo-EE is depicted.

The cofactor composition of holo-EE purified from *E. coli* TOP10 cells was also determined using mass spectrometry. The flavin cofactor was extracted from the enzyme using 60% ethanol. FAD was detected in positive mode for the transition of 786.15 to 136.10 m/z and from 786.15 to 348.10 m/z at 8.53 min. FMN was detected in negative mode for the transition of 455.00 to 97.00 m/z and from 455.00 to 78.90 m/z at 8.64 min. From the measured transitions for the purified flavin cofactor the concentrations for FMN and FAD can be calculated, which indicates that about 74% of the flavin cofactor in holo-EE is FMN and only 26% is FAD, matching perfectly with the fluorescence emission properties. This FAD/FMN ratio in holoenzyme might depend on the cellular conditions, and therefore this ratio might differ per protein batch.

### Crystal structure of *Tt*ProDH $\Delta$ ABC

Crystallization of EE was hampered by inconvenient removal of the MBP tag [47]. We created a *Tt*ProDH variant ( $\Delta$ ABC), which lacks the N-terminal helices  $\alpha$ A,  $\alpha$ B and  $\alpha$ C.  $\Delta$ ABC is poorly active but binds the flavin cofactor in stoichiometric amounts. From this variant, the MBP-tag could be successfully removed (Fig. 7A) and the purified ProDH fragment was used for crystallization. Crystals of *Tt*ProDH  $\Delta$ ABC reached their maximum size in 21 days (Fig. 7B). Collection statistics and refinement data of the crystals obtained are summarized in Table 2. The coordinates and structure factors have been deposited in the Protein Data Bank (PDB) with accession code 5M42.

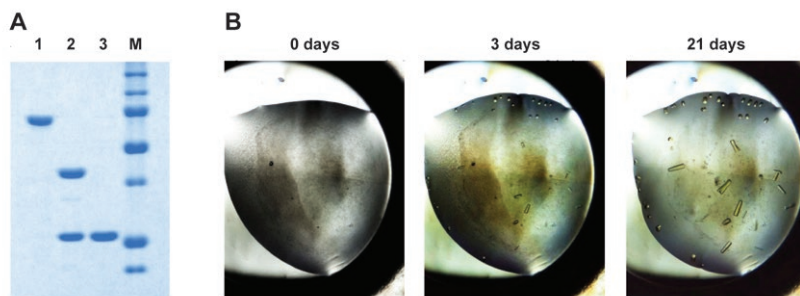


**Figure 7.**

Preparation of  $\Delta$ ABC for crystallization. (A) Removal of the MBP-tag and purification of native  $\Delta$ ABC, visualized on SDS-PAGE. From left to right: (1) purified MBP-*Tt*ProDH  $\Delta$ ABC; (2) MBP-*Tt*ProDH  $\Delta$ ABC after limited trypsinolysis; (3) purified native  $\Delta$ ABC. Molecular masses of marker proteins (M) from top to bottom: 150, 100, 75, 50, 37, 25, 20 kDa. (B) Growth of *Tt*ProDH  $\Delta$ ABC crystals.

The three-dimensional model for *Tt*ProDH  $\Delta$ ABC comprises residues 38-279 (Fig. 8A). Superposition of this structure onto that of *Tt*ProDH (2G37) showed an rmsd value of 0.338 Å (for 221 C $\alpha$  atoms of A chains) demonstrating a similar overall structure and no gross conformational changes. Using ESI-MS, we detected that the C-terminal helix  $\alpha$ 8 of MBP-*Tt*ProDH  $\Delta$ ABC is unstable and becomes proteolytically cleaved in *E. coli* after Thr287.

While MBP-TtProDH has a predicted denatured mass of 74401 Da, the truncated form has a measured mass of 71899 Da. This points to removal of a part of the C-terminal tail with sequence (288-RRIAERPENLLLVLRSLVSGLE-309). This truncated form has a predicted subunit mass of 71885 Da. Deletion of the last 22 residues might increase the flexibility of the remaining C-terminal end of the protein and explain why residues 280-287 are not visible in the crystal structure. For the FAD cofactor, no electron density was observed for the adenosine 5'-monophosphate (AMP) moiety (Fig. 8A). This suggests that either the AMP part of the FAD shows multiple orientations and therefore is highly mobile, or that (part of) the bound cofactor is FMN instead of FAD. The mode of binding of the FMN-part of the flavin cofactor is strictly conserved compared to that of TtProDH (Fig. 8B).

**Table 2.**

Data collection and refinement statistics for TtProDH  $\Delta$ ABC.

Data collection statistics	
Space group	P 6 <sub>2</sub>
Cell dimensions a, b, c (Å)	131.92 131.92 36.58
Wavelength, Å	0.9794
Resolution, Å	65.96 – 2.2 (2.32 – 2.2)
Total no. of reflections	159591 (23667)
No. of unique reflections	18892 (2730)
Redundancy	8.4 (8.7)
Completeness, %	100 (100)
Average I/ $\sigma$	11 (2.2)
R <sub>merge</sub> <sup>a</sup>	0.138 (0.897)
CC(1/2)	0.997 (0.714)
Refinement statistics	
Resolution range, Å	60-2.2
Protein non-hydrogen atoms	1977
Ligand non-hydrogen atoms	31
Solvent non-hydrogen atoms	65
R <sub>work</sub> (%)	18.2
R <sub>free</sub> <sup>b</sup> (%)	22.5
rmsd bond length, Å	0.019
rmsd bond angles, °	2.081
Average B-factor, Å <sup>2</sup>	37.67

Values in parentheses correspond to the highest resolution shell.

<sup>a</sup>  $R_{\text{merge}} = \Sigma(I - I_{\text{av}}) / \Sigma I_{\text{av}}$ , where the summation is over symmetry-equivalent reflections

<sup>b</sup> R calculated for 5% of data excluded from the refinement.

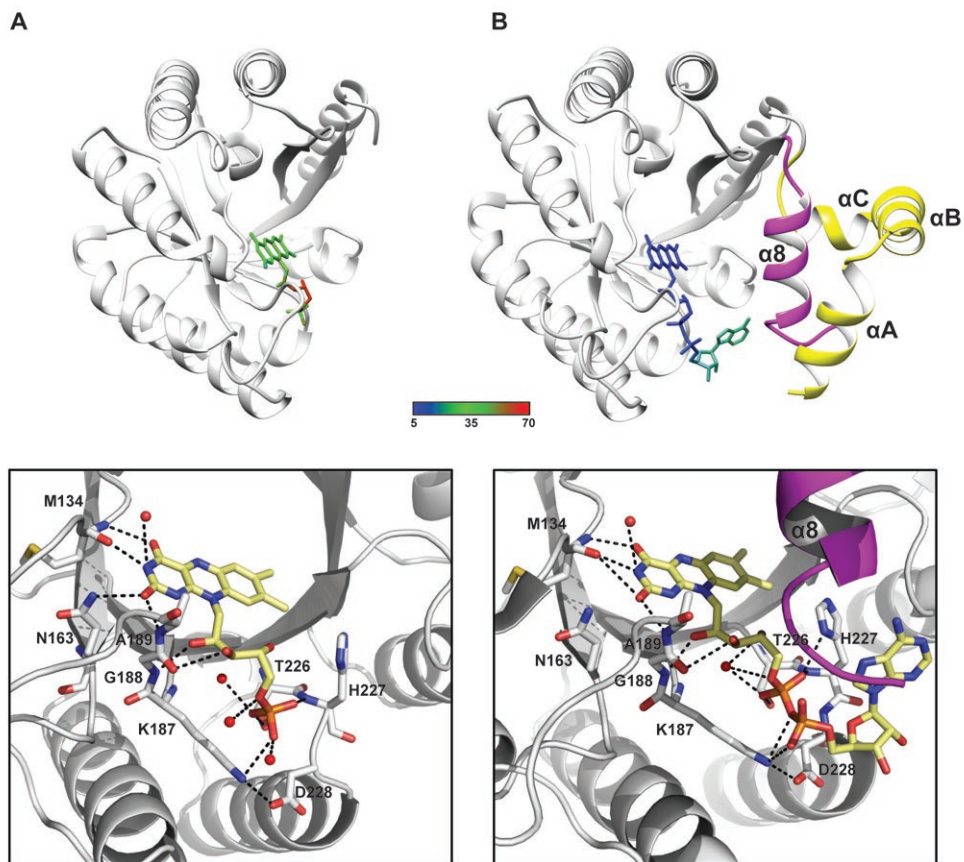


**Figure 8.**

Cartoon representation of the three-dimensional models of the crystal structures of (A) *TtProDH*  $\Delta ABC$  and (B) *TtProDH* (PDB entry 2G37). In the top panels, the flavin cofactors are colored by B-factor. N-terminal helices  $\alpha A$ ,  $\alpha B$ , and  $\alpha C$  and the C-terminal  $\alpha 8$  are colored in yellow and magenta, respectively, in *TtProDH* and are missing in *TtProDH*  $\Delta ABC$ . The bottom panels show the H-bond network contributing to stabilization of the cofactor. Involved residues are labeled and represented as CPK sticks and flavin cofactors show their C $\alpha$  in pale yellow. Water molecules are depicted as red spheres.

## Discussion

This research describes the production of fully reconstitutable apoprotein of proline dehydrogenase for the first time. Using the riboflavin auxotrophic *E. coli* strain BSV11, we obtained an apoprotein preparation that contained 17% residual activity. Spectral analysis confirmed the presence of some holoenzyme, analogous to observations made with sarcosine oxidase and vanillyl-alcohol oxidase [28,29]. More striking, the obtained apoenzyme can be fully reconstituted with either FMN or FAD, leading to quite identical catalytic properties.

ProDH and MTHFR are the only FAD-binding enzymes with a  $(\beta\alpha)_8$  TIM-barrel fold [7]. The presence of a non-covalent FAD cofactor in ProDH was first described by Scarpulla and Soffer in 1978 [56]. They showed that the activity of ProDH, which was solubilized from *E. coli* membranes, is stimulated by FAD but not FMN. After that, it was shown that the flavin cofactor of PutA from *Salmonella typhimurium*, assumed to be FAD, could be reduced by proline [57,58]. Since these observations, ProDH has been denoted as an FAD-containing enzyme. We show here that *Tt*ProDH does not limit itself to FAD as cofactor; it also binds FMN with equal affinity and has similar kinetic parameters with both cofactors. Moreover, heterologously overproduced MBP-*Tt*ProDH contains more FMN than FAD. The fact that apo-EE and holo-EE have similar spectral and hydrodynamic properties suggests that apo-EE is fully folded and awaits flavin binding. This is similar as in e.g. flavodoxin [59], *para*-hydroxybenzoate hydroxylase [12] and VAO [24]. However, in VAO, initial non-covalent binding of FAD to the apo dimer stimulates enzyme octamerization and autocatalytic flavinylation [25].

Up to now, all known crystal structures of PutAs and ProDHs contain an FAD cofactor [32,44,60-62]. In the crystal structure of *Tt*ProDH (PDB entry 2G37), the high B-factor around the adenosine part of the cofactor is due to the fact that the adenosine is not in contact with any atoms or water molecules in the structure (Fig. 8B). This supports an increased flexibility or absence of the adenosine moiety in a fraction of the enzyme.

The PutAs and ProDHs that have been analyzed so far have a similar location for the isoalloxazine ring system and diphosphoribose moiety of the FAD cofactor, but the orientation of the adenosine group differs between the two enzyme groups. This diverse orientation might be caused by the structural differences between PutAs and ProDHs. First, PutAs contain an additional helix,  $\alpha 5a$ , which is replaced by a loop in monofunctional ProDHs. Helix  $\alpha 5a$  contains a tryptophan that stacks against the adenine group in the FAD in PutAs. The loop in ProDHs does not have an equivalent of this tryptophan for interaction with the FAD. Second, PutAs have extra helical stretches that follow after helix  $\alpha 8$ . These additional C-terminal helices in PutAs would clash with the conformation of the adenine ring of the FAD cofactor as it is found in monofunctional ProDHs [32,63].



Often, the ADP moiety strongly contributes to the interaction between FAD and the apoprotein [24,64-66]. However, in *TtProDH*, the adenosine moiety of FAD does not show any interaction with the enzyme [32] (Fig. 8B). The flavin cofactor inserts its ribityl pyrophosphate moiety next to strands 5 and 6. There are several interactions between *TtProDH* and the pyrophosphate of FAD. Thr226 and His227, present in the  $\beta 6$ - $\alpha 6$  loop, interact with the FMN phosphate. Lys187, stabilized by Asp228, contacts the AMP phosphate. These residues are all present in conserved sequence motifs of the PutA/ProDH family, with His227 and Lys187 being strictly conserved throughout the family [32].

Flavoenzymes that adopt TIM-barrel folds and bind FMN, such as glycolate oxidase [67], flavocytochrome  $b_2$  [68], old yellow enzyme [69], trimethylamine dehydrogenase [70], and dihydroorotate dehydrogenase [71], insert the ribityl phosphate moiety next to strands 7 and 8. With these enzymes, the phosphate group interacts with amides in the initial turn of the short helix  $\alpha 8'$ . In MTHFR [45], the only other known TIM-barrel enzyme that binds FAD, the ribityl chain extends between barrel strands 4 and 5, and the FMN phosphate binds to the  $\beta 4$ - $\alpha 4$  loop. In addition, the adenosine moiety of the FAD cofactor in MTHFR does show several contacts with the enzyme. These data suggest that *TtProDH* has a different binding mode for the FAD/FMN cofactor compared to other FMN-binding TIM-barrel enzymes, and to the FAD-binding MTHFR.

The *TtProDH* variant  $\Delta ABC$  reveals that helices  $\alpha A$ ,  $\alpha B$ ,  $\alpha C$  and  $\alpha 8$  are not essential for binding of the flavin cofactor in *TtProDH*. Based on these observations and the present results, we conclude that there is no structural reason why *TtProDH* should not bind FMN. Thus, we suggest that PutAs might be specific for FAD, whereas monofunctional ProDHs do not necessarily discriminate between FAD and FMN as cofactor.

When purified from *E. coli*, the majority of the EE variant of MBP-*TtProDH* contains FMN as prosthetic group. This might be explained by the availability of FMN and FAD in the cell. To the best of our knowledge, *TtProDH* is the first example of a flavoenzyme that does not discriminate between FAD and FMN as cofactor. Therefore, classification of *TtProDH* as an FAD-binding enzyme should be revised.

## **Acknowledgements**

We thank Prof. Dr. Marco Fraaije (Molecular Enzymology Group, University of Groningen) for kindly providing us with the *E. coli* BSV11 strain. We thank Prof. Dr. Jacques Vervoort (Laboratory of Biochemistry, Wageningen University & Research) for help with mass spectrometry. We thank Arjan Barendregt (Biomolecular Mass Spectrometry and Proteomics Group, Bijvoet Centre for Biomolecular Research, Utrecht University) for help with ESI-MS. This work is supported by the Netherlands Organization for Scientific Research (NWO) and The Graduate School VLAG (Wageningen, The Netherlands) through the ERA-NET Industrial Biotechnology program (ERA-IB-2, project EIB.10.004) of the European Community and by Spanish Ministry of Economy and Competitiveness (BIO2013-42978-P).

## References

- [1] Joosten, V. and van Berkel, W. J. H., Flavoenzymes. *Curr. Opin. Chem. Biol.* (2007), 11, 195-202.
- [2] Santos, M. A., Jiménez, A., Revuelta, J. L., Molecular characterization of *FMN1*, the structural gene for the monofunctional flavokinase of *Saccharomyces cerevisiae*. *J. Biol. Chem.* (2000), 275, 28618-28624.
- [3] Wu, M., Repetto, B., Glerum, D. M., Tzagoloff, A., Cloning and characterization of FAD1, the structural gene for flavin adenine dinucleotide synthetase of *Saccharomyces cerevisiae*. *Mol. Cell. Biol.* (1995), 15, 264-271.
- [4] Mack, M., van Loon, A. P. G. M., Hohmann, H. P., Regulation of riboflavin biosynthesis in *Bacillus subtilis* is affected by the activity of the flavokinase/flavin adenine dinucleotide synthetase encoded by *ribC*. *J. Bacteriol.* (1998), 180, 950-955.
- [5] Manstein, D. J. and Pai, E. F., Purification and characterization of FAD synthetase from *Brevibacterium ammoniagenes*. *J. Biol. Chem.* (1986), 261, 16169-16173.
- [6] Serrano, A., Ferreira, P., Martínez-Júlvez, M., Medina, M., The prokaryotic FAD synthetase family: a potential drug target. *Curr. Pharm. Des.* (2013), 19, 2637-2648.
- [7] Macheroux, P., Kappes, B., Ealick, S. E., Flavogenomics - a genomic and structural view of flavin-dependent proteins. *Febs J.* (2011), 278, 2625-2634.
- [8] de Gonzalo, G., Smit, C., Jin, J., Minnaard, A. J., Fraaije, M. W., Turning a riboflavin-binding protein into a self-sufficient monooxygenase by cofactor redesign. *Chem. Commun.* (2011), 47, 11050-11052.
- [9] Hevel, J. M., White, K. A., Marletta, M. A., Purification of the inducible murine macrophage nitric oxide synthase. Identification as a flavoprotein. *J. Biol. Chem.* (1991), 266, 22789-22791.
- [10] Vermilion, J. L. and Coon, M. J., Identification of the high and low potential flavins of liver microsomal NADPH-cytochrome P-450 reductase. *J. Biol. Chem.* (1978), 253, 8812-8819.
- [11] van Berkel, W. J. H., Benen, J. A. E., Snoek, M. C., On the FAD-induced dimerization of apo-lipoamide dehydrogenase from *Azotobacter vinelandii* and *Pseudomonas fluorescens*. Kinetics of reconstitution. *Eur. J. Biochem.* (1991), 197, 769-779.
- [12] Müller, F. and van Berkel, W. J. H., A study on *p*-hydroxybenzoate hydroxylase from *Pseudomonas fluorescens*. A convenient method of preparation and some properties of the apoenzyme. *Eur. J. Biochem.* (1982), 128, 21-27.
- [13] Müller, F., NMR spectroscopy on flavins and flavoproteins, *Flavins and Flavoproteins: Methods and Protocols*, Springer New York, 2014, 229-306.
- [14] Ghisla, S. and Massey, V., New flavins for old: artificial flavins as active site probes of flavoproteins. *Biochem. J.* (1986), 239, 1-12.
- [15] Krzek, M., van Beek, H. L., Permentier, H. P., Bischoff, R., Fraaije, M. W., Covalent immobilization of a flavoprotein monooxygenase via its flavin cofactor. *Enzyme Microb. Technol.* (2016), 82, 138-143.
- [16] Hefti, M. H., Vervoort, J., van Berkel, W. J. H., Dechlorination and reconstitution of flavoproteins - Tackling fold and function. *Eur. J. Biochem.* (2003), 270, 4227-4242.
- [17] Husain, M. and Massey, V., Reversible resolution of flavoproteins into apoproteins and free flavins, *Methods Enzymol.*, Vol 53, Academic Press, 1978, 429-437.
- [18] Müller, F. and van Berkel, W. J. H., Methods used to resolve reversible flavoproteins into the constituents apoflavoprotein and prosthetic group, *Chemistry and biochemistry of flavoenzymes*, CRC Press, Boca Raton 1991, 261-274.
- [19] Van Berkel, W. J. H. and Müller, F., The elucidation of the microheterogeneity of highly purified *p*-hydroxybenzoate hydroxylase from *Pseudomonas fluorescens* by various biochemical techniques. *Eur. J. Biochem.* (1987), 167, 35-46.
- [20] Mewies, M., McIntire, W. S., Scrutton, N. S., Covalent attachment of flavin adenine dinucleotide (FAD) and flavin mononucleotide (FMN) to enzymes: the current state of affairs. *Protein Sci.* (1998), 7, 7-20.
- [21] Heuts, D. P. H. M., Scrutton, N. S., McIntire, W. S., Fraaije, M. W., What's in a covalent bond? On the role and formation of covalently bound flavin cofactors. *Febs J.* (2009), 276, 3405-3427.
- [22] Fraaije, M. W., van den Heuvel, R. H. H., van Berkel, W. J. H., Mattevi, A., Covalent flavinylation is essential

- p>for efficient redox catalysis in vanillyl-alcohol oxidase.
- J. Biol. Chem.*
- (1999), 274, 35514-35520.
- [23] Brandsch, R. and Bichler, V., Autoflavinylation of apo6-hydroxy-D-nicotine oxidase. *J. Biol. Chem.* (1991), 266, 19056-19062.
- [24] Fraaije, M. W., van den Heuvel, R. H. H., van Berkel, W. J. H., Mattevi, A., Structural analysis of flavinylation in vanillyl-alcohol oxidase. *J. Biol. Chem.* (2000), 275, 38654-38658.
- [25] Tahallah, N., van den Heuvel, R. H. H., van den Berg, W. A. M. *et al.*, Cofactor-dependent assembly of the flavoenzyme vanillyl-alcohol oxidase. *J. Biol. Chem.* (2002), 277, 36425-36432.
- [26] Bandrin, S. V., Rabinovich, P. M., Stepanov, A. I., 3 linkage groups of genes of riboflavin biosynthesis in *Escherichia coli*. *Genetika* (1983), 19, 1419-1425.
- [27] Abbas, C. A. and Sibirny, A. A., Genetic control of biosynthesis and transport of riboflavin and flavin nucleotides and construction of robust biotechnological producers. *Microbiol. Mol. Biol. Rev.* (2011), 75, 321-360.
- [28] Hassan-Abdallah, A., Bruckner, R. C., Zhao, G., Jorns, M. S., Biosynthesis of covalently bound flavin: isolation and *in vitro* flavinylation of the monomeric sarcosine oxidase apoprotein. *Biochemistry* (2005), 44, 6452-6462.
- [29] Jin, J., Mazon, H., van den Heuvel, R. H. H. *et al.*, Covalent flavinylation of vanillyl-alcohol oxidase is an autocatalytic process. *FEBS J.* (2008), 275, 5191-5200.
- [30] Adams, E. and Frank, L., Metabolism of proline and the hydroxyprolines. *Annu. Rev. Biochem.* (1980), 49, 1005-1061.
- [31] Phang, J. M., The regulatory functions of proline and pyrroline-5-carboxylic acid. *Curr. Top. Cell. Regul.* (1985), 25, 91-132.
- [32] White, T. A., Krishnan, N., Becker, D. F., Tanner, J. J., Structure and kinetics of monofunctional proline dehydrogenase from *Thermus thermophilus*. *J. Biol. Chem.* (2007), 282, 14316-14327.
- [33] Tanner, J. J., Structural biology of proline catabolism. *Amino Acids* (2008), 35, 719-730.
- [34] Mitsubuchi, H., Nakamura, K., Matsumoto, S., Endo, F., Inborn errors of proline metabolism. *J. Nutr.* (2008), 138, 2016S-2020S.
- [35] Phang, J. M., Hu, C. A., Valle, D., Disorders of proline and hydroxyproline metabolism, Metabolic and Molecular Bases of Inherited Disease, McGraw-Hill, 2001, 1821-1838.
- [36] Hu, C. A., Williams, D. B., Zhaorigetu, S. *et al.*, Functional genomics and SNP analysis of human genes encoding proline metabolic enzymes. *Amino Acids* (2008), 35, 655-664.
- [37] Bender, H. U., Almashanu, S., Steel, G. *et al.*, Functional consequences of PRODH missense mutations. *Am. J. Hum. Genet.* (2005), 76, 409-420.
- [38] Jacquet, H., Demily, C., Houy, E. *et al.*, Hyperprolinemia is a risk factor for schizoaffective disorder. *Mol. Psychiatry* (2004), 10, 479-485.
- [39] Jacquet, H., Raux, G., Thibaut, F. *et al.*, PRODH mutations and hyperprolinemia in a subset of schizophrenic patients. *Hum. Mol. Genet.* (2002), 11, 2243-2249.
- [40] Willis, A., Bender, H. U., Steel, G., Valle, D., PRODH variants and risk for schizophrenia. *Amino Acids* (2008), 35, 673-679.
- [41] Donald, S. P., Sun, X. Y., Hu, C. A. A. *et al.*, Proline oxidase, encoded by p53-induced gene-6, catalyzes the generation of proline-dependent reactive oxygen species. *Cancer Res.* (2001), 61, 1810-1815.
- [42] Polyak, K., Xia, Y., Zweier, J. L., Kinzler, K. W., Vogelstein, B., A model for p53-induced apoptosis. *Nature* (1997), 389, 300-305.
- [43] Liu, W. and Phang, J. M., Proline dehydrogenase (oxidase) in cancer. *Biofactors* (2012), 38, 398-406.
- [44] Lee, Y. H., Nadaraia, S., Gu, D., Becker, D. F., Tanner, J. J., Structure of the proline dehydrogenase domain of the multifunctional PutA flavoprotein. *Nat. Struct. Biol.* (2003), 10, 109-114.
- [45] Guenther, B. D., Sheppard, C. A., Tran, P. *et al.*, The structure and properties of methylenetetrahydrofolate reductase from *Escherichia coli* suggest how folate ameliorates human hyperhomocysteinemia. *Nat. Struct. Biol.* (1999), 6, 359-365.
- [46] Huijbers, M. M. E. and van Berkel, W. J. H., High yields of active *Thermus thermophilus* proline dehydrogenase are obtained using maltose-binding protein as a solubility tag. *Biotechnol. J.* (2015), 10,

- 395-403.
- [47] Huijbers, M. M. E. and van Berkel, W. J. H., A more polar N-terminal helix releases *Thermus thermophilus* proline dehydrogenase from self-association. *J. Mol. Catal. B* (2016), 134, 340-346.
  - [48] Kabsch, W., XDS. *Acta Crystallogr. D Biol. Crystallogr.* (2010), 66, 125-132.
  - [49] Collaborative Computational Project, N., The CCP4 suite: programs for protein crystallography. *Acta Crystallogr. D Biol. Crystallogr.* (1994), 50, 760-763.
  - [50] Vagin, A. A., New translation and packing functions. *Newsletter on protein crystallography, Daresbury Laboratory* (1989), 24, 117-121.
  - [51] Murshudov, G. N., Vagin, A. A., Dodson, E. J., Refinement of macromolecular structures by the maximum-likelihood method. *Acta Crystallogr. D Biol. Crystallogr.* (1997), 53, 240-255.
  - [52] Emsley, P., Lohkamp, B., Scott, W. G., Cowtan, K., Features and development of Coot. *Acta Crystallogr. D Biol. Crystallogr.* (2010), 66, 486-501.
  - [53] Laskowski, R. A., MacArthur, M. W., Moss, D. S., Thornton, J. M., PROCHECK: a program to check the stereochemical quality of protein structures. *J. Appl. Cryst.* (1993), 26, 283-291.
  - [54] Weber, G., Fluorescence of riboflavin and flavin-adenine dinucleotide. *Biochem. J.* (1950), 47, 114-121.
  - [55] Visser, A. J. W. G., Kinetics of stacking interactions in flavin adenine dinucleotide from time-resolved flavin fluorescence. *Photochem. Photobiol.* (1984), 40, 703-706.
  - [56] Scarpulla, R. C. and Soffer, R. L., Membrane-bound proline dehydrogenase from *Escherichia coli*. Solubilization, purification and characterization. *J. Biol. Chem.* (1978), 253, 5997-6001.
  - [57] Menzel, R. and Roth, J., Enzymatic properties of the purified *putA* protein from *Salmonella typhimurium*. *J. Biol. Chem.* (1981), 256, 9762-9766.
  - [58] Menzel, R. and Roth, J., Purification of the *putA* gene product - A bifunctional membrane-bound protein from *Salmonella typhimurium* responsible for the two-step oxidation of proline to glutamate. *J. Biol. Chem.* (1981), 256, 9755-9761.
  - [59] Bollen, Y. J. M., Nabuurs, S. M., van Berkel, W. J. H., van Mierlo, C. P. M., Last in, first out: the role of cofactor binding in flavodoxin folding. *J. Biol. Chem.* (2005), 280, 7836-7844.
  - [60] Singh, H., Arentson, B. W., Becker, D. F., Tanner, J. J., Structures of the PutA peripheral membrane flavoenzyme reveal a dynamic substrate-channeling tunnel and the quinone-binding site. *Proc. Natl. Acad. Sci. USA* (2014), 111, 3389-3394.
  - [61] Srivastava, D., Schuermann, J. P., White, T. A. *et al.*, Crystal structure of the bifunctional proline utilization A flavoenzyme from *Bradyrhizobium japonicum*. *Proc. Natl. Acad. Sci. USA* (2010), 107, 2878-2883.
  - [62] Luo, M., Arentson, B. W., Srivastava, D., Becker, D. F., Tanner, J. J., Crystal structures and kinetics of monofunctional proline dehydrogenase provide insight into substrate recognition and conformational changes associated with flavin reduction and product release. *Biochemistry* (2012), 51, 10099-10108.
  - [63] Zhang, M., White, T. A., Schuermann, J. P. *et al.*, Structures of the *Escherichia coli* PutA proline dehydrogenase domain in complex with competitive inhibitors. *Biochemistry* (2004), 43, 12539-12548.
  - [64] van der Laan, J. M., Schreuder, H. A., Swarte, M. B. A. *et al.*, The coenzyme analog adenosine 5-diphosphoribose displaces FAD in the active site of p-hydroxybenzoate hydroxylase. An x-ray crystallographic investigation. *Biochemistry* (1989), 28, 7199-7205.
  - [65] Sato, K., Nishina, Y., Shiga, K., The binding of adenine nucleotides to apo-electron-transferring flavoprotein. *J. Biochem.* (1992), 112, 804-810.
  - [66] Tedeschi, G., Negri, A., Ceciliani, F., Mattevi, A., Ronchi, S., Structural characterization of L-aspartate oxidase and identification of an interdomain loop by limited proteolysis. *Eur. J. Biochem.* (1999), 260, 896-903.
  - [67] Lindqvist, Y., Refined structure of spinach glycolate oxidase at 2 Å resolution. *J. Mol. Biol.* (1989), 209, 151-166.
  - [68] Xia, Z. X. and Mathews, F. S., Molecular structure of flavocytochrome  $b_2$  at 2.4 Å resolution. *J. Mol. Biol.* (1990), 212, 837-863.
  - [69] Fox, K. M. and Karplus, P. A., Old yellow enzyme at 2 Å resolution: overall structure, ligand binding, and comparison with related flavoproteins. *Structure* (1994), 2, 1089-1105.

- [70] Lim, L. W., Shamala, N., Mathews, F. S. *et al.*, Three-dimensional structure of the iron-sulfur flavoprotein trimethylamine dehydrogenase at 2.4 Å resolution. *J. Biol. Chem.* (1986), 261, 15140-15146.
- [71] Rowland, P., Nielsen, F. S., Jensen, K. F., Larsen, S., The crystal structure of the flavin containing enzyme dihydroorotate dehydrogenase A from *Lactococcus lactis*. *Structure* (1997), 5, 239-252.







# Chapter 7

**General discussion**





L-proline is one of the proteinogenic amino acids and a central compound in metabolism (**Chapter 1**). Proline catabolism involves the conversion of L-proline to L-glutamate, which starts with the oxidation of L-proline to  $\Delta^1$ -pyrroline-5-carboxylate (P5C) by the flavin-dependent enzyme proline dehydrogenase (ProDH) (Fig. 1A). In addition, L-proline also serves as a building block for the synthesis of a wide range of antibiotics.

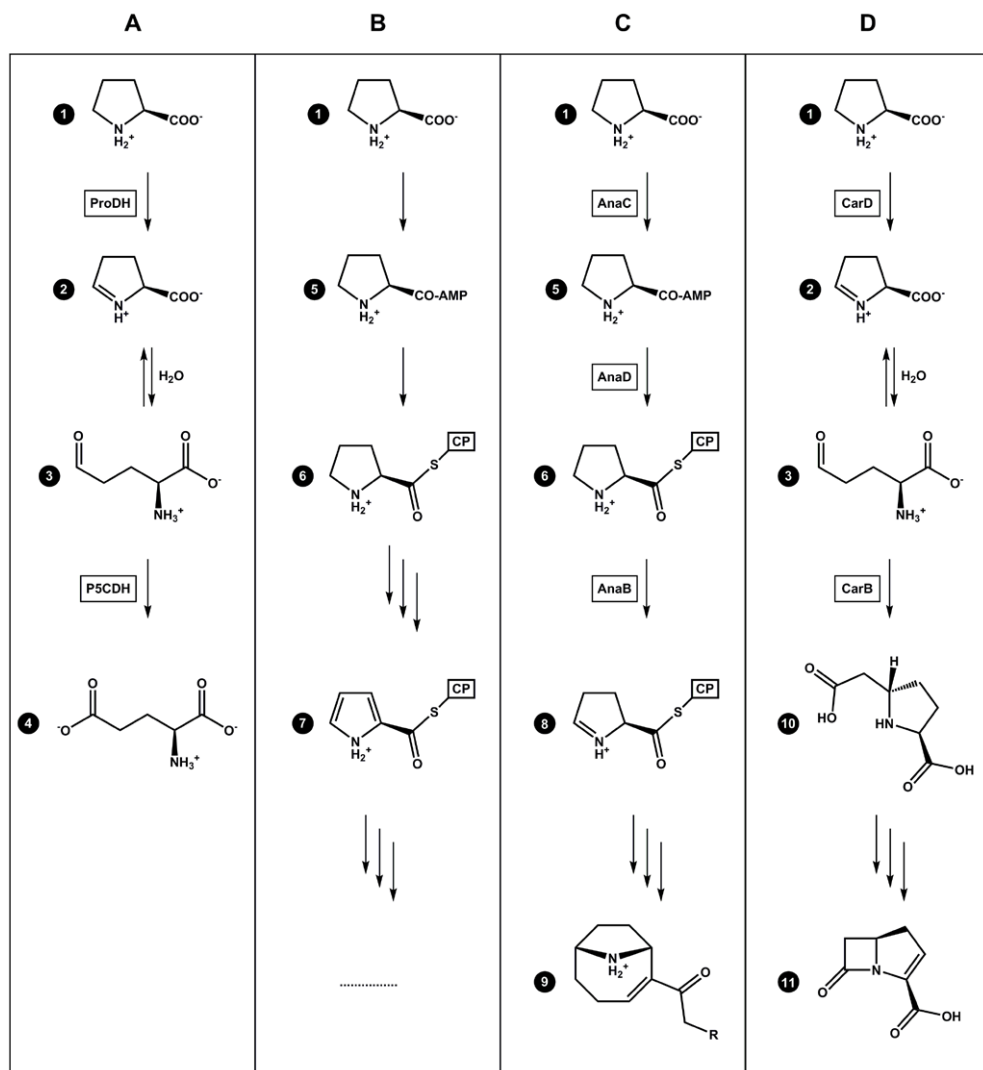
### Proline as a building block

Pyrrole rings are commonly encountered in natural products [1], and L-proline often serves as one of the precursors of pyrrole-containing secondary metabolites [2-8]. Biosynthesis of these compounds starts with the adenylation of L-proline, followed by loading of the adenylated proline onto an acyl-carrier protein (ACP) or peptidyl carrier protein (PCP). Subsequently, a four-electron oxidation takes place and prolyl-CP is converted to pyrrole-2-carboxylate (P2C)-CP, which can serve as one of the building blocks for polyketide synthases (PKSs) or nonribosomal peptide synthases (NRPSs) (Fig. 1B) [1]. However, there are also examples in which L-proline is oxidized and incorporated in a different way into natural products.

The neurotoxic alkaloids anatoxin-a and homoanatoxin-a are produced by certain species of cyanobacteria and are potent agonists of the nicotinic acetylcholine receptor [9]. Biosynthesis of these compounds is initiated by the conversion of L-proline and resembles the biosynthesis of pyrrole-containing secondary metabolites. However, in this case, a two-electron oxidation takes place instead of a four-electron oxidation. As a result, the product is P5C, as for ProDH, rather than P2C (Fig. 1C) [10,11]. Sequence alignments show that the enzyme responsible for this reaction is not related to ProDHs, but belongs to the acyl-CoA dehydrogenases (ACAD) family [11,12].

L-proline is also an important building block for the biosynthesis of carbapenems, which are promising sources for clinically useful antibiotics. After conversion of proline to glutamic semialdehyde (GSA), malonyl-CoA is condensed with GSA and subsequent biosynthesis steps lead to the production of the basic carbapenem (Fig. 1D) [13]. The enzyme that converts proline to GSA in this biosynthetic route, CarD, shows significant sequence homology to ProDH, and the fingerprint motifs of the PutA/ProDH family are easily recognized [14]. Therefore, in the biosynthesis of carbapenem antibiotics, proline is not adenylated and CP-bound, but directly oxidized by ProDH.

In summary, L-proline is an important building block of many metabolites and antibiotics. Most often, proline oxidation occurs on prolyl-CPs by ACAD-like enzymes. However, sometimes ProDH plays a direct role in the oxidation of proline.

**Figure 1.**

Involvement of L-proline in different biosynthetic pathways. **(A)** Conversion of L-proline to L-glutamate. **(B)** L-proline as the precursor of pyrrole-containing secondary metabolites. **(C)** Incorporation of L-proline into (homo)anatoxin-a. **(D)** Incorporation of L-proline into (5R)-cabapenem. Reaction intermediates: (1) L-proline, (2)  $\Delta^1$ -pyrroline-5-carboxylate (3) glutamic semialdehyde, (4) L-glutamate, (5) adenylated L-proline, (6) CP-loaded L-proline, (7) CP-loaded pyrrole-2-carboxylate, (8) CP-loaded  $\Delta^1$ -pyrroline-5-carboxylate, (9) R=H: anatoxin-a, R=Me: homoanatoxin-a, (10) (2S,5S)-carboxymethylproline, (11), (5R)-cabapenem.

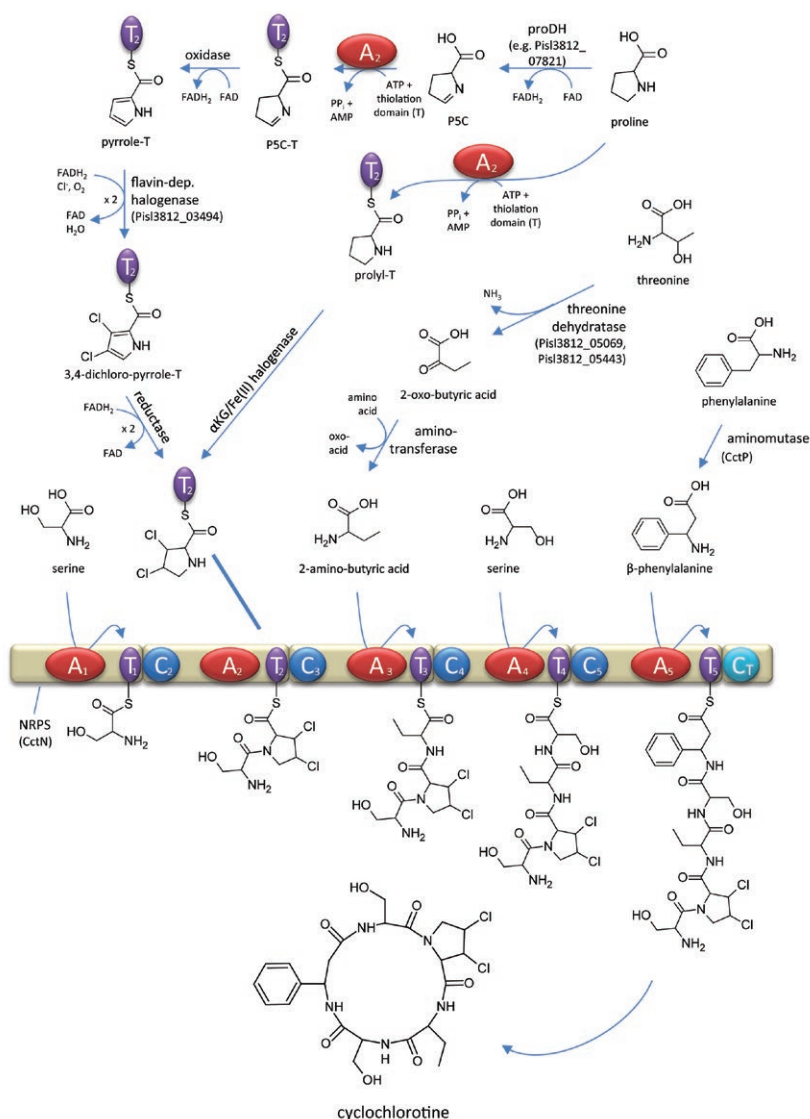


Figure 2.

Model for cyclochlorotine biosynthesis. The upper part proposes pathways for the nonproteinogenic amino acid building blocks. Where applicable, candidate enzymes are indicated. Synthesis of 3,4-dichloroproline most likely is achieved on a carrier protein (e.g. T domain of module 2), and two possible pathways are shown. Halogenation occurs either directly by a 2KG/Fe(II)-dependent halogenase or by a flavin-dependent halogenase via a pyrrole carboxylic acid intermediate. The proline dehydratase (*ProDH*) Pisl3812\_07821 is considered to initiate the latter pathway by oxidation of free proline to form  $\Delta^1$ -pyrroline-5-carboxylic acid (P5C). Subsequent steps likely involve a P5C-carrier protein oxidase (according to [7,11]). In the lower part, NRPS domains are abbreviated as A for adenylation, T for thiolation, C for condensation and CT for terminal condensation-like domains. The T domains are post-translationally modified by phosphopantetheinylation. Release and cyclization of cyclochlorotine is mediated by the CT domain. Figure from [15].



Cyclochlorotine, an astin analogue produced by *Talaromyces islandicus*, contains a dichlorinated proline. This cyclic peptide is synthesized by an NRPS [15] (Fig. 2). As part of the European Research Area Industrial Biotechnology (ERA-IB) project “Multi Enzyme Systems Involved in Astin Biosynthesis and their use in heterologous astin production (MESIAB)”, we expressed three ProDHs from *T. islandicus* that might play a role in the biosynthesis of cyclochlorotine (**Chapter 1**). So far, it remains to be elucidated whether initial proline oxidation occurs directly by ProDH, or after adenylation and loading onto an CP (Fig. 2) [15].

## Recombinant production of ProDH

So far, the *in vitro* properties of eukaryotic ProDHs have been poorly characterized and it has remained challenging to produce these enzymes in heterologous hosts. Expression of eukaryotic proteins in a prokaryotic system is often hampered by the lack of suitable chaperones, post-translational modifications, and compartmentalization, which can result in protein misfolding and aggregation [16]. Nevertheless, production of recombinant proteins in *Escherichia coli* remains one of the most popular methods to obtain proteins for basic research. The advantages of using *E. coli* as a host are high levels of heterologous gene expression, a wide range of available genetic tools, easy scalability of experiments, fast production and low costs. Therefore, we initiated expression trials of His-tagged *T. islandicus* ProDHs (*Ti*ProDH) in *E. coli*. However, this was not straightforward, as production levels were low, the enzymes ended up in inclusion bodies, and were sensitive to proteolytic degradation.

Because of the instability of *Ti*ProDH during purification, we simultaneously started expression trials with ProDH from *Thermus thermophilus* (*Tt*ProDH). The crystal structure of this enzyme has been elucidated [17], but relatively little is known about its biochemical properties. Since *T. thermophilus* and its thermostable enzymes are often used as model systems [18], *Tt*ProDH was a good candidate to find out more about the structure-function relationship of ProDHs. This knowledge would also be useful for the production of proline-derived chemicals, including astins.

Although *Tt*ProDH has been crystallized, production yields of this prone-to-aggregate enzyme have not been reported. In **Chapter 2**, we describe the heterologous production of *Tt*ProDH in *E. coli*. Initially, we attempted to express this enzyme with a polyhistidine-tag; however, this was not readily achieved.

Many strategies are available to enhance protein solubility and decrease protein aggregation during production in a heterologous host. Such strategies include, amongst others, procedures to control the expression of genes encoding the protein, development of specialized bacterial host strains, and screening of growth and induction conditions [19]. In addition, the development of solubility- and purification tags has enhanced the possibilities for protein expression and purification. Nowadays, many affinity-tag systems are available

that can contribute to an increased protein solubility and an easier purification process [20]. Such tags are characterized by a minimal effect on the tertiary structure and biological activity of the protein of interest, and an easy and specific removal in order to produce the native form of the protein.

To boost the production of *TtProDH* in *E. coli*, we constructed an N-terminal fusion between this enzyme and maltose-binding protein (MBP). Vectors that harbor MBP in order to facilitate the expression and purification of proteins were first described in 1988 [21]. Nowadays, MBP is widely recognized as an efficient solubility tag, especially during the purification of eukaryotic proteins [22–24]. Using MBP as a fusion tag for *TtProDH* was very successful, as MBP-*TtProDH* was easily produced in *E. coli* and purified as active holoenzyme. Impressive yields of the fusion enzyme were obtained: after expression in *E. coli*, MBP-*TtProDH* comprised about 50% of the total protein content of the cells and more than 250 mg fusion protein per liter of *E. coli* culture was purified (Fig. 3). MBP-*TtProDH* could also be successfully cleaved with trypsin in order to obtain native *TtProDH* (**Chapter 2**). However, cleavage was not achieved with Factor Xa, for which a cleavage site was constructed in the linker sequence.



**Figure 3.**

Purification of MBP-*TtProDH* WT. The left panel depicts the amylose column with the bound fusion protein. The right panel shows the impressive yield of the purified enzyme, as deduced from the intense yellow color, which originates from the non-covalently bound flavin cofactor.

One of the ProDHs from *T. islandicus* could be also produced and purified using the MBP-tag (Fig. 4), and ProDH activity of this enzyme could be demonstrated [15]. However, this fungal enzyme appeared to be less stable during purification than MBP-tagged *TtProDH*.

One of the reasons for the poor expression and solubility of *TiProDH* might be its N-terminal sequence. ProDHs adopt a distorted ( $\beta\alpha$ )<sub>8</sub> TIM-barrel fold, which is conserved throughout the PutA/ProDH family; however, the N-terminal sequence of ProDH is poorly conserved and varies among species. Eukaryotic ProDHs have an elongated N-terminus compared to prokaryotic ProDHs (Fig. 5). The function of this N-terminal sequence is currently unknown. As for human ProDH [25], successful production of *TiProDH* in *E. coli* might require the

(partial) removal of the N-terminal sequence. Furthermore, the involvement of this enzyme in the production of cyclochlorotine remained elusive. Therefore, we did not continue with an extensive characterization of this fungal enzyme but rather focused on the biochemical characterization of *Tt*ProDH.

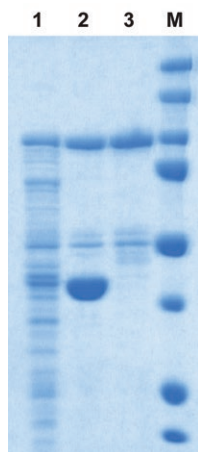


**Figure 4.**

SDS-PAGE analysis of *Tt*ProDH purification. Lanes: (1) cell extract, (2) after amylose column and concentration (3) after Superdex 200 column and concentration. As a molecular weight marker, Precision Plus Protein Standard (Biorad) was used. Molecular masses of marker proteins (M), from top to bottom: 250, 150, 100, 75, 50, 37, 25, 20 kDa. 43 mg of MBP-*Tt*ProDH was purified from a 6 L *E. coli* culture. Purified MBP-*Tt*ProDH has an apparent molecular mass of 97 kDa, which matches the predicted theoretical mass of 98.7 kDa for the construct. A weak band of smaller size (51 kDa) is also visible. It is assumed that this band is free *Tt*ProDH which has a predicted theoretical mass of 56.2 kDa. The intense band corresponding to 41 kDa in lane 2 is due to free MBP, which has a predicted theoretical mass of 42.5 kDa. Figure from [15].

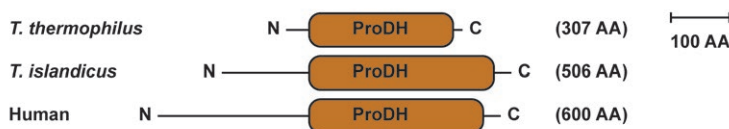


**Figure 5.**

Cartoon representation of the domain composition of *T. thermophilus*, *T. islandicus* and human ProDH. The N- and C-termini are indicated as black lines, and the catalytic ProDH domain is indicated as a brown box. The total lengths of the protein sequences are indicated in parentheses.

## Self-association of *Tt*ProDH

Purified MBP-*Tt*ProDH, as well as native *Tt*ProDH, appeared to be prone to aggregation through non-native self-association. In **Chapter 3**, we provide evidence that the hydrophobic N-terminal helix of *Tt*ProDH is responsible for the self-association. A more polar helix, created by replacing Phe10 and Leu10 for glutamates (EE), prevents the protein from aggregating and the MBP-*Tt*ProDH EE variant exclusively forms tetramers. Unfortunately, although MBP-*Tt*ProDH WT can easily be cleaved with trypsin to obtain the native protein, this is not the case for MBP-*Tt*ProDH EE. The MBP-tag is very stable against trypsinolysis, but *Tt*ProDH EE gets readily degraded (**Chapter 3**). Also for additional MBP-*Tt*ProDH variants (described in **Chapters 4 and 5**), production was very successful, but cleavage of the fusion enzyme, either with Factor Xa, chymotrypsin or trypsin, in order to obtain native *Tt*ProDH remained elusive. This suggests that aggregation of *Tt*ProDH protects the enzyme against trypsinolysis.

In **Chapter 2**, we showed that the MBP-tag does not influence the spectral, hydrodynamic and kinetic properties of *Tt*ProDH. However, removal of the MBP-tag is of interest in order to study the enzyme in its native state, for example with regard to its thermostability and three-dimensional structural properties. Although thermal unfolding and thermoinactivation of the fusion enzymes can be studied (**Chapter 5**), more detailed structure-function relationship studies require removal of the MBP-tag. Furthermore, removal of the fusion tag would allow us to confirm that the tag does not influence the oligomerization state of *Tt*ProDH. Also for biocatalytic applications, such as cascade reactions with glutamate-1-semialdehyde aminomutase [26], quantitative removal of the tag is desirable. Attempts to optimize cleavage of the fusion enzyme by altering the conditions of trypsinolysis, by mutating suspect trypsin cleavage sites, and by cleaving in the presence of the substrate proline or the inhibitor L-tetrahydro-2-furoic acid (THFA), did not protect native *Tt*ProDH from further degradation. An additional possibility to obtain the native enzyme from MBP-*Tt*ProDH could be to change the linker between the fusion tag and the native enzyme.

### Catalytic properties of *Tt*ProDH

As described in **Chapter 1**, ProDH oxidizes L-proline to P5C. This oxidation involves the transfer of two electrons from the proline substrate to the flavin cofactor, which is subsequently re-oxidized by transferring its electrons to the electron transport chain via the reduction of membrane-bound ubiquinone [27-29]. *Tt*ProDH has a restricted substrate scope: next to L-proline, only 3,4-dehydro-L-proline becomes oxidized [17]. In addition, *Tt*ProDH has a high  $K_M$  value for proline. This value likely reflects the availability of proline in the cell, and the fact that proline should, besides being converted to P5C, also be available for various other cellular processes and protein synthesis.

It has been shown for the ProDH domain of *E. coli* PutA (*Ec*PutA) [30] and ProDH from *M. tuberculosis* (*Mt*ProDH) [31] that the substrate-induced reduction of the flavin is not the rate-limiting step in the overall reaction. In order to determine the rate of proline oxidation, we performed anaerobic stopped-flow kinetics on MBP-*Tt*ProDH WT and *Tt*ProDH WT. When recording steady-state kinetics, proline concentrations up to 200 mM are used (**Chapter 3-6**) and the maximal rate is not yet reached at that substrate concentration. The high proline concentrations complicate the anaerobic stopped-flow experiments of the reductive half-reaction. As can be seen in Fig. 6, maximum rates are not reached yet at a substrate concentration of 400 mM proline. Using higher proline concentrations gives severe mixing problems in the stopped-flow machine due a high viscosity of the substrate solution. Nevertheless, it is clear that the maximum rate of the reductive half-reaction of *Tt*ProDH WT is an order of magnitude higher than the overall rate of this enzyme. Furthermore, the estimated dissociation constant ( $K_D$ ) of the enzyme-proline complex underscores the low affinity for the substrate.

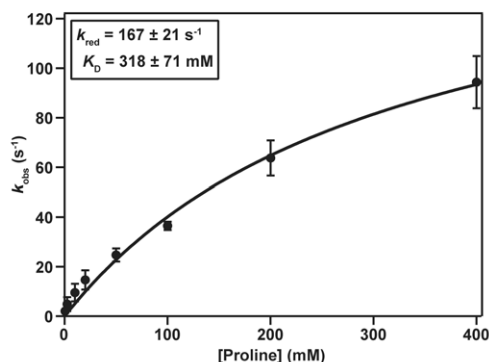


**Figure 6.**

Proline reductive half-reaction of *Tt*ProDH WT, as determined by anaerobic stopped-flow experiments. The measurements were performed at 25 °C, in 50 mM sodium phosphate, pH 7.4.

The overall reaction rate of MBP-*Tt*ProDH is strongly temperature dependent. Increasing the temperature from 25 °C to 45 °C, which is closer to the physiological temperature of *T. thermophilus*, leads to a remarkable tenfold increase in catalytic efficiency (**Chapter 3**). This corresponds with the idea that thermostable enzymes are rather rigid at room temperature. In line with this, incubation of various MBP-*Tt*ProDH variants at elevated temperatures leads to an initial increase in activity (**Chapters 2 and 5**), which is probably related to an increase in protein flexibility. It would be interesting to determine the kinetic parameters of the MBP-*Tt*ProDH variants described in **Chapters 4 and 5** at elevated temperatures to determine if the variants behave equally with proline.

To gain more insight into the reactivity of the flavin cofactor of the MBP-*Tt*ProDH variants, we used a suicide inhibitor to mimic the behavior of the proline substrate (**Chapter 4**). Suicide inhibitors, also called mechanism-based inhibitors, initially react with an enzyme in a similar way as the substrate. However, a chemically reactive intermediate is generated during the reaction and the enzyme is inactivated through covalent modification by this intermediate. *N*-propargyl derivatives can function as suicide inhibitors and can be used as drugs to inhibit flavoenzymes. This has been demonstrated for example for monoamine oxidases [32,33]. *Tt*ProDH can be irreversibly inactivated by the suicide inhibitor *N*-propargylglycine due to formation of a bicovalent linkage between flavin N(5) and the  $\epsilon$ -amino group of Lys99 [34]. *N*-propargylglycine turned out to be a perfect probe to mimic the proline substrate of *Tt*ProDH. Upon reaction of the enzyme with this suicide inhibitor, the absorption maximum of *Tt*ProDH at 450 nm disappears, while the maximum at 380 nm gradually increases and shifts to longer wavelengths. This behavior is indicative of initial flavin reduction and subsequent formation of the covalent Lys99-flavin adduct. Thus, the reactivity of the flavin cofactor can easily be monitored using this probe. In **Chapter 4**, we describe the reactivity of different MBP-*Tt*ProDH variants with *N*-propargylglycine to see the changes in reactivity of the flavin with this substrate analogue.

## Functionality of *Tt*ProDH

As stated above, ProDHs adopt a distorted  $(\beta\alpha)_8$  TIM-barrel fold, which is conserved throughout the PutA/ProDH family; however, the N-terminal sequence of ProDH is poorly conserved and varies in length (Fig. 5). *Tt*ProDH contains an N-terminal arm consisting of three helices:  $\alpha$ A,  $\alpha$ B and  $\alpha$ C. We show in **Chapter 3** that aggregation of MBP-*Tt*ProDH is due to the hydrophobicity of helix  $\alpha$ A. After solving the issue of self-association by replacing the hydrophobic amino acids Phe10 and Leu10 for polar glutamates (EE), we subsequently removed one ( $\Delta$ A), two ( $\Delta$ AB) or three ( $\Delta$ ABC) N-terminal helices in order to obtain more information about their function (**Chapter 4**). It became evident that N-terminal helices  $\alpha$ A and  $\alpha$ B play no role in catalysis of the enzyme, nor in protein tetramerization. In fact, the  $k_{\text{cat}}$  of WT is the lowest of all MBP-*Tt*ProDH variants. This is probably due to its self-association, which makes the enzyme less flexible. Solving the problem of self-association (EE), and removal of one or two N-terminal helices ( $\Delta$ A and  $\Delta$ AB) increases the  $k_{\text{cat}}$ , with  $\Delta$ AB being the most active truncated variant. This indicates that helices  $\alpha$ A and  $\alpha$ B are not required for catalysis. As described above, *N*-propargylglycine can be used to mimic the proline substrate and monitor the reactivity with the flavin cofactor. We show that removal of one or two N-terminal helices increases the rate of covalent flavin modification, indicating that the reaction with the suicide inhibitor has improved.

In contrast to helices  $\alpha$ A and  $\alpha$ B, helix  $\alpha$ C is crucial for *Tt*ProDH catalysis and tetramerization. Removal of this helix leads to inactive dimers and partial cleavage of C-terminal helix  $\alpha$ 8 during production of the enzyme in *E. coli*. The crystal structure of *Tt*ProDH  $\Delta$ ABC (PDB: 5M42), as determined in **Chapter 6**, confirms a similar overall structure and no gross conformational changes compared to *Tt*ProDH WT (PDB: 2G37). However, in this structure, an even larger part of C-terminal helix  $\alpha$ 8 is missing, suggesting an increased flexibility or even removal of the remaining part of helix  $\alpha$ 8. V32D and V36D variants show that a hydrophobic patch between helix  $\alpha$ C and  $\alpha$ 8 is involved in retaining activity and tetramerization (**Chapter 4**). Therefore, we conclude that helix  $\alpha$ C is involved in positioning of C-terminal helix  $\alpha$ 8. This is important for catalysis, since helix  $\alpha$ 8 contributes several strictly conserved residues that interact with the proline substrate.

To gain more insight into the functionality of *Tt*ProDH, we selectively disrupted two ion pairs in the dimerization domain of MBP-*Tt*ProDH variants EE,  $\Delta$ A,  $\Delta$ AB and  $\Delta$ ABC (**Chapter 5**). Changing two negatively charged residues (Asp205 and Glu207) in helices  $\alpha$ 5 into positively charged lysines (KK) alters the oligomerization state of the enzyme from tetramer to monomer. This monomerization improves the catalytic efficiencies of the enzymes, although this is at the cost of their thermostability. The monomeric variant  $\Delta$ AB KK might be used for studying the interactions between helices  $\alpha$ C and  $\alpha$ 8 and their influence on catalysis in more detail. A crystal structure does not always show the influence of destabilizing interactions, since the protein is in a fixed state in the structure, but it might be possible to study such



destabilizing interactions using 2D NMR [35]. Due to its monomeric nature, *Tt*ProDH  $\Delta$ AB KK would be an interesting candidate for such studies, although this would require removal of the MBP-tag.

In conclusion, we have achieved to obtain fully activity monomers of MBP-tagged *Tt*ProDH. We have also shown that it is possible to selectively remove parts of the N-terminus, without influencing the *in vitro* functionality of the enzyme. Therefore, MBP-*Tt*ProDH variant  $\Delta$ AB KK is the smallest, fully functioning variant of this enzyme with a molecular mass of the catalytic domain of 33 kDa. This domain contains all parts that are crucial for catalysis. However, it has to be taken into account that this concerns *in vitro* activity. *In vivo*, the N-terminal parts that we removed might serve as a docking interface for P5CDH during channeling, or might be involved in interaction with the cytoplasmic surface of the plasma membrane. Nevertheless, the fact that for *Tt*ProDH most of the N-terminus can be deleted without affecting the enzyme suggests that it should be possible to rationally design N-terminal truncated constructs for the recombinant expression of eukaryotic ProDHs, with a special interest in human ProDH (*vide infra*).

### Thermostability of *Tt*ProDH

In this thesis, we have investigated several properties of *Tt*ProDH that are of interest for industrial purposes. The use of enzymes in industrial processes is expanding since green alternatives to chemical processes and the production of enantiomerically pure compounds is becoming increasingly important. Enzymes from thermophilic organisms are very promising industrial biocatalysts. They often display a high operational stability and co-solvent compatibility. This facilitates the use of non-natural substrates in industrial processes, since such substrates are often more soluble at higher temperatures and in the presence of organic solvents. Thermophilic enzymes are applicable in, for example, biorefinery [36], bioremediation [37], and in the production of chiral compounds to produce optically pure pharmaceuticals. Thermostable enzymes from *Thermus thermophilus* often serve as models and have widespread biotechnological applications [18,38].

In **Chapter 2**, we show that *Tt*ProDH has a melting temperature over 80 °C and has a rather good co-solvent compatibility. In **Chapter 5**, we took a closer look at the thermostability of *Tt*ProDH. The oligomerization state of this enzyme appeared to be a crucial factor in providing thermostability. As explained before, the dimerization domain of *Tt*ProDH, formed by helices  $\alpha$ 5, was disrupted by changing two negatively charged residues (Asp205 and Glu207) into positively charged lysines (KK). This leads to the formation of functional monomers rather than dimers. These monomers have an increased catalytic activity at moderate temperatures, but their thermostability has decreased severely. This might be caused by the increased flexibility of the free monomers compared to the monomeric units in a tetrameric composition. So in this enzyme, a trade-off is made between thermostability

and catalytic activity. Since a high thermostability combined with a high activity at moderate temperatures does not provide an evolutionary advantage for thermophilic organisms, this trade is probably not maintained during evolution. Therefore, trade-offs between catalytic activity and stability are commonly found in enzymes [39-41].

As we described in **Chapter 5**, proteins from (hyper)thermophilic organisms have been found to be structurally similar to their mesophilic counterparts and there are many examples of thermostable enzymes that occur in a higher oligomeric state compared to their mesophilic counterparts. The observation that a higher oligomerization state is crucial to retain thermostability of *Tt*ProDH combined with the observation that thermophilic and mesophilic enzymes are structurally very alike might be used to increase the thermostability of other mesophilic enzymes while maintaining their catalytic activity.

### Cofactor binding of *Tt*ProDH

In **Chapter 6**, we studied the cofactor binding of *Tt*ProDH. Flavoenzymes contain a flavin adenine dinucleotide (FAD) or flavin mononucleotide (FMN) cofactor that serves as a redox-active prosthetic group. FAD- and FMN-containing enzymes are dominated by different enzyme folds. The Rossmann fold is very common among FAD-containing proteins, while FMN-containing proteins mostly adopt a TIM-barrel or flavodoxin-like fold [42]. The preference for FAD or FMN for different enzyme folds is clearly demonstrated in the family of flavin-dependent monooxygenases, which constitutes the largest family of flavoenzymes with at least 130 members described thus far [42,43]. Members of groups A, B, E, F and G of flavin-dependent monooxygenases adopt a Rossmann fold and bind FAD, while members of group C and H adopt a TIM-barrel fold and bind FMN (Fig. 7). Members of group D adopt an acyl-CoA dehydrogenase fold and bind either FAD or FMN [43].

In **Chapter 6**, we show that *Tt*ProDH can bind both FAD and FMN with similar kinetic parameters and dissociation constants. To the best of our knowledge, this is the first example of a flavoenzyme that shows no preference for either of the cofactors. It might be that this is rather unique; however, it also indicates that caution should be taken before describing an enzyme as an FAD- or FMN-binding enzyme. Our results suggest that there are examples of enzymes belonging to the same family but originating from different organisms that do not necessarily contain the same flavin cofactor.

Purified MBP-tagged *Tt*ProDH contains a mixture of FAD and FMN (**Chapter 6**). The ratio between both cofactors might depend on the purified batch of enzyme, since the enzyme has no preference for either of the cofactors and the availability of both cofactors in the cell might differ between different enzyme production processes.

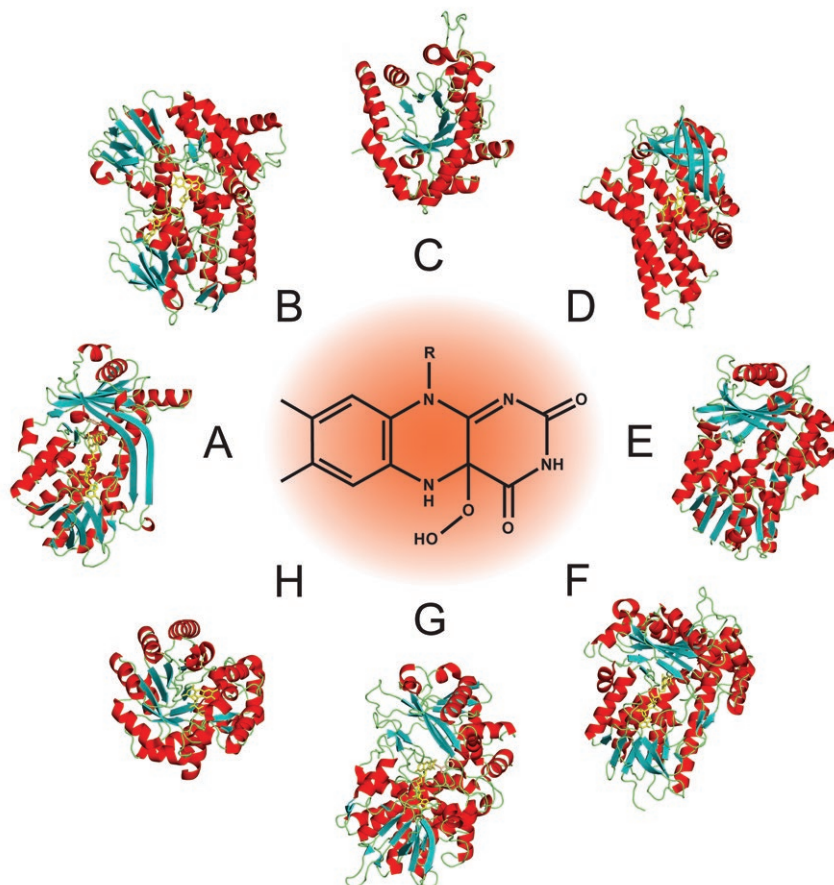


**Figure 7.**

Protein folds of flavin-dependent monooxygenases. Members of groups A, B, E, F and G adopt a Rossmann fold and bind FAD and members of groups C and H adopt a TIM-barrel fold and bind FMN. Members of group D adopt an acyl-CoA dehydrogenase fold and bind either FAD or FMN. (A) 4-hydroxybenzoate 3hydroxylase (PDB: 1PBE), (B) phenylacetone monooxygenase (PDB: 1W4X), (C) bacterial luciferase (PDB: 1LUC), (D) 4-hydroxyphenylacetate 3-hydroxylase (PDB: 2JBS), (E) styrene monooxygenase (PDB: 3IHM), (F) tryptophan 7-halogenase (PDB: 2ARD), (G) tryptophan 2-monooxygenase (PDB: 4IV9), (H) nitronate monooxygenase (PDB: 2GJL). In the center, the hydroperoxyflavin oxygenation species of flavin-dependent monooxygenases is shown. Figure from [43].

## ProDH in health and disease

In **Chapter 1**, the important role of proline in various cellular processes is discussed. The gene encoding for human ProDH is a hotspot for mutations, and the most commonly encountered mutations are presented in Table 1. These missense mutations influence ProDH activity, leading to various degrees of increased plasma proline levels (hyperprolinemia) and an increased susceptibility for schizophrenia [44-48].

**Table 1.**

Human ProDH missense mutations and their effect on ProDH activity [44-48]. Activity classifications: mild (<30%), moderate (30-70%) and severe (>70%) reduction of ProDH activity.

Mutation	Reduction of ProDH activity
R185Q, L289M, A455S, A472T	mild
Q19P, A167V, R185W, D426N, V427M, R431H	moderate
P406L, L441P, R453C, T466M, Q521E	severe

Although soluble and active human ProDH has been purified before [25], thorough studies on the structure-function relationship of this eukaryotic enzyme are lacking. In **Chapter 4** and **5**, we gained more insight into the minimal ProDH domain that is required for catalysis. This information might be used to better appreciate the effects of the different mutations in human ProDH. Mutating a bacterial homologue to study clinically relevant mutations in a human enzyme variant is done more often, for example for methylenetetrahydrofolate reductase [49]

We showed that most of the N-terminal part of *Tt*ProDH can be removed without affecting the catalytic properties of the enzyme (**Chapter 4**). Human ProDH has an elongated N-terminus compared to *Tt*ProDH (Fig. 5), and several missense mutations are located in the N-terminal region (Table 1). None of these mutations has severe consequences for the activity of the enzyme. Although the N-terminal region is not important for ProDH activity, this part of the protein likely has an important role *in vivo*, for example in cellular localization, membrane association, or intermolecular interactions. In addition, many eukaryotic proteins are co- or post-translationally modified, for example by acetylation or methylation. Such modifications are often essential for protein regulation and cellular signaling and might also occur in the N-terminal region of ProDH.

The human ProDH mutations that severely affect the enzyme activity are all located in the catalytic domain of the enzyme; however, most of the mutations are not situated in conserved sequence motifs (Table 1 and Fig. 8). Only Leu441, one of the residues that show a missense mutation with severe effects on ProDH activity, is a highly conserved residue. It is located in strand  $\beta$ 5 and flanked by residues that are involved in binding the flavin cofactor. Likely, replacing Leu441 by proline disrupts  $\beta$ -sheet formation and/or flavin binding. This could

explain the severe implications of this mutation. It has been shown for the ProDH domain of *EcPutA* that introducing the mutation homologous to the human mutation L441P decreases  $k_{\text{cat}}$  and severely decreases the thermostability of the enzyme. This suggests indeed that by introducing a proline at this position, flavin-protein interactions are disrupted and that the packing of the hydrophobic core of the enzyme is altered, destabilizing the protein [50].

Mutating Ala455 in human ProDH has mild consequences for the activity of the enzyme (Table 1). This residue is present at the ProDH dimerization interface that we identified for *TtProDH* in **Chapter 5**. This dimerization interface is important for stability of the thermophilic enzyme. Purified human ProDH is described as a dimer [25], but the dimer interface is not identified. However, it is likely that this interface is comparable to that of *TtProDH*. This might suggest that replacement of Ala455 by serine has mild consequences (Table 1) because the stability of the enzyme is affected.

Mutations R453C and A455S are located in a region that is not present in *TtProDH*. Possibly, human ProDH contains an extra helix that is also present in PutAs, denoted as  $\alpha 5a$  [25,50]. It is not surprising that replacement of an arginine by a cysteine has a large impact on the enzyme.

For most of the mutations, their implication is not clear. They are not localized in conserved regions and from the available ProDH crystal structures their impact is difficult to deduce. They might influence, for example, protein stability, protein folding, or protein-protein interactions. Besides that, it might also be that the effect is already at the translational level. Biochemical studies on recombinant human ProDH as well as *in vivo* studies are needed to gain a deeper understanding of this issue.

Since most biochemical studies on ProDH are based on enzymes from prokaryotic origin, studying eukaryotic ProDHs would greatly expand our knowledge on the ProDH family. In this research, we obtained knowledge about the minimal domain necessary for ProDH catalysis. Using this knowledge combined with our successful production and purification system (**Chapter 1**), it would be worthwhile to attempt to purify human ProDH, as well as other eukaryotic ProDHs. Besides expanding our biochemical knowledge on ProDHs to eukaryotic variants, studying the human enzyme might also shed more light on the molecular effects of missense mutations in ProDH. Nonetheless, a combination of *in vitro* and *in vivo* experiments will be needed since it cannot be excluded that several of these mutations are related to cellular processes.

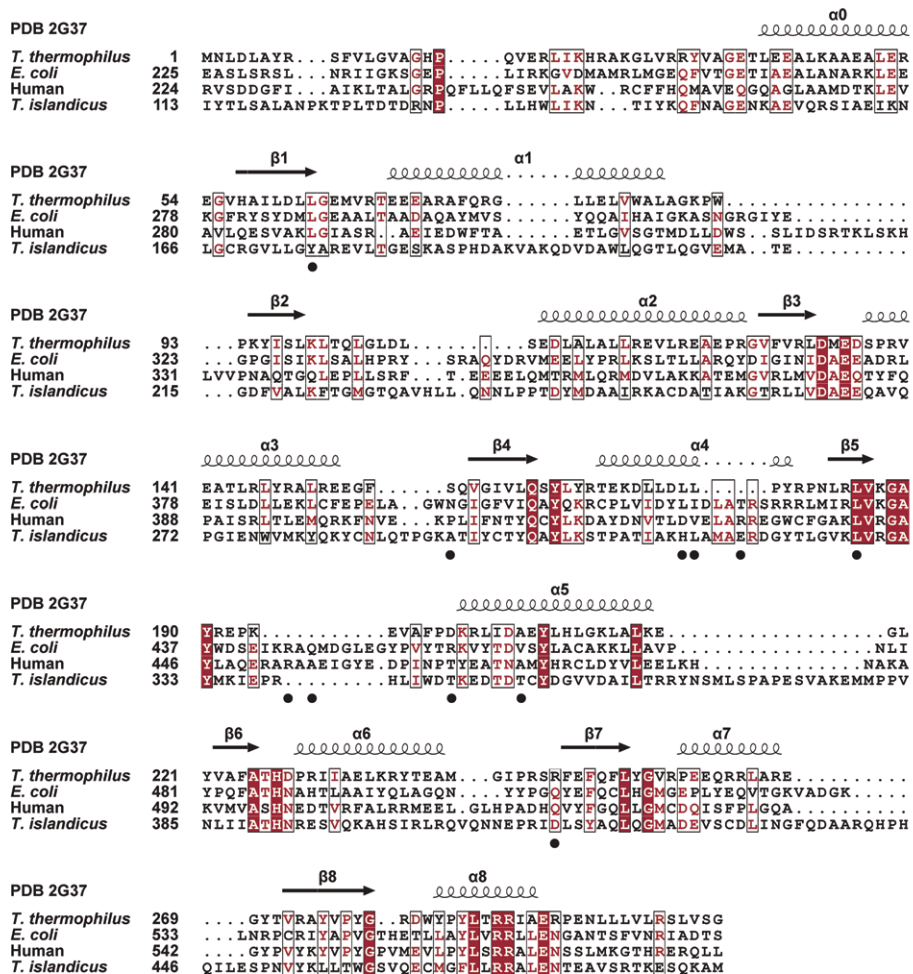


Figure 8.

Commonly found missense mutations in human ProDH indicated in a structure-based multiple alignment of ProDHs from different organisms. The ProDH amino acid sequences of *T. thermophilus* (UniProt: Q72IB8, PDB: 2G37), *E. coli* (UniProt: P09546, PDB: 4O8A), Human (UniProt: O43272) and *T. islandicus* (UniProt: A0A0U1M791) were aligned using the PROMALS3D server [51], which also uses structural information in constructing the alignment. The figure showing the alignment was made using ESPrict 3.0 software [52]. Strictly conserved residues are shown in white on a red background and similar residues are shown in red on a white background. Black boxes indicate similarity in a group of residues. Below the sequence, commonly found missense mutations in human ProDH are indicated with a black circle.



## Conclusions and future perspectives

In this thesis, we investigated multiple facets of the thermostable flavoenzyme *TtProDH*, including heterologous protein production, aggregation and oligomerization behavior, thermostability and cofactor binding. This expanded our knowledge on the structure-function relationship of this enzyme. We have created a minimalist ProDH that is still an excellent catalyst, but is deprived of all structural features that are unnecessary for *in vitro* functioning. These results contribute to fundamental insights of the biochemical properties of *TtProDH* and provide a basis for further structure-function studies on ProDHs, which is also a step forward in understanding the impact of missense mutations of human ProDH. In addition, this work gives insight into enzyme functionality from an industrial perspective by supplying tools for efficient recombinant ProDH production and by elucidating factors that govern thermostability of the enzyme. Finally, this work presents the first example of an enzyme that does not discriminate between FAD and FMN as cofactor, adding another surprise to the rich repertoire of flavoenzymes.

## References

- [1] Walsh, C. T., Garneau-Tsodikova, S., Howard-Jones, A. R., Biological formation of pyrroles: nature's logic and enzymatic machinery. *Nat. Prod. Rep.* (2006), 23, 517-531.
- [2] Cerdeño, A. M., Bibb, M. J., Challis, G. L., Analysis of the prodiginine biosynthesis gene cluster of *Streptomyces coelicolor* A3(2): new mechanisms for chain initiation and termination in modular multienzymes. *Chem. Biol.* (2001), 8, 817-829.
- [3] Garneau-Tsodikova, S., Dorrestein, P. C., Kelleher, N. L., Walsh, C. T., Protein assembly line components in prodigiosin biosynthesis: characterization of PigA,G,H,I,J. *J. Am. Chem. Soc.* (2006), 128, 12600-12601.
- [4] Li, C., Roege, K. E., Kelly, W. L., Analysis of the indanomycin biosynthetic gene cluster from *Streptomyces antibioticus* NRRL 8167. *ChemBioChem* (2009), 10, 1064-1072.
- [5] Meiser, P., Weissman, K. J., Bode, H. B. *et al.*, DKxanthene biosynthesis - understanding the basis for diversity-oriented synthesis in myxobacterial secondary metabolism. *Chem. Biol.* (2008), 15, 771-781.
- [6] Nowak-Thompson, B., Chaney, N., Wing, J. S., Gould, S. J., Loper, J. E., Characterization of the pyoluteorin biosynthetic gene cluster of *Pseudomonas fluorescens* Pf-5. *J. Bacteriol.* (1999), 181, 2166-2174.
- [7] Thomas, M. G., Burkart, M. D., Walsh, C. T., Conversion of L-proline to pyrrolyl-2-carboxyl-S-PCP during undecylprodigiosin and pyoluteorin biosynthesis. *Chem. Biol.* (2002), 9, 171-184.
- [8] Zhang, X. and Parry, R. J., Cloning and characterization of the pyrrolomycin biosynthetic gene clusters from *Actinosporangium vitaminophilum* ATCC 31673 and *Streptomyces* sp. Strain UC 11065. *Antimicrob. Agents Chemother.* (2007), 51, 946-957.
- [9] Wonnacott, S. and Gallagher, T., The chemistry and pharmacology of anatoxin-a and related homotropanes with respect to nicotinic acetylcholine receptors. *Mar. Drugs* (2006), 4, 228.
- [10] Méjean, A., Mann, S., Maldiney, T. *et al.*, Evidence that biosynthesis of the neurotoxic alkaloids anatoxin-a and homoanatoxin-a in the cyanobacterium *oscillatoria* PCC 6506 occurs on a modular polyketide synthase initiated by L-proline. *J. Am. Chem. Soc.* (2009), 131, 7512-7513.
- [11] Méjean, A., Mann, S., Vassiliadis, G. *et al.*, *In vitro* reconstitution of the first steps of anatoxin-a biosynthesis in *Oscillatoria* PCC 6506: from free L-proline to acyl carrier protein bound dehydroproline. *Biochemistry* (2010), 49, 103-113.
- [12] Moncoq, K., Regad, L., Mann, S., Méjean, A., Ploux, O., Structure of the prolyl-acyl carrier protein oxidase involved in the biosynthesis of the cyanotoxin anatoxin-a. *Acta Crystallogr. D Struct. Biol.* (2013), 69, 2340-2352.
- [13] Coulthurst, S. J., Barnard, A. M. L., Salmond, G. P. C., Regulation and biosynthesis of carbapenem antibiotics in bacteria. *Nat. Rev. Microbiol.* (2005), 3, 295-306.
- [14] McGowan, S. J., Sebahia, M., Porter, L. E. *et al.*, Analysis of bacterial carbapenem antibiotic production genes reveals a novel  $\beta$ -lactam biosynthesis pathway. *Mol. Microbiol.* (1996), 22, 415-426.
- [15] Schafhauser, T., Kirchner, N., Kulik, A. *et al.*, The cyclochlorotine mycotoxin is produced by the nonribosomal peptide synthetase CctN in *Talaromyces islandicus* ('*Penicillium islandicum*'). *Environ. Microbiol.* (2016).
- [16] Dyson, M. R., Shadbolt, S. P., Vincent, K. J., Perera, R. L., McCafferty, J., Production of soluble mammalian proteins in *Escherichia coli*: identification of protein features that correlate with successful expression. *BMC Biotechnol.* (2004), 4.
- [17] White, T. A., Krishnan, N., Becker, D. F., Tanner, J. J., Structure and kinetics of monofunctional proline dehydrogenase from *Thermus thermophilus*. *J. Biol. Chem.* (2007), 282, 14316-14327.
- [18] Cava, F., Hidalgo, A., Berenguer, J., *Thermus thermophilus* as biological model. *Extremophiles* (2009), 13, 213-231.
- [19] Lebendiker, M. and Danieli, T., Production of prone-to-aggregate proteins. *FEBS Lett.* (2014), 588, 236-246.
- [20] Terpe, K., Overview of tag protein fusions: from molecular and biochemical fundamentals to commercial systems. *Appl. Microbiol. Biotechnol.* (2003), 60, 523-533.
- [21] di Guana, C., Lib, P., Riggsa, P. D., Inouyeb, H., Vectors that facilitate the expression and purification of foreign peptides in *Escherichia coli* by fusion to maltose-binding protein. *Gene* (1988), 67, 21-30.
- [22] Sachdev, D. and Chirgwin, J. M., Fusions to maltose-binding protein: control of folding and solubility in

- protein purification, *Methods Enzymol.*, Academic Press, 2000, 312-321.
- [23] Reuten, R., Nikodemus, D., Oliveira, M. B. *et al.*, Maltose-binding protein (MBP), a secretion-enhancing tag for mammalian protein expression systems. *PLoS ONE* (2016), 11, e1-15.
  - [24] Sachdev, D. and Chirgwin, J. M., Properties of soluble fusions between mammalian aspartic proteinases and bacterial maltose-binding protein. *J. Protein Chem.* (1999), 18, 127-136.
  - [25] Tallarita, E., Pollegioni, L., Servi, S., Molla, G., Expression in *Escherichia coli* of the catalytic domain of human proline oxidase. *Protein Expr. Purif.* (2012), 82, 345-351.
  - [26] Hennig, M., Grimm, B., Contestabile, R., John, R. A., Jansonius, J. N., Crystal structure of glutamate-1-semialdehyde aminomutase: an  $\alpha_2$ -dimeric vitamin B<sub>6</sub>-dependent enzyme with asymmetry in structure and active site reactivity. *Proc. Natl. Acad. Sci. USA* (1997), 94, 4866-4871.
  - [27] Moxley, M. A., Tanner, J. J., Becker, D. F., Steady-state kinetic mechanism of the proline:ubiquinone oxidoreductase activity of proline utilization A (PutA) from *Escherichia coli*. *Arch. Biochem. Biophys.* (2011), 516, 113-120.
  - [28] Schertl, P. and Braun, H., Respiratory electron transfer pathways in plant mitochondria. *Front. Plant Sci.* (2014), 5.
  - [29] Wanduragala, S., Sanyal, N., Liang, X. W., Becker, D. F., Purification and characterization of Put1p from *Saccharomyces cerevisiae*. *Arch. Biochem. Biophys.* (2010), 498, 136-142.
  - [30] Moxley, M. A. and Becker, D. F., Rapid reaction kinetics of proline dehydrogenase in the multifunctional proline utilization A protein. *Biochemistry* (2012), 51, 511-520.
  - [31] Serrano, H. and Blanchard, J. S., Kinetic and isotopic characterization of L-proline dehydrogenase from *Mycobacterium tuberculosis*. *Biochemistry* (2013), 52, 5009-5015.
  - [32] Hubálek, F., Binda, C., Li, M. *et al.*, Inactivation of purified human recombinant monoamine oxidases A and B by rasagiline and its analogues. *J. Med. Chem.* (2004), 47, 1760-1766.
  - [33] Binda, C., Hubálek, F., Li, M. *et al.*, Crystal structures of monoamine oxidase B in complex with four inhibitors of the *N*-propargylaminoindan class. *J. Med. Chem.* (2004), 47, 1767-1774.
  - [34] White, T. A., Johnson Jr., W. H., Whitman, C. P., Tanner, J. J., Structural basis for the inactivation of *Thermus thermophilus* proline dehydrogenase by *N*-propargylglycine. *Biochemistry* (2008), 47, 5573-5580.
  - [35] Lienhart, W. D., Gudipati, V., Uhl, M. K. *et al.*, Collapse of the native structure caused by a single amino acid exchange in human NAD(P)H:quinone oxidoreductase<sup>1</sup>. *FEBS J.* (2014), 281, 4691-4704.
  - [36] Turner, P., Mamo, G., Karlsson, E. N., Potential and utilization of thermophiles and thermostable enzymes in biorefining. *Microb. Cell Fact.* (2007), 6, 9-9.
  - [37] Tango, M. S. A. and Islam, M. R., Potential of extremophiles for biotechnological and petroleum applications. *Energy Sources* (2002), 24, 543-559.
  - [38] Pantazaki, A., Pritsa, A., Kyriakidis, D., Biotechnologically relevant enzymes from *Thermus thermophilus*. *Appl. Microbiol. Biotechnol.* (2002), 58, 1-12.
  - [39] Beadle, B. M. and Shoichet, B. K., Structural bases of stability–function tradeoffs in enzymes. *J. Mol. Biol.* (2002), 321, 285-296.
  - [40] Georges, F., Protein stability and enzyme activity at extreme biological temperatures. *J. Phys. Condens. Matter* (2010), 22, 323101.
  - [41] Sterner, R. and Liebl, W., Thermophilic adaptation of proteins. *Crit. Rev. Biochem. Mol. Biol.* (2001), 36, 39-106.
  - [42] Macheroux, P., Kappes, B., Ealick, S. E., Flavogenomics - a genomic and structural view of flavin-dependent proteins. *FEBS J.* (2011), 278, 2625-2634.
  - [43] Huijbers, M. M. E., Montersino, S., Westphal, A. H., Tischler, D., van Berkel, W. J. H., Flavin dependent monooxygenases. *Arch. Biochem. Biophys.* (2014), 544, 2-17.
  - [44] Bender, H. U., Almashanu, S., Steel, G. *et al.*, Functional consequences of PRODH missense mutations. *Am. J. Hum. Genet.* (2005), 76, 409-420.
  - [45] Hu, C. A., Williams, D. B., Zhaorigetu, S. *et al.*, Functional genomics and SNP analysis of human genes encoding proline metabolic enzymes. *Amino Acids* (2008), 35, 655-664.
  - [46] Jacquet, H., Demily, C., Houy, E. *et al.*, Hyperprolinemia is a risk factor for schizoaffective disorder. *Mol.*

- Psychiatry* (2004), 10, 479-485.
- [47] Jacquet, H., Raux, G., Thibaut, F. *et al.*, PRODH mutations and hyperprolinemia in a subset of schizophrenic patients. *Hum. Mol. Genet.* (2002), 11, 2243-2249.
- [48] Liu, H., Heath, S. C., Sobin, C. *et al.*, Genetic variation at the 22q11 *PRODH2/DGCR6* locus presents an unusual pattern and increases susceptibility to schizophrenia. *Proc. Natl. Acad. Sci. USA* (2002), 99, 3717-3722.
- [49] Guenther, B. D., Sheppard, C. A., Tran, P. *et al.*, The structure and properties of methylenetetrahydrofolate reductase from *Escherichia coli* suggest how folate ameliorates human hyperhomocysteinemia. *Nat. Struct. Biol.* (1999), 6, 359-365.
- [50] Zhang, M., White, T. A., Schuermann, J. P. *et al.*, Structures of the *Escherichia coli* PutA proline dehydrogenase domain in complex with competitive inhibitors. *Biochemistry* (2004), 43, 12539-12548.
- [51] Pei, J., Kim, B. H., Grishin, N. V., PROMALS3D: a tool for multiple protein sequence and structure alignments. *Nucl. Acids Res.* (2008), 36, 2295-2300.
- [52] Robert, X. and Gouet, P., Deciphering key features in protein structures with the new ENDscript server. *Nucl. Acids Res.* (2014), 42, W320-W324.





# Summary

**English summary**  
**Nederlandse samenvatting**





## English summary

Proline is one of the proteinogenic amino acids and one of the most abundant amino acids in the cell. Next to serving as one of the non-essential amino acids, proline also has a central role in metabolism. In **Chapter 1**, the different functions of this imino acid are described, as well as the proline metabolic enzymes. The focus is on the enzyme proline dehydrogenase (ProDH), which catalyzes the flavin-dependent conversion of L-proline to  $\Delta^1$ -pyrroline-5-carboxylate (P5C). Malfunctioning of this enzyme has severe implications for human health and has been associated with tumorigenesis and schizophrenia.

This thesis deals with the engineering and biochemical characterization of *Thermus thermophilus* ProDH (*TtProDH*) in order to gain more insight into the structure-function relationship of this thermo-resistant flavoenzyme. *TtProDH* is a membrane-associated protein and recombinant soluble forms of the enzyme have only been obtained in limited amounts. **Chapter 2** describes the heterologous production of *TtProDH* in *Escherichia coli*. Using maltose-binding protein (MBP) as solubility tag, high yields of active holoenzyme are obtained. The MBP-tag can be efficiently removed from the fusion protein with trypsin, yielding native *TtProDH*. This enzyme is thermotolerant as well as solvent tolerant; however, both fused and clipped *TtProDH* are prone to aggregation. In **Chapter 3**, we show that the hydrophobic N-terminal helix of *TtProDH* is responsible for this non-native self-association. Phe10 and Leu12, located at the protein surface, were replaced by glutamates, generating the F10E/L12E (EE) variant of MBP-*TtProDH*. This more polar variant exclusively forms tetramers and exhibits excellent catalytic features. Specific removal of the MBP-tag of the EE variant is less easy than for WT, as trypsinolysis of the fusion enzyme leads to degradation of *TtProDH*. Since the MBP tag does not influence the spectral and catalytic properties of the enzyme, further experiments were performed with MBP-tagged variants of *TtProDH*.

ProDH has a distorted ( $\beta\alpha$ )<sub>8</sub> TIM-barrel fold which is conserved throughout the PutA/ProDH family. In contrast, the N-terminal sequence of ProDH is poorly conserved. *TtProDH* contains, next to the distorted TIM-barrel, three N-terminal helices,  $\alpha$ A,  $\alpha$ B and  $\alpha$ C, of which the function is not well understood. In **Chapter 4**, we describe the characterization of helical arm-truncated variants, lacking respectively one ( $\Delta$ A), two ( $\Delta$ AB), or three ( $\Delta$ ABC) N-terminal helices. All three variants show flavin properties that are highly similar to EE, indicating no changes in the microenvironment of the flavin isoalloxazine ring.  $\Delta$ A and  $\Delta$ AB are highly active tetramers, whereas removal of the complete N-terminal arm ( $\Delta$ ABC) results in poorly active dimers. Furthermore, EE,  $\Delta$ A and  $\Delta$ AB rapidly react with the suicide inhibitor *N*-propargylglycine, while  $\Delta$ ABC is not capable of forming a flavin adduct with *N*-propargylglycine. This indicates that helix  $\alpha$ C has a crucial role in both the oligomerization and activity of *TtProDH*. Closer examination revealed an ionic interaction as well as a hydrophobic patch between helices  $\alpha$ C and  $\alpha$ 8, the latter helix being crucial for substrate recognition. To investigate the functional role of helix  $\alpha$ C in further detail, additional enzyme

variants were created that disrupt the interactions between both helices. While disrupting the ionic interaction had minor effects, disrupting the hydrophobic patch leads to dimer formation, loss of activity and decreased reactivity with *N*-propargylglycine. This supports that helix  $\alpha$ C is crucial for *Tt*ProDH catalysis and tetramerization through positioning of helix  $\alpha$ 8.

The quaternary structure of *Tt*ProDH was investigated in more detail in **Chapter 5**. Two ionic interactions at the dimeric interface were selectively disrupted by changing Asp205 and Glu207 of *Tt*ProDH variants EE,  $\Delta$ A,  $\Delta$ AB and  $\Delta$ ABC into lysines. These KK-variants form monomers (except for EE KK, which forms dimers) and have improved catalytic properties at moderate temperatures compared to their non-KK counterparts. However, their melting temperatures are decreased by more than 20 °C. This indicates that a trade-off is made between thermostability and catalytic activity.

In **Chapter 6**, we studied the cofactor binding of *Tt*ProDH. Flavoenzymes contain either FAD or FMN as cofactor. FAD often binds to a Rossmann fold, while FMN prefers a TIM-barrel or flavodoxin-like fold. Proline dehydrogenase is denoted as an exception: it possesses a TIM barrel-like fold while binding FAD. To study the cofactor binding of *Tt*ProDH, we produced MBP-*Tt*ProDH EE in its apoform using a riboflavin auxotrophic *E. coli* strain. Reconstitution of the enzyme with either FAD or FMN revealed that MBP-*Tt*ProDH has no preference for FAD as cofactor. Kinetic parameters of both holo-FAD and holo-FMN are similar, as are the dissociation constants for FAD and FMN release. We show that the holo form of MBP-*Tt*ProDH, as produced in *E. coli* TOP10 cells, contains about three times more FMN than FAD. In addition, we obtained the crystal structure *Tt*ProDH  $\Delta$ ABC, which shows no electron density for an AMP moiety of the cofactor. This indicates the presence of mainly FMN in the enzyme. The capability of *Tt*ProDH to display equal properties with both cofactors is unique for flavoenzymes, and classification of *Tt*ProDH as an FAD-containing enzyme should be reconsidered.

In **Chapter 7**, we discuss the novel findings described in this thesis and put them in a broader perspective. We have created a minimalist ProDH that is an excellent catalyst, but is deprived of all structural features that are unnecessary for *in vitro* functioning. Our results expand the knowledge on the structure-function relationship of ProDHs, and give insight into enzyme functionality from an industrial perspective. We also discuss how this knowledge might be used in future studies for a better understanding of the properties of eukaryotic ProDHs, with a special interest in the human enzyme.

## Nederlandse samenvatting

Proline is één van de proteïnogene aminozuren en tevens een van de meest voorkomende aminozuren in de cel. In **Hoofdstuk 1** worden de verschillende functies van dit niet-essentiële aminozuur beschreven. De nadruk ligt hierbij op de centrale rol van proline en het enzym proline dehydrogenase (ProDH) in de cellulaire metabolisme. ProDH katalyseert de omzetting van L-proline naar  $\Delta^1$ -pyrroline-5-carboxylaat (P5C). Slecht functioneren van dit flavine-afhankelijke enzym heeft ernstige gevolgen voor de mens en wordt in verband gebracht met de ontwikkeling van tumoren en met schizofrenie.

Dit proefschrift beschrijft de biochemische karakterisatie en proteïne engineering van ProDH afkomstig uit *Thermus thermophilus* (TtProDH). Het doel hiervan is om meer inzicht te verkrijgen in de structuur-functie relatie van dit thermostabiele enzym. TtProDH is een membraan gebonden enzym en oplosbare vormen van dit eiwit zijn tot nu toe slechts in geringe hoeveelheden verkregen. **Hoofdstuk 2** beschrijft de heterologe productie van TtProDH in *Escherichia coli*. Door het fuseren van TtProDH met maltose-bindend eiwit (MBP) kunnen grote hoeveelheden actief enzym verkregen worden. Het MBP kan verwijderd worden door het fusie-eiwit te knippen met trypsine. Dit levert natief TtProDH op; dit enzym is bestand tegen hoge temperatuur en organische oplosmiddelen. Echter, zowel het fusie-eiwit als het natieve enzym hebben de neiging te aggregeren. In **Hoofdstuk 3** laten we zien dat de N-terminale helix van TtProDH verantwoordelijk is voor dit aggregatiegedrag. Door twee hydrofobe aminozuren (Phe10 en Leu12) aan het oppervlak van het eiwit te vervangen door polaire glutamaten werd een F10E/L12 (EE) variant verkregen die homogene tetrameren vormt en prima actief is. Helaas leidt het knippen van MBP-TtProDH EE met trypsine tot afbraak van EE. Omdat de MBP-tag geen invloed heeft op de activiteit van het enzym zijn verdere experimenten uitgevoerd met gefuseerde varianten van TtProDH.

ProDH heeft een katalytisch domein dat lijkt op een TIM-barrel, een achtvoudige herhaling van  $\beta\alpha$  eenheden. Deze manier van vouwen is geconserveerd in de PutA/ProDH familie. De N-terminale sequentie van ProDH is echter slecht geconserveerd. Naast de TIM-barrel bevat TtProDH drie N-terminale helixen,  $\alpha A$ ,  $\alpha B$  and  $\alpha C$ , waarvan de functie niet bekend is. In **Hoofdstuk 4** beschrijven we de eigenschappen van ingekorte varianten, die respectievelijk één ( $\Delta A$ ), twee ( $\Delta AB$ ), of drie ( $\Delta ABC$ ) N-terminale helixen missen. Alle drie varianten binden de flavine cofactor op vergelijkbare wijze als de EE variant.  $\Delta A$  en  $\Delta AB$  zijn tetrameren en goed actief, terwijl het verwijderen van de complete N-terminale arm ( $\Delta ABC$ ) resulteert in een dimeer die nauwelijks activiteit vertoont. In tegenstelling tot EE,  $\Delta A$  en  $\Delta AB$  kan  $\Delta ABC$  geen flavine adduct vormen met de zelfmoordremmer *N*-propargylglycine. Dit toont aan dat helix  $\alpha C$  een belangrijke rol speelt in zowel de oligomerisatie als de activiteit van TtProDH. Verdere aminozuur veranderingen lieten zien dat de hydrofobe interactie tussen helix  $\alpha C$  en helix  $\alpha 8$  cruciaal is voor de positionering van helix  $\alpha 8$ . Deze positionering beïnvloedt niet alleen de vorming van het tetrameer, maar is ook belangrijk voor de juiste interactie met het substraat.

De quaternaire structuur van *TtProDH* is verder onderzocht in **Hoofdstuk 5**. Twee ionogene interacties in het dimeer grensvlak zijn selectief verbroken door de negatief geladen aminozuren Asp205 en Glu207 van EE,  $\Delta A$ ,  $\Delta AB$  and  $\Delta ABC$  te veranderen in positief geladen lysines. Deze KK varianten vormen monomeren (behalve EE KK, deze vormt dimeren) en vertonen een toegenomen activiteit in vergelijking met de varianten waarbij de dimeer-interacties niet verbroken zijn. Echter, de smelttemperaturen van de KK varianten zijn verlaagd met meer dan 20 °C. Dit geeft aan dat er een compromis is bereikt tussen de katalytische activiteit en thermostabiliteit van het enzym.

In **Hoofdstuk 6** hebben we de cofactor binding van *TtProDH* bestudeerd. Flavine-afhankelijke enzymen bevatten FAD of FMN als cofactor. FAD bindt meestal in een dinucleotide bindend domein, terwijl FMN de voorkeur heeft voor binding in een TIM-barrel of flavodoxine domein. Proline dehydrogenase is een uitzondering: dit TIM-barrel enzym bindt FAD. Om de cofactor binding van *TtProDH* nader te bestuderen hebben we MBP-*TtProDH* geproduceerd in zijn apovorm door gebruik te maken van een riboflavine deficiënte *E. coli* stam. Reconstitutie van het apo enzym met FAD of FMN liet tot onze verrassing zien dat MBP-*TtProDH* geen voorkeur heeft voor FAD als cofactor. De kinetische parameters en dissociatie constanten van de holo-FAD en holo-FMN complexen zijn gelijk. Verder tonen we aan dat de holo vorm van MBP-*TtProDH*, zoals geproduceerd in *E. coli* TOP10 cellen, ongeveer drie keer meer FMN dan FAD bevat. Ook laten we zien dat de kristalstructuur verkregen van *TtProDH*  $\Delta ABC$  geen elektronendichtheid bezit voor het AMP deel van de cofactor. Dit is een verdere aanwijzing dat het enzym voornamelijk FMN bevat. Het feit dat *TtProDH* geen voorkeur heeft voor één van beide cofactoren is uniek voor flavine-bevattende eiwitten. We stellen dan ook voor de klassificering van *TtProDH* als FAD-bindend eiwit te herzien.

In **Hoofdstuk 7** bediscussiëren we de resultaten die beschreven zijn in dit proefschrift en plaatsen we deze in een breder perspectief. We hebben een minimalistische ProDH gecreeërd die nog steeds een uitstekende katalysator is, maar verlost is van alle structurele delen die onnodig zijn voor het *in vitro* functioneren. Onze resultaten verbreden de kennis met betrekking tot de structuur-functie relatie van ProDHs. Daarnaast geven ze inzicht in het functioneren van enzymen vanuit een industrieel perspectief. Tenslotte bediscussiëren we hoe deze kennis mogelijk gebruikt kan worden in toekomstige studies om de werking van eukaryote ProDHs, en met name het humane enzym, beter te begrijpen.









# About the author

**Acknowledgements**

**Curriculum vitae**

**Publications**

**Overview of completed training activities**





## **Acknowledgements**

Yellow has always been my favorite color. No wonder I was a bit unhappy during the first year of my PhD, since there was a serious lack of yellow in the lab. Luckily, the tide turned. Four years and large amounts of yellow protein later, I look back at an amazing experience and I feel both happy and sad to have finished this thesis. Since finishing a thesis is not something you do by yourself, I would like to thank everyone who contributed directly or indirectly to this thesis.

First and foremost, I would like to thank my promoter and supervisor Willem van Berkel. I am very grateful that you provided me with the opportunity to do my PhD within the Enzymes@Work group. The start of the project was not easy; I remember that you kept asking me to deliver 'geel en veel'. Luckily, we managed to achieve this mission, I am very glad we did not give up on ProDH. Thank you for your guidance and support throughout these years and for always pushing me to go a step further. Your extensive knowledge and help was always available and your door was always open. During the last months of my PhD, I was constantly sending you manuscripts and I was amazed how quickly you could find the time to correct them. I am very grateful for all your support and I think I could not have wished for a more enthusiastic supervisor. I hope we can continue to collaborate in the future.

Sacco, after my MSc thesis and internship, it was very nice that you welcomed me to do my PhD in the Biochemistry lab. Thank you for providing the vibrant atmosphere in the department.

To my colleagues of the Enzymes@Work group: thank you for the great time and all the scientific discussions we had. Adrie, you are a walking encyclopedia in case we encounter difficulties in the lab. I really admire your extensive knowledge and I am very grateful for your help and enthusiasm, both in the lab and behind the computer. A special thanks to my fellow PhDs Joseline, Tom, Gudrun and Antsje. It was great to share the PhD-experience with you and I enjoyed our dinners, drinks and gaming nights a lot. Joseline and Tom, I am very happy and honored to have you as my paranymphs. Joseline, it has been great spending not only our studies, but also our PhD together, thanks for all your support (and often distraction...). Tom, we shared an office from the beginning, which I really enjoyed. Thanks for keeping up with all my talking, that must have been hard sometimes.

Thanks to Laura for keeping up with all our administration. Jacques and Sjef, thank you for your help with MS measurements, which contributed to several chapters in this thesis. Walter, thank you for guiding me during the practicals of the Enzymology course. I enjoyed assisting during the practicals very much and learned a lot from your teaching skills.

A big thank you also goes to all the past and current members of the Laboratory of Biochemistry not mentioned above. I enjoyed our lunchbreaks, borrels, dinners, and all kind of activities very much. There is a great atmosphere in the Biochemistry group, I will miss it a lot and I hope we will stay in touch!

I had the opportunity to spend some weeks in Zaragoza (Spain) during my PhD. I would like to thank Milagros Medina for welcoming me in the lab. Milagros and Patricia Ferreira Neila, thank you for your help with the stopped-flow measurements. Marta Martínez-Julvéz, thank you for your help with the crystallization experiments. I am really happy with the positive outcomes of this collaboration!

I would like to thank Arjan Barendregt from Utrecht University for helping me with ESI-MS measurements. This was a really valuable contribution to several chapters in this thesis.

Thanks also to all the members of the MESIAB project. It was very interesting to see our different research fields combined in one project and I had a lot of fun during our biyearly meetings.

During my PhD I supervised several students during their BSc/MSc thesis or HBO internship. I am very happy you all decided to spend a significant part of your studies on this project. In chronological order: Wiebe, Evans, Maja, Maikel, Robbert, Ilona, Jenny, Estela and Stijn, I very much appreciate your hard work and contribution to this thesis. It was very nice to see you all grow in the lab. Thank you and I wish all of you the best with your future careers!

Mede-Moleculairen Henriëtte, Leonie, Bas en (ook latere PhD-collega's) Joseline en Antsje, super bedankt voor de gezellige en motiverende studiejaren en daarna voor het delen van ons 'PhD-leed' tijdens etentjes en borrels. Ik heb hier altijd erg van genoten; hopelijk kunnen we ook onze ervaringen uit het PhD afterlife nog lang blijven delen!

Bijzonder dankbaar ben ik ook de vriendinnen buiten het lab voor alle gezellige jaren in Wageningen en daar buiten. Jullie hebben ervoor gezorgd dat ik het leven buiten mijn thesis zeker niet vergat! Harriët en Jeltje, het is alweer meer dan 10 jaar geleden dat we samen op Asserpark kwamen wonen. Nu wonen we allemaal in een ander land, maar dat verandert niets aan onze vriendschap. Bedankt voor alle fantastische tijden en steun waar nodig! Marleen, Paulien, Ina: bedankt voor alle thee-, klets- en een heleboel andere momenten! Iris en Florence, onze geweldige Spanje-avonturen zal ik nooit vergeten! Tenslotte een bedankje aan al mijn hardloopmaatjes bij Tartlétos en Pallas voor de gezellige trainingen en activiteiten waarbij ik mijn werk altijd volledig van me af kon zetten!

Lieve Bas, ik had me geen betere steun én afleiding kunnen bedenken tijdens mijn laatste PhD-jaar. Jij hebt de laatste loodjes een heel stuk minder zwaar gemaakt. Ook was je mijn reddende engel bij al mijn last-minute lay-out issues, dankjewel!

Deze laatste alinea is voor mijn ouders, zus Loes en broertje Fons. Ik ben heel blij dat jullie me gemotiveerd hebben iets te gaan studeren wat ik leuk vond en achter mij stonden toen ik naar Wageningen vertrok. Tijdens mijn studie en PhD heb ik altijd op jullie hulp kunnen rekenen op wat voor manier dan ook. Ik beloof jullie dat ik weer vaker langs zal komen nu mijn PhD afgerond is!

**Mieke**

## Curriculum vitae

Mieke Huijbers was born on the 15th of January 1988 in Beek en Donk, the Netherlands and she moved to Someren in 1995. During her teenage years, a broad fascination for Science and Life started to develop. Therefore, it was no surprise that, after finishing her secondary education (VWO) at het Varendonck College in Asten in 2006, she started her Bachelor Molecular Life Sciences at Wageningen University & Research. During this BSc program, her interest became more focused on biochemistry in general and proteins in specific. The BSc degree was obtained *with distinction* in 2009, and followed by a few months of travelling and language courses in Spain. Back in the Netherlands, Mieke continued with the Master's program of



Molecular Life Sciences at Wageningen University & Research. In line with her growing interest in proteins, she started her thesis at the Laboratory of Biochemistry, in the group of Prof. Dr. Sacco de Vries. Under the daily supervision of Marije aan den Toorn she studied structural and activational changes upon unfolding of the kinase domain of a somatic embryogenesis receptor-like kinase, which resulted in a co-authorship on a scientific paper. For a second thesis, she went to the Structural and Computational Biology Programme of the Institute for Research in Biomedicine (IRB) in Barcelona, Spain. Under the supervision of Dr. Roeland Boer, she continued her work on somatic embryogenesis receptor-like kinases by improving purification protocols and setting up crystallization trials. To complete her MSc, Mieke went to Utrecht University for an internship at the Medicinal Chemistry and Chemical Biology group. Under supervision of Dr. Ir. John Kruijtzer and Dr. Johan Kemmink, she worked on the synthesis of a new protective group for histidine residues during the synthesis of sulfated-tyrosine containing peptides. In addition, she synthesized sulfated peptides and studied peptide-protein interactions. Mieke received her Master's degree *with distinction* in June 2012 and shortly after she was appointed as a PhD candidate in the Enzymes@Work group of Prof. Dr. Willem van Berkel in the Laboratory of Biochemistry at Wageningen University & Research. The results of the research performed in the four years that followed are described in this thesis. She now continues her career as a postdoctoral researcher in the Biocatalysis group of Dr. Frank Hollmann at the Department of Biotechnology at Delft University of Technology.



## Publications

### This thesis

- **Huijbers, M. M. E.**, Wu, J. W., van Berkel, W. J. H. (2017) Dimerization of proline dehydrogenase from *Thermus thermophilus* is crucial for its thermostability. *Manuscript in preparation*.
- **Huijbers, M. M. E.**, van Alen, I., Wu, J. W., Barendregt, A., Heck, A. J. R., van Berkel, W. J. H. (2017) Functional impact of the N-terminal arm of proline dehydrogenase from *Thermus thermophilus*. *Manuscript submitted*.
- **Huijbers, M. M. E.**, Martínez-Júlvez, M., Westphal, A. H., Delgado-Arciniega, E., Medina, M., van Berkel, W. J. H. (2017) Proline dehydrogenase from *Thermus thermophilus* does not discriminate between FAD and FMN as cofactor. *Sci. Rep.*, *manuscript accepted*.
- **Huijbers, M. M. E.** and van Berkel, W. J. H. (2016) A more polar N-terminal helix releases MBP-tagged *Thermus thermophilus* proline dehydrogenase from tetramer-polymer self-association. *J. Mol. Catal. B. Enzym.* 134, 340-346.
- **Huijbers, M. M. E.** and van Berkel, W. J. H. (2015) High yields of active *Thermus thermophilus* proline dehydrogenase are obtained using maltose-binding protein as a solubility tag. *Biotechnol. J.* 10, 395-403.

### Other work

- Jahn, L., Schafhauser, T., Pan, S., Weber, T., Wohlleben, W., Fewer, D., Sivonen, K., Flor, L., van Pée, K., Caradec, T., Jacques, P., **Huijbers, M. M. E.**, van Berkel, W. J. H., Ludwig-Müller, J. (2017) A new ostropalean fungus (*Villosirosea asteris* gen. nov., sp. nov.) from the inflorescence axis of *Aster tataricus*. *Manuscript submitted*.
- Schafhauser, T., Kirchner, N., Kulik, A., **Huijbers, M. M. E.**, Flor, L., Caradec, T., Fewer, D. P., Gross, H., Jacques, P., Jahn, L., Jokela, J., Leclère, V., Ludwig-Müller, J., Sivonen, K., van Berkel, W. J. H., Weber, T., Wohlleben, W., van Pée, K. (2016) The cyclochlorotine mycotoxin is produced by the nonribosomal peptide synthetase CctN in *Talaromyces islandicus* ('*Penicillium islandicum*'). *Environ. Microbiol.* 18, 3728–3741.
- Schafhauser, T., Wibberg, D., Rückert, C., Winkler, A., Flor, L., van Pée, K., Fewer, D. P., Sivonen, K., Jahn, L., Ludwig-Müller, J., Caradec, T., Jacques, P., **Huijbers, M. M. E.**, van Berkel, W. J. H., Weber, T., Wohlleben, W., Kalinowski, J. (2016) Draft genome sequence of *Talaromyces islandicus* ("*Penicillium islandicum*") WF-38-12, a neglected mold with significant biotechnological potential. *J. Biotechnol.* 211, 101-102.
- **Huijbers, M. M. E.**, Montersino, S., Westphal, A. H., Tischler, D., van Berkel, W. J. H. (2014) Flavin dependent monooxygenases. *Arch. Biochem. Biophys.* 544, 2-17.
- aan den Toorn, M., **Huijbers, M. M. E.**, de Vries, S. C., van Mierlo, C. P. M. (2012) The *Arabidopsis thaliana* SERK1 kinase domain spontaneously refolds to an active state *in vitro*. *PLoS ONE* 7, e50907.

## Overview of completed training activities



### Discipline specific activities

#### Courses

Training on stopped-flow and crystallography – University of Zaragoza	Zaragoza (Spain)	2015
European summer school on industrial biotechnology – Stability, folding, and misfolding of recombinant proteins	Milan (Italy)	2014
Applied biocatalysis (VLAG, GBB)	Wageningen (NL)	2014
Bioinformatic tools for PKS and NRPS discovery – From genomic data to the products	Lille (France)	2013
3DM course (Bio-Product)	Nijmegen (NL)	2012

#### Conferences and meetings

8 <sup>th</sup> European meeting onOxiZymes *	Wageningen (NL)	2016
11 <sup>th</sup> International conference on protein stabilisation * <sup>‡</sup>	Istanbul (Turkey)	2016
CHAINS – chemistry as innovating science * <sup>‡</sup>	Veldhoven (NL)	2015
Mini symposium ‘Pack and Go’ –Nanopackaging of biomacromolecules (VLAG, BIC, PCC)	Wageningen (NL)	2015
CHAINS – chemistry as innovating science *	Veldhoven (NL)	2014
18 <sup>th</sup> International symposium on flavins and flavoproteins *	Cha-Am (Thailand)	2014
7 <sup>th</sup> European meeting onOxiZymes *	Vienna (Austria)	2014
NWO protein study group meeting	Veldhoven (NL)	2013
Mini symposium WBox2: redox biocatalysis (NBV, BIC)	Wageningen (NL)	2013
BCF career event – academic expo * <sup>‡</sup>	Amsterdam (NL)	2013
NWO protein study group meeting *	Veldhoven (NL)	2012

#### General courses

Adobe Indesign essential training (WUR library)	Wageningen (NL)	2016
Scientific artwork with Photoshop and Illustrator (WUR library)	Wageningen (NL)	2016
Career orientation (WGS)	Wageningen (NL)	2015
Scientific writing (WGS)	Wageningen (NL)	2015
Project and time management (WGS)	Wageningen (NL)	2015
Reviewing a scientific paper (WGS)	Wageningen (NL)	2015
Mini symposium ‘How to write a world-class paper’ (WUR library, Elsevier)	Wageningen (NL)	2013
Teaching and supervising thesis students (WGS)	Wageningen (NL)	2013
VLAG PhD week (VLAG)	Baarlo (NL)	2013

#### Optional activities

Biochemistry weekly group meetings and colloquia	Wageningen (NL)	2012 – 2016
ERA-IB biannual meetings	Wageningen (NL)	2012 – 2014
Biochemistry PhD retreat (member of organizing committee)	United Kingdom	2013
Preparing PhD research proposal	Wageningen (NL)	2012

\* poster presentation, <sup>‡</sup> oral presentation

The research presented in this thesis was performed at the Laboratory of Biochemistry, Wageningen University & Research, and was financially supported by the Netherlands Organization for Scientific Research (NWO) and The Graduate School VLAG (Wageningen, The Netherlands) through the ERA-NET Industrial Biotechnology program (ERA-IB-2, project EIB.10.004) of the European Community.

Financial support from the Laboratory of Biochemistry for printing this thesis is gratefully acknowledged.

Cover design and layout by Mieke Huijbers

Printed by GVO drukkers & vormgevers, Ede, the Netherlands





